UNIVERSITY OF CALIFORNIA,
IRVINE

Toward enhancing the durability and integration of engineered articular cartilage

DISSERTATION

Submitted in partial satisfaction of the requirements for the degree of

DOCTOR OF PHILOSOPHY

in Biomedical Engineering

by

Jarrett Marshall Link

Dissertation Committee:
Distinguished Professor Kyriacos Athanasiou, Chair
Principal Development Engineer Jerry Hu
Associate Professor Wendy Liu

2020

DEDICATION

To Shriners Hospitals for Children and all those who walk in pain

TABLE OF CONTENTS

LIST OF FIGURES ..... *xiii*

LIST OF TABLES ..... *xviii*

ACKNOWLEDGEMENTS ..... *xx*

CURRICULUM VITAE ..... *xxii*

ABSTRACT ..... *xxiv*

INTRODUCTION *1*

CHAPTER 1 The self-assembling process and applications in tissue engineering 7

Abstract **7**

Introduction **7**

Tissue engineering **8**

Self-assembling process **9**

Other scaffold-free techniques **12**

Advantages of scaffold-free techniques **15**

Scaffold-free tissue engineering in the clinic **17**

Functional tissue engineering **19**

Primarily mechanically functional tissues **20**

Bone 20

Cartilage 21

Ligaments and tendons 22

Cardiac 23

Vascular 24

Non-mechanical tissues **26**

Liver 26

Cornea 27

Conclusions and future directions **29**

CHAPTER 2 A modified hydroxyproline assay based on hydrochloric acid in Ehrlich's solution accurately measures tissue collagen content ***33***

Abstract **33**

Introduction **34**

Methods **38**

Tissue preparation 38

Hydroxyproline assay overview 38

Suggested hydroxyproline assay protocol 39

Optimization of hydrochloric acid concentration 40

Absorbance measurements 41

Comparison of Ehrlich's solution using hydrochloric or perchloric acid for collagen quantification 41

Amino acid analysis 42

Statistics 42

Results **43**

Discussion **47**

CHAPTER 3 Facet joints of the spine: structure-function relationships, problems and treatments, and the potential for regeneration ***52***

Abstract **52**

Introduction **52**

Facet joint anatomy and biomechanics **54**

Articular processes 55
Articular cartilage 57
Synovium, synovial fold, and fibrous capsule 58
Nerve endings 59
Role of the facet joint in spine biomechanics 59
Biomechanical alterations postdegeneration and surgical intervention 60

Pain and pathology associated with the facet joint 61

Facet joint injury 61
Facet joint pain 61
Facet joint degeneration 62
The relationship between the facet joint and intervertebral disc degeneration 65
Comorbidities 66

Management of back pain related to facet joint pathology 67

Conservative management 67
Operative management 69

Future directions: could tissue engineering provide a new treatment strategy for facet-related morbidity? 72

Key criteria to engineer facet cartilage 74
Potential strategies to engineer facet cartilage 76
Key criteria for an engineered total facet joint 78
Envisioning an engineered total facet joint 79

Conclusion 80

CHAPTER 4 The tribology of cartilage: mechanisms, experimental techniques, and relevance to translational tissue engineering 81

Abstract 81

Introduction **82**

Commonly examined tribological characteristics in cartilage **84**

Surface roughness 84

Coefficient of friction 84

Tribological structure-function relationships in diarthrodial joints **85**

Cartilage components essential for tribological function 87

Regulation of lubrication modes in diarthrodial joints 91

Pathologies affecting diarthrodial joint tribology 92

Methods for quantifying tribological properties **94**

Tribometers 95

Atomic force microscopy 97

Toward engineering native tribological properties **97**

Biolubricants 97

Scaffolds 99

Bioactive factors 101

Mechanical stimulation 103

Perspectives **104**

CHAPTER 5 Chondroitinase ABC enhances integration of self-assembled articular cartilage, but its dosage needs to be moderated based on neocartilage maturity ***106***

Abstract **106**

Introduction **107**

Methods **110**

Cell and tissue harvest 110

Construct formation and culture 110
Construct integration 111
Histology of constructs and composites 112
Biochemical analyses of constructs 112
Construct and composite mechanical testing 113
Statistics 113

Results 114

Phase I: C-ABC$_{int}$ and TCL enhanced cartilage integration synergistically 114
Phase II: Construct mechanical properties were preserved regardless of C-ABC$_{int}$ concentration, but local, histologic effects of C-ABC$_{int}$ were observed for both immature and mature constructs 116
Phase II: Effective C-ABC$_{int}$ dose to enhance cartilage integration is greater for mature constructs than for immature constructs 118

Discussion 121

Supplementary material 128

CHAPTER 6 Bioactive factors confer protection to self-assembled cartilage against macrophage challenge in a novel co-culture system 130

Abstract 130

Introduction 131

Methods 133

Isolation, expansion, and aggregate redifferentiation of chondrocytes 133
Isolation of bone marrow-derived monocytes and differentiation into macrophages 135
Formation of self-assembled cartilage constructs 135
Co-culture of macrophages and self-assembled cartilage constructs 136
Sample processing and biochemical analyses 137
Mechanical testing 138

Histology 138
ELISA cytokine analysis 139
Statistics 139
Results 139
Study 1: C-ABC modulates compressive stiffness in CHG-treated constructs 139
Study 1: Stiff, CHG-treated constructs are protected from macrophage inflammatory challenge even in the presence of an elevated proinflammatory response 141
Study 2: C-ABC modulates compressive stiffness in TCL-treated constructs 145
Study 2: TCL-treated constructs can withstand macrophage challenge regardless of stimulation and stiffness 146
Study 2: TCL-treated constructs diminish TNF-α production, and increased stiffness enhances the anti-inflammatory effect of IL-10-stimulated macrophages 146
Discussion 150
CHAPTER 7 Establishing the safety of self-assembled articular cartilage implants in the Yucatan minipig 154
Abstract 154
Introduction 155
Materials and Methods 157
Fabrication of tissue engineered implants 157
Quality control of engineered implants 160
Acquisition of Yucatan minipigs 160
Surgical set #1 161
Surgical set #2 164
Safety assessments 167
Statistics 169

Results **170**

Surgical set #1 170

Surgical set #2 174

Discussion **178**

Supplementary Material **181**

CONCLUSIONS AND FUTURE DIRECTIONS ***182***

REFERENCES ***187***

APPENDIX 1 Characterization of facet joint cartilage properties in the human and interspecies comparisons ***243***

Abstract **243**

Statement of significance **244**

Introduction **244**

Materials and methods **247**

Specimens 247

Histology 248

Biochemistry 248

Creep indentation testing 248

Statistical analysis 249

Results **249**

Gross morphology 249

Histology 251

Biochemistry 252

Mechanical testing 253

Discussion **254**

APPENDIX 2 Exogenous lysyl oxidase-like 2 and perfusion culture induce collagen crosslink formation in osteogenic grafts 271

Abstract 271

Introduction 272

Materials and methods 274

Scaffold preparation 274

Cell culture 274

Hydroxylysine and copper sulfate treatment 275

Detection of LOX activity 275

Seeding MSCs on HA-PLG constructs in bioreactors and stimulation with LOXL2 275

Quantification of collagen content 278

Statistical analysis 278

Results 278

HL and CuSO4 influence collagen deposition and LOX activity 278

LOXL2 treatment influences MSC proliferation after 21 days of culture 279

Functional properties of engineered constructs are not affected by LOXL2 280

Extended culture duration sustains MSC osteogenic differentiation 280

Exogenous LOXL2 supplementation leads to pyridinoline crosslink formation 281

Discussion 281

APPENDIX 3 Characterization of adult and neonatal articular cartilage from the equine stifle 297

Abstract 297

Introduction 298

Materials and methods 300

Native tissue sample preparation 300
Biomechanical evaluation 301
Biochemical evaluation 302
High-performance liquid chromatography 302
Histological and immunohistochemical evaluation 303
Statistical Analysis 303
Results 303
Gross morphology 303
Histology 304
Biochemical properties 305
Biomechanical properties 307
Discussion 308
Conclusion 314
APPENDIX 4 In Vitro Effects of Bupivacaine on the Viability and Mechanics of Native and Engineered Cartilage Grafts 332
Abstract 332
Introduction 333
Materials and methods 335
Explant harvest 335
Neocartilage engineering 335
Bupivacaine exposure 336
Viability assessment 337
Histological evaluation 337
Quantitative biochemistry 337
Creep indentation testing 338

Statistical analysis 338

Results 339

Chondrocyte viability 339

Histology 339

Quantitative biochemistry 340

Compressive mechanical properties 340

Discussion 341

LIST OF FIGURES

Figure 1-1. Scaffold-free tissue engineering. 9

Figure 1-2. The phases of self-assembly and cartilage development. 10

Figure 1-3. Energy usage and achievable dimensions in scaffold-free processes. 12

Figure 2-1. Overview of the hydroxyproline assay. 36

Figure 2-2. Spectrophotometric absorbance as a function of collagen concentration....43

Figure 2-3. Absorbance as a function of light wavelength and collagen concentration for paired hydroxyproline assays 45

Figure 2-4. Concentrations of collagen measured by the hydroxyproline assay using DMAB dissolved in 30% HClO4 or HCl plus 70% isopropanol. 46

Figure 2-5. Concentrations of hydroxyproline, from lowest to highest collagen content, in rabbit liver, rabbit testis, engineered bovine articular cartilage, bovine articular cartilage, rabbit meniscus, and rabbit tendon 47

Figure 3-1. Facet joint anatomy. 56

Figure 3-2. Common facet-related problems. 63

Figure 3-3. Conservative and operative management strategies for facet joint pathologies 68

Figure 3-4. Tissue-engineering the facet joint. 77

Figure 4-1. Lubrication regimes (A-D) within a synovial joint. 86

Figure 4-2. A summary of how the gross morphology, biochemical content, and mechanical properties of cartilage feed into the maintenance of tribological function in the diarthrodial joint. 88

Figure 4-3. Tribometer configurations. 95

Figure 5-1. A schematic diagram describes the integration of engineered cartilage to native cartilage. 109
Figure 5-2. C-ABC$_{int}$ and TCL synergistically enhanced cartilage integration (Phase I). 115
Figure 5-3. A higher C-ABC$_{int}$ dose is required for local GAG depletion in 5-week constructs due to increased collagen density at the edge (Phase II). 116
Figure 5-4. Properties of engineered constructs were found to be preserved regardless of C-ABC$_{int}$ dose (Phase II). 118
Figure 5-5. Effective C-ABC$_{int}$ dose to achieve integration for immature constructs is lower than for mature constructs (Phase II). 119
Figure 5-6. C-ABC$_{int}$ dose required for enhanced mechanical integration is higher for mature constructs than for immature constructs (Phase II). 121
Figure 6-1. A schematic representation of the co-culture system. 137
Figure 6-2. C-ABC application modulates CHG-treated construct biochemical properties. 140
Figure 6-3. H&E from CHG-treated constructs following 2 weeks of co-culture. 141
Figure 6-4. CHG-treated construct biochemical properties after 2 weeks of macrophage co-culture. 143
Figure 6-5. Mechanical properties and inflammatory cytokine data for CHG-treated constructs. 144
Figure 6-6. Histology of TCL-treated constructs after C-ABC application at t=0. 145
Figure 6-7. Saf O staining of TCL-treated constructs after two weeks of macrophage co-culture. 148

Figure 6-8. Biochemical, mechanical, and cytokine data for TCL-treated constructs. .149
Figure 7-1. Surgical set #1 timeline and surgical approach: A schematic depicting a timeline for the creation of the tissue engineered neocartilage implants, to implantation and sacrifice. 163
Figure 7-2. Surgical set #2 timeline and surgical approach: A schematic depicting a timeline from the creation of the tissue engineered neocartilage implants, implantation, and sacrifice. 166
Figure 7-3. Surgical set #2 post-operative care: Immediately after surgery, minipigs were placed in a custom-made, IACUC-approved, sling. 168
Figure 7-4. Surgical set #1 defect maps and resulting gross morphology 171
Figure 7-5. Histopathology of graft sites from the fibrin minipig. 173
Figure 7-6. Surgical set #2 results: Defect maps for control (a) and treated (b) minipigs 175
Figure 7-7. Surgical set #2 8-week endpoint complete blood count normalized to presurgical values. 176
Figure 7-8. Surgical set #2 8-week endpoint blood phenotyping chemistry panel normalized to presurgical values. 177
Figure A1-1. Illustration of the facet joint anatomy and the gross morphological measurements of the facet joint surface. 266
Figure A1-2. Human facet joint pathology grading. 267
Figure A1-3. Interspecies comparison of the average A) length B) width and C) percentage depth of the inferior (I) and superior (S) facet surfaces. 267
Figure A1-4. Facet joint histology. 268

Figure A1-5. Comparison of the biochemical properties of facet cartilage among spinal levels within one species and also among species. 269
Figure A1-6. Comparison of the mechanical properties of facet cartilage among spinal levels within one species and also among species. 270
Figure A2-1. Full-factorial study to determine concentrations of HL and CuSO4 required for LOX-mediated crosslinking. 292
Figure A2-2. Effect of exogenous LOXL2 application on morphology and DNA content of constructs cultured for 21 days. 293
Figure A2-3. Effect of exogenous LOXL2 application on osteogenic differentiation and functional outputs for constructs in perfusion culture for 21 days. 294
Figure A2-4. Effect of extended culture time on morphology and DNA content. 295
Figure A2-5. Effect of extended culture time on osteogenic differentiation and functional outputs. 296
Figure A3-1. Articular cartilage from 17 sites across six regions of the distal femur and patella were characterized morphologically, histologically, biochemically, and biomechanically. 321
Figure A3-2. Thickness of adult articular cartilage. 322
Figure A3-3. Histological evaluation of neonatal and adult articular cartilage cross sections from site 2 of each region. 323
Figure A3-4. Immunohistochemical evaluation of neonatal and adult articular cartilage from site 2 of each region. 324
Figure A3-5. Biochemical characterization of regions and overall average for each age group: neonatal and adult. 325

Figure A3-6. Characterization of compressive properties at each site within each region and overall average for each age group: neonatal and adult. 326
Figure A3-7. Characterization of tensile properties within each region and overall average for each age group: neonatal and adult. 327
Figure A4-1. Chondrocyte viability in native explants and neocartilage constructs after bupivacaine exposure. 349
Figure A4-2. Gross and microscopic histology of native explants and neocartilage constructs after exposure to bupivacaine. 350
Figure A4-3. Biochemical composition of the extracellular matrix. 351
Figure A4-4. Compressive mechanical properties of native explants and neocartilage. 351

LIST OF TABLES

Table 1-1. Advantages of scaffold-free techniques 29

Table 2-1. A cost and safety comparison between perchloric acid and hydrochloric acid 37

Table 3-1. Structural and functional properties of the human facet joint 56

Table 3-2. A comparison of the facet joint to the knee 73

Table 4-1. Coefficients of friction (μ) for native articular cartilage and meniscus in the boundary lubrication regime 89

Table 4-2. Coefficients of friction (μ) for engineered articular cartilage and meniscus in the boundary lubrication regime 102

Table 5-S1. Self-assembled articular cartilage construct properties prior to integration 128

Table A1-1. Patient details of human lumbar spine samples. 266

Table A1-2. Interspecies sample numbers and methods used to characterize the facet cartilage. 266

Table A1-3. Biochemical properties of human facet cartilage as a function of degeneration severity. 268

Table A3-1. Thickness, hydration, and crosslinks per collagen of neonatal and adult articular cartilage from specific regions and sites within each region. 328

Table A3-2. GAG, collagen, and cell number on a per wet weight (WW) and per dry weight (DW) basis of neonatal and adult articular cartilage from specific regions and sites within each region. 329

Table A3-3. Compressive properties of neonatal and adult articular cartilage from specific regions and sites within each region. 330
Table A3-4. Tensile properties of neonatal and adult articular cartilage from specific regions and sites within each region. 331
Table A4-1. Biochemical composition of extracellular matrix 351

ACKNOWLEDGEMENTS

From start to finish, graduate school was an incredibly immersive, challenging, stimulating, educational, and, ultimately, transformative period in my life. I have developed substantially as a scientist, engineer, and, perhaps most palpably, as a human being during my PhD studies and research. While there were many unexpected twists and turns along the way, including a transfer from UC Davis to UC Irvine at the midpoint, I will be forever grateful to the many people and organizations that helped me navigate this journey.

First and foremost, I would like to thank Dr. Kyriacos Athanasiou, my primary advisor and principal investigator at both UC Davis and UC Irvine, for: his guidance and mentorship that motivated me to mature personally and professionally; his contagious and ceaseless pursuit of scientific advance; his ability to convey his knowledge, wisdom, and upstanding ethics; and his encouragement of all of his students to have a positive impact on the world as both scientists and people. I would also like to thank Dr. Jerry Hu, another crucial advisor throughout graduate school, for his unwavering energy, support, and ability to encourage me to ask every question possible. Additionally, I would like to thank all of my past and present graduate student and postdoctoral colleagues from the Athanasiou laboratories at both UC Davis and UC Irvine. Without their personal and professional support, passion, insight, and humor, I would not be where I am today. I would also like to acknowledge people specific to UC Davis who had a profoundly positive impact on my development, including Dr. Hari Reddi, Christal Wintersmith, and all of the graduate students who were a part of the Biomedical Engineering Student Association (BESA). I have missed all of you ever since moving to UC Irvine.

Next, I would like to thank UC Irvine as an organization and environment that made it as seamless as possible to transition from one university to another midway through graduate school. Many individuals were responsible for the ease of that transition, including, but not limited to Clare Cheng, Sally Avila, Maggie Mulcare, and Thomas Pitcher. I would also like to express

gratitude to Dr. Wendy Liu, who became a mentor of mine, collaborator to the Athanasiou laboratory, and a member of my dissertation committee. Her insights and immunology expertise were instrumental in developing my research trajectory at UC Irvine. Susan Demas also will forever have my gratitude for her willingness to care for our research animals as if there were her own pets, for her diligence and expertise in the operating room, and for supporting me through challenging moments at the UCI Medical Center.

I would also like to thank the National Science Foundation Graduate Research Fellowship Program for their financial and professional development support, and acknowledge all of the organizations that have provided me with funding throughout graduate school, including the National Institutes of Health, UC Davis, and UC Irvine.

While I developed substantially in graduate school, my training began prior to starting my PhD studies. I would like to thank Dr. Peter Augat of the Institute of Biomechanics at BGU Murnau for giving me an opportunity to complete an undergraduate summer research internship in 2012 that set the stage for my future research engagements. Additionally, the mentorship I received from Dr. Farshid Guilak and Dr. Katherine Glass at Duke University as a Pratt Undergraduate Research Fellow, as well as the rigorous cartilage tissue engineering research experience, was indispensable in helping me reach and prepare for PhD level work.

Finally, I would like to thank my partner Ashleigh, parents Mary Kay and Ken, sister Nicole, extended family, and close friends for their unconditional love and support, consistent interest in the progression of my work, and ability to give my life a deeper meaning and purpose beyond the pursuit of scientific excellence.

CURRICULUM VITAE

Jarrett Marshall Link

2013-2014, Pratt Undergraduate Research Fellow, Orthopaedic Bioengineering Laboratory, advisor: Farshid Guilak, Duke University

2014, BSE in Biomedical Engineering, Graduate with Departmental Distinction, Duke University

2014-2017, Graduate Student Researcher, Musculoskeletal Bioengineering Laboratory, advisor: Kyriacos A. Athanasiou, University of California, Davis

2016-2019, National Science Foundation Graduate Research Fellowship Program Awardee

2017-2020, Graduate Student Researcher, DELTA*i*, advisor: Kyriacos A. Athanasiou, University of California, Irvine

2018, MS in Biomedical Engineering, University of California, Irvine

2020, PhD in Biomedical Engineering, University of California, Irvine

Field of Study

Toward enhancing the durability and integration of engineered articular cartilage

Publications

Link JM, Hu JC, and Athanasiou KA. Chondroitinase ABC Enhances Integration of Self-assembled Articular Cartilage, but its Dosage Needs to be Moderated Based on Neocartilage Maturity. Cartilage. (Online Ahead of Print 2020)

Link JM*, Salinas EY*, Hu JC, Athanasiou KA. The tribology of cartilage: mechanisms, experimental techniques, and relevance to translational tissue engineering. Clinical Biomechanics. (*these authors contributed equally to this work) (Online Ahead of Print 2019)

O'Leary SA, Paschos NK, **Link JM**, Klineberg EO, Hu JC, Athanasiou KA. Facet joints of the spine: structure-function relationships, problems and treatments, and the potential for regeneration. Annual Review of Biomedical Engineering. 20:1 (2018)

Mitra D, Yasui OW, Harvestine JN, **Link JM**, Hu JC, Athanasiou KA, Leach JK. Exogenous lysyl oxidase-like 2 and perfusion culture induce collagen crosslink formation in osteogenic grafts. Biotechnology Journal. 0, 1700763 (2018)

Lee JK*, **Link JM***, Hu JC, Athanasiou KA. The self-assembling process and applications in tissue engineering. Cold Spring Harbor Perspectives in Medicine. (2017) (*these authors contributed equally to this work)

O'Leary SA, **Link JM**, Klineberg EO, Hu JC, Athanasiou KA. Characterization of facet joint cartilage properties in the human and interspecies comparisons. Acta Biomaterialia, 54:367-376 (2017)

Cissell DD*, **Link JM***, Hu JC, Athanasiou KA. A modified hydroxyproline assay based on hydrochloric acid in Ehrlich's solution accurately measures tissue collagen content. Tissue

Engineering Part C: Methods. 23(4):243-250 (2017) (*these authors contributed equally to this work)

Glass KA, **Link JM**, Brunger JM, Moutos FT, Gersbach CA, Guilak F. Tissue engineered cartilage with inducible and tunable immunomodulatory properties. Biomaterials. 35(22):5921-5931 (2014)

ABSTRACT

Toward enhancing the durability and integration of engineered articular cartilage

by

Jarrett Link

Doctor of Philosophy in Biomedical Engineering

University of California, Irvine, 2020

Distinguished Professor Kyriacos Athanasiou, Chair

Articular cartilage, a connective tissue that provides a lubricious surface for the movement of diarthrodial joints, does not naturally heal and can degenerate to osteoarthritis due to age, disease, or trauma. Although tissue-engineering has the potential for joint restoration, deploying engineered implants in the clinical setting depends on factors such as 1) whether implanted neocartilage constructs can integrate with adjacent, native tissue; and 2) whether the implant can withstand the proinflammatory environment that can result from surgery, trauma, or disease, such as osteoarthritis. Using self-assembled articular cartilage as a model, the global objectives of this work were: 1) to enhance cartilage integration; 2) to investigate how bioactive factors may protect neocartilage against macrophage challenges; and 3) to validate *in vivo* the preclinical safety profile of our tissue-engineering strategies using a preclinical model.

Using chondroitinase ABC for integration (C-ABC_{int}), the following cartilage integration hindrances were targeted: 1) lack of cells at the interface; 2) repulsive negative charges induced by cartilage glycosaminoglycans (GAGs); 3) extracellular matrix density; and 4) a limited number of stabilizing collagen crosslinks at the interface. It was hypothesized that a combination of C-ABC_{int} and bioactive factors (i.e., TGF-β1, C-ABC, and lysyl oxidase like 2) would enhance integration between native and engineered articular cartilage. Also, it was hypothesized that effective C-ABC_{int} dose would depend on construct maturity, but would not affect construct

mechanical properties. It was found that C-ABC$_{int}$, whose dose depended on construct maturity, and TCL enhanced interface Young's modulus synergistically and led to increases in interface Young's modulus up to 11.4-fold. Importantly, construct mechanical properties were not affected. The process of administering a GAG-removal agent such as C-ABC$_{int}$ at the periphery of engineered cartilage could be readily adapted to a clinical setting, due to its simplicity, efficacy, and dose control.

Using a novel, direct co-culture system designed to probe cartilage mechano-immunology, the interplay between differentially stimulated macrophages and engineered neocartilage was also examined. It was hypothesized that stiffer engineered neocartilage would elicit an enhanced inflammatory response, but that the addition of bioactive factors would mitigate tissue damage. Although, confirming our hypothesis, stiff constructs caused a 2.5-fold increase in tumor necrosis factor alpha (TNF-α) secretion compared to softer groups, these stiff tissues also demonstrated an improved ability to withstand macrophage challenge. Regardless of stimulation, macrophages did not decrease TCL-treated construct aggregate modulus when compared to baseline values. The unexpected robustness of stiff constructs against inflammatory factors bodes well for the implantation of these constructs *in vivo*.

Finally, to validate the preclinical safety of the approaches developed to this point, this work concluded with a large animal study examining the effects of tissue-engineered constructs in an orthotopic defect. Allogeneic, self-assembled constructs were implanted into full-thickness chondral defects in the minipig distal femur. As hypothesized, the allogeneic implants did not lead to adverse local or systemic reaction and, thus, were deemed safe for investigation of the efficacy of repair, moving our approach one step closer to clinical translation.

INTRODUCTION

Articular cartilage is an avascular, hypocellular tissue composed primarily of water, collagen II, and glycosaminoglycans (GAGs); it lines the ends of diarthrodial joints, bears mechanical load, and provides a nearly frictionless surface for joint articulation.[1] Loss of this musculoskeletal tissue, which can manifest as focal articular cartilage defects, can occur through traumatic injury, pathology, or age and ultimately leads to osteoarthritis (OA). Significantly, OA is a leading cause of disability because roughly 50 million adults in the United States experience its symptoms.[2] Focal defects alone prior to OA development can lead to reduced joint function. Because articular cartilage lacks an adequate intrinsic repair response, surgical techniques, such as microfracture, have been developed for relatively small (<5 cm^2) cartilage lesions.[2] However, the clinical efficacy of this procedure is variable because it often results in the formation of mechanically inferior fibrocartilage. Thus, there is a clinical need for the development of better treatments for focal articular cartilage defects.

To further improve treatment of cartilage lesions, tissue-engineering strategies have been explored as potential therapies. One such method is the self-assembling process in cartilage tissue engineering, in which high-density chondrocyte culture in non-adherent wells recapitulates aspects of cartilage morphogenesis leading to the generation of scaffold-free, engineered cartilage constructs.[3] With the addition of biochemical, biophysical, and mechanical stimuli during *in vitro* culture, functional properties (e.g., aggregate modulus) of self-assembled neocartilage have approached those of native tissues.[4-6] Self-assembled neocartilage represents a cartilage tissue-engineering strategy with great translational potential, particularly when combined with an allogeneic cell source to alleviate cell sourcing issues.

While the self-assembling process in cartilage tissue engineering is a promising technique, there are impediments to its clinical translation that can first be approached through *in vitro* experiments, such as a lack of horizontal integration between engineered constructs and native

tissue. Following surgery, integration of self-assembled neocartilage implants to native tissue would be vital for the long-term *in vivo* durability of this approach. Stress concentrations resulting from incomplete integration could irreparably damage both engineered and native cartilage through delamination,[7] excess mechanical load,[8] and rough articulation.[1] By developing strategies to enhance cartilage integration *in vitro*, self-assembled articular cartilage will have a higher likelihood of success *in vivo*, thereby driving clinical translation.

Another obstacle to clinical translation of engineered cartilage implants is the unknown nature of the effects of immune cells (e.g., macrophages) on self-assembled neocartilage. Following surgical implantation of self-assembled neocartilage, the accumulation of immune cells such as macrophages at the implant site could hamper cartilage repair and regeneration.[9,10] Macrophages can initiate signaling cascades that cause chondrocytes to upregulate the production of catabolic enzymes (e.g., matrix metalloproteinases or MMPs), which can damage cartilage extracellular matrix (ECM).[11] Loss of intact cartilage ECM will degrade cartilage mechanical properties, potentially leading to more catabolic activity and, thus, more degeneration. Engineered neocartilage and native tissue are both potentially susceptible to the deleterious effects of inflammatory factors produced by macrophages. Thus, characterizing the impact of inflammation on engineered cartilage *in vitro* is important to elucidating its potential for long-term durability in an *in vivo* environment.

Ultimately, to progress along the translational paradigm, *in vitro* studies must lead to preclinical assessments in a representative animal model. The pillars of the preclinical assessment criteria are safety and efficacy.[12] Especially for allogeneic implants, first establishing the safety of the approach in a small cohort of animals is a viable and ethical strategy. The minipig has emerged as an attractive animal model for assessing the safety of neocartilage implants due to its anatomical and physiologic similarities to humans, docile nature, and success as a model for allogeneic temporomandibular joint disc repair.[9] Demonstrating that an allogeneic approach to

focal articular cartilage defect repair is safe would indicate that approaches of this nature can proceed toward preclinical studies geared more toward assessing durability and efficacy.

Considering the desire for translation of promising engineered cartilage techniques, this work in part aimed to address potential pitfalls to neocartilage clinical success in an *in vitro* setting, and also sought to establish the safety of allogeneic, self-assembled neocartilage implants. The global objectives of this work were three-fold: 1) to enhance cartilage integration, 2) to investigate the protective capacity of bioactive factors applied to neocartilage against macrophage challenge, and 3) to validate the preclinical safety profile of the tissue-engineering strategies developed *in vitro*. Toward these objectives, three specific aims were investigated:

Specific Aim 1: To identify appropriate construct maturation time and C-ABC concentration for improving integration between self-assembled constructs and native articular cartilage. Through removal of anti-adhesive, dense glycosaminoglycans, chondroitinase ABC (C-ABC_{int}) targeted integration hindrances in both immature and mature self-assembled articular cartilage. It was hypothesized that a combination of C-ABC_{int} and bioactive agents applied to constructs would enhance integration between native and engineered articular cartilage, the effective dose of C-ABC_{int} would be dependent on construct maturity, and no dose of C-ABC_{int} would affect construct mechanical integrity.

Specific Aim 2: To examine the effect of bioactive stimuli on self-assembled neocartilage subjected to inflammatory cytokine and macrophage challenge. A novel, direct co-culture system was developed to assess the interaction between differentially stimulated macrophages and neocartilage constructs of varying stiffnesses. It was hypothesized that stiff neocartilage treated with bioactive factors would be protected from the deleterious effects of pro-inflammatory macrophages, despite eliciting an enhanced inflammatory response from the macrophages.

Specific Aim 3: To validate the safety of allogeneic, self-assembled articular cartilage implants in an orthotopic large animal model. The best integration and construct formation approaches identified in Specific Aims 1 and 2 were combined to generate allogeneic neocartilage constructs that were implanted into the Yucatan minipig to determine their safety. It was hypothesized that neocartilage implants would elicit neither a local nor a systemic immune response.

The aims have been completed as proposed, and this thesis describes all work that contributed to their fulfillment. Chapters 1, 2, 3, and 4 establish background information and techniques related to cartilage tissue engineering. Chapter 1 describes the self-assembling process, scaffold-free tissue engineering, as well as scaffold-based approaches, in the context of functional tissue engineering as a whole, including perspectives on various musculoskeletal and cardiac tissues. Chapter 2 presents research that enabled safer and more effective colorimetric quantification of hydroxyproline, a key amino acid in the structural protein collagen that is in large part responsible for the function of cartilage. In the contexts of the facet joint and articular cartilage lubrication, Chapters 3 and 4, respectively, delineate the tissue engineering methodology that involves identification of structure-function relationships, pathophysiologic processes, unmet clinical needs, and, ultimately, tissue engineering strategies to address those needs. These two chapters guided the execution of the specific aims laid out in this thesis.

For the investigation of Aim 1, Chapter 5 presents research that developed new strategies for enhancing the integration of self-assembled neocartilage to native articular cartilage. In two experimental phases, three factors that could mitigate specific obstacles to cartilage integration were examined: C-ABC$_{int}$, bioactive stimuli (i.e., TCL: transforming growth factor beta-1 (TGF-β1), chondroitinase ABC (C-ABC), and lysyl oxidase like 2 (LOXL2)), and neocartilage construct maturity. An engineered-native composite integration model, which involved placing discs of engineered constructs into rings of native cartilage tissue, was developed to determine the efficacy of these factors toward enhancing interface strength and stiffness without reducing the

properties of the engineered construct. C-ABC$_{int}$, whose dose was dependent on construct maturity, and bioactive factors synergistically enhanced interface stiffness and significantly increased interface strength, but did not affect neocartilage mechanical properties.

Aim 2 is addressed in Chapter 6, which describes the development of a co-culture system that enabled elucidation of the interaction between differentially stimulated macrophages and neocartilage constructs, as well as the potential chondroprotective effect of bioactive stimuli. The effect of neocartilage stiffness on macrophage mechano-immunology was also investigated. As hypothesized, bioactive stimuli improved preservation of the mechanical integrity of neocartilage constructs even in the presence of pro-inflammatory macrophages, thus supporting their use in an *in vivo* environment.

Finally, to address Aim 3, Chapter 7 examined the safety of allogeneic, neocartilage implants stimulated with the bioactive factors investigated in Aim 2 and treated with C-ABC$_{int}$ from Aim 1 in the Yucatan minipig. Local and systemic immune responses to implants were evaluated, as were animal wellbeing and behavior. Also described in this chapter is the development and deployment of a custom, adjustable immobilization sling that improved minipig comfort during postoperative recovery from anesthesia. Importantly, histopathology, systemic biochemical assays, and observation of animal behavior indicated that allogeneic neocartilage implants did not generate a local or systemic immune response and, thus, are safe to use.

Additional work not directly related to the aims of this work, but nonetheless contributive to the scientific community at large is presented in the appendices. Appendix 1 presents an interspecies facet joint characterization study that established structure-function relationships for the facet joint in multiple animal model candidates to establish design criteria and inform model selection for the future. Appendix 2 describes the application of LOXL2 and perfusion culture on osteogenic grafts, which was shown to increase collagen crosslinking and osteogenic potential in constructs. Appendix 3 details the characterization and comparison of adult and neonatal equine articular cartilage, which established comprehensive, topographical structure-function

relationships that can be utilized in tissue engineering studies moving forward. Appendix 4 studies the effects of bupivacaine on both neocartilage and native articular cartilage and illustrates that bupivacaine can lead to chondrotoxicity and mechanical degradation in neocartilage constructs. Together, the works presented in the appendices detail my additional efforts toward advancing the fields of musculoskeletal biology, tissue engineering, and orthopedics.

The product of this body of work and potential future directions it has illuminated are contained in the Conclusion and Future Directions Chapter. Particularly, this work has established a foundation to motivate additional studies to further enhance cartilage integration, continue to explore the emerging field of cartilage mechano-immunology, and work toward demonstrating the efficacy of neocartilage implants in healing cartilage defects.

CHAPTER 1 The self-assembling process and applications in tissue engineering

Abstract

Tissue engineering strives to create neotissues capable of restoring function. Scaffold-free technologies have emerged that can recapitulate native tissue function without the use of an exogenous scaffold. This chapter will survey, in particular, the self-assembling and self-organization processes as scaffold-free techniques. Characteristics and benefits of each process are described, and key examples of tissues created using these scaffold-free processes are examined to provide guidance for future tissue engineering developments. This chapter aims to explore the potential of self-assembly and self-organization scaffold-free approaches, detailing the recent progress in the *in vitro* tissue engineering of biomimetic tissues with these methods, toward generating functional tissue replacements.

Introduction

The field of tissue engineering aims to recapitulate native tissue function toward replacing damaged or diseased tissues and organs. The tissue-engineering paradigm is traditionally composed of living cells, scaffolds, and signals. The scaffolds used in tissue engineering are highly diverse, ranging from synthetic to natural polymers, hydrogels to woven meshes. The emergence of scaffold-free processes—tissue-engineering platforms that do not require the addition of an exogenous scaffold—have expanded the capabilities of the field. Scaffold-free techniques have been successfully used in engineering musculoskeletal[13] as well as cardiovascular, metabolic, and corneal tissues.[14] Within scaffold-free approaches, two primary,

Chapter published as: Lee JK*, Link JM*, Hu JC, Athanasiou KA. The self-assembling process and applications in tissue engineering. Cold Spring Harbor Perspectives in Medicine. (2017) (*authors contributed equally to this work)

thermodynamically driven modalities have been described: self-organization and self-assembly[14] (Figure 1-1).

In this chapter, a summary of the progress in tissue engineering will be covered. While a wide variety of cell sources and stimuli can be applied in tissue engineering, the focus of this chapter will be related to scaffold-free approaches. Herein, we focus specifically on the *in vitro* tissue-engineering techniques that generate biomimetic tissues (i.e., those that recapitulate native tissue). *In vivo* tissue engineering can also include the injection of cell suspensions and matrix-associated cells for continued development and maturation in an *in vivo* environment, but are not extensively covered in this chapter. Finally, the progress in engineering functional tissues with a particular emphasis on self-assembling and scaffold-free techniques to treat a wide range of diseases will be highlighted.

Tissue engineering

Classical tissue engineering approaches combine cells, biomaterials, and bioactive stimuli to generate robust implants capable of restoring the structure and function of tissues damaged by trauma, pathology, or age. Often referred to as the tissue-engineering "triad," this foundational concept of cells, scaffolds, and signals has informed strategies for numerous outcomes, such as bone regeneration following complex fractures or the development of vasculature *in vitro* to replace diseased vessels.[15,16] Significant advances in the field have resulted from this paradigm. However, scaffold-free techniques have emerged which may better apply to certain tissues where cells may not require exogenous scaffolds. In this manner, biomimetic and functional tissues of clinically relevant dimensions may be created. Scaffold-free techniques may thus improve the likelihood for clinical translation, which remains the ultimate goal of the field.

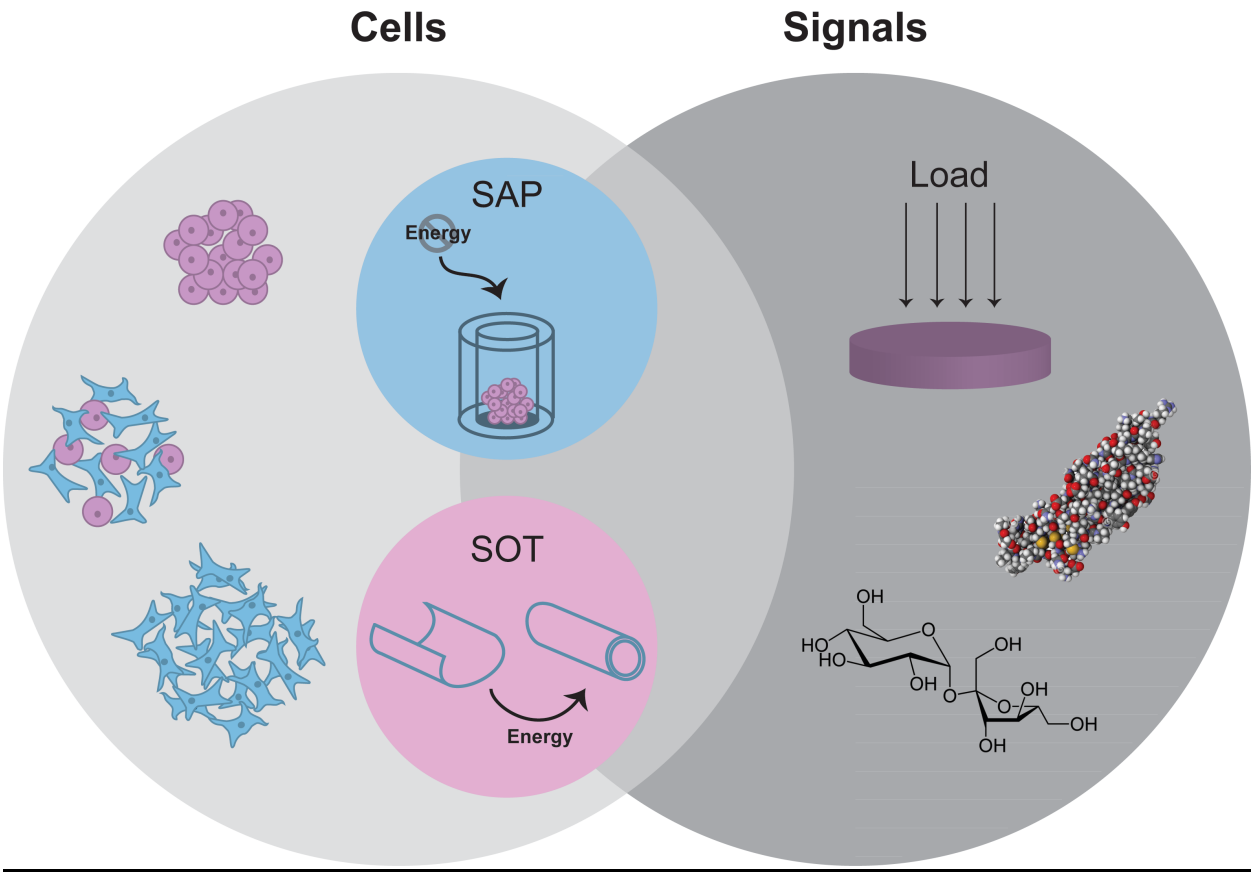

Figure 1-1. Scaffold-free tissue engineering. The tissue-engineering paradigm typically consists of cells, scaffolds, and signals. The benefits of scaffold-free approaches have motivated the use of only cells and signals. Depicted here are example modalities within this paradigm, using homogeneous or heterogeneous cell populations in concert with mechanical (e.g., compressive loading) and/or biochemical stimuli (e.g., TGF-β1 or sucrose) to enhance neotissue properties. Two distinct forms of scaffold-free tissue engineering exist, termed the self-assembling process (SAP) and the self-organization technique (SOT). While self-organization requires the exogenous input of energy, self-assembly occurs in a closed system.

Self-assembling process

One promising tissue-engineering technique, especially in cartilage tissue engineering, is the self-assembling process.[14,17] Without the influence of external energy, self-assembly mimics developmental events to generate functional cartilaginous tissue with characteristics reminiscent of native tissue (Figure 1-2). Non-adherent culture substrates—typically agarose—support high density chondrocyte seeding, prevent cell attachment, and encourage cell-cell interactions, facilitating the chondrogenic phenotype. Indeed, cell adhesion is up-regulated in chondrocytes[18] during the initial phase of the self-assembling process, reminiscent of mesenchymal condensation

during cartilage morphogenesis.[19,20] For example, increased levels of N-cadherin on the cell surface can minimize free energy, according to the differential adhesion hypothesis, as described below. Critically, no external energy is provided to the system during self-assembly (i.e., it is a closed system). Since the development of the self-assembling process, substantial efforts toward understanding the mechanisms of action have been investigated to refine the technique further. In particular, the differential adhesion and differential interfacial tension hypotheses have been used to describe the self-assembling process.

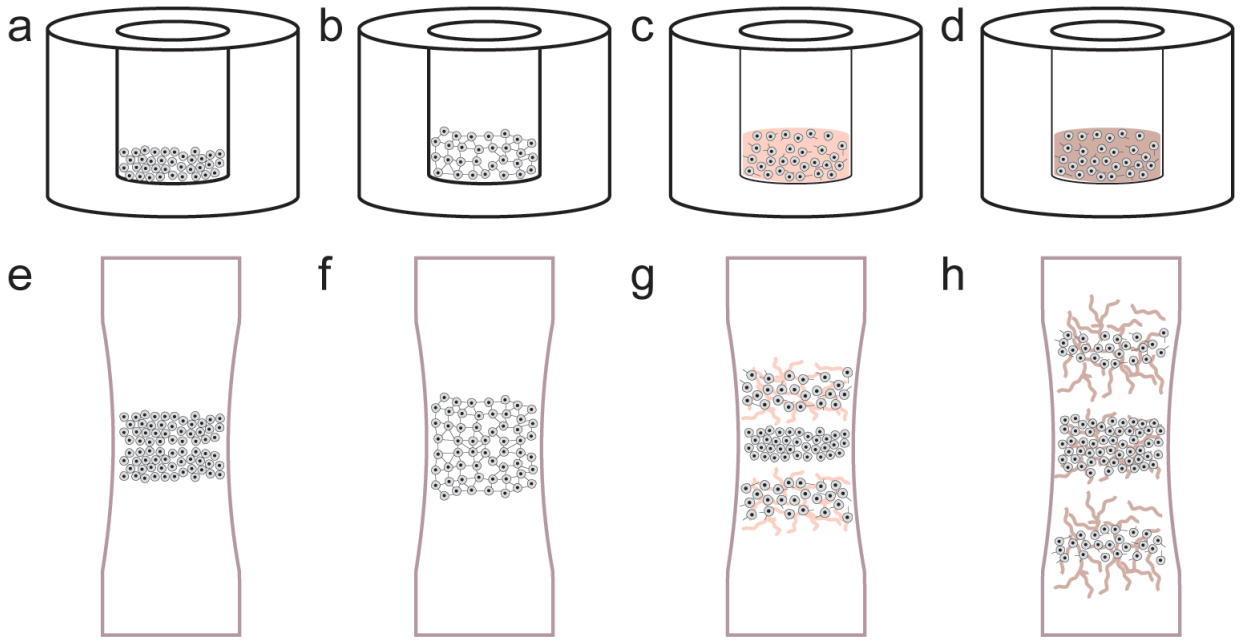

Figure 1-2. The phases of self-assembly and cartilage development. Self-assembling articular cartilage forms in a manner reminiscent of cartilage morphogenesis. In the first phase of self-assembly (a), a high-density cell solution is seeded in a non-adherent well. During phase two (b), minimization of free energy occurs as cells bind to one another via cell-adhesion receptors like N-cadherin. In phase three (c), extracellular matrix synthesis is up-regulated. Finally, the engineered tissue matures as distinct regions develop and native tissue-like functional properties are approached (d). Similarly, the process of long bone formation is mediated first by mesenchymal condensation (e). Robust matrix deposition begins as cells differentiate (f), following chemotactic agents to elongate the bone in opposite directions (g). Over time, the core forms a site for vascularization to become bone (h).

Informing the mechanism of the self-assembling process, the differential adhesion hypothesis posits that tissues minimize free energy via cell-cell binding. The type and number of adhesion proteins present on a cell surface give rise to cell-cell interactions. Correspondingly, a mass of cells behaves analogously to a liquid and will minimize its surface tension, known as

tissue surface tension. This tension will determine the sorting behavior of cells in a mixed population, as cells with higher surface tension will sort to the center, maximizing intercellular adhesion. Consequently, tissue surface tension will be minimized. Similarly, in the self-assembling process, the non-adherent substrate forces a homogeneous cell population to minimize free energy via cell-cell adherence, facilitated by increased levels of N-cadherin and other adhesion molecules.[18,21] The development of this continuous aggregate is critical to neotissue development, reflects the process of mesenchymal condensation, and can potentially drive chondrogenic gene expression.[18,21] The mechanism of self-assembly can thus be partly explained by the differential adhesion of surface-bound molecules.

Another mechanism that may contribute to the self-assembling process is differential interfacial tension. Cortical cell tension, driven by contractility of the actin cytoskeleton and cell surface tension, has been implicated in cell sorting.[22-24] As in differential adhesion, the minimization of free energy drives the cellular behavior in the differential interfacial tension hypothesis, with cell sorting dictated by forces generated by the cell cytoskeleton and at the cell membrane. Specifically, cells generating similar tensions will tend to aggregate as compared to those exhibiting different tensions. The differential adhesion and differential interfacial tension hypotheses may be related.[24] Increased understanding of the relative contributions and/or interactions of these processes would help elucidate self-assembly mechanisms.

Drawing from knowledge of developmental biology, biomedical engineers can utilize the self-assembling process to drive cell sorting, gene expression, and tissue formation in a manner similar to morphogenesis. Our enhanced understanding of underlying mechanisms in self-assembly will drive the rational selection of agents that can positively modulate the formation of tissues with increased functional properties.

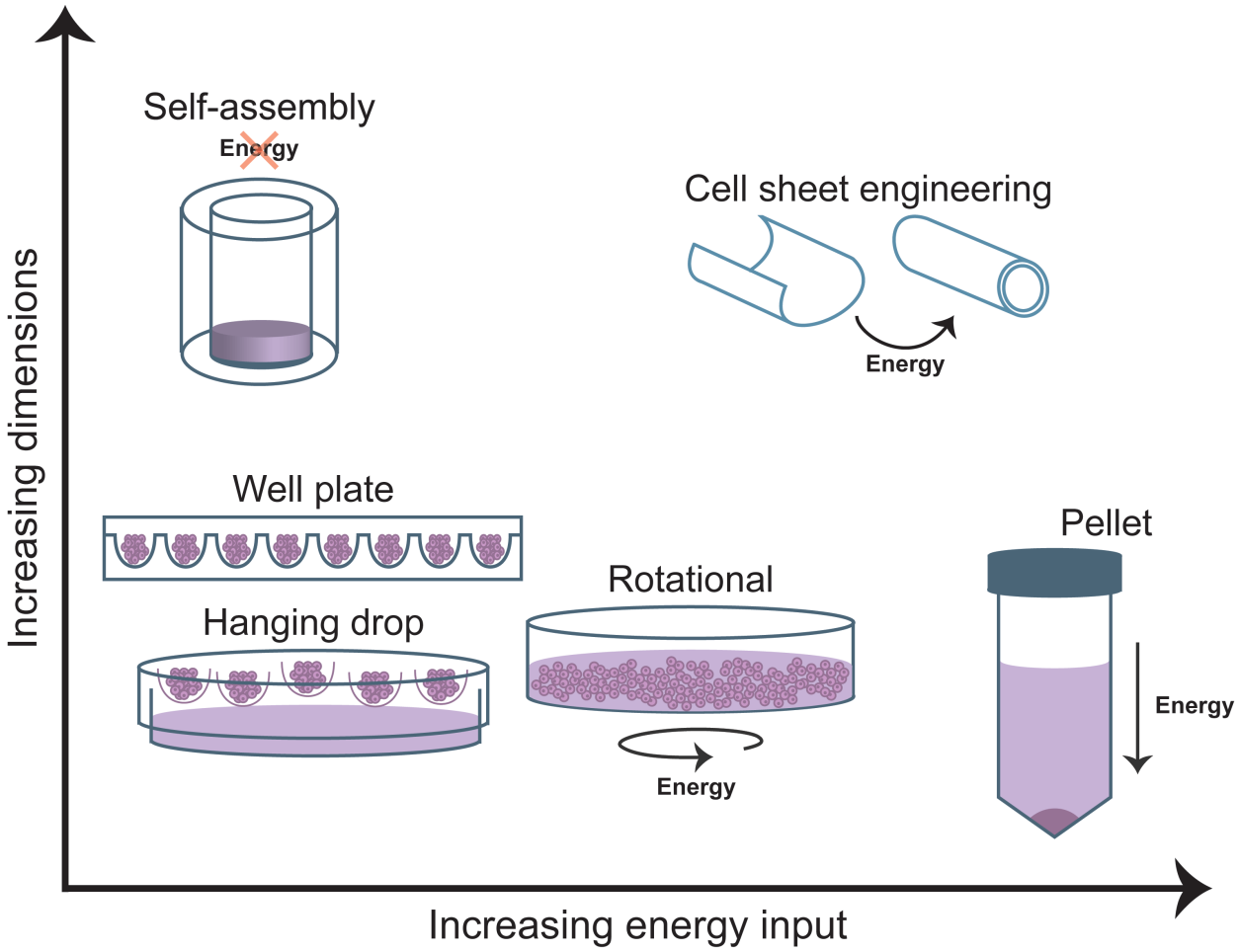

Figure 1-3. Energy usage and achievable dimensions in scaffold-free processes. Scaffold-free processes differ with respect to the energy required for tissue formation and the dimensions that can be achieved. Spheroid or aggregate formation based on the methods of hanging drop, round or v-bottom well plates, or rotational culture requires minimal energy and forms aggregates of small dimensions. Pellet culture requires substantial energy in the form of centrifugation and similarly forms small-diameter cellular aggregates. Finally, self-assembly and larger self-organization techniques such as cell sheet engineering are able to generate sizeable constructs of clinically relevant dimensions.

Other scaffold-free techniques

While promising, self-assembly is but one example of a variety of scaffold-free tissue engineering methodologies that have gained traction and present unique advantages. For instance, scaffold-free systems do not produce synthetic degradation by-products, can maintain the rounded phenotype of cells such as chondrocytes, and do not require harsh processing chemicals involved in scaffold production.[25] Many of these alternate techniques can be grouped within the self-organizing tissue-engineering paradigm, which is a distinct subset of scaffold-free tissue

engineering that requires external energy input into the system for tissue formation (Figure 1-1). Moreover, these varied techniques are able to form tissues with a range of dimensions (Figure 1-3). Within this paradigm exist methods such as pellet culture, aggregate culture, and cell sheet engineering.

Pellet culture is a fundamental method of scaffold-free tissue engineering. Requiring substantial external energy, pellet culture is mediated by centrifugation of cells inside a conical-shaped tube. Subsequently, cell pellets are cultured in medium specific to a certain tissue, driving cellular differentiation to achieve tissue-specific gene expression and extracellular matrix (ECM) deposition. Bone, liver, and cartilage tissues have all been formed in this manner.[26-28] Despite the ability to create tissues with relevant ECM components, pellet culture fails to meet many clinical translation criteria, such as robust mechanical properties and anatomically relevant geometries and dimensions. Thus, biomedical engineers interested in translational medicine typically focus on strategies other than pellet culture for use in *in vitro* biomimetic tissue engineering.

A variety of methods exist to generate cellular aggregates or spheroids, and these terms are often used interchangeably in the literature. Similar to pellet culture, aggregate culture maintains cells in a 3D environment and can be used to enhance tissue-specific gene and protein expression. Multiple methods are used to induce aggregate formation: hanging drop, round or v-bottom well plates, and rotational culture. In hanging drop culture, cell suspensions are placed in droplets on the lid of a culture plate; after inverting, gravity assists cells in coalescing at the base of the drop and forming an aggregate. Similar to self-assembly, the well plate method uses non-adherent round- or v-bottom plates to statically induce aggregate formation. Finally, by subjecting a cell population to rotational culture in the presence of tissue-specific growth factors, aggregation and differentiation is encouraged through cell-cell and cell-matrix interactions. Subsequently, relevant ECM proteins are synthesized and neotissue begins to form. Though these methods are able to form aggregates that can serve as important tools in understanding mechanisms of

differentiation and phenotypic maintenance, they may not be suitable for *in vitro*, biomimetic tissue engineering.

Aggregate or spheroid culture, like pellet culture, produces small-diameter cellular aggregates and may not be a feasible approach to engineer mechanically functional tissues when used alone, likely due to the limited number of cells in each aggregate. If the approach is part of a larger tissue engineering effort,[29] however, then it can be used to engineer anatomically relevant tissues. For instance, aggregate culture can encourage both differentiation of stem cells and redifferentiation of passaged primary cells, followed by their application in other tissue engineering methods, such as self-assembly, to create larger constructs.[30] Bioprinting has emerged as a method to employ directly these small diameter aggregates as "bioink," which are fed through a small nozzle and deposited in specific locations during 3D printing. Additionally, with fusion of multiple spheroids, larger, continuous constructs can be generated. Indeed, application of compression to mesenchymal stem cell (MSC) aggregates within a mold has been able to generate large and continuous cartilage constructs.[31] Thus, though the tissues formed by both pellet and aggregate/spheroid culture may not reach clinically relevant dimensions, these methods are important for the phenotypic maintenance of many cell types and can be integrated as part of a larger tissue engineering process.

Cell sheet engineering is a scaffold-free approach using external manipulations and thermal energy to form 3D tissues. Cells are cultured in monolayer on functionalized substrates or on a thermoresponsive polymer. In the case of direct cellular attachment, cells are removed via enzymatic cleavage of their cell-matrix attachments to the surface; to avoid enzymatic detachment, cell scraping can also be used. The cell sheet can be draped over a mandrel to form, for example, a hollow vascular structure.[32] Alternatively, thermoresponsive polymers have been developed where, subject to a change in temperature, the polymer changes conformation and induces detachment of the cell layer.[33] The polymer method avoids the use of mechanical or enzymatic cell detachment to preserve the cell-matrix binding interactions. Further, fusion of

multiple cell sheet layers can be employed to generate tissues of greater thickness to recapitulate the zonal architecture of target tissues .[34] As compared to pellet and aggregate culture techniques, cell sheet engineering can form substantially larger structures.

Advantages of scaffold-free techniques

The process of engineering tissues using scaffold-free techniques exhibits distinct advantages. For instance, scaffold-free methods may promote native tissue integration, facilitate enhanced matrix deposition and, thus, more direct mechanotransduction, and avoid the release of harmful byproducts. In the case of self-assembled articular cartilage, the neotissue has an abundance of cells at the construct edge, which likely encourages tissue growth into native cartilage and promotes integration.[35] Direct cell-ECM interactions in self-assembled cartilage prevent cells from experiencing stress-shielding, which has been shown to impede matrix production and remodeling.[17] Scaffold-free approaches can avoid issues of cytotoxicity due to the harsh processing conditions—particulate-leaching polymerizing chemicals and plasticizers, for example—required for manufacturing of some biomaterials.[36] Without the use of foreign materials, scaffold-free processes can reduce the likelihood of a foreign material-associated immune response; this response is known to limit the durability of the implanted construct and potentially compromise the health of the patient.[37] Biocompatibility issues, assuming a cell source is chosen appropriately, are mitigated in the scaffold-free paradigm since synthetic materials are avoided. Scaffold-free techniques thus possess several advantages for use in tissue engineering strategies.

Yet, there are limitations associated with the scaffold-free paradigm. If scaffold-free techniques cannot match native tissue functional properties at implantation, clinical translation is complicated. For instance, if engineered cartilage with inferior mechanical properties were placed into a femoral focal defect, stress concentrations could develop within the engineered cartilage and at the native-engineered tissue interface. Especially in the case of load-bearing tissues,

mismatch in functional properties could result in destruction of the implant if not appropriately unloaded post-surgery. Physicians may have to devise rehabilitation regimens specific to scaffold-free constructs to improve the clinical viability of these approaches. To ensure clinical success of scaffold-free approaches, application of biomimetic stimuli is crucial to driving the development of functionally relevant neotissues.[8,25,38]

Scaffold-free approaches often require a high cell seeding density, which brings into question the issue of cell sourcing. It is important to note that certain cell types are anchorage-dependent and require the presence of an exogenous scaffold at seeding; these cells may not be suitable for a scaffold-free approach. Primary autologous cell harvesting techniques often do not meet cell number requirements and can be associated with donor site morbidity.[39] Passaged primary autologous cells are available in higher quantities, but may be limited by expansion potential and do not address the issue of donor site morbidity. Furthermore, passaged primary cells may experience epigenetic changes that affect gene expression,[40] leading to an altered ECM profile and, potentially, reduced functional properties. Stem cells, such as MSCs and dermis-derived stem cells, represent an attractive cell source, as they are more widely available and have demonstrated the ability to differentiate into many different cell and tissue types. In many cases, however, stem cells do not fully differentiate into the target cell, which may affect the ultimate properties of generated neotissue. Moreover, differentiation protocols are often complex and may result in non-homogeneous cell populations. Cell sourcing remains a critical issue in tissue engineering and must be solved to improve the prospects of clinical translation for scaffold-free approaches.

Tissue-specific design criteria must be considered when choosing a particular tissue-engineering approach. In some cases, a self-assembly model may be ideal. For example, chondrocytes are particularly amenable to the self-assembling process: passaged rabbit cells treated with a combination of bioactive (i.e., transforming growth factor-β1 (TGF-β1) and chondroitinase-ABC) and mechanical (i.e., hydrostatic pressure) stimuli can create tissues with

clinically relevant dimensions with a tensile stiffness reaching 6.3MPa.[41] On the other hand, a scaffold may be necessary for recapitulating the structure-function relationship in a large segmental defect of bone, as osteoblasts require a scaffold for survival. Researchers must continue to refine these techniques and further define native tissue structure and function to develop the most effective tissue-engineering strategies. We would like to emphasize the importance of biomimetic, functional tissue engineering, which will be discussed at length later in this chapter.

Scaffold-free tissue engineering in the clinic

While obstacles still exist, promisingly, a few scaffold-free processes have reached the clinic. Autologous chondrocyte implantation (ACI), while not an *in vitro* biomimetic tissue-engineering method, was established in 1994 as a clinical treatment for focal articular cartilage defects.[42] Requiring two surgical steps—one to harvest tissue, the other to implant cells into a defect—ACI has been shown to be superior to other surgical techniques such as mosaicplasty,[43] although other studies have demonstrated that ACI is no better functionally than other cheaper orthopaedic procedures like microdrilling or microfracture.[44,45] In ACI, the defect may be filled with reparative tissue synthesized by implanted articular chondrocytes; this fibrocartilaginous tissue exhibits functional properties inferior to native hyaline articular cartilage. Thus, ACI may lead to a limited repair response. Furthermore, this technique may be less effective in older patients, who are more likely to suffer from musculoskeletal maladies, due to the reduced proliferative and regenerative capabilities of aged cells. However, the clinical development pathway for ACI can inform the translation of scaffold-free, *in vitro* biomimetic tissue-engineering techniques.

In a biomimetic, scaffold-free approach, cell-sheet engineered vasculature for end-stage renal disease patients undergoing hemodialysis has demonstrated promise in clinical trials.[46] Scaffold-free techniques for vascular tissue engineering have demonstrated a higher propensity for achieving native tissue structure and can withstand higher burst pressures.[47] Additionally,

removing the influence of a biomaterial reduces the chance of dangerous thrombosis formation and leukocyte activation. In this clinical trial, concerns related to unrolling of the cell sheet arose.[46] Reported cases of unrolling identify a critical shortcoming of cell-sheet engineering for vascular tissue engineering; methods to ensure fusion of the cell sheet via improved nutrient transport may promote long-term closure.[46] If the issues of extended culture times and the potential for unrolling can be solved, *in vitro* cell-sheet engineering for diseased vasculature may experience broad clinical use.

In a biomimetic tissue-engineering approach akin to self-assembly, ISTO Technologies, in concert with Zimmer Biologics, has produced scaffold-free neocartilage that successfully completed Phase I/II trials and continues on the path of commercialization. The RevaFlex product is generated from a high-density cell culture derived from juvenile donors; the authors previously determined that chondrocytes derived from younger donors possessed enhanced neocartilage generation potential.[48] RevaFlex was implanted into 12 patients in a Phase I/II clinical trial initiated in late 2006.[49] In this clinical study, clinical efficacy was assessed via patient-reported outcome measures, MRI, and elective second-look arthroscopy and biopsy.[49] Of second-look arthroscopies (9/12 patients), RevaFlex reportedly resulted in "~66% of lesions demonstrat[ing] gross anatomical cartilage characteristics with adequate fill with promising histologic characteristics".[49] Additionally, no immunological response to allograft neocartilage was found; these findings of a lack of graft rejection address many clinical concerns associated with using juvenile cells from an allogeneic source for graft production.[49,50] RevaFlex received FDA approval for an Investigational New Drug (IND) Application prior to clinical trials and is thus regulated as a biologic, rather than a device. Ultimately, the commercial success of RevaFlex paves the way in regulatory aspects of scaffold-free tissues—particularly in terms of cell sourcing and immune rejection—and will inform the clinical development of cartilage constructs generated from self-assembling or self-organization techniques.

Though translation of scaffold-free techniques to the clinic is limited, these advances serve as informative examples of the required regulatory path for clinical success. For instance, cell-based therapies like ACI may provide some insight into clinical translation of scaffold-free tissue-engineered therapies. Though these cell therapies do not fall in the scope of biomimetic *in vitro* tissue engineering, they are informative examples of clinical translation of cell-derived products. RevaFlex is an example of an *in vitro* engineered, biomimetic articular cartilage tissue replacement; the path to FDA approval of RevaFlex highlights the challenges of clinical translation of such a product. Given the similarities between the self-assembling process and the methods used to generate the RevaFlex graft, the RevaFlex pathway provides guidance for clinical translation of a self-assembled articular cartilage replacement. While continued refinement of these scaffold-free tissue-engineering techniques is required, lessons from approved, clinically available cell-based and biomimetic tissue-engineered therapies should be noted.

Functional tissue engineering

Biomimetic tissue engineering aims to generate functional tissues *in vitro*, toward achieving certain properties of target tissues; these properties depend on the tissues' primary roles *in vivo*. The benchmarks for engineered tissues are derived from their native counterparts. For instance, musculoskeletal tissue engineers focus on forming tissues with appropriate mechanical strength and stiffness to function in the tissues' native load-bearing capacities. Hepatic tissue engineers focus on forming tissues able to express specific enzymes and proteins necessary to mimic liver function. Some of these commonly reported parameters are presented in Table 1-1. Scaffold-free tissue engineering techniques aiming to recapitulate native tissue function should bear in mind these reported properties and strive to bring them closer to native tissue values. The following sections highlight recent progress in engineering musculoskeletal, cardiovascular, liver, and corneal tissues using scaffold-free, biomimetic *in vitro* tissue engineering.

Primarily mechanically functional tissues

Bone

Bone is a mineralized collagen matrix responsible for primary load bearing in the musculoskeletal system. In addition, bone serves as an anchorage point for ligaments, tendons, and muscles to facilitate movement. Clinical applications of tissue-engineered bone often relate to the repair of critical-sized defects that cannot heal on their own. The primary objective of tissue engineers, therefore, is to engineer bone with compressive and tensile stiffness and strength reminiscent of native bone. Additionally, indicators of vascularization and mineralization are used to assess bone quality. Scaffold-free approaches used in bone engineering are primarily cell sheet-based, with few using aggregate culture.

Osteogenic cell sheets are used to generate tissue-engineered bone targeting the compressive and mineral properties of native bone. Osteogenically differentiated mesenchymal stem cell sheets rolled into cylindrical constructs exhibited mineralization and a compressive strength of nearly 1.6MPa.[51] The cell sheet structure can be placed into critical-sized defects to facilitate new tissue formation, though additional validation of the mechanical properties of the newly formed bone is needed.[52] *In vivo* implantation promoted expression of bone genetic markers (i.e., collagen type I, osteocalcin, and osterix) in cell sheet co-cultures of osteogenic stromal cells and endothelial cells as compared to mono-cultures of osteogenic cells.[53] Though bone tissue engineering with scaffold-free cell sheets has been attempted, most of these studies do not assess the mechanical properties of formed tissues. As such, additional work analyzing the functional mechanical properties of cell sheet-based, *in vitro* tissue-engineered bone is needed.

Few studies examine aggregate or spheroid culture for engineering large bone tissue constructs, as aggregate studies are primarily used for differentiating progenitor cells into osteogenic cells for future application in larger scaffold-free or scaffold-based techniques. Various

scaffold-free aggregate techniques are able to generate mineralizing spheroids, but larger constructs are not often formed in subsequent steps.[54] Studies using scaffold-free processes from cellular differentiation to large construct formation would improve our understanding of the potential applicability of scaffold-free techniques in bone tissue engineering.

Cartilage

Articular cartilage is a load-bearing tissue that also serves to facilitate the smooth translation of diarthrodial joints. Unlike bone, however, articular cartilage does not heal itself; clinical application of tissue-engineered articular cartilage, then, serves to replace degenerated cartilage tissues. The primary benchmarks of articular cartilage tissue engineering are sufficient compressive and tensile properties. In addition, lubrication properties and integration ability are desirable. Scaffold-free methods including the self-assembling process, cell sheet engineering, and aggregate culture have been applied in articular cartilage tissue engineering toward achieving the mechanical properties of native tissues.

The self-assembling process as a scaffold-free tissue formation technique has been extensively studied[17] for engineering of articular cartilage. With this scaffold-free process, primary articular chondrocytes treated with matrix cross-linking enzyme lysyl oxidase-like protein 2 (LOXL2) can generate tissues achieving compressive and tensile stiffnesses up to 220kPa and 2.3MPa, respectively.[55] Using combinations of bioactive stimuli (i.e., TGF-β1, chondroitinase-ABC) and/or mechanical stimuli (i.e., hydrostatic pressure), tissues with tensile stiffnesses up to 6.3MPa and 2.1MPa can be generated from passaged leporine and porcine cells, respectively.[41,56] Self-assembled articular cartilage derived from primary chondrocytes cultured in chondrogenic-inducing medium expressed superficial zone protein, imparting the tissue with lubrication capacity and frictional properties approaching those of native articular cartilage.[57] The self-assembling process, thus, can be used to engineer native tissue-like neocartilage. Future

work investigating the implantation of these lubricated and mechanically robust tissues in an orthotopic location would lead the field in generating functional tissue-engineered cartilage.

Other scaffold-free methods for cartilage tissue engineering include cell sheet engineering and aggregate culture. In a technique similar to self-assembly, chondrocytes placed in a non-adherent well self-aggregate into “cartilage tissue analogs” expressing collagen type II and native tissue levels of glycosaminoglycan.[58] Moreover, these tissues were reported to have an equilibrium compressive Young’s modulus on par with native tissue.[59] Cell sheet engineering has also been used to engineer cartilage tissues; contraction of a MSC-derived cell sheet led to a tensile strength of ~1.2 MPa.[60] Scaffold-free aggregate and cell sheet culture methods are able to generate cartilage tissues that are mechanically viable. Additional investigation using these methods to achieve native tissue-like mechanical properties as well as lubrication would benefit efforts to engineer scaffold-free cartilage.

Ligaments and tendons

Ruptured ligaments and tendons are often repaired with autologous or cadaver-derived grafts, which are limited in supply. Tissue engineering of ligaments and tendons thus aims to fill this need for mechanically robust replacements. Engineered ligaments and tendons are commonly assessed for various tensile testing criteria, such as tensile stiffness, strength, and force. Scaffold-free methods used in forming these tissues are akin to cell sheet engineering, while spheroids have been used to a limited extent.

Cell sheet methods in ligament and tendon engineering rely on the strong contractile forces of seeded cells. Monolayers of stromal cells cultured on laminin-coated substrates detached and organized into rod-like tissues anchored by silk sutures; these tissues reached a tensile force of 0.26N, a tangent modulus up to 15.4MPa, and a tensile stress of 2.11MPa.[61] Rolling of a tenocyte-derived cell sheet stimulated with ascorbic acid and connective tissue growth factor achieved a reported tensile stiffness of nearly 200N/mm^2 (MPa) and strongly expressed

collagen type I and tenomodulin.[62] Additional work exploring layering or bundling of scaffold-free ligaments and tendons to achieve mechanically robust tissues with larger geometries would move the field closer to a replacement ligament or tendon.

The use of spheroid culture in tendon and ligament engineering is limited primarily to differentiation and phenotypic maintenance of cells for seeding on woven scaffolds. Scaffold-free spheroids derived from anterior cruciate ligament cells became smaller over time, but increasingly expressed collagen and tenascin C and could colonize scaffolds.[63] Hanging-drop spheroid culture of tenocytes similarly enhanced expression of tendon-associated genes (e.g., collagen type III, scleraxis) as compared to monolayer cultures, with ascorbic acid, insulin, and TGF-β1 achieving higher expression levels than TGF-β1 and insulin-like growth factor-1 (IGF-1) use.[64] Though the use of spheroids in tendon and ligament engineering demonstrates the ability of scaffold-free culture to enhance relevant gene expression, these studies did not examine the functional mechanical properties of engineered tissues. As such, additional work exploring the mechanical properties achievable through a combination of scaffold-free and scaffold-based methods for tendon and ligament engineering would benefit the field.

Cardiac

Cardiac tissues function primarily in contraction, relying on rapid electrical conductance to synchronize the heartbeat. In cases of myocardial infarction, large portions of the heart are damaged and cannot properly conduct these electrical signals. Cardiac tissue engineering aims to repair and replace damaged tissues to restore electrical conductivity and contractility toward reestablishing normal heart function. Cell sheet engineering as a scaffold-free method dominates cardiac tissue engineering and aims primarily to achieve electrical conductance for synchronous contractility. More recently, efforts to vascularize engineered cardiac tissues prior to implantation have emerged.

Cell sheet engineering techniques have been developed to form 3D cardiac tissues capable of electrical communication. Synchronous and spontaneous beating was achieved by layering cardiac cell sheets derived from embryonic cardiomyocytes.[65] Electrical connectivity via the formation of gap junctions, as indicated by connexin43 staining, has been observed in layered cardiac tissues.[34,66] Due to the metabolic requirements of cardiac cells, vascularization of layered cardiac sheets is important for *in vivo* survival of the graft.[67] Multi-step transplantation of ten three-layer cardiac sheets co-cultured with endothelial cells promoted vascularization *in vivo*, resulting in a fused, 30-layer-thick cardiac tissue beating simultaneously.[34] Electrical conductivity and synchronous beating in engineered cardiac tissues can thus be achieved with cell sheet engineering. These studies demonstrate that *in vivo* tissue engineering of cell sheets induces vascularization. Additional studies exploring *in vitro* vascularization and *in vivo* integration of vascular cardiac tissues are needed to promote repair of damaged heart tissues.

Vascular

Diseases affecting the vascular system can lead to myocardial infarction, stroke, or peripheral limb ischemia. Vascular tissue engineering aims to replace segments of diseased vessels. To recapitulate native tissue function, engineered vessels should be able to withstand physiological burst pressures; additionally, they should resist cyclic loading fatigue and maintain an endothelium layer.[68] In the last two decades, vascular tissue engineering has diversified to include scaffold-free systems that include self-assembly, cell sheet, and spheroid-based techniques.

The self-assembling process has seen limited application in vascular tissue engineering. Vascular rings were formed through self-assembly of smooth muscle cells before they were placed sequentially on a silicone mandrel and underwent fusion (self-organization).[69] Though the tensile mechanical properties of individual vascular rings were assessed (ultimate tensile strength of 100-500kPa), the functional properties of the fused tubular structure were not. In addition to examining burst pressure, future work using both self-assembly and self-organization could

control cell placement (e.g., endothelial cells at the vascular ring center, smooth muscle cells in the media layer, and fibroblasts at the outermost edge) to create a tissue-engineered vessel with structural morphology and mechanical properties reminiscent of vascular tissues.

Vascular tissue formation using cell sheet engineering is the most popular scaffold-free system used. Sequential sheets of human vascular smooth muscle cells and fibroblasts wrapped around a mandrel fused to form a tubular vessel capable of endothelialization and exhibited a reported "burst strength" over 2,000mmHg (~265kPa).[32] Subsequent iterations of this method produced fibroblast- and endothelial cell-based vessels with reported burst pressures of more than 3,500mmHg (~465kPa).[47] Ascorbic acid-treated MSCs can also be used in a similar process to generate a cell sheet-based vascular tissue with suitable suture loading strength.[70] Finally, cell sheet methods can be combined with scaffold-based technologies to enhance functional properties. Primary smooth muscle cell-derived sheets seeded onto electrospun collagen/poly(ε-caprolactone) scaffolds achieved additional increases in tensile strength of vessels compared to the scaffold alone.[71] These increases in tensile properties are encouraging, though burst pressure was not assessed in this study.[71] These studies demonstrate that cell sheet-based vascular tissue engineering can achieve functional burst pressure properties exceeding those of native tissue. Toward potentially engineering contractile arterial vessels, future work should include smooth muscle cell phenotypic maintenance and/or differentiation and their incorporation into a mechanically robust vascular graft.

Finally, a combination of scaffold-free spheroid formation and the self-organizing technique of bioprinting has been used to a limited extent in vascular tissue engineering. This process used agarose as a mold to support the build process in bioprinting spheroids (formed via pellet culture) composed of smooth muscle cells and fibroblasts.[72] Layer-by-layer composition in this study allowed for the design of a double-layered vascular wall exhibiting patterns of smooth muscle cell and fibroblast organization.[72] Interestingly, placement of stem cell-based spheroids on a pre-stretched electrospun scaffold resulted in incomplete fusion and hole formation in tissue-

engineered vessels, suggesting that the scaffold may impede fusion.[73] Though burst pressure as a functional parameter was not assessed in these spheroid-based studies, the results demonstrate the ability to finely control structural architecture in vascular tissue engineering and achieve small-diameter vessels (<5mm). Additional work to enhance fusion of spheroid structures and produce mechanically viable vessels, toward achieving branching vasculature capable of withstanding burst pressures, would greatly benefit the field.

Non-mechanical tissues

Liver

Liver diseases including fibrosis and viral infections have driven the need for alternative sources of healthy liver tissue since donors are limited. The most successful option for complete liver failure remains liver transplantation. Primary hepatocyte transplantation involving injection of a cell suspension has been used, but transplantation of engineered tissues is still under development. Liver tissue engineering is meant to both maintain hepatocyte phenotype in culture and to differentiate progenitor cells into mature hepatocytes. To create a functional tissue-engineered solution, engineers focus on protein and metabolite secretion—primarily, production of albumin, alpha 1 anti-trypsin (A1AT), and the P450 cytochrome enzyme. Scaffold-free methods of aggregate or spheroid culture and cell sheet techniques have been used to achieve these objectives.

Scaffold-free spheroids are formed from a variety of cell sources and are the primary scaffold-free method used in liver tissue engineering, as spheroids provide a means to maintain the phenotype of liver cells. The dimensions of pelleted aggregates can influence both the immediate and long-term expression levels of liver-specific albumin[74] and should be considered in liver tissue engineering. Additionally, hepatocyte spheroids have been shown to survive and maintain their phenotype at least 3 days when implanted *in vivo*.[75] Co-culture of hepatocytes and other cell types can further enhance the phenotypic maintenance of hepatocytes. For instance,

co-cultures of hepatocytes and hepatic stellate cells induced increased expression of albumin and cytochrome P450 compared to hepatocytes alone.[76] Similarly, aggregates formed via co-culture of hepatocytes and pancreatic islet cells not only maintained hepatocytic (and pancreatic) phenotypes, but enhanced expression of liver-specific proteins over hepatocyte aggregates.[77] These studies thus demonstrate the importance of scaffold-free spheroid culture not only to maintain but also to enhance hepatocyte phenotype, especially when hepatocytes are cultured with support cells. Future work should validate the long-term phenotypic stability of hepatocytes cultured as spheroids and their potential in long-term restoration of liver function when implanted *in vivo*.

Cell sheet culture in liver tissue engineering involves co-culture of hepatocytes with an additional cell source or layering of multiple hepatocyte sheets. Hepatocyte cell sheets demonstrated robust expression of albumin as evaluated via immunohistochemistry; increases in protein production correlated with enhanced liver tissue volume as a result of layering multiple cell sheets.[78] In addition to robust albumin and A1AT production, cell sheets derived from hepatocytes co-cultured with fibroblasts promoted enhanced vascularization after subcutaneous implantation when compared to hepatocyte-derived sheets.[79] This scaffold-free co-culture technique could address the pressing need for vascularization after transplantation to ensure survival of engineered liver tissues. It is important to note that the *in vivo* vascularization of engineered liver tissues is encompassed within the *in vivo* tissue engineering methodology; successful *in vitro* engineering of liver vasculature would greatly advance the field. Scaffold-free cell sheets of hepatocytes alone or in co-culture are thus able to express proteins indicative of liver function and induce vascularization of implanted tissues.

Cornea

The cornea is a transparent and avascular ocular structure that provides physical protection to the eye and serves as an optical interface. An epithelium and endothelium layer comprise a

combined ~10% of the corneal thickness and act primarily as a barrier and integration point to the remainder of the eye, respectively. Structurally, aligned collagen fibrils, termed lamellae, comprise the bulk of the corneal stroma, which represents 90% of corneal thickness.[80] Proteoglycans between lamellae layers contribute to corneal transparency, a unique attribute of this tissue. Diseased or damaged corneal tissues can lead to vision loss and blindness, creating a clinical need for tissue-engineered corneas for transplantation. The primary challenge of engineering the cornea is to create a transparent structure with suitable matrix organization that confers substantial refractive power and mechanical protection.[80] Full-thickness corneal tissue engineering has primarily been completed with scaffold-based methods, though cell sheet systems have been used to engineer certain layers.

Cell sheet engineering is the predominant scaffold-free method studied for corneal regeneration. Researchers created autologous epithelial-cell sheets that were able to restore the cornea's transparency and natural barrier function and improve visual acuity in human patients;[81] this technique was previously demonstrated in a rabbit corneal model.[33] Though these studies successfully created an epithelial cell sheet, they did not create the stroma. Other cell sheet work attempted to create thicker corneal tissues by altering the cell sheet growth substrate[82] or by engineering specifically the endothelium layer.[83] Despite this exciting work in stroma or endothelium engineering, these studies have not yet examined the functional parameters of transparency and physical protection. Cell sheets are promising for the creation of transparent and protective corneal layers. Additional studies combining various cell sheet layers may elucidate the potential of generating full-thickness corneal transplants.

Table 1-1. Advantages of scaffold-free techniques

TARGET TISSUES	EXAMPLES OF COMMONLY REPORTED PARAMETERS
PRIMARILY MECHANICAL FUNCTION (E.G., MUSCULOSKELETAL, CARDIOVASCULAR)	
BONE	Compressive and tensile stiffness, strength
ARTICULAR CARTILAGE	Compressive and tensile stiffness, strength
TENDON, LIGAMENT	Tensile stiffness, strength; maximum force
HEART	Electrical conductance, contractility
VESSEL	Burst pressure; recapitulation of layered structures
NON-MECHANICAL TISSUES (E.G., METABOLIC, CORNEAL)	
LIVER	Albumin; α-1 anti-trypsin; P450 cytochrome
CORNEA	Transparency; refractive power

Conclusions and future directions

In the last few decades, the tissue-engineering field has made tremendous strides toward creating functional tissues able to replace those damaged by disease, trauma, or age. Scaffold-free tissue engineering recently emerged as an alternative approach that uses only cells and signals, aiming to exploit the benefits of scaffold-free systems. Within scaffold-free systems, self-organization and self-assembling processes can be defined based on whether external energy is applied (Figure 1-1). As the field progresses in the continued use of scaffold-free systems, it will become critical to create stricter definitions for terminology used to denote various techniques; this issue is particularly important in the development of spheroid, aggregate, and pellet-based technologies, terms often used interchangeably. Depending on the target tissue of interest, a given scaffold-free (or even scaffold-based) method may be preferable. This chapter summarized the current progress in the tissue-engineering field, focusing primarily on scaffold-free techniques. Specifically, we highlight the recent advances and existing limitations in biomimetic *in vitro* tissue engineering, toward creating tissues that truly restore the function of the intended tissue targets. Though the field has seen expansive growth with the advent of new technologies, this chapter highlighted remaining hurdles that need to be addressed for clinical translation.

Extensive progress in tissue engineering has resulted in tissues that recapitulate certain metrics of target tissues; to assess the long-term functionality and facilitate clinical translation, however, increased development and standardization of appropriate animal models are needed. These tissue-engineering models should match not only the disease characteristic, but the defect characteristics as well. For example, osteoarthritis models should aim to better recapitulate not only the inflammatory environment, but also the size and shape of a cartilage defect. In addition to appropriately modeling the disease state, standardization of animal models across research groups would assist in direct comparisons of studies. Use of select FDA-approved models may guide animal selection. In scaffold-free systems, specifically, achievement of sufficient mechanical properties is critical to the survival of the implant within the host environment. In the case of articular cartilage replacement, until mechanically biomimetic tissues can be engineered using scaffold-free systems, it may be advisable to explore rehabilitation techniques that use unloading of the patient's joint until the neotissue has matured mechanically. Due to the dependence on high numbers of cells, scaffold-free tissue-engineered constructs may need to address the permanence of these cells within the construct to determine that cells do not leave the implanted neotissue and elicit adverse effects elsewhere in the host. Continued improvements to animal models will facilitate the translation of engineered tissues to human patients. Until truly biomimetic tissue is created, use of scaffold-free techniques in the clinic may progress with appropriate rehabilitation and post-operative procedures in place to ensure neotissue maturation and development.

Cell sourcing is arguably the most limiting step of tissue engineering—both scaffolds and signals can be synthetically created while cells must be derived from a natural source and are thus a limited resource. The high cell numbers needed for scaffold-free techniques renders them particularly vulnerable to cell sourcing issues. Using aggregate culture protocols, cell-sourcing limitations can be addressed, as these approaches can be an effective means to promote the desired cell phenotype in a 3D environment. Because primary cells are limited in availability, most

tissue engineers select progenitor cells that can be differentiated using aggregate culture. Once the desired phenotype has been obtained, these cells can be employed in a subsequent scaffold-free or scaffold-based method to generate constructs of clinically relevant dimensions. Increased development of our ability to differentiate progenitor cells or maintain primary cells in 3D culture can ultimately address the significant cell numbers needed in scaffold-free, *in vitro* biomimetic tissue engineering.

Though this chapter focused on scaffold-free systems, continued progress in tissue engineering may require the simultaneous use of scaffold-free and scaffold-based techniques as the complexity of engineered tissues increases. As mentioned previously, many cells are anchorage-dependent and are not suitable for use in scaffold-free systems. For instance, osteoblasts require a scaffold for their survival. Therefore, to form a biphasic osteochondral graft, a cell-laden bone scaffold may be used in conjunction with scaffold-free neocartilage. Identification of the appropriate system—scaffold-free or scaffold-based—for independent cell types will further the field in developing more complex tissues through the combination of various systems.

Finally, enhanced understanding of the development of various tissue types will aid in identification of whether scaffold-free or scaffold-based systems are most appropriate. In this chapter, we highlight the parallels between scaffold-free neocartilage generation and *in vivo* development of articular cartilage (Figure 1-2). Mesenchymal condensation of cartilaginous precursors occurs in the absence of a scaffold; tissue engineering with chondrocytes in a scaffold-free process thus reflects the developmental environment. The work in developmental biology can thus inform the selection of tissue engineering modalities. Increased understanding of the processes by which various tissues and organs develop will aid the selection of scaffold-free or scaffold-based techniques.

A key focus of this chapter is the self-assembling process, which results in functional tissue formation in a cell-driven manner that requires no external input of energy. In some tissue types

(i.e., cartilage), the self-assembling process mimics natural mechanisms of developmental biology. By studying the self-assembling platform, enhanced understanding of development may be achieved. Conversely, our current understanding of developmental processes may be applied to self-assembling techniques, toward discovering methods to enhance the functional properties of neotissue. Ultimately, engineered neotissue will reach a level of complexity recapitulating native tissue functions, allowing neotissue not just to repair, but also to regenerate diseased tissues.

CHAPTER 2 A modified hydroxyproline assay based on hydrochloric acid in Ehrlich's solution accurately measures tissue collagen content

Abstract

Collagen quantification has long been relevant to biomedical research and clinical practice to characterize tissues and determine disease states. The hydroxyproline assay, while a broadly employed method of quantifying collagen, uses perchloric acid to dissolve Ehrlich's reagent. Since perchloric acid poses occupational safety hazards and high costs, in this study, a new hydroxyproline assay was developed that replaces perchloric acid with a relatively safer and cheaper alternative, hydrochloric acid. To validate this biochemical technique, first, using either acid to dissolve Ehrlich's reagent, the assays were completed for native and engineered collagenous tissues. No statistical differences were identified between the assays ($p = 0.32$). Subsequently, both biochemical techniques were compared to amino acid analysis, considered a proteomics gold standard. Interestingly, utilizing hydrochloric acid in lieu of perchloric acid yielded greater concordance with amino acid analysis ($\rho_c = 0.980$) than did the traditional assay ($\rho_c = 0.947$); i.e., the hydrochloric acid-based assay more closely estimates hydroxyproline content, and, consequently, true collagen content. Thus, using Ehrlich's reagent containing hydrochloric acid in the hydroxyproline assay represents an advance in both mitigating laboratory safety hazards and improving biochemical collagen quantification.

Chapter published as: Cissell DD*, Link JM*, Hu JC, Athanasiou KA. A modified hydroxyproline assay based on hydrochloric acid in Ehrlich's solution accurately measures tissue collagen content. Tissue Engineering Part C: Methods. 23(4):243-250 (2017) (*authors contributed equally to this work)

Introduction

Collagen, the most abundant protein in mammals, has been heavily studied for over a century.[84,85] It primarily gives rise to the mechanical integrity of connective tissues, such as those of the musculoskeletal system, including bone, cartilage, and tendon.[86-88] Additionally, other biological structures (e.g., skin, eye, lung, gut, and vasculature) incorporate copious collagen.[89] For any of these systems, a change in collagen density could alter tissue biomechanics leading to impaired biological function.[90] The importance of structure-function relationships is paramount, and the specific role of collagen has been extensively characterized. At a smaller scale, collagen also affects cellular behavior via cell-matrix mechanotransduction. Collagen bound to cell-surface proteins (e.g., integrins) can either promote proper cell phenotype, as in chondrocytes, or contribute to cell dysregulation, as in tumor progression.[91,92] Degradation or loss of collagen due to age or trauma remains clinically relevant since these processes can adversely affect physiologic function of the aforementioned organ systems. Excessive collagen production associated with chronic or severe tissue damage can also deteriorate normal tissue function.[93] Thus, in both healthy and diseased states, collagen is a biologically important protein; for research and clinical purposes, methods to accurately quantify collagen in a target tissue or as a metabolite in urine, for example, have been developed since the mid-1900s.[94]

It was recognized that collagen could be quantified indirectly through hydroxyproline content since this amino acid is present almost exclusively in collagen. The gold standard for measuring hydroxyproline is chromatographic amino acid analysis, but this technique is not practical for all experiments due to its low-throughput nature and relatively high cost. As such, Neuman and Logan [94] devised a simple colorimetric assay that generates a chromophore from hydroxyproline via reaction with p–dimethylaminobenzaldehyde (DMAB, a.k.a. Ehrlich's reagent). Uniquely, their assay required relatively small amounts of protein, which represented a marked advance in hydroxyproline quantification compared to previous methods. Since that initial breakthrough, hydroxyproline quantification, and its use towards quantifying collagen, has been

continually improved [95-102] and was eventually commercialized. An alternative approach to quantifying collagen, based on Sirius Red dye binding, was later introduced [103] and is also available as a commercial assay. More recently, a method was described for quantifying collagen in collagenase-digested tissue based on binding of a fluorescent molecule to peptides containing N-terminyl glycine residues.[104] Each of these biochemical methods for measuring collagen exploits a different, unique attribute of collagen's amino acid sequence or structure.

Despite the advent of additional techniques for measuring collagen content, the colorimetric hydroxyproline assay remains a commonly used protocol in biologic research; however, the safety and cost of this assay could be improved. To dissolve DMAB, a solution of perchloric acid ($HClO_4$) and 2-propanol is typically used as the solvent for this assay. $HClO_4$, an unstable and oxidative strong acid, must be used in specially designed fume hoods with wash-down capabilities to prevent accumulation of unstable, explosive perchlorate salts in ventilation systems. Failure to use an appropriate fume hood could create a safety hazard, and not all laboratories contain fume hoods rated for $HClO_4$. The need for specialty fume hoods thus potentially increases assay cost. Additionally, $HClO_4$ is more expensive to purchase than other strong acids, such as hydrochloric acid (HCl). Due to occupational hazards, as defined by the Occupational Health and Safety Administration (OSHA), [105] and relatively high cost, an alternative to $HClO_4$ in the broadly used hydroxyproline assay is desirable (Table 2-1).

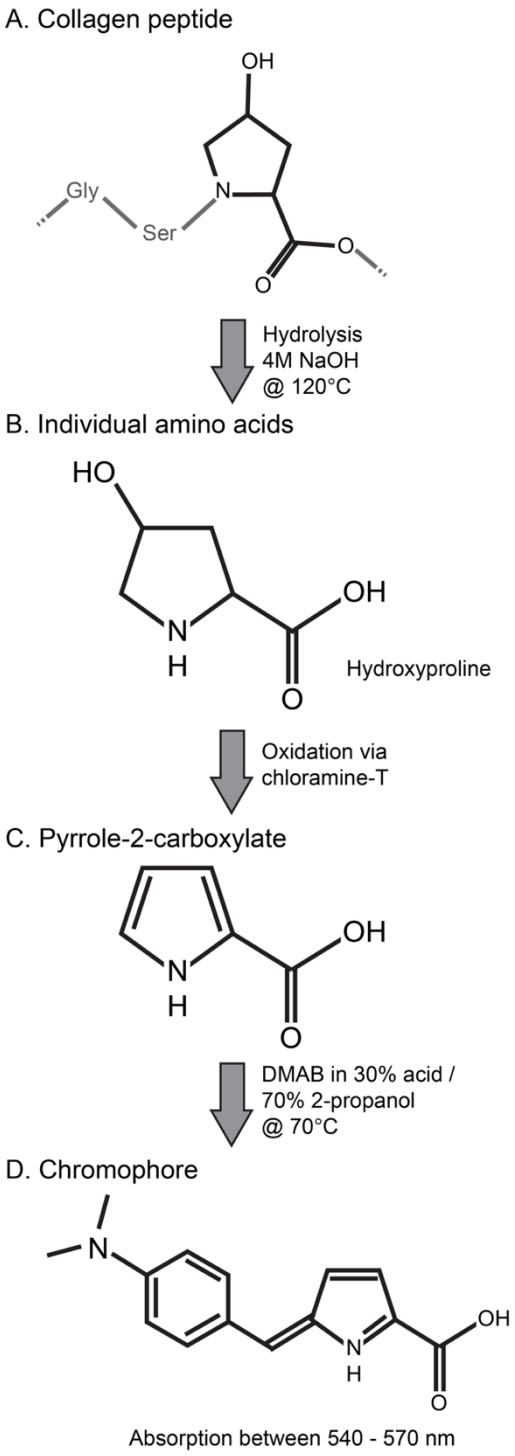

Figure 2-1. Overview of the hydroxyproline assay. Collagen peptides (A) are hydrolyzed in 4M sodium hydroxide (NaOH) to individual amino acids including hydroxyproline (B). Oxidation of the hydroxylated amino ring of hydroxyproline by chloramine-T yields a pyrrole (C) that reacts with p-dimethylaminobenzaldehyde (DMAB) to produce a chromophore (D) with peak absorption of light with wavelengths between 540 – 570 nm.

HCl, which does not need a wash-down capable fume hood, is a less expensive and safer alternative to $HClO_4$. It is also widely used in research laboratories. While $HClO_4$ is often used in the hydroxyproline assay to dissolve DMAB, HCl acts as the strong acid solvent to dissolve DMAB for a recreational drug spot test assay based on similar biochemistry.[106] Since the chemistry involved in both cases is similar—chromophore development from heterocyclic organic compounds—we hypothesized that HCl could replace $HClO_4$ in the hydroxyproline assay while causing no differences in hydroxyproline detection for various tissues. To ensure validity of this modified assay across a range of samples, tissue types tested included articular cartilage, tendon, meniscus, liver, and testis, as well as self-assembled articular cartilage. The primary purpose of this experiment was to ensure hydroxyproline assays, using both acid formulations, yield comparable results for various tissue explants and tissue-engineered constructs.

Table 2-1. A cost and safety comparison between perchloric acid and hydrochloric acid

		$HClO_4$	**HCl**
Cost		$374.00/2.5 L bottle (Sigma, ACS reagent, 60%)	$94.80/2.5 L bottle (Sigma, ACS reagent, 37%)
Fume Hood	Type	Wash-down capable	Conventional
	Cost	$18,470*	$7,705**
OSHA Safety Symbols			

*Labconco 4' Protector Stainless Steel Perchloric Acid Laboratory Hood (cat #: 130400002)
**Labconco 4' Protector XL Benchtop Laboratory Hood (cat #: 111400000)

 flammables, pyrophorics, self-heating, emits flammable gas, self-reactives, organic peroxides

 skin corrosion/burns, eye damage, corrosive to metals

 irritant (skin and eye), skin sensitizer, acute toxicity (harmful), narcotic effects, respiratory tract irritant

 carcinogenic, mutagenicity, reproductive toxicity, respiratory sensitizer, target organ toxicity, aspiration toxicity

Methods

Tissue preparation

Samples of bovine articular cartilage were obtained from the distal femora of juvenile bovine pelvic limbs obtained from a commercial provider of animal tissues (Research 87, Boylston, MA). The femorotibial joints were dissected using sterile technique and osteochondral explants were obtained using an 8-mm dermal biopsy punch. Subchondral bone was removed, and the cartilage trimmed to a thickness of 2mm from the articular surface using a custom jig. Tissue engineered neocartilage samples were produced according to previously published methods[55]. Briefly, bovine chondrocytes were isolated from distal bovine femora, seeded into non-adherent 5mm agarose wells, and fed daily with chondrogenic media. Neocartilage samples were cultured for 16 to 28 days. Select samples were treated with chondroitinase-ABC or transforming growth factor β-1 to vary the neocartilage glycosaminoglycan (GAG) and collagen contents. Samples of leporine liver, testis, meniscus, and common calcanean tendon were obtained from an adult New Zealand White rabbit humanely euthanized as part of a separate study that was approved by the University Institutional Animal Care and Use Committee. Approximately 5 mg portions of each hydrated tissue were weighed, subject to lyophilization for 72 hours, and then re-weighed to determine tissue water content. Each dehydrated sample underwent enzymatic digestion in a papain solution (3.75 U/mL) containing 5mM N-acetyl-L-cysteine and 5mM ethylenediaminetetraacetic acid (EDTA) in 50mM potassium phosphate buffer (pH = 6.9) at 60°C for 18 hours. Liver and testis tissues were sonicated at ~5 W for 1 second to achieve complete dissolution (QSonica, Newton, CT). Samples were stored at 4°C following papain digestion and allowed to come to room temperature prior to conducting the hydroxyproline assay.

Hydroxyproline assay overview

A collagen standard curve was prepared from serial dilutions of a bovine collagen reference standard (Biocolor Ltd., Carrickfergus, UK) diluted with papain solution. Aliquots of 10 – 30 μL of

tissue digest were diluted to a final volume of 100 μL with excess papain solution to achieve a concentration of collagen expected to fall within the range of the standard curve. Specifically, 10 μL of tissue digest were used for tendon and meniscus, 20 μL were used for engineered and native bovine articular cartilage, and 30 μL were used for leporine liver and testis. An overview of the assay chemistry is provided in Figure 2-1. Soluble peptides and proteins in each standard and tissue sample were hydrolyzed to individual amino acids by adding 100 μL of 4 N sodium hydroxide and incubating at 120°C and 15 psi above atmospheric pressure for 15 minutes. Samples were allowed to cool to room temperature and then neutralized with 100 μL of 4 N HCl. Hydroxyproline amino acids were converted to pyrolle-2-carboxylate by oxidation via addition of 0.625 mL of 0.05 M chloramine-T in 74% v/v H_20, 26% v/v 2-propanol, 0.629 M NaOH, 0.140 M citric acid (monohydrate), 0.453 M sodium acetate (anhydrous), and 0.112 M acetic acid (glacial), followed by incubation at room temperature for 20 minutes. Finally, 0.625 mL of 15% w/v DMAB (1 M) in 2-propanol plus concentrated acid (a.k.a. Ehrlich's solution) was added to each sample and vortexed immediately to facilitate mixing. Samples were incubated at 65°C for 20 minutes and then rapidly cooled by immersion in room temperature water to stop chromophore development.

Suggested hydroxyproline assay protocol

- Digest tissue in papain solution for 18 hours at 60°C.
    - Papain solution: 3.875 U/mL papain in 5 mM EDTA tetrasodium hydrate, 5 mM N-acetyl-L-cysteine, and 50 mM potassium phosphate buffer at pH 7
- Dilute samples with excess papain solution to bring expected concentration of collagen within the assay standard range and to a final volume of 100 μL in an autoclave safe, screw-top tube (e.g., 2 mL cryovial). Leave cap loose.
- Add 100 μL of 4N NaOH to each sample.

- Autoclave at 120°C and 15 psi above atmospheric pressure (i.e., typical liquid cycle) for 15 minutes.
- Allow samples to return to room temperature.
- Add 100 µL of 4N HCl to neutralize the pH.
- Add 625 µL Chloramine-T solution.
    - Chloramine-T solution: 0.05 M Chloramine-T in 74% v/v H_20, 26% v/v 2-propanol, 0.629 M NaOH, 0.140 M citric acid (monohydrate), 0.453 M sodium acetate (anhydrous), and 0.112 M acetic acid (glacial)
- Let stand at room temperature for 20 minutes.
- Add 625 µL Ehrlich's solution and vortex immediately to ensure complete mixing.
    - Ehrlich's solution: 1 M DMAB in 30% v/v HCl and 70% v/v 2-propanol
- Incubate in water bath at 65°C for 20 minutes.
- Immediately quench reaction by immersing tubes in cool water
- Plate standards and samples in triplicate in a 96-well clear, flat-bottomed plate (200 µL/well).
- Read plate in a spectrophotometer at an absorbance wavelength between 550-565 nm.

Optimization of hydrochloric acid concentration

To identify the optimum proportion of HCl for the Ehrlich's solution, formulations with 50%, 30%, and 10% v/v concentrated HCl (Fisher Scientific, Waltham, MA) were prepared in a balance of 2-propanol. The different proportions of HCl were compared to 30% $HClO_4$ Ehrlich's solution for quantifying hydroxyproline content via the hydroxyproline assay as described above.

Absorbance measurements

Aliquots of 100 μL of each sample were added in triplicate to a clear 96-well plate. To evaluate potential differences in wavelength of maximal light absorption, absorbance measurements were made at varying wavelengths in 10 nm increments from 300 – 500 nm, in 5 nm increments from 500 – 600 nm, and in 10 nm increments from 600 – 800 nm using a microplate reader (Synergy HT, BioTek Instruments, Winooski, VT). Background absorbance was measured from samples of papain solution without added collagen standard or tissue digest subject to the same reaction steps as described above. Subsequently, absorbance measurements were made within the range of the optimal absorbance wavelengths using a microplate reader (Tecan Group Ltd., Männedorf, Switzerland).

Comparison of Ehrlich's solution using hydrochloric or perchloric acid for collagen quantification

Samples of tissue with differing collagen content and extracellular matrix compositions were used to assess agreement between collagen quantification by the hydroxyproline assay using DMAB dissolved in $HClO_4$ or HCl. Paired samples of each collagen standard and tissue digest were prepared and treated identically as described above up to the final chromophore development step. Chromophore development was then performed with DMAB dissolved in either 30% v/v $HClO_4$ or 30% v/v HCl combined with 70% v/v 2-propanol.

Four separate iterations of the assay were performed using different samples of tissue-engineered neocartilage, native bovine articular cartilage, and native leporine tissues. Samples in the first iteration of the assay consisted of neocartilage and native cartilage that were prepared exactly as described above. In the second iteration, samples with varying collagen content were prepared by performing three serial, 1:1 dilutions of native cartilage digest in papain solution. For the third iteration, samples of neocartilage were chosen with low GAG or high GAG content, and 0, 1.25, 2.50, or 5.00 μg of soluble collagen (Sircol bovine collagen standard, Biocolor Ltd., Carrickfergus, UK) per 100 μL were added to each digest solution. Samples in the fourth iteration

consisted of leporine tissues prepared as described above. For each iteration of the hydroxyproline assay, absorbance measurements were recorded and the concentration of collagen in each original specimen calculated based on standard curves created for each microplate.

Amino acid analysis

For comparison of colorimetric assay results to a proteomics gold standard, papain digested samples underwent amino acid analysis at the UC Davis Proteomics Core Facility. Selected samples of bovine native cartilage, bovine neocartilage, and leporine tissues were subjected to formic acid/acetonitrile transfer, dried, subjected to liquid phase hydrolysis in 6 N HCl with 1% phenol at 110°C for 24 hours, and dried again. Finally, samples were resuspended in S-2-aminoethyl-L-cysteine dilution buffer and loaded into the amino acid analyzer (Hitachi L-8900, Tokyo, Japan) for quantification. Sircol bovine collagen reference standard (Biocolor Ltd., Carrickfergus, UK) was also analyzed to relate results to the hydroxyproline assay.

Statistics

Standard curves were fit between measured absorbance values and standards of known collagen concentration by least squares linear regression for all repetitions of the hydroxyproline assay. Coefficients of determination (R^2) were calculated for each standard curve. Potential differences in measurements of sample collagen or hydroxyproline content among the different assays were examined by matched pairs two-tailed t-tests with significant differences defined by $p < 0.05$. Additionally, reproducibility between the different assays was assessed by calculating the Lin's concordance correlation coefficient (ρ_c), a measure of agreement between paired results that accounts for linearity as well as proximity to a line with a slope of one and a y-intercept of 0.[107,108] Finally, *a posteriori* power analyses (power = 0.8 or 0.9, $p < 0.05$) were completed to determine how many samples would be necessary to observe potentially significant differences between groups.

Results

Hydroxyproline assay standard curves for each acid formulation were generated (Figure 2-2). A standard curve using a 50% HCl concentration was developed and yielded the lowest absorbance, whereas the 30% $HClO_4$ formulation led to the greatest absorbance. The 30% $HClO_4$ and 30% HCl solutions produced standard curves with R^2 values of 0.998 and 0.999, respectively. While the 10% HCl group exhibited similar absorbance to the 30% HCl group, it had a lower R^2 value (0.969 vs. 0.999) and demonstrated phase separation during chromophore development. Thus, the 10% HCl group along with 50% HCl were not considered as replacements for 30% $HClO_4$.

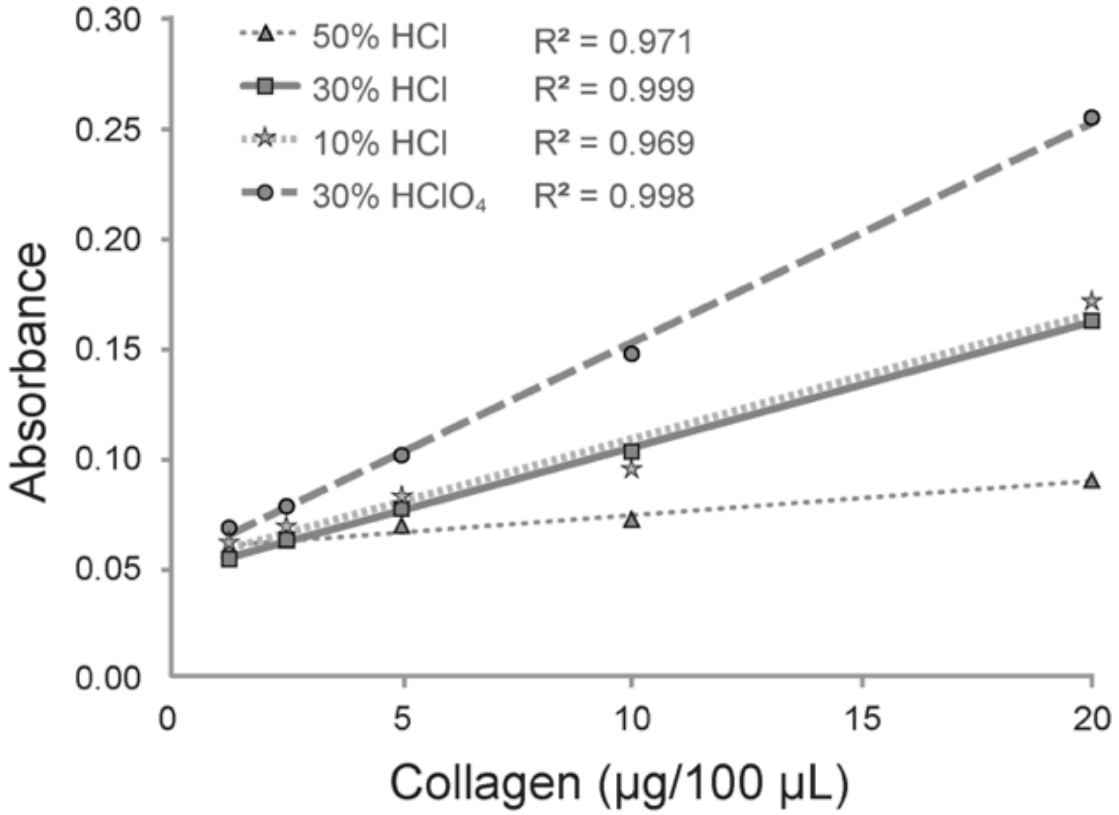

Figure 2-2. Spectrophotometric absorbance as a function of collagen concentration. Sircol collagen standard at different concentrations was quantified via hydroxyproline assay using DMAB dissolved in a solution consisting of isopropanol and strong acid (30% $HClO_4$, 10% HCl, 30% HCl, or 50% HCl). The $HClO_4$ group generated a curve with the greatest slope. For the groups using HCl, a 30% strong acid solution most closely mimicked the results of $HClO_4$ and displayed the greatest linearity. These two groups were carried forward into later phases of this project for further comparison.

Ehrlich's solutions produced with $HClO_4$ or HCl resulted in similar absorption spectra (Figure 2-3). Both formulations of the reagent reacted with collagen to yield the greatest specific absorbance at light wavelengths between 540 – 575 nm and peak absorbance occurring at 565 nm (Figure 2-3A-B). Due to unreacted DMAB, other reagents, and solutions involved in the assay, marked non-specific absorbance occurred for wavelengths less than 500 nm regardless of solvent and collagen concentration. Ehrlich's solution produced with $HClO_4$ achieved greater absolute absorbance and greater absorbance to background ratio compared to HCl (Figure 2-3A-D), but both versions of the reagent exhibited highly linear responses to concentrations of collagen between 1.25 – 20 μg/100μL for wavelengths of light between 545 – 575 nm (Figure 2-3E-F).

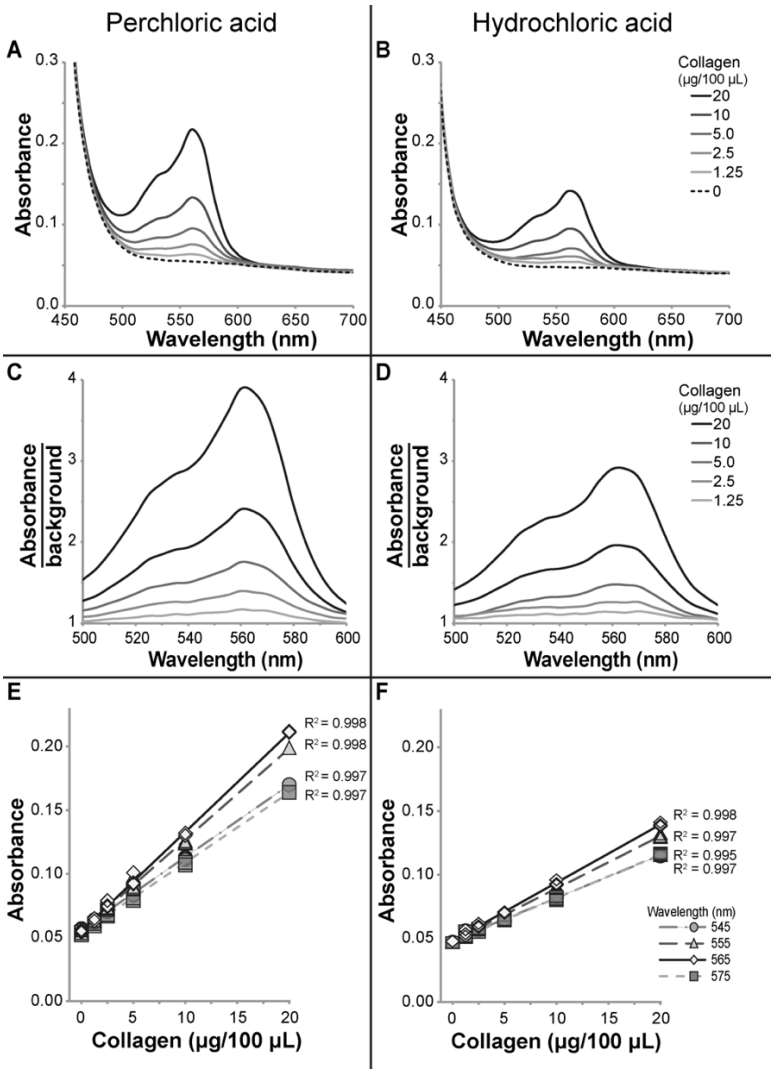

Figure 2-3. Absorbance as a function of light wavelength and collagen concentration for paired hydroxyproline assays using Ehrlich's solution made with HClO4 (A, C, E) or HCl (B, D, F). Marked non-specific absorption occurred at wavelengths less than 500 nm and negligible absorption occurred at wavelengths greater than 600 nm (A, B). Both solutions produced peak absorption and absorption:background ratios at wavelengths of 560-565 nm (C, D). The maximum absorption and absorption:background was less for Ehrlich's solution made from HCl, but both solutions produced a linear absorption response for concentrations of collagen between 1.25 - 20 µg/100 µL for wavelengths between 545-575 nm (E, F).

Quantification of collagen using the colorimetric hydroxyproline assay achieved a concordance correlation coefficient of ρ_c = 0.976 for all paired samples assayed with Ehrlich's solution using either $HClO_4$ or HCl (Figure 2-4). Within specific tissue types, ρ_c was 0.972, 0.986, and 0.991 for engineered cartilage (n=36), native cartilage (n=16), and leporine tissues (n=4), respectively. No significant difference was observed between the two collagen assays applied in samples of bovine native cartilage, tissue-engineered cartilage, or leporine liver, testis, meniscus, or tendon (n = 58,

p = 0.321). Based on our power analysis, 89 or 118 measurements would be necessary to achieve power of 0.8 or 0.9, respectively, to identify a statistically significant difference ($p < 0.05$) if the small, observed differences between the two assays are not due to random variation.

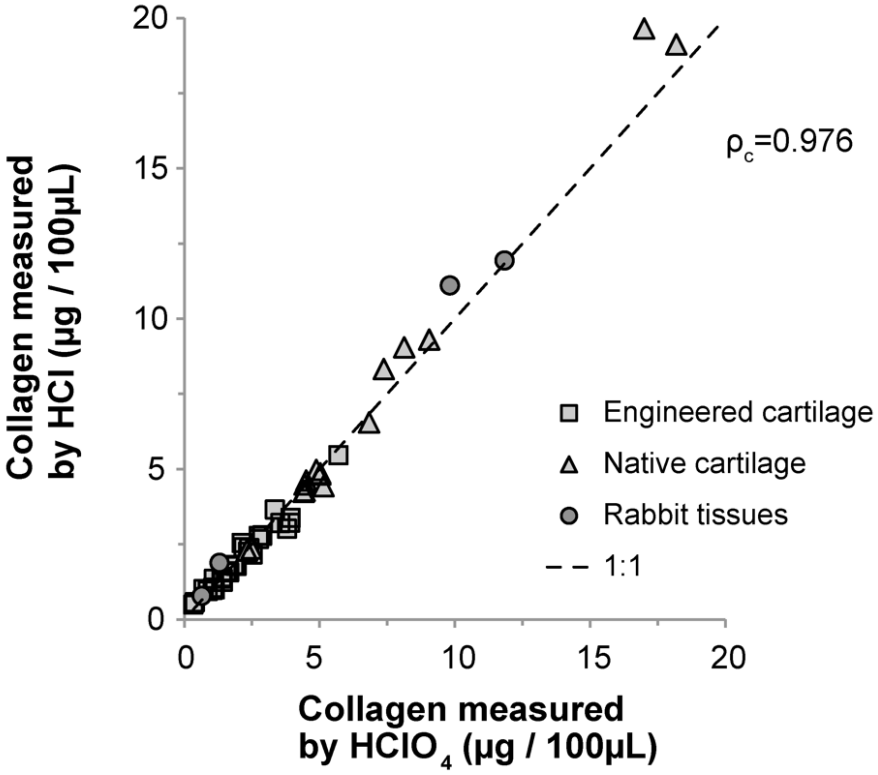

Figure 2-4. Concentrations of collagen measured by the hydroxyproline assay using DMAB dissolved in 30% HClO4 or HCl plus 70% isopropanol. Source tissues, which were differentially treated, included native (n=16) or engineered (n=36) bovine cartilage and leporine tissues (n=4). The leporine tissues included, in ascending order of collagen concentration, liver, testis, meniscus, and tendon. Aliquots of each tissue digest were diluted with a variable amount of excess papain solution to a volume of 100 µL to achieve concentrations of collagen within the limits of the assay standard curve. There was excellent concordance ($\rho_c = 0.976$) between collagen concentrations measured using $HClO_4$ or HCl.

Hydroxyproline biochemical assay results were compared to hydroxyproline amino acid quantification (Figure 2-5). The HCl group correlated more strongly with amino acid quantification data than the $HClO_4$ group. Furthermore, the slope of the regression line for the HCl group was closer to unity. Thus, ρ_c was greater for HCl than for $HClO_4$ (0.980 vs. 0.947). Although both versions of the colorimetric assay underestimated hydroxyproline content compared to chromatographic amino acid analysis, the observed differences were not statistically significant

($p = 0.195$ for HCl and $p = 0.110$ for $HClO_4$). To identify a statistically significant difference with power of 0.8 and $p < 0.05$, 20 measurements would be necessary for $HClO_4$, while 43 measurements would be necessary for HCl.

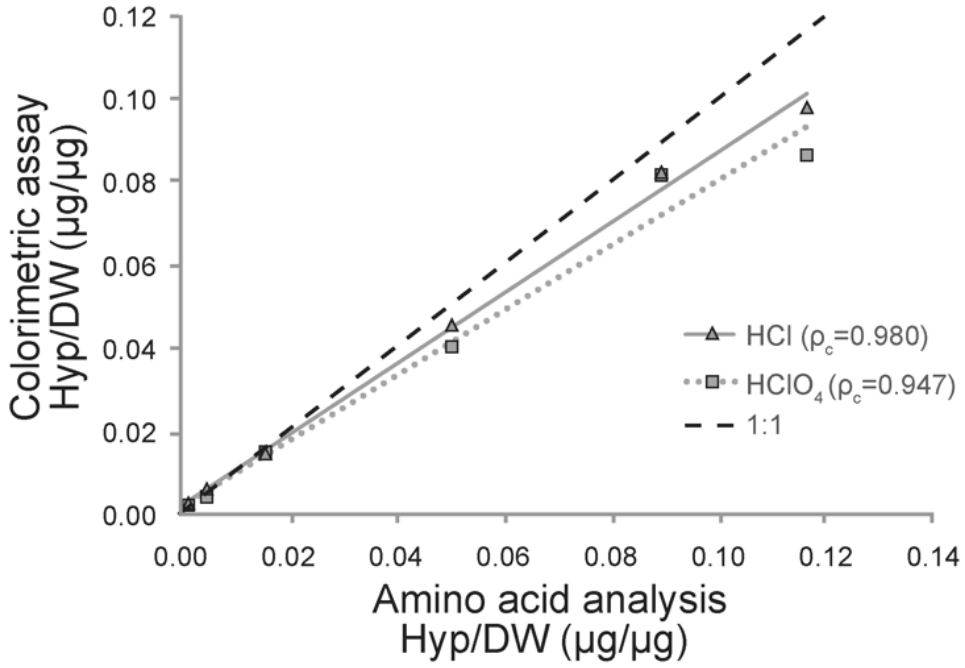

Figure 2-5. Concentrations of hydroxyproline, from lowest to highest collagen content, in rabbit liver, rabbit testis, engineered bovine articular cartilage, bovine articular cartilage, rabbit meniscus, and rabbit tendon, as measured by colorimetric assay or by amino acid analysis. The dotted line corresponds to the hydroxyproline assay using Ehrlich's solution made with 30% $HClO_4$, while the solid line represents the hydroxyproline assay that replaces 30% $HClO_4$ with 30% HCl. Amino acid analysis quantification shared the greatest concordance with the HCl group (ρ_c=0.980), while the $HClO_4$ group did not agree as closely with amino acid quantification (ρ_c=0.947). Concordance is illustrated by experimental curve proximity to the 1:1 unity dashed line. Both colorimetric assays underestimated hydroxyproline content as determined by amino acid analysis.

Discussion

Measurement of collagen is an important aspect of biological research toward characterizing the composition of normal tissues, understanding certain pathologic processes, and for development of biomaterials and tissue-engineered constructs. Collagen content of a tissue or biomaterial can be measured by different commonly used approaches; examples include (1) quantification of hydroxyproline; (2) detection of a dye that binds to solubilized collagen molecules; and (3) quantification of antibody binding via an enzyme-linked immunosorbent assay (ELISA). Here we report a modification to colorimetric hydroxyproline measurement for collagen quantification that

improves on assay safety and cost, and achieves similar or improved accuracy. The modified assay substitutes HCl for $HClO_4$ to make Ehrlich's solution; no difference was observed between measurements of collagen using either formulation of Ehrlich's solution for any of the tissues tested, including liver, testis, cartilage, meniscus, and tendon. Additionally, the hydroxyproline content of samples measured using the colorimetric assay with HCl strongly agrees with results obtained by the gold standard, chromatographic amino acid analysis.

Our proposed colorimetric assay represents a simple improvement for the quantification of hydroxyproline and collagen in biologic tissues by substituting HCl for $HClO_4$ in the formulation of Ehrlich's solution (15% w/v DMAB, 70% 2-propanol, 30% concentrated acid). Colorimetric quantification of collagen is based on oxidation of hydroxyproline residues to form pyrrole-2-carboxylate followed by reaction with DMAB to yield a detectable chromophore.[94] Multiple revisions of the original colorimetric hydroxyproline assay have been introduced;[101,102] in the case of this study, we have replaced $HClO_4$ with HCl in Ehrlich's solution, which achieved more accurate quantification of hydroxyproline content in tissues as confirmed by amino acid analysis. The HCl-based assay exhibited strong concordance with amino acid analysis ($\rho_c = 0.980$) and on average differed from amino acid analysis by 10.3%, whereas $HClO_4$ had weaker concordance ($\rho_c = 0.947$) and erred by an average of 14.8%. The limited number of samples included in amino acid analysis prevents evaluating assay accuracy as a function of tissue type, but trends suggest that both colorimetric assays slightly underestimate hydroxyproline content in collagen-rich samples. The ~33% greater absorbance to background ratio produced by Ehrlich's solution with $HClO_4$ may provide slightly greater sensitivity for detecting very small differences in collagen between tissues. Thus, future refinements of the assay should be aimed at achieving greater absorption to background to further improve the assay sensitivity. Nonetheless, substituting HCl for $HClO_4$ in Ehrlich's solution improves the assay's accuracy.

The results of this study indicate that both acid formulations result in a highly linear absorbance response for concentrations of collagen between 0 and 20 μg/100 μL. The assay as

presented here is capable of accurately quantifying hydroxyproline in a wide variety of tissues, from those with minimal collagen (e.g., liver) to those composed of nearly 100% collagen (e.g., tendon). A limitation of our study is that the upper limit of linearity using HCl was not explored. Previous research using $HClO_4$ demonstrated linearity of the absorbance response for dilutions of hydroxyproline up to 20 µg/50 µL, far exceeding any concentrations tested in this study.[16] Linearity of the absorbance response should be validated for concentrations of collagen in excess of 20 µg/100 µL prior to using the HCl-based assay for measuring highly concentrated hydroxyproline or collagen samples. Nonetheless, our modified hydroxyproline assay exhibits a linear absorbance range sufficient for accurately measuring collagen content in most biologic tissues.

Commonly used assays indirectly measure collagen content in biological samples by exploiting its unique amino acid sequence, which can over- or underestimate the true sample collagen content.[94,109] Using hydroxyproline to measure collagen in a sample relies on the repeating amino acid sequence and predictable proportion of hydroxyproline in a given type of collagen. All types of collagen exhibit a repeating glycine-X-Y amino acid sequence in which “X” and “Y” most often represent proline and hydroxyproline residues.[110] The proportion of hydroxyproline by mass is highly conserved within a given type of collagen and ranges from 11.3% in type I collagen to 15% in type III collagen.[111] Importantly, these assays are not specific to detection of hydroxyproline in collagen and the presence of hydroxyproline associated with other proteins could inflate the apparent collagen content. Serum complement, acetylcholinesterase, and elastin are all proteins with relatively high hydroxyproline contents, and their potential presence should be considered when choosing an appropriate assay for collagen quantification.[112] Similarly, the hydroxyproline assay is not specific to fibrillar collagen, because hydroxylation of proline to hydroxyproline occurs very soon after translation. Thus, intracellular procollagen and extracellular tropocollagen are also detected by the hydroxyproline assay. Although the assay reported here demonstrates strong agreement with amino acid analysis for

measurement of hydroxyproline, the assay shares the same limitations as previous hydroxyproline-based methods of collagen quantification.

Other methods for quantifying collagen include Sirius red dye binding and ELISA, each associated with their own advantages and disadvantages. For example, Sirius red dye binds to the highly basic residues of solubilized fibrillar collagen amino acid side chains [113] and does not bind to most non-collagenous proteins that are high in hydroxyproline content.[111,112] The Sirius red binding assay also obviates the need for hydrolysis of collagen to individual amino acids and allows for quantification of different collagen fractions based on their solubility.[114,115] Nonetheless, binding of Sirius red to non-collagen proteins has been reported to cause inaccurate results, and modification of the assay may be necessary depending on the tissue source.[116] Moreover, a direct comparison of the hydroxyproline and dye-binding based methods for quantifying collagen in a pulmonary fibrosis model found the hydroxyproline-based assay to more accurately reflect total collagen and differences among samples than Sirius red binding.[109] Assays based on hydroxyproline or Sirius red binding do not distinguish between different types of collagen. ELISA is typically the best choice for quantifying a specific type of collagen and is capable of discriminating between collagen types that may be present in the same tissue, such as type I and type II collagen in fibrocartilage.[117] Disadvantages of using ELISA for collagen quantification include cost and potential need for more than one assay when working with tissues from different species. The specific goals of a study, tissue sources, and limitations of each assay should be considered when choosing an appropriate collagen quantification method.

Using HCl in place of $HClO_4$ improves the cost and safety of this assay. Since this assay uses relatively large volumes of reagent in comparison to other biochemical assays, the 75% reduction in cost for the strong acid component of this assay can provide significant cost savings for laboratories.[118] In terms of safety, HCl is not associated with the build-up of explosive salts, which is known to occur with $HClO_4$. Therefore, HCl does not necessitate the use of an expensive wash-down capable fume hood. $HClO_4$ also presents the potential issues of flammability, toxicity,

and mutagenicity, while HCl can be used without these concerns. Based on improvements in efficacy, cost, and safety, this modified assay represents an improved tool for measuring hydroxyproline and collagen content in biological samples.

In conclusion, the extra hazard, cost, and need for specialized fume hoods can be obviated for the purposes of collagen quantification via the hydroxyproline assay by substituting concentrated HCl for $HClO_4$ to produce Ehrlich's solution. Use of HCl accurately quantifies hydroxyproline and collagen in enzymatically digested collagenous tissues with no change in the wavelength of peak absorption. As when using $HClO_4$, care must be taken to avoid phase separation upon addition of Ehrlich's solution containing HCl. Although Ehrlich's solution containing $HClO_4$ yielded greater absorption than HCl for the same concentration of collagen/hydroxyproline, both versions of the assay were accurate over the range of collagen concentrations and tissues tested in this study, and HCl more closely corresponded to values obtained by amino acid analysis.

CHAPTER 3 Facet joints of the spine: structure-function relationships, problems and treatments, and the potential for regeneration

Abstract

The zygapophyseal joint, a diarthrodial joint commonly referred to as the facet joint, plays a pivotal role in back pain, a condition that has been a leading cause of global disability since 1990. Along with the intervertebral disc, the facet joint supports spinal motion and aids in spinal stability. Highly susceptible to early development of osteoarthritis, the facet is responsible for a significant amount of pain in the low-back, mid-back, and neck regions. Current noninvasive treatments cannot offer long-term pain relief, while invasive treatments can relieve pain, but fail to preserve joint functionality. This review presents an overview of the facet in terms of its anatomy, functional properties, problems, and current management strategies. Furthermore, this review introduces the potential for regeneration of the facet and particular engineering strategies that could be employed as a long-term treatment.

Introduction

The highly innervated, diarthrodial, zygapophysial joint, or the facet joint, is located at either side of the posterior vertebral body. The facet joint's opposing bony surfaces are covered by a layer of hyaline articular cartilage, and the joint is encapsulated by the synovium and fibrous capsule. This joint can have meniscus-like structures that improve joint congruency. Facet joints work in pairs, along with the intervertebral disc (IVD), to constrain the motion of the vertebrae while aiding in the transmission of spinal loads.[119]

Chapter published as: O'Leary SA, Paschos NK, Link JM, Klineberg EO, Hu JC, Athanasiou KA. Facet joints of the spine: structure-function relationships, problems and treatments, and the potential for regeneration. Annual Review of Biomedical Engineering. 20:1 (2018)

The facet joint is frequently dislocated or fractured due to motor vehicle- or sports-related trauma.[120-122] These events impair normal spine function, cause pain, and potentially can lead to varying degrees of degeneration within the facet joint. Whether induced by trauma or age-related changes, facet joint degeneration, which has been implicated as a possible cause of pain, is prevalent. Facet degeneration may develop in patients as young as 15 years old;[123] almost two-thirds of people are affected to some degree by the time they reach the age of 30 years.[124] Severe and potentially symptomatic lumbar osteoarthritis (OA) usually affects the elderly population.[125] Not all cases of facet degeneration result in patient pain; however, advanced OA, concomitant hypertrophy of the facet, and IVD degeneration all contribute to spinal canal nerve impingement in symptomatic spinal stenosis,[126] the most common reason for lumbar surgery in the United States.[127] These pathological conditions also play a role in other back-related morbidities such as spondylolisthesis[128] and scoliosis.[129]

The facet joint is severely understudied. Consequently, the mechanism of facet joint pain and its relationship to degeneration is not fully understood and often debated; however, the facet joint is increasingly being recognized as a source of back pain. Low-back pain is common, affecting ~59.1 million people in the United States.[130] In 2011, 28.9% of all US adults experienced low-back pain, and 15.5% suffered from neck pain.[131] Back pain burdens both the nation's health and health care system, at a total cost of $100–200 billion per year, rivaling heart disease, diabetes, and cancer as the nation's top health concerns.[132,133] The developing recognition of the facet joint's contribution to back pain is reflected in the dramatic increase of facet joint interventions in recent years (e.g., during 2000–2011, there was an increase of 308% per 100,000 Medicare beneficiaries).[134] Although diagnosing facet joint pain is difficult, it is estimated to be responsible for 16–40%,[135-141] 34–48%,[138-140] and 39–67%[139,140,142] of pain felt in the low-back, mid-back, and neck regions, respectively. Thus, the facet joint is the locus of highly significant pathology.

Conservative pain-relieving facet joint treatments such as intraarticular injections, medial branch blocks, and radio-frequency denervation offer only short-term pain relief and aim to relieve symptoms rather than to treat underlying mechanisms or damaged tissues.[143] Invasive, surgical options for stenosis, spondylolisthesis, and scoliosis often require removal of the facet joints to reduce pain. However, such procedures are commonly accompanied by spinal fusion, known to induce adjacent segment disease,[144,145] as well as complete immobilization of the fused spinal segments. Thus, there is a need to develop a surgical option for pain management that does not compromise the function of the treated facet or the integrity of adjacent facets . To that end, researchers and clinicians alike are seeking new treatment modalities for this troubled joint. For instance, metallic prostheses are currently in clinical trials.[146] However, due to their inability to recapitulate healthy spine biomechanics and kinematics, prostheses and other therapies in the clinic often fall short in providing a durable, motion-preserving solution. Considering these shortcomings, tissue engineering of a biomimetic facet joint may serve as an attractive solution for motion preservation and long-term pain management since it would recreate the characteristics of a healthy spine.

This article presents an overview of the facet joint in terms of its anatomy, functional properties, problems, and current treatment and management strategies. Discussion of the diagnosis of facet joint pain, a controversial issue, can be found elsewhere.[147,148] To provide context to a more extensively characterized joint, this review compares the facet joint with the knee. This review aims to discuss, for the first time, how tissue-engineering may be a viable option for treating the facet joint.

Facet joint anatomy and biomechanics

Together, the IVD and the facet joints, known as the three-joint complex, connect adjacent vertebrae, stabilize the spine, and facilitate articulation.[149] Primary constituents of the facet joint include the subchondral bone, articular cartilage, synovium, and fibrous capsule. These joints are

densely innervated, actively supporting motor function and transmission of pain. Because the spine's biomechanics are regionally dependent, the facet orientation relative to the sagittal and transverse planes and shape of the articulating surface vary, both among and within the cervical, thoracic, and lumbar spinal regions.[150-152] Furthermore, variation in facet joint structure and number can be observed across species.[153] Altogether, these anatomical components form a joint that bears nontrivial loads when the spine experiences compression, flexion, extension, and/or torsion.

Articular processes

The inferior aspect of the facet joint extends from the lamina of the superior vertebral body and meets the superior aspect of the facet joint extending from the inferior vertebral body (Figure 3-1A). Relative to the sagittal plane, the orientation of the articular surfaces (angle θ), for which these protrusions provide support, changes from one spinal level to the next (Figure 3-1B) (Table 3-1). The largely sagittal orientation of the lumbar facet joint, in combination with the high degree of mutual convexity and concavity of the opposing joint surfaces in this region, enables a greater range of motion in terms of flexion, as well as higher resistance to axial rotation.[154] Furthermore, the smaller inclination angle (see Table 3-1 for definition and data) of the lumbar facets provides increased protection against forward displacement of the spinal segment. In the cervical and thoracic regions, a less sagittal orientation of the joint, a greater inclination angle, and roughly planar articular surfaces facilitate a greater range of both axial rotation and lateral bending in comparison to the lumbar region, especially at C5 and C6.[150] In general, the shape and orientation of the articular processes of the facet joint at each spinal level serve to modulate range of motion and effectively bear loads to maintain spinal function.

Table 3-1. Structural and functional properties of the human facet joint

	Cervical	Thoracic	Lumbar	Refs
Surface Area	0.80-1.07 cm^2	0.69-1.15 cm^2	0.97-2.12 cm^2	155
Sagittal Orientation Angle*	70-96°	93-110°	27-46°	151,152,156
Inclination Angle**	31-59°	62-78°	71-86°	155
Range of Motion Per Motion Segment	Flexion/Extension: 8-17° Lateral Bending: 4-11° Axial Rotation: 8-12°	Flexion/Extension†: 4-12° Lateral Bending†: 6-9° Axial Rotation†: 2-9°	Flexion/Extension: 12-20° Lateral Bending: 3-8° Axial Rotation: 2-5°	157,158
Contact Forces on Facet Surfaces	Flexion/Extension: 17-27 N Lateral Bending: 17-40 N Axial Rotation: 26-30 N	No Data	Flexion/Extension: 46-109 N Lateral Bending: 10-75 N Axial Rotation: 56-120 N	159-163

*Sagittal orientation angle is displayed in Figure 3-1. **Inclination angle is defined as the angle between the transverse plane and the best-fit plane between the articulating surfaces of the facet. †Ribcages were removed from thoracic spines before range of motion testing.

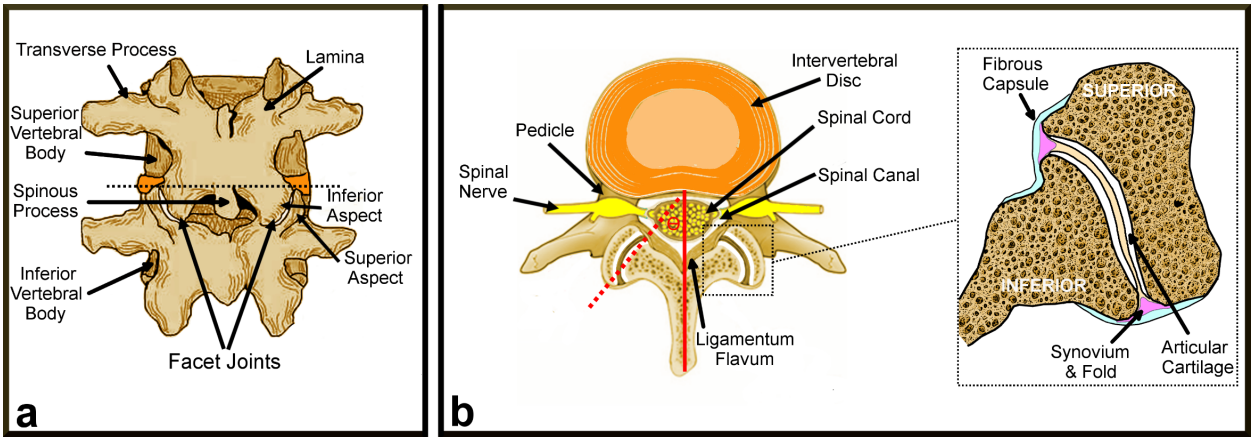

Figure 3-1. Facet joint anatomy. a) Posterior view of the motion segment. b) Axial view of the motion segment and a closer look at the facet joint and its individual components. Sagittal orientation angle (Θ) refers to the facet joint's orientation with reference to the sagittal plane.

Given that researchers often use large animal models for facet joint research, it is important to note that differences exist in facet joint structure and biomechanics between humans and other species. All commonly used large animal models are quadrupedal, leading to marked differences in facet joint size and shape.[164] Additionally, the number of facet joints changes from species to species because the sum of functional spinal units varies from species to species. These differences yield loading patterns different from those in bipedal humans, which may limit the applicability of quadrupedal animal models.

Articular cartilage

Articular cartilage, covering the surfaces of the inferior and superior subchondral bone protrusions, enables low-friction movement and experiences tensile, compressive, and shear loads.[165] Unlike cartilages of other joints, the cartilage of human facet joints is not well characterized. The histological, mechanical, and biochemical characteristics of lumbar facet joint cartilage of the minipig, monkey, and rabbit have recently been reported.[164] Like articular cartilage found elsewhere, facet joint cartilage is organized into superficial, middle, and deep zones. In the superficial zone, collagen fibers are oriented tangential to the joint surface, and chondrocytes appear flattened; in the middle (or transitional) zone, collagen fibers are arranged in a more isotropic fashion, and chondrocytes increase in number and roundness; in the deep zone, both the collagen and chondrocytes are oriented perpendicular to the joint surface. Facet joint cartilage's aggregate modulus is similar across species, between opposing surfaces of the joint (i.e., inferior and superior), and across lumbar spinal levels. The average values for the aggregate modulus ranged from 0.159 to 0.174 MPa, and the thickness ranged from 290 to 370 μm. Similarly, the glycosaminoglycan (GAG), collagen, and DNA contents of the minipig and rabbit cartilage were comparable between joint surfaces and spinal levels ranging from 2.4% to 4.2%, from 15.77% to 16.62%, and from 0.029% to 0.034% per wet weight, respectively. A separate study reported that in canine L3–L4 and L4–L5 superior facet joint cartilage, the tensile modulus

and aggregate modulus are 10.08 ± 8.07 MPa and 0.55 ± 0.13 MPa, respectively.[165] Additionally, the compressive Young's modulus of ovine cervical facet joint cartilage was found to be 0.76 ± 0.35 MPa,[166] and the compressive stiffness of equine cervical facet joint cartilage was found to be ~0.118 MPa.[167] Aside from animal data, a comprehensive description of normal human facet joint cartilage of the lumbar, thoracic, or cervical region has yet to be reported. Performing these characterizations in humans will aid in the selection of an appropriate animal model for facet joint research.

Synovium, synovial fold, and fibrous capsule

The synovium, synovial folds, and fibrous capsule enclose the facet joint space and play a biomechanical role. The synovium directly surrounds the facet joint, while the synovial fold—sometimes termed a meniscoid—folds into the area between the inferior and superior facet.[168] Cervical synovial folds comprise fibrous, adipose, or fibroadipose tissue. The synovium prevents synovial fluid from escaping; the synovial fold increases surface contact area, improving joint congruence. Within the cervical spine, posterior synovial folds protrude into the joint space by a median of 2.81 mm, whereas anterior synovial folds extend by a median of 3.52 mm.[168] Superposed to the synovium, the fibrous capsule is composed of ligamentous tissue and completely surrounds the joint. It regulates the internal environment of the facet in terms of nutrients and immune cells. Furthermore, in conjunction with the ligamentum flavum (ligaments that connect to the lamina of adjacent vertebrae), the fibrous capsule provides mechanical stability to ensure that opposing facet surfaces remain close to one another (Figure 3-1B). In the lumbar spine, the fibrous capsule tensile strength parallel and perpendicular to the axis of collagen fiber orientation is 1.90 MPa and 0.95 MPa, respectively.[169] The complex modulus of elasticity parallel to collagen fiber orientation is 1.63 MPa; perpendicular to collagen fiber orientation, the viscous and elastic secant moduli are 1.81 and 1.00 MPa, respectively.[169] Altogether, the synovium, synovial fold, and fibrous capsule preserve and augment the mechanical function of the

underlying articular cartilage, and thus must be considered when addressing any aspect of the facet joint for the purposes of basic research or therapy development.

Nerve endings

Whereas the articular cartilage of the facet joint is aneural, the subchondral bone, synovium, synovial folds, and joint capsule are innervated extensively.[170] These nerve endings, which form part of the medial branch emanating from the dorsal ramus, are involved in pain sensation and proprioception.[171] The medial branch is particularly important because it is responsible for sensory input from the midline of the spine to the facet joint line.[171] As such, many facet joint diagnostics and interventions rely on mitigating pain by blocking medial branch nervous signals.

Role of the facet joint in spine biomechanics

Biomechanically, the facet joint, together with the IVD and spinal ligaments, bears some of the compressive load in the spine and inhibits excessive flexion, translation, and torsion that could lead to pathological conditions. In the lumbar spine, in vitro studies have shown that the facet articular surface alone bears 6–30% of axial compressive loads, depending on the mode of spinal motion.[172,173] The cervical and upper thoracic facet joints transmit 23% of axial compressive loads. Note that loads in the cervical spine are smaller than those in the lumbar spine (Table 3-1).[172,173] The loading profile changes from level to level according to the curvature of the spine and the geometry of the individual facet joints, making generalizations about the biomechanics of the facet joint difficult.[149] As shown by measurements of the effects of facetectomy, the facet joint ensures that the spinal column resists joint distraction, shear forces, and lateral or anteroposterior translation and imparts sufficient torsional stiffness.[149] For example, joint distraction increased under the same tensile load following facetectomy.[174] When combined with other loading types, such as flexion, the risk of joint distraction and subsequent trauma can increase further. Thus, biomechanically competent facet joints preserve normal spinal motion and mitigate potential trauma or degeneration.

Biomechanical alterations postdegeneration and surgical intervention

Facet joint biomechanics change significantly because of tissue degeneration and spinal surgical intervention. For example, degeneration of the IVD, as part of the three-joint complex, is expected to affect the facet. Similarly, degeneration of the facet joint can lead to a compromised IVD.[121] Disc degeneration has been associated with an increased range of motion in the lumbar facet joints, which could lead to increased compressive stress and promote cartilage degeneration.[175] Disc narrowing also increases axial compressive loads in the lumbar facet surface by 70%, far exceeding normal load-bearing capacity.[176] Disc replacement has been employed to treat disc degeneration; however, this procedure may also result in kinematic and biomechanical changes that could have adverse effects on the facet. The effects of a disc implant at the L5–S1 spine segment were assessed in a finite-element model of the lumbar spine. Depending on the anteroposterior location of the implant, the sum of flexion and extension range of motion can vary from 11.5° to 15°, demonstrating that the range of motion depends on where the surgeon places the implant.[177] Furthermore, under lateral bending on the ipsilateral side, lumbar facet joint forces as a function of cranial/caudal implant location can range from 70 to 115 N, possibly leading to disruption of articular cartilage homeostasis.[177] Another study concluded that, after cervical disc replacement, range of motion in the associated facet joints increased from 9.6° ± 5.1° to 16.2° ± 3.6° postimplantation.[178] Interestingly, in the same study, facet contact pressures in extension or flexion did not change significantly. Despite conflicting results based on experimental methods, patient population, or intervention type, degeneration and surgical intervention often lead to deviations from the biomechanics observed in a healthy, intact facet joint. Generally, in cases of advanced, extensive degeneration, all affected tissues, for instance both the IVD and the facet joint, must be treated to restore the joint to a healthy state.

Pain and pathology associated with the facet joint

Facet joint injury

The facet joint is a common site of traumatic injury. It is estimated to sustain damage in 70% of all subaxial cervical spine injuries (Figure 3-2D).[179] Damage to the cervical spine usually occurs because of single or combined abnormal movements (i.e., flexion, extension, rotation, lateral bending, and compression) primarily due to motor or sports-related accidents.[180,181] Trauma to the cervical spine encompasses a wide spectrum of injuries, ranging from displaced and nondisplaced fractures to subluxed, perched, locked, or dislocated facets, and can be unilateral or bilateral in nature.[122,182] The facet capsule, ligamentum flavum, and disc are the most frequently cited areas of soft tissue disruption by these injuries.[183-185] Cervical injuries most frequently occur at levels C5–C6 and C6–C7[120] and are more common among males,[181,186] people 15–45 years old, and people older than 65. Although the cervical levels are particularly vulnerable, the facet joint is also involved in 22.5% of all of injuries related to the thoracic and lumbar levels.[187]

Facet joint pain

Aside from facet related trauma, where imaging is primarily used as the diagnostic tool, the diagnosis of facetogenic pain is difficult and remains a significant source of controversy within the field.[147,148] Currently, the use of repeated nerve blocks as a diagnostic tool is the most validated approach.[188] Use of this tool reveals that the incidence rate of facet pain in people without evidence of disc herniation, radiculitis, or sacroiliac joint arthritis is 16–40%,[135,137-141,189] 39–67%,[138-140] and 34–48%[139,140,142] in cases of chronic low-back pain, cervical pain**,** and thoracic pain, respectively. In these cases, repeated nerve blocks elicited pain relief response of at least 80%. The prevalence of lumbar facet joint pain also increases with age.[190] The facet is considered a source of back and neck pain inasmuch as pain can be removed by treating the facet joint alone.

Facet joint degeneration

OA of the facet joint is a progressive degenerative disease (Figure 3-2A). The development of OA usually begins with changes in articular cartilage and spreads to the synovium, capsule, subchondral bone, ligaments, and musculature, leading to failure of the entire joint.[191,192] In advanced stages, degeneration is usually not limited to specific sites and tends to affect the entire cartilage surface.[164] There is no consensus on whether the inferior or superior surface is more disease prone. Typical radiographic features of OA include joint space narrowing from cartilage thinning, osteophytes, subchondral cysts, articular process hypertrophy, and subchondral bone sclerosis.[193]

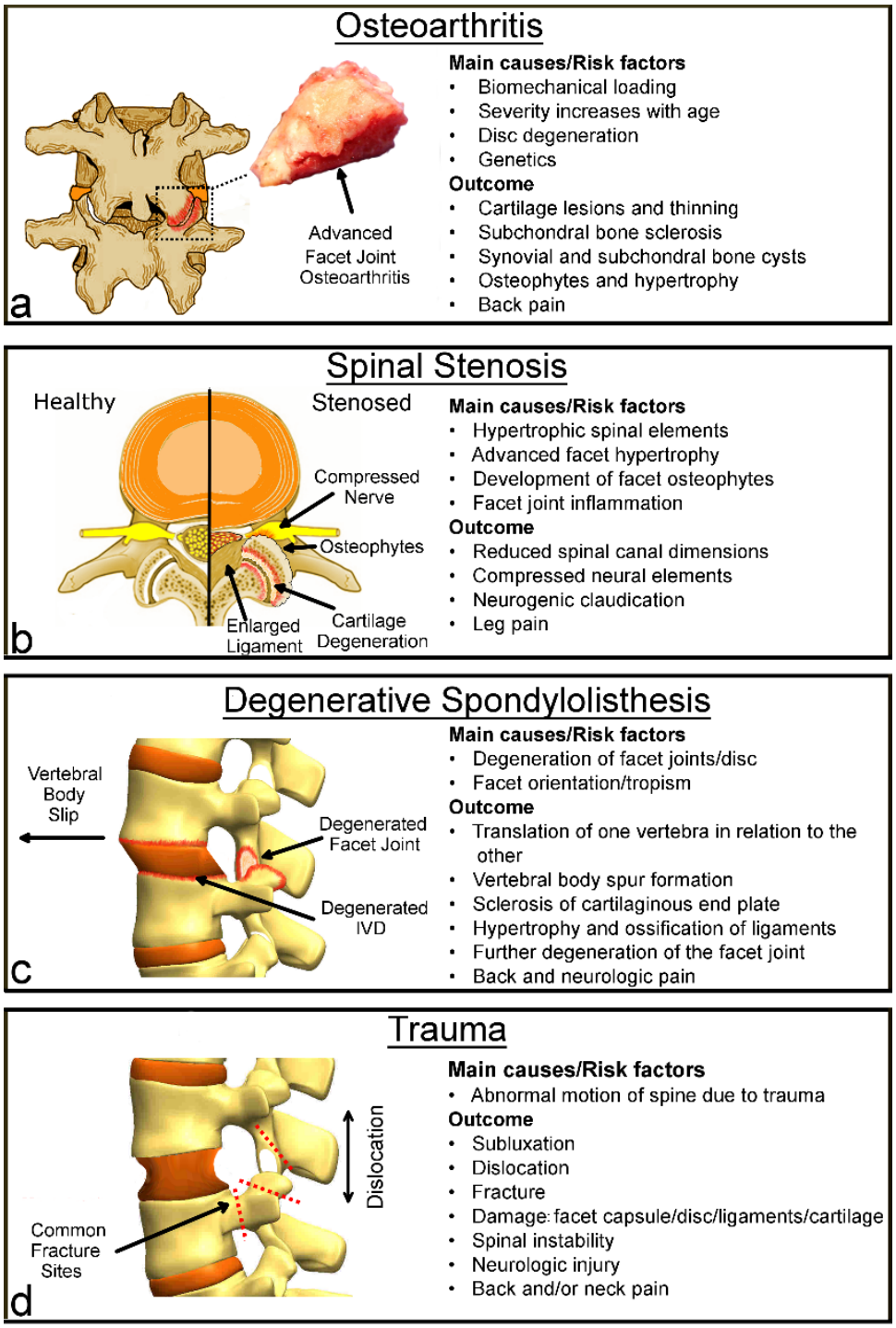

Figure 3-2. Common facet-related problems. Illustration and description of a) osteoarthritis, b) spinal stenosis, c) degenerative spondylolisthesis, and d) trauma, and the associated causes, risk factors, and potential outcome. IVD, intervertebral disc

Facet OA occurs frequently. According to a cadaveric study based on the presence of osteophytes in the lumbar facets, OA (ranging from mild to severe) is a universal finding in adults

older than 60 years, and severity increases with age.[124] A computed tomography (CT)-based study of people with a mean age of 67 years found severe lumbar facet OA in 54% of patients.[125] Prevalence may vary by ethnicity; a recent CT-based study of the lumbar spine of Korean patients reported a prevalence as low as ~18%.[194] Lumbar facet degeneration is most commonly found at L4–L5 and L5–S1; however, all lumbar levels are considered susceptible.[124,194-197] OA's prevalence is strongly associated with increasing age, bone mass index [198,199] and a more sagittal orientation of the joint;[200-202] whether the last of these is a result or cause of degeneration is unknown. Regarding the cervical facet joint, the severity of degeneration increases with age,[203,204] is slightly more common in men, and typically manifests at C2–C3, C3–C4, and C4–C5.[203,205,206] Population-based assessments of the prevalence of OA in the thoracic spine appear to be lacking.

Despite the reported prevalence of facet degeneration, the relationship between facet degeneration and back pain is unclear. It is often assumed that facet degeneration is the source of back pain, however there is little evidence to support such a general claim. For example, in two CT based studies performed by the same authors, facet degeneration was reported to be between 60 and 70%, however an association between degeneration and low back pain could not be established.[193,207] In contrast, more recent CT based studies have concluded that severe degeneration is associated with back pain in older adults and degeneration at spinal levels L4-L5 and L5-S1 correlate with back pain among women.[194] Establishing a distinct relationship between joint degeneration and pain has always been challenging and similar inconsistencies can be found within the context of other osteoarthritic joints within the body, for example the knee. Possible reasons for this have been mainly attributed to the lack of specificity of degeneration on current imaging techniques and the use of unreliable and under-developed grading scales. Although the specificity of diagnostic tools can be improved when detecting facet degeneration, it is important to note that facet degeneration should not be considered synonymous with back pain.

The relationship between the facet joint and intervertebral disc degeneration

Facet joint OA is strongly associated with IVD degeneration due to their intrinsically linked biomechanics. This relationship was originally described as a cascade of degenerative events initiated either by the facet joints or by the disc.[208] It is believed that facet degeneration usually follows disc degeneration, with facet overloading resulting from disc incompetence.[195,197] However, this sequence has been challenged by studies that have found facet joint OA in the absence of disc degeneration.[198,209] For example, one magnetic resonance imaging (MRI)-based study reported that 22% of individuals, recruited as part of the Framingham Heart Study, had facet joint OA without disc degeneration, occurring most frequently at levels L4–L5 and L5–S1.[198] Although this study did not find an association between age and facet joint OA in the absence of disc degeneration, an earlier, cadaveric study found facet OA without disc degeneration to be common among individuals younger than 30 years.[209]

Methods used in studies that examine associations between IVD degeneration and facet OA have been subject to criticism. It has been suggested that studies reporting facet joint OA only in the company of disc degeneration may contain population bias because all study participants had low-back pain and, thus, were not representative of the general population.[198] The ability of current imaging techniques to detect early OA changes in the facet joint has been questioned; such changes may be underreported.[210] A cadaveric study of facet joint OA in association with disc degeneration noted that mild OA occurred in subjects as young as 15 years old,[211] suggesting higher prevalence in adults if modalities other than current imaging techniques are employed. To date, all studies assessing the relationship between disc degeneration and facet joint OA are cross-sectional in design; therefore, an assessment of a causal relationship between them is difficult despite the observation of a strong relation between the two.

Ironically, surgical treatments of degenerated discs can encourage facet OA progression. Despite the popularity of spinal fusion for treating a plethora of pathologies, this technique can

induce adjacent segment disease (ASD). ASD describes degeneration of motion segments adjacent to the treated level, including the development of facet OA.[145,212] The reported annual incidence of symptomatic ASD is the cervical and lumbar spine is 2.9%[213] and 2.5%,[144] respectively, and it has a 10-year prevalence rate of 22.2% and 19.2%. Disc arthroplasty was introduced to preserve motion and to prevent ASD. However, disc prosthesis surgery accelerates the rate of facet OA at the index level,[214] and the incidence of ASD has not changed substantially.[214,215] In this respect, there is insufficient evidence to support disc arthroplasty as being superior to fusion. Despite surgical advancements, current treatments may continue to adversely affect the facet.

Comorbidities

Degeneration of the facet joint plays a significant role in other back-related morbidities, such as degenerative spinal stenosis, spondylolisthesis, and scoliosis. Spinal stenosis usually develops later in life and is the most frequently cited reason for lumbar spine surgery in the United States and some European countries (Figure 3-2B).[127,216-218] Advancement of degenerative spinal stenosis and progression of facet joint hypertrophy with subsequent development of osteophytes can compress the spinal neural elements, leading to neurogenic intermittent claudication.[126,219,220] Degenerative spondylolisthesis (Figure 3-2C) occurs in ~14% of adults,[221] whereas scoliosis affects 2–32% of adults[222,223] and 60% of elderly population.[129] Although the involvement of facet pathology in degenerative spondylolisthesis and scoliosis is not fully understood, facet degeneration and its contribution to spinal instability are thought to be associated with these conditions.[222,224-227] Additional studies to understand facet joint structure–function relationships may further elucidate our understanding of the facet's role in these conditions.

Management of back pain related to facet joint pathology

Conservative management

When analgesics or physical therapy fail to resolve facet related pain, additional conservative interventions are considered. Such interventions include medial branch blocks, intra-articular injections, and radio-frequency denervation.

Medial branch blocks.

Medial branch block injections, also known as nerve blocks, are typically used to diagnose facetogenic pain (Figure 3-3A). Their usefulness in the treatment of facet-related pain has also been investigated, although their effectiveness in providing pain relief is a topic of debate.[147] Injections targeting the medial branch nerve interrupt pain signal transmission. Some studies report greater than 50% pain relief in ~85% of patients after lumbar facet joint nerve blocks,[228,229] whereas other studies report 50% pain relief after a single or double nerve block in 40–58% of patients.[230,231] The duration of these interventions is temporary, as it remains effective in fewer than 10% of patients after 1 year.[232] Medial branch blocks are typically indicated only for diagnostic purposes; additional data would be useful to evaluate their therapeutic effectiveness.

Intra-articular injections (or facet block injections)

Intra-articular facet injections (Figure 3-3A), typically consisting of anesthetics and corticosteroids,[233] have been evaluated for their potential effectiveness in mitigating facetogenic pain. The effectiveness of these injections has become a subject of controversy. Most systematic reviews and high-level randomized control trials conclude that there is no benefit in pain and functional status from intra-articular injection compared with placebo.[234-237] The use of ultrasonography to accurately guide injections has recently become more popular than fluoroscopy, as ultrasonography appears to be more effective.[238] However, any potential positive effect of these injections is considered temporary and requires multiple subsequent injections to

maintain relief. Thus, currently, there is not enough evidence to recommend their use for the treatment of facetogenic pain.

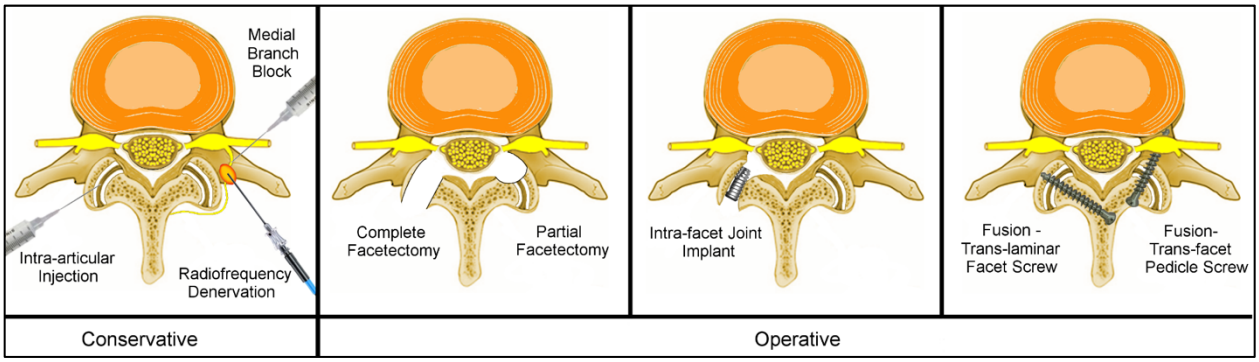

Figure 3-3. Conservative and operative management strategies for facet joint pathologies, including (a) injections, (b) facetectomies, (c) fusion systems, and (d) implants.

Radio-frequency denervation of the facet joint

Radio-frequency denervation is considered the most successful treatment approach for chronic facetogenic pain (Figure 3-3A).[233] Briefly, this technique uses radio-frequency energy, delivered percutaneously, to heat and temporarily damage medial branch fibers, preventing the transmission of pain signals originating from the facet.[239] When compared with placebo, radio-frequency denervation provided improved back motion, pain relief, and functional outcomes over a 1- to 6-month period.[240-242] However, several studies found no difference in pain relief between this technique and a sham treatment. Reasons cited for studies that do not find a significant association between pain relief and radio-frequency often include the use of inconsistent criteria for patient selection as well as differences in the positioning of the electrodes.[243,244] These results imply that the efficacy of radio-frequency denervation may be adversely affected by patient- and technique-specific factors. In general, radio-frequency denervation is widely accepted as the most effective intervention for facetogenic pain; however, most reports emphasize that pain relief from this technique is temporary.[147,242,245]

Operative management

If conservative management fails, operative management can be considered, including facet joint excision as well as fusion and replacement systems. An increasing number of newly introduced facet interventions exist, indicating a growing appreciation for the contribution of the facet joints in back pain. Considering that many of these interventions have not been fully developed, clinical evidence is often lacking and, thus, assessment of their potential benefits has to rely on biomechanical studies. However, despite the importance of biomechanical studies in research and development of new interventions, they provide a limited indication of the expected clinical performance and, therefore, results should be interpreted with caution.

Facet joint excision (facetectomy)

Facet joint excision, including both partial and complete facetectomy, is usually performed when neurological symptoms are present. Nerve root impingement due to stenosis is common (Figure 3-3B), but can also occur due to trauma. Facetectomy is rarely performed for degenerative facet joints alone and is considered an important adjunct to operative management.[147]

Partial facetectomy involves the excision of the medial facet portion with the lateral attachments of the ligamentum flavum. The total removal of the joint, as well as the ligamentum flavum, is considered a complete facetectomy. The main indication for this technique is persistent degenerative spine disease, associated with advanced facet joint hypertrophy and osteophytes, that does not respond to conservative treatments.[234,246] Because facetectomy is typically combined with other techniques, it is challenging to evaluate its efficacy. One clinical study reported that following a partial facetectomy alone, at least 70% of patients no longer had pain radiating to the lower limbs.[247]

The main concern with either partial or complete facetectomy is resulting spinal instability. Using a finite-element model, a comparison between partial and complete facetectomy showed that spinal instability was associated with the extent of resection.[248] In addition a biomechanical study found that with substantial facet resection, the main concern is resulting iatrogenic spinal

instability, which can reduce failure strength by up to 50%.[249] Therefore, facetectomy is frequently accompanied by fusion techniques that restore spinal stability.

Facet joint fusion systems

Facet joint fusion is considered advantageous because it can theoretically ensure spinal stability postfacetectomy.[250] Furthermore, it is a relatively straightforward technique with minimal risk of complications.[251] Several facet joint fusion systems are used clinically, yet the published research detailing patient outcomes for these systems is limited. Spinal instability is the primary indication for fusion which can be caused by facet trauma, as well as following decompression surgeries in cases of symptomatic spinal stenosis, spondylolisthesis etc.

Translaminar facet screws (TLFSs), placed into the facet joints via the lamina (Figure 3-3C), are considered important elements to enhance fusion.[252] In a cohort study of 120 patients that used the Core Outcome Measure Index (ratings of leg and back pain intensity, function symptom-specific well-being, general quality of life, and social and work disability) to assess outcomes of TLFS fixation versus transforaminal lumbar interbody fusion, found that both procedures had similar scores (3.6 versus 4.0) and 78% of patients in both groups reported a good global outcome (the operation helped or helped a lot). However, ~18% of the patients who underwent TLFS fixation required additional surgery, mainly due to pseudoarthrosis or ASD, in a mean period of 3.4 years.[253]

Transfacet pedicle screws (TFPSs), placed through the facet joint extending into the pedicle, provide another alternative to the traditional pedicle screw fixation technique (Figure 3-3C).[254] According to biomechanical studies, both techniques are reported to have comparable strength in both thoracic and lumbar spine fixation.[254,255] The minimally invasive nature of this technique is promising, but additional long-term data are necessary to evaluate its safety and ability to achieve solid fusion.[256,257]

Intrafacet joint implants (wedge body/spacers) inserted into the facet joint space to engage the opposing joint surfaces can provide necessary distraction for stabilization (Figure 3-3D).[258] A

laboratory studies involving the assessment of biomechanical function found that the implants could also improve rotational stability.[259] A clinical study involving placement of facet spacers in the cervical facet as a treatment for cervical spondylotic disease was assessed using the Odom Criteria and an excellent outcome (i.e., all preoperative symptoms and abnormal findings improved) was reported for 25 out of 36 patients following surgery.[260] Despite these promising results, studies that report the long-term benefits of implants involving a large number of patients are required for further validation of the device.

Facet replacement systems

In the last decade, the increasing need for more effective management of facetogenic pain and thorough decompression without fusion-associated morbidity has led to the development of techniques akin to total knee or hip arthroplasty. Similar to the operative management techniques mentioned above, limited data have been published; thus, conclusions about the efficacy of these systems are largely based on biomechanical studies and may be premature.

The anatomic facet replacement system (AFRS) is composed of two separate implants that are fixated with pedicle screws to the vertebra and with a cross-linking component to one another. As shown with a finite-element model, the implant demonstrated kinematics similar to those of the intact facet joint.[261] No clinical studies have been reported so far.[261]

Biomechanical test results indicate the total facet arthroplasty system (TFAS) also has promise to restore facet joint motion and provide stabilization.[262-264] Fixed to the vertebral body with pegs, this device incorporates a sphere sliding along a curved plate to preserve joint movement and articulation.[262] The TFAS allows for more motion in all directions compared with a rigid fixation system.[262] Despite these promising preliminary studies, no clinical data have been reported yet.

The total posterior arthroplasty prosthesis, commonly referred to as TOPS, is a posterior dynamic fixation device that involves removal of all of the posterior elements of the spine, including the affected facet joints and spinous process. A biomechanical evaluation of the device

found that it can restore lateral bending and axial rotation kinematics of the intact spine.[265] In a preliminary clinical report, TOPS was associated with a decrease in pain of 76% after 1 year.[266] Outcomes were maintained at 7 years' follow-up, as indicated by the Oswestry disability index of 7.8 at 7 years versus 49.1 preoperatively. However, 1 out of 10 patients experienced a device-related failure 3 months after surgery.[267] Further research is necessary to evaluate the exact role and applicability of this system in facet joint degeneration.

In addition to the larger arthroplasty systems described above, a facet joint resurfacing system has also been proposed as a solution to facet joint degeneration. Limited preliminary data report improved pain and functionality at 24 months after surgery.[268] One out of eight patients (12.5%) suffered an implant dislocation that required reoperation with posterior lumbar interbody fusion, indicating that additional studies are needed to evaluate safety.

Future directions: could tissue engineering provide a new treatment strategy for facet-related morbidity?

Despite the facet's contribution to the economic and social burdens of back pain, no treatment can provide an effective, long-term, restorative solution for this joint. Tissue engineering, however, offers promise for treating maladies in numerous tissues. Specifically, engineering articular cartilage has long been a priority, considering its susceptibility to pathology, its innate inability to regenerate, and the failure of current treatments to produce robust neotissue.[8] Within the last two decades, investigations of various cell sources, biomaterials, and stimuli have brought the field closer to functional biologic replacements of both cartilage and underlying bone.[25] Yet, despite similar joint pathology, facet tissue engineering remains almost completely unexplored (Table 3-2).[269] Thus, the application of tissue engineering principles to the facet may provide a much-needed, long-term, motion-preserving solution.

Table 3-2. A comparison of the facet joint to the knee

	Knee	Facet Joint	Refs
Articular Surface Area	Femur: 29.5 ± 2.5 cm^2 Tibial plateau: 22.5 ± 2.4 cm^2	Inferior: 0.69-1.97 cm^2 Superior: 0.74-2.12 cm^2	155,270
Articular Cartilage Properties	Thickness: 2-3 mm GAG/WW: 5-10% Collagen/WW: 15-20% Aggregate Modulus: 80-2000 kPa Young's Modulus: 5-25 MPa Tensile Strength**: 3-11 MPa	Thickness*: 0.49 ± 0.10 mm GAG/WW*: 3.8 ± 1.3% Collagen/WW*: 16.8 ± 2.6% Aggregate Modulus*: 554 ± 13 kPa Young's Modulus*: 10.1 ± 8.1 MPa Tensile Strength*: 4.44 ± 2.4 MPa	165,271-273
Contact Forces	Medial Condyle: ~1750 N Lateral Condyle: ~500 N Patellofemoral: ~925 N	Cervical†: ~17-40 N Thoracic: No Data Lumbar††: ~10-120 N	159,160,162,163,274
Reasons for Hospital Visits	Degenerative changes and traumatic events due to, for example, focal lesions, osteochondritis dissecans, OA, meniscus tears, ligament tears, etc. (**1.8%** of hospital visits due to knee symptoms)	Degenerative changes and traumatic events due to, for example, spinal stenosis, spondylolisthesis, traumatic injury, whiplash, etc. (**1.3%** of hospital visits due to back symptoms)	275
Example Treatments	NSAIDs, intra-articular injections, microfracture, ACI, MACI, meniscectomy, and total knee arthroplasty	NSAIDs, intra-articular injections, medial branch blocks, partial facetectomy, spine fusion, and arthroplasty systems	25,149
PubMed Searches‡	799 results for "knee, tissue engineering" 3815 results for "knee, properties" 521 results for "knee, characterization"	6 results for "facet joint, tissue engineering" 39 results for "facet joint, properties" 13 results for "facet joint, characterization"	

*Facet joint cartilage properties from canine tissue. **Knee cartilage tensile strength from equine tissue. †Forces measured with strain gauges and neural network models at C5-C6 in human cadaveric spines (C3-T1). ††Forces measured with pressure sensors at L5-S1 in human cadaveric spines (L5-S1). ‡PubMed searches did not include MeSH terms; GAG, glycosaminoglycan; WW, wet weight; OA, osteoarthritis;

As discussed above, the facet joint is part of a highly complex system that includes an IVD, ligaments, musculature, and so forth, all of which are susceptible to both degenerative changes and trauma. Therefore, the proposal to tissue-engineer a replacement for this joint cannot currently be considered an all-encompassing solution for all facet-related issues. Instead,

to begin with, one can consider facet joint trauma and spinal afflictions such as spondylolisthesis as targets for tissue engineering, as these indications would benefit from the development of a biological replacement. As described above, in these cases, facet degeneration and concomitant hypertrophy are key contributors to nerve impingement, necessitating the complete or partial removal of facets and/or laminae. The development of a tissue-engineered replacement can be considered for regaining spinal stability and eliminating fusion. As mentioned above, these indications are already the target of at least four facet arthroplasty systems that are currently in clinical trials. Thus, a biological replacement for the facet would provide a novel solution to an already well-recognized and significant problem.

Such a replacement may also offer a long-term solution for facet-mediated pain in the absence or presence of disc pain. Although it is difficult to isolate the facet joint as the sole source of axial pain, use of the best diagnostic tools available has revealed that its prevalence is significant. In these cases, replacement of the facet with a biological solution may provide a longer-term treatment strategy compared with currently available treatments. In addition, considering that facet OA is currently a contraindication to disc replacement, the development of a biological facet replacement may become an adjunct to biological disc replacement. Finally, as the technology matures, a tissue-engineered solution may serve to target the facet in a broader context and may extend to the treatment of other facet-related issues. The following section discusses the criteria, strategies, and challenges associated with tissue engineering a facet cartilage replacement, as well as a total joint replacement.

Key criteria to engineer facet cartilage

Creating a facet cartilage replacement through tissue engineering can restore joint function and treat pathology of the joint. It is increasingly recognized that developing a biomimetic replacement is integral to achieving functionality.[25] On the basis of what is known about facet cartilage, it may possess properties more amenable to functional tissue engineering than other synovial joints

(e.g., the knee). Facet cartilage is thinner and has a much smaller surface (Table 3-2), so it requires less neotissue volume, potentially negating nutrient diffusion issues associated with engineering thicker cartilage.[276] Furthermore, it may be possible to engineer an entire synovial joint surface, not merely cartilage constructs for focal defects, which would avoid well-known integration issues between native and engineered cartilage.[277] Also, the facet experiences lower compressive loads than the knee (Table 3-2). In fact, the range of compressive stiffness values in engineered cartilage already approaches those observed in native facet cartilage of several animal models.[164,278] In addition, a recent report demonstrates that the mechanical, biochemical, and histological properties of various animal models are not significantly different between the opposing facet joint surfaces and spinal levels in which they are located.[164] Such uniformity in properties avoids the need to tissue-engineer site-specific replacements and reduces the complexity of the task. Although these design aspects bode well for potentially engineering a facet cartilage replacement, further design criteria must first be established.

Although data exist describing the human facet's anatomical and geometric characteristics (Table 3-1), the properties of human facet articular cartilage have not been reported. The ubiquitous nature of facet joint degeneration has rendered the acquisition of healthy human spines a challenge. As such, an appropriate large animal model for the facet has yet to arise. Not only are these properties necessary for the design of a functional facet replacement, they would also contribute to our understanding of the facet's structure–function relationships and pathophysiology. The articular cartilage of canine, porcine, leporine, primate,[164] and equine models has been extensively characterized;[164] thus, significant progress has been made in this area. However, deeper analysis of facet tissues in humans will be paramount for establishing design criteria toward engineering functional tissue replacements.

Cell sources for tissue-engineered facet neocartilage also need to be explored. As mentioned above, the volume of required engineered tissue is small; thus, the necessary number of initial cells may be lower. However, using an autologous source of chondrocytes from healthy

facet cartilage, a strategy commonly used in the knee, may not be an option. Several confounding factors, such as small surface area and facet cartilage degeneration, limit the applicability of this strategy. Therefore, alternative cell sources that are currently being researched for replacements of other joint cartilage—including autologous chondrocytes harvested from other sites in the body, allogeneic chondrocytes, or mesenchymal stem cells (MSCs) (e.g., marrow-, synovial membrane–, or adipose-derived)—may be viable for tissue-engineering a facet cartilage replacement.

Potential strategies to engineer facet cartilage

To engineer a biological replacement for the entire facet joint, there are numerous important considerations. To achieve a positive clinical outcome, tissue-engineered facet cartilage must allow for replication of tissue function as well as maintenance of long-term stability after implantation. The following is a discussion of the key aspects that should be considered when developing a strategy to tissue-engineer the facet joint.

Scaffold based

Traditional tissue-engineering approaches often use biodegradable, polymeric scaffolds to mimic the three-dimensional (3D) structure of native cartilage (Figure 3-4A). Scaffolds provide temporary mechanical support and biological cues for embedded cells to maintain phenotype and promote growth of neocartilage. Many scaffold-based approaches are currently being investigated, some of which are available clinically for treatment of the knee and other joints. For example, MSCs harvested from the iliac crest and embedded in collagen or hyaluronic acid matrices are beneficial for treatment of talus osteochondral defects.[279] Also, autologous matrix-induced chondrogenesis (AMIC) is considered a promising one-step cartilage repair technique that combines microfracture with the implantation of an acellular biomaterial.[280] In addition to these, scaffolds made of polylactides and/or polyglycolides result in tissue with similar histomorphology to native

cartilage.[281,282] While these scaffold-based methods appear promising, their durability warrants further investigation to assess long-term success.

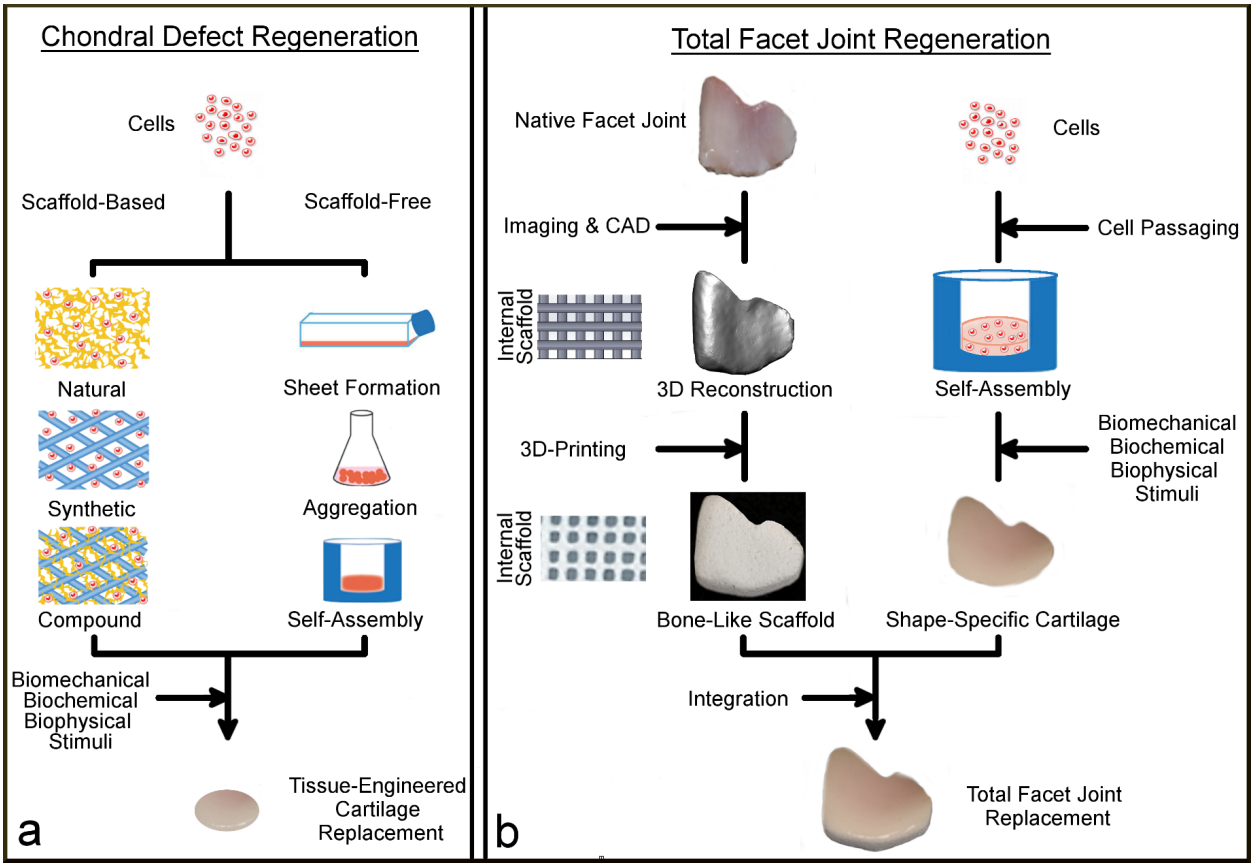

Figure 3-4. Tissue-engineering the facet joint. Potential strategies towards regeneration of a) facet cartilage to treat chondral defects and b) the joint to treat total joint afflictions. Strategies to tissue-engineer a cartilage replacement can be scaffold-based, requiring the use of a natural, synthetic, or compound scaffold, or can be scaffold-free, using cell sheet and aggregate engineering techniques or the self-assembly process. Many of these strategies may also have the potential to engineer the entire facet joint surface. One such strategy, the self-assembly process, generates neotissue without a scaffold and without external energy input, thus mimicking developmental events. Shape-specificity is also achievable using this method. Shape-specific self-assembled cartilage integrated with 3D-printed bone could represent the first biologic total joint replacement, which would be an important step in advancing the field of tissue-engineering. CAD, computer aided design.

Scaffold free

A promising, emerging paradigm that may potentially be applied to facet cartilage is scaffold-free tissue engineering (Figure 3-4A). Scaffold-free strategies aim to produce tissues by mimicking developmental processes while also reducing the risk of scaffold degradation toxicity, stress shielding, and cell-signaling hindrance. Revaflex, which consists of an expanded sheet of juvenile allogeneic chondrocytes, is in clinical trials for use in cartilage repair in the knee, and preliminary

results have been positive.[49] Similarly, Chondrosphere, a product that is also targeted for the knee, uses only autologous cell aggregates and is also in clinical trials. At a 1-year follow up, all assessment scores were significantly increased.[283] An approach known as the self-assembling process yields neocartilage that, when treated with biochemical and biomechanical stimuli, has compressive and tensile properties approaching those of native knee cartilage.[55,278] Considering that functional properties of self-assembled cartilage are similar to those of animal facet cartilage,[55,165,278] this method may have the capacity to regenerate human facet cartilage. Furthermore, self-assembly allows for control over tissue shape, potentially leading to replication of the complex curvature of the facet's articular surface.[284] Although these scaffold-free strategies are promising, long-term clinical trials need to be performed to assess their efficacy.

Key criteria for an engineered total facet joint

A challenge for tissue-engineered facet cartilage may involve difficulty accessing the joint. Due to the facet's anatomical positioning, small size, and high congruence, distracting and/or disarticulating the joint using current surgical equipment is challenging. This problem is exacerbated by the facet's tendency toward hypertrophy, often resulting in excessive bony overgrowth. Therefore, surgical instruments and techniques need to be developed in parallel to match the needs of this treatment strategy. Encouragingly, total facet joint arthroplasty systems and associated surgical techniques have already been developed and are currently in clinical trials. Therefore, these techniques could be adopted and refined to implant a biological facet replacement. Interestingly, a replacement of the entire facet (opposing articular surfaces and underlying bone) may obviate the issues associated with accessing the articular surface while addressing the overarching problem of joint degeneration. Of course, the degree to which the facet is degenerated and the quality of the remaining bone for the purposes of attachment would have to be assessed on a patient-specific basis. Indeed, due to the facet's favorable design (discussed above), it could be a suitable candidate for the first total biologic joint replacement.

To successfully engineer a total facet replacement, the implant must fully function upon implantation, conform to the facet shape, and be fixed securely. Current chondral and osteochondral engineering strategies rely on the surrounding native tissue for structural support, fixation, cells, and bioactive factors. Therefore, a design for a readily implantable total biologic joint necessitates engineering and maturation of both cartilage and bone layers within a single integrated structure in vitro. Like cartilage regeneration strategies, both layers need to mimic properties of their respective native structures. Furthermore, implant fabrication processes need to be capable of replicating facet geometry, which is known to be level and patient specific.[156] Other considerations, such as implant fixation and development of appropriate surgical techniques, would need to be addressed. However, current osteochondral engineering strategies developed primarily for repairing focal defects in the knee, in particular those involving 3D printing, may hold translational potential for entire facet joint regeneration.

Envisioning an engineered total facet joint

A potential approach to engineering a total biologic joint prosthesis may involve an in vitro, self-assembled, shape-specific cartilage construct integrated with a 3D-printed shape–specific, underlying bone-like substrate (Figure 3-4B). As discussed above, native cartilage properties have been achieved in vitro via self-assembly in concert with various stimuli; thus, the self-assembling process can be considered a promising option for the creation of a biomimetic cartilage replacement.[55,278] Typically, engineering bony tissue requires the use of a scaffold. Unlike conventional scaffold fabrication methods, 3D printing can precisely control external geometry as well as internal pore size, porosity, and spatial distribution to meet design needs.[285] Ceramics, known for their excellent bioactivity, osteoconductivity, and compositional similarity to bone, have successfully been 3D printed and shown to support bone formation.[286] Thus, integration of self-assembled cartilage with 3D-printed ceramic scaffolds may be an attractive design for a total biologic joint prosthesis. Furthermore, precise control of both the internal bone

architecture and the external implant shape may enhance integration between cartilage and bone, as well as enable the design of a fixation method. Although many current tissue-engineering strategies would need refinement to account for facet-specific design criteria and tissues such as the fibrous capsule, tissue engineering may provide a durable, motion-preserving treatment modality for this troubled joint.

Conclusion

In a healthy state, facet joints facilitate and guide spinal motion, ensuring proper kinematics at each level. However, since facets are the locus of highly significant pathology, pain, and disability, new management strategies continue to be explored. Unfortunately, a durable, motion-preserving solution still has not been identified. While continued characterization of facet structure–function relationships and refinement of tissue-engineering techniques are necessary, a biologic facet joint replacement may one day emerge as an all-inclusive treatment for local facetogenic trauma and degeneration as well as being an important aspect toward solving more pervasive issues within the spine.

CHAPTER 4 The tribology of cartilage: mechanisms, experimental techniques, and relevance to translational tissue engineering

Abstract

Diarthrodial joints, found at the ends of long bones, function to dissipate load and allow for effortless articulation. Essential to these functions are cartilages, soft hydrated tissues such as hyaline articular cartilage and the knee meniscus, as well as lubricating synovial fluid. Maintaining adequate lubrication protects cartilages from wear, but a decrease in this function leads to tissue degeneration and pathologies such as osteoarthritis. To study cartilage physiology, articular cartilage researchers have employed tribology, the study of lubrication and wear between two opposing surfaces, to characterize both native and engineered tissues. The biochemical components of synovial fluid allow it to function as an effective lubricant that exhibits shear-thinning behavior. Although tribological properties are recognized to be essential to native tissue function and a critical characteristic for translational tissue engineering, tribology is vastly understudied when compared to other mechanical properties such as compressive moduli. Further, tribometer configurations and testing modalities vary greatly across laboratories. This review aims to define commonly examined tribological characteristics and discuss the structure-function relationships of biochemical constituents known to contribute to tribological properties in native tissue, address the variations in experimental set-ups by suggesting a move toward standard testing practices, and describe how tissue-engineered cartilages may be augmented to improve their tribological properties.

Chapter published as: Link JM*, Salinas EY*, Hu JC, Athanasiou KA. The tribology of cartilage: mechanisms, experimental techniques, and relevance to translational tissue engineering. Clinical Biomechanics. (*authors contributed equally to this work) (online ahead of print 2019)

Introduction

Diarthrodial joints, such as the knee, contain hyaline articular cartilage, fibrocartilage, and intra-articular space filled with synovial fluid. Hyaline articular cartilage is a highly hydrated, anisotropic tissue composed primarily of collagen II, proteoglycans, and chondrocytes that covers the ends of long bones and acts as a load-bearing, lubricated surface during joint articulation. [272] Fibrocartilage structures, such as the meniscus in the knee, confine motion, dissipate loads, and contribute to essentially frictionless articulation of diarthrodial joints as well. Synovial fluid is confined to the joint space by the articular capsule and contains macromolecular components, such as superficial zone protein (SZP) and hyaluronan, which are essential to joint lubrication. [287,288] This review will focus on the articular surfaces of hyaline articular cartilage and the knee meniscus, as well as synovial fluid, since they are the components responsible for maintaining low-friction motion and lubrication, or tribological functions, in diarthrodial joints.

Tribology is the study of the interactions between two surfaces moving relative to one another. While it traditionally refers to the study of non-biological materials, tribological principles have been extended to understand the loading environment of diarthrodial joints. The quantitative properties when studying the tribology of diarthrodial joints are surface roughness, R_a, and coefficient of friction, μ. This review will utilize both of these properties for evaluation of tribological properties of the native and engineered tissues described in subsequent sections. A crucial characteristic of native hyaline articular cartilage is its ability to exhibit minimal friction at joint-gliding speeds between 0-0.03m/s when subjected to loads that are five times bodyweight.[289,290] The replication of tribological properties is crucial to the translation of tissue-engineered articular cartilages, yet they remain under-characterized in tissue-engineered constructs. For instance, a PubMed search for “articular cartilage lubrication” yielded 422 results, but a search for “articular cartilage mechanical properties” produced 1,789 references. Building on some of the tissue-engineering strategies described in this review to improve the tribological properties of engineered constructs could decrease this discrepancy.

It is predicted that by the year 2050 osteoarthritis, an articular cartilage degeneration disease, will affect at least 130 million people world-wide.[291] Articular cartilage degeneration causes pain and inflammation of the joint, loss in mechanical function, as well as loss in tribological function. As health care technologies expand and life expectancy in the United States consequently increases, incidences of articular cartilage degeneration will also increase, necessitating viable treatment options such as implantable tissue-engineered articular cartilage constructs with adequate mechanical and tribological properties.

In this review, the components, such as SZP and hyaluronan, and mechanisms, such as shear-thinning of synovial fluid, known to contribute to the tribological properties of articular cartilages will be described. The pathologies that compromise articular cartilage tribological function will also be discussed. Specifically, this review will delve into how surface roughness, coefficient of friction, and lubrication regimes affect and are affected by the state of biochemical components known to regulate tribological function. Tribological properties will be compared quantitatively by looking at the spread of the coefficient of friction obtained across laboratories using a variety of tribometer modalities. Although there is a consensus toward testing articular cartilages under boundary lubrication regimes, variations exist from laboratory to laboratory in terms of tribometer configurations, testing substrates, and lubricants. A recommendation will be made toward reconciling and standardizing tribological measurements for articular cartilages. Therapeutic targeting of tribological properties will be presented and discussed, including the current state of recapitulating tribological properties in tissue-engineered articular cartilages for translation. Finally, the areas of articular cartilage tribology that remain understudied will be presented.

Commonly examined tribological characteristics in cartilage

The two quantitative tribological characteristics measured in both native and engineered articular cartilage are surface roughness and coefficient of friction. In this section, surface roughness and coefficient of friction are defined, and the values of native articular cartilage are presented. Finally, the coefficient of friction and surface roughness of synthetic materials are juxtaposed to native cartilage tribological properties for added context and perspective.

Surface roughness

A common measure of surface roughness, R_a, quantifies asperities on the articulating surface. Surface roughness is derived by measuring the average height deviation from the surface midline and is typically reported in nanometers.[292] Surface roughness ranges from 1-150 nm in native hyaline articular cartilage across the body. In comparison, the femoral head components of total hip replacements typically range from 40-200 nm in surface roughness.[293-295]

Coefficient of friction

Coefficient of friction, μ, refers to the ratio of the horizontal force needed to move two surfaces across each other relative to the normal force. Coefficient of friction is the tribological property most studied in the field of articular cartilage. In both native and experimental settings, coefficient of friction is dependent on the articular surface roughness, normal load, lubrication mode, as well as experimental conditions such as testing modality. Coefficient of friction may be determined under static or kinetic conditions. Furthermore, the initial and equilibrium coefficient of friction can also be measured. The coefficients of friction that will be examined in this review were obtained under kinetic, equilibrium conditions in the boundary lubrication regime. The coefficient of friction of native articular cartilage has been reported to range broadly from 0.001-0.45 (Table 4-1).[272,296,297] For comparison, typical new and cleaned rolling bearings offer a coefficient of friction

of 0.005, indicating that articular cartilage can be more frictionless than a man-made bearing under certain conditions.[298]

Tribological structure-function relationships in diarthrodial joints

In this section, the cartilage components that are essential for tribological function are identified. The capacity of lubricin and hyaluronan to modify the tribological characteristics of a diarthrodial joint is described. The importance of the interaction between lubricin and hyaluronan in the synovial fluid is also described and further discussed in the context of different lubrication modes. Lubrication modes, including boundary, mixed, elastohydrodynamic, and hydrodynamic, are defined, and the loading conditions that yield these lubrication modes are also established.

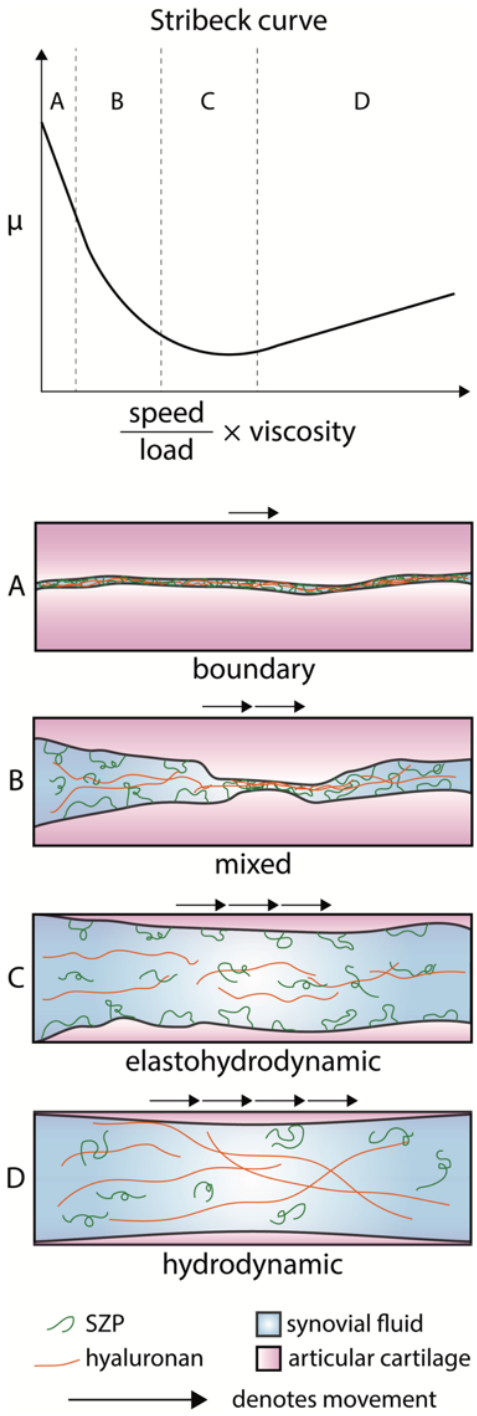

Figure 4-1. Lubrication regimes (A-D) within a synovial joint. The speed of articulation, magnitude of load, and fluid viscosity determine the mode of lubrication and affect the coefficient of friction (μ), as demonstrated in the Stribeck curve. Boundary lubrication (A) involves interaction of both articular surfaces resulting in a lack of fluid film. Mixed lubrication (B) combines aspects of boundary lubrication and fluid film lubrication. Elastohydrodynamic lubrication (C) is characterized by both a fluid film and deformation of articular cartilage. Hydrodynamic lubrication (D) involves a fluid film alone.

Cartilage components essential for tribological function

Among the components of diarthrodial joints, synovial fluid and the articular cartilage surface, or lamina splendens, play particularly important roles in cartilage lubrication.[272] Two key synovial fluid constituents are hyaluronan and SZP.(Majd et al., 2014). Hyaluronan, among other roles, gives rise to the shear-thinning properties of synovial fluid, critical to fluid film lubrication in articulating joints.[299] Matrix molecules present at the articular cartilage surface, primarily collagen II, can form molecular associations with SZP and hyaluronan in synovial fluid.[300,301] These complexes at the cartilage surface create a "sacrificial layer" vital in mediating boundary lubrication.[302] Due to their vital functions in mediating cartilage lubrication, SZP and hyaluronan are discussed in more detail below.

Lubricin/SZP/proteoglycan 4: Lubricin, SZP, and proteoglycan 4 (PRG4) are terms often used interchangeably throughout the literature to describe one of the critical lubricants in diarthrodial joints. While each is a product of the *PRG4* gene, they are distinct macromolecules of varying sizes (SZP: 345 kDa, lubricin: 227 kDa, PRG4: 460 kDa).[303] However, because it is difficult to distinguish unique functions among them, this review will refer to the products of the *PRG4* gene collectively as SZP. This is a mucinous glycoprotein secreted into synovial fluid by superficial zone chondrocytes and synoviocytes, shown to mitigate superficial zone cartilage damage and chondrocyte death.[288]

The globular N- and C- termini of SZP can interact with a variety of molecules at the cartilage surface, such as collagen II, fibronectin, and cartilage oligomeric protein to form a lubricating boundary layer.[288,300] SZP has also demonstrated strong adsorption to denatured, amorphous, and fibrillar collagen II, suggesting its adsorption is not dependent on the conformation of collagen.[304] Meniscus surfaces can also benefit from this lubricating layer, because SZP localization at its surface has been observed.[305] In general, SZP has been shown to reduce coefficients of friction across a variety of tissues and materials.[288,303,304] Its function can be further enhanced in the presence of hyaluronan, with which it can interact to form complexes.[306]

Hyaluronan: The non-sulfated glycosaminoglycan (GAG) hyaluronan is a large polysaccharide (2000 kDa in diarthrodial joints) that is found both floating freely in synovial fluid and as part of the extracellular matrix of articular cartilage.[307] GAGs are thought to be responsible for interstitial fluid pressurization in articular cartilage, and the depletion of GAGs, in particular hyaluronan, has adverse effects on its frictional and lubricating properties.[308,309] For example, gradually removing hyaluronan from a lubricating solution was shown to increase the coefficient of friction of the native articular cartilage surfaces being examined.[308] Hyaluronan in a matrix is known to act as a viscoelastic material, and, because of its large size, hyaluronan induces steric hindrance that attenuates fluid flow within a solution.[299,309,310] Since these properties of hyaluronan contribute to joint tribology, several hyaluronan-based clinical products have been developed to mitigate the symptoms of osteoarthritis.[299,311]

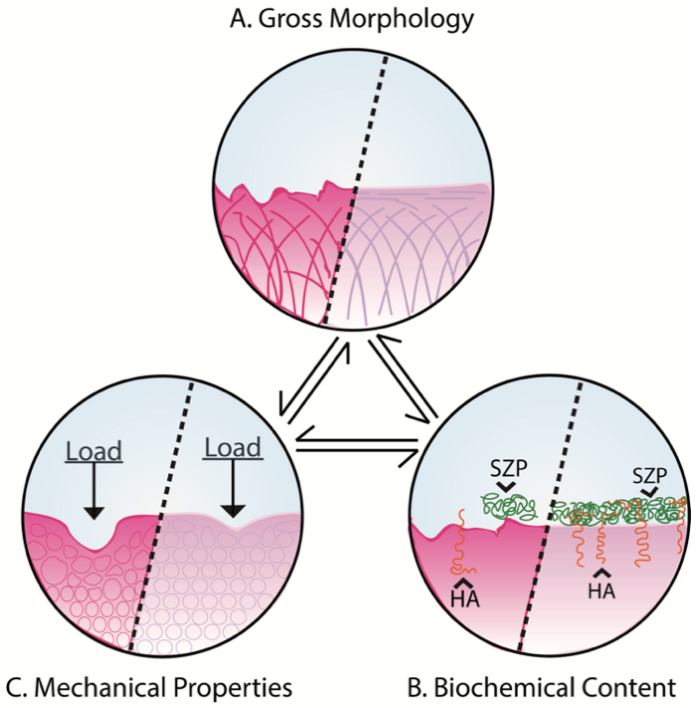

Figure 4-2. A summary of how the gross morphology, biochemical content, and mechanical properties of cartilage feed into the maintenance of tribological function in the diarthrodial joint. In all panels, diseased cartilage is shown on the left and healthy cartilage is shown on the right. The gross morphology (A), biochemical content (B), and mechanical properties (C) of diseased cartilage (left) are compromised in comparison to healthy cartilage (right).

In experimental laboratory settings, hyaluronan has been studied as a joint lubricating agent using cartilage-cartilage, cartilage-steel, and cartilage-glass interactions.[308,312,313] Furthermore, hyaluronan alone, and its complexing with SZP, contribute greatly to the shear-thinning behavior of synovial fluid, suggesting that a healthy joint necessitates both hyaluronan and SZP for tribological function.[306] Therefore, when studying and characterizing the tribology of diarthrodial joint tissues, both hyaluronan and SZP should be present in the testing solution if one is to expect coefficients of friction approximating *in vivo* values.

Table 4-1. Coefficients of friction (μ) for native articular cartilage and meniscus in the boundary lubrication regime

Tissue type	Species	Modality	Substrate	Lubricant	μ*	Reference
AC	ovine	pin-on-plate	stainless steel	FBS	0.46	(Kanca et al., 2018b)
AC	ovine	pin-on-plate	AC	FBS	0.03	(Kanca et al., 2018b)
AC	human	pin-on-plate	glass	PBS	0.22	(Middendorf et al., 2017)
AC	porcine	pin-on-plate	glass	SF	0.001-0.11	(McCutchen, 1962)
AC	bovine	ball-on-disc	glass	N/A	0.19	(Blum and Ovaert, 2013)
AC	bovine	rolling-ball-on-disc	glass	PBS	0.12-0.16	(Jia et al., 2016)
AC	bovine	ball-on-disc	glass	N/A	0.121	(Grad et al., 2012)
AC	bovine	pin-on-plate	stainless steel	PBS	0.025	(Moore and Burris, 2015)
AC	bovine	pin-on-plate	glass	PBS	0.13	(Oungoulian et al., 2015)
AC	bovine	pin-on-plate	CoCr HC	PBS	0.15	(Oungoulian et al., 2015)
AC	bovine	pin-on-plate	CoCr LC	PBS	0.13	(Oungoulian et al., 2015)

AC	bovine	pin-on-plate	stainless steel	PBS	0.24	(Oungoulian et al., 2015)
AC	bovine	pin-on-disc	glass	PBS	0.069-0.13	(Peng et al., 2015)
AC	bovine	annulus-on-disc^{+}	AC	PBS	0.24	(Schmidt et al., 2007)
AC	bovine	annulus-on-disc^{+}	AC	BSF	0.028	(Schmidt et al., 2007)
AC	bovine	disc-on-disc^{+}	AC	PBS	0.08	(Waller et al., 2013)
AC	bovine	disc-on-disc^{+}	AC	CACP-SF	0.04	(Waller et al., 2013)
AC	bovine	disc-on-disc^{+}	AC	HSL	0.03	(Waller et al., 2013)
AC	bovine	disc-on-disc^{+}	AC	HSF	0.01	(Waller et al., 2013)
AC	bovine	disc-on-disc^{+}	AC	CACP-SF+HSL	0.005	(Waller et al., 2013)
AC	bovine	pin-on-plate	AC	BSF	0.014	(Warnecke et al., 2017)
AC	bovine	pin-on-plate	glass	BSF	0.215	(Warnecke et al., 2017)
meniscus	bovine	pin-on-plate	glass	PBS	0.17-0.24	(Bonnevie et al., 2014)
meniscus	bovine	pin-on-plate	glass	PBS	0.20	(Bonnevie et al., 2016)
meniscus	bovine	pin-on-plate	glass	PBS	0.032	(Peng et al., 2015)
meniscus	bovine	pin-on-plate	AC	BSF	0.021	(Warnecke et al., 2017)
meniscus	bovine	pin-on-plate	glass	BSF	0.10	(Warnecke et al., 2017)
meniscus	ovine	pin-on-plate	glass	PBS	0.25-0.3	(Galley et al., 2011)
meniscus	ovine	pin-on-plate	glass	ESF	0.09-0.14	(Galley et al., 2011)

Abbreviations. AC: articular cartilage; BSF: bovine synovial fluid; CACP-SF: camptodactyly-arthropathy-coxa vara-pericarditis syndrome synovial fluid; CoCr LC: cobalt chromium low carbon; CoCr HC: cobalt chromium high carbon; ESF: equine synovial fluid;

FBS: fetal bovine serum; HSF: human synovial fluid; HSL: human superficial zone protein; PBS: phosphate buffered saline; SF: synovial fluid;
*Boundary lubrication, average, equilibrium, kinetic coefficient of friction (μ)
+Tribological testing modalities analogous to pin-on-disc

Regulation of lubrication modes in diarthrodial joints

The shear-thinning properties of synovial fluid allow it to act as a viscous fluid at low shear rates or sliding speeds.[314,315] The loading and shear rates that affect the viscosity of synovial fluid also influence the lubrication mode (boundary or fluid-film) and tribological properties of articulating joints. Because of the inherent porosity of articular cartilage, it is theorized that the articular cartilage "weeps" interstitial fluid into the intra-articular space when pressurized. When in fluid-film lubrication, pressure on the fluid in the intra-articular space drives fluid into the tissue, theoretically "boosting" its mechanical properties.[316-318] Stribeck curves, such as the one shown in Figure 4-1, are used to plot the dependence of the coefficient of friction on sliding speed, applied normal load, and viscosity of the fluid between the sliding surfaces, and illustrate how these parameters determine the mode (i.e., boundary or fluid-film) and regime of lubrication. These lubrication regimes are boundary (Figure 4-1A), mixed (Figure 4-1B), elastohydrodynamic (Figure 4-1C), and hydrodynamic lubrication (Figure 4-1D), which will be discussed in greater detail below.

Boundary lubrication plays a crucial role in articular cartilage tribology and mediates frictional properties of articular cartilages if the joint is functioning under high loads, low sliding speeds, or high fluid viscosity.[319,320] *In vivo* and cadaveric studies have shown that under physiological loads, the pressure distribution and lubrication regimes across the articular cartilage surface are not uniform, and, in areas of high load, articular cartilage surfaces experience boundary lubrication.[316] Most studies examining the tribological properties of articular cartilage surfaces conduct measurements under a boundary lubrication regime because of its translational relevance, since this regime interrogates sample properties rather than lubricant properties (Table 4-1 and Table 4-2). In the boundary lubrication regime, articular cartilage surfaces are separated by only one or two molecules, known as a sacrificial layer.[302] The primary molecules responsible

for forming the layer of separation are hyaluronan and SZP, which shelter the articular cartilage surface from high friction.[321] Other molecules involved in forming the sacrificial layer are aggrecans and surface-activated phospholipids.[322] This sacrificial layer of molecules lining articular cartilage in boundary lubrication mode is replenished at an equal or higher rate than it is depleted, which maintains a low coefficient of friction on the articular cartilage surface. Studies have shown that in healthy articular cartilage, the boundary lubrication layer would be replenished at least 10 times faster than the development of wear caused by an increase in friction coefficient.[302]

Fluid-film lubrication occurs at high articulation speeds or low loads. Fluid-film lubrication can be either elastohydrodynamic or hydrodynamic depending on these loading conditions, but is classified as fluid film lubrication if the interacting articular cartilage surfaces are fully separated by a fluid-film distance larger than the surface roughness of the tissue.[323] If the articular cartilage surface is deformed by the fluid-film, then lubrication is considered to be in the elastohydrodynamic regime. Under the elastohydrodynamic regime, joint physiological loads are initially borne by the synovial fluid; the corresponding fluid pressure is then transferred onto the articulating surfaces. In fluid-film mode, the complex formed by SZP and hyaluronan is disassembled because of their weak physical interaction.[292] This allows SZP to float freely in the synovial fluid and disperse evenly throughout the intra-articular space.[306]

Pathologies affecting diarthrodial joint tribology

Conditions that can induce cartilage degeneration and, consequently, a reduction in tribological properties, include congenital disorders, wear and tear, traumatic injury, and inflammation. One congenital disease with particular relevance to cartilage lubrication is camptodactyly-arthropathy-coxa vara-pericarditis (CACP) syndrome, caused by a mutation in the *PRG4* gene.[288] Inherited in an autosomal recessive fashion, affected patients exhibit non-inflammatory, juvenile-onset joint failure, suggesting SZP is necessary for joint health and function.[324] The ability of SZP to rescue

function in tissues affected by CACP has been tested *in vitro* using bovine articular cartilage.[325] These explants demonstrated a boundary mode friction coefficient of 0.04 when lubricated with synovial fluid taken from patients with CACP (i.e., lacking functional SZP). When SZP was added to the CACP synovial fluid, however, the coefficient of friction dropped to 0.005. Thus, functional SZP appears to be a critical regulator of cartilage lubrication.

In addition to genetic conditions, general wear and tear of the articular surface can lead to local collagen depletion, one of the first stages of osteoarthritis.[326] Superficial collagen loss likely depletes the cartilage surface of key boundary lubrication components, such as SZP, hyaluronan, and binding domains, and can increase surface roughness, potentially furthering the progression of osteoarthritis.[327,328] Differences in gross morphology, biochemical content, and mechanical properties between healthy and diseased cartilages are depicted in Figure 4-2. Healthy human femoral head articular cartilage has demonstrated a boundary mode coefficient of friction of 0.119, whereas early osteoarthritic tissue and advanced osteoarthritic tissue had friction coefficients of 0.151 and 0.409, respectively.[329] Values were determined using atomic force microscopy (AFM), thus surface roughness was simultaneously measured. The increase in friction coefficients with osteoarthritis progression correlated with higher tissue surface roughness, as it was determined healthy, early osteoarthritic, and advanced osteoarthritic tissue each had a surface roughness of 104, 382, and 537 nm, respectively. These findings indicate osteoarthritis progression is closely related to deteriorating cartilage lubrication.

Traumatic injury often induces post-traumatic osteoarthritis, a condition that can inhibit the lubrication of articular cartilages. For example, in an equine injury model, synovial fluid hyaluronan concentration and molecular weight decreased following the injury, which impacted the fluid's lubrication abilities. The boundary mode friction coefficient of bovine articular cartilage tested in healthy equine synovial fluid was 0.026, whereas it was 0.036 when tested with synovial fluid from injured horses.[330]

Inflammatory pathways can also be activated by traumatic injury and osteoarthritis, leading to the upregulation of inflammatory cytokines such as interleukin-1β (IL-1β), known to adversely affect lubrication of articular cartilage.[331] In an *in vitro* study, 48-hour IL-1β treatment of bovine cartilage explants increased the boundary mode equilibrium coefficient of friction from 0.26 to 0.36. It has also been shown that an important regulator of cartilage lubrication and superficial zone maintenance is epidermal growth factor receptor (EGFR). In an animal study, EGFR-deficient mice developed early cartilage degeneration and demonstrated little to no hyaluronan and SZP localization at the cartilage surface.[332] In bovine articular cartilage explants, transforming growth factor alpha (TGF-α), known to activate EGFR-signaling, led to nearly a six-fold increase in *PRG4* mRNA and a 28% reduction in the explant friction coefficient. Thus, if EGFR-signaling is disrupted in articular cartilage, for instance through upregulation of IL-1β, key lubrication components, tissue tribological properties, and overall tissue health can be damaged.[332,333] In general, regardless of the mechanism of depletion, a lack of boundary lubricant will increase frictional forces in the superficial zone of articular cartilage, potentially leading to dysregulated chondrocyte metabolism, apoptosis, and degeneration.[325]

Methods for quantifying tribological properties

In this section, methods for quantifying tribological properties are listed and discussed. The most commonly used tribometer configurations, pin-on-disc, pin-on-plate, and rolling-ball-on-disc, for articular cartilage are described and compared. The use of atomic force microscopy to quantify surface roughness is also included. Because different testing configurations can lead to disparities in coefficient of friction and surface roughness values, suggestions for standardized practices are also presented.

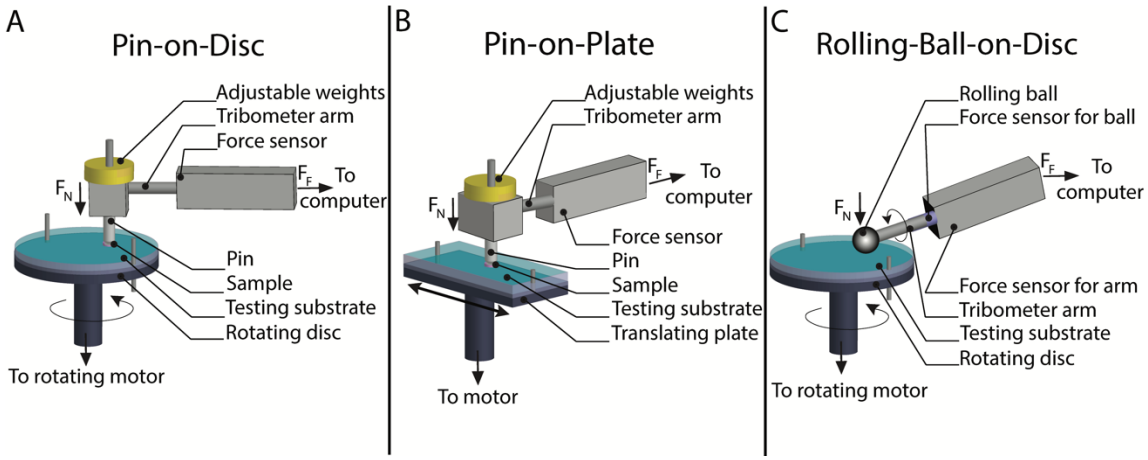

Figure 4-3. Tribometer configurations. Schematic of a pin-on-disc tribometer (A) where a sample is glued to the pin and tested on a substrate attached to the rotating disc. Schematic of pin-on-plate tribometer (B), which uses a translating plate instead of a disc. Schematic of rolling-ball-on-disc tribometer (C), primarily used to test orthopedic implants, where both the tribometer arm and the disc can be rotated independently. In each setup, the coefficient of friction is calculated by dividing the friction force (F_F), obtained from the force sensor, by the known F_N created by the adjustable weights or the movement of the tribometer arm.

Tribometers

A tribometer quantifies tribological properties, such as coefficient of friction. There are many different tribometer configurations across engineering, but the most popular in articular cartilage research are pin-on-disc, pin-on-plate, and rolling-ball-on-disc (Figure 4-3). Regardless of the configuration, all tribometers aim to measure the properties of two materials rubbing against each other and the effectiveness of lubricants between them. Usually, articular cartilages are tested against a substrate of either stainless steel or glass, with lubricants ranging from phosphate buffered saline (PBS) solution to fetal bovine serum. To showcase the multitude of ways tribological properties are studied, Table 4-1 and Table 4-2 compare recent tribology studies on hyaline articular cartilage, as well as the knee meniscus, by describing sample types, tribometer configurations, substrates, and lubricants. In particular, Table 4-1 demonstrates how these experimental methodological variations yield large discrepancies in the coefficient of friction of native articular cartilages. For example, quantifying coefficient of friction by using cartilage-on-cartilage will yield lower values compared to using glass-on-cartilage.[305] Furthermore, the testing solution also has an effect on coefficient of friction, such as BSF yielding lower values compared

to PBS.[334] It is emerging that having a standard practice of quantifying coefficient of friction of native and engineered articular cartilage would be useful in facilitating comparisons between laboratories. For instance, this standard method could involve a pin-on-plate or pin-on-disc tribometer configuration with the tissue submerged in PBS under boundary lubrication.

Pin-on-disc/plate: The pin-on-disc and pin-on-plate tribometer configurations are the most popular amongst articular cartilage research groups. Usually, they contain an acrylic pin to which articular cartilage samples may be glued and then placed in contact with a substrate (Figure 4-3A and Figure 4-3B).[335-337] The disc or plate substrate, generally made of glass or stainless steel, is completely submerged in a lubricating fluid, such as PBS, for testing. Adjustable weights are used to apply a known normal force on the articulating surfaces. A strain gauge, or other force sensor types, is used to measure the friction force of the sample as the disc or plate rubs against it. Boundary lubrication mode should be the lubrication modality used for this tribometer configuration to ensure that the properties that are observed reflect the properties of the sample against the substrate. If identification of the lubrication properties of a solution is desired, both boundary and fluid-film lubrication studies should be performed to fully characterize the lubricant.

Rolling-ball-on-disc: Tribometers may also take the form of a rolling-ball-on-disc (Figure 4-3C). In this configuration, both the ball and the disc can be driven independently allowing for a variety of kinematic conditions.[338] This configuration is generally used to test the interaction of substrates used in total knee replacements and is useful for testing the wear characteristics of plastic inserts and metal components in synthetic joint replacements over time. Although useful for certain applications, the rolling-ball-on-disc tribometer does not feasibly allow the testing of a small articular cartilage tissue sample. Ball-on-disc tribometers, although rarely used, also exist and differ from rolling-ball-on-disc tribometers in that the ball is used to translate against a sample without rolling.[339,340]

Atomic force microscopy

AFM is capable of surface imaging and force measurements at the nanoscale, making this approach valuable for measuring tribological properties such as surface roughness and "microscale" coefficient of friction.[341] Through the use of AFM, it has been found that the surface roughness, R_a, of immature bovine articular cartilage is around 72 nm.[295] AFM is particularly useful for testing tribological properties occurring under boundary lubrication because of its ability to operate at single asperity, high pressure contact.[320] However, studies have shown that AFM tip size and scan size affect surface roughness measurements.[342] Therefore, when presenting AFM measurements for surface roughness, it is also important to report the tip size and scan size, as well as a native tissue measurement with the same tip size and scan size, for comparison.

Toward engineering native tribological properties

Because adequate lubrication is vital for diarthrodial joint health and function, various strategies to engineer biomimetic tribological properties for both native tissue and engineered constructs have been explored. Approaches include the development of biolubricants to alter both fluid-film and boundary lubrication, low-friction scaffolds, as well as bioactive factors and mechanical stimulation regimens that promote endogenous lubrication mechanisms.

Biolubricants

Biolubricants can augment boundary lubrication properties by binding to articular cartilage to replace components often depleted in damaged or degenerated articular cartilage, such as GAGs. For example, hyaluronan-binding peptides were attached to cartilage via heterobifunctional polyethylene glycol (PEG) chains to recruit hyaluronan from solution to the cartilage surface.[343] This strategy significantly decreased coefficients of friction in both healthy and osteoarthritic cartilage explants by ~50% relative to control conditions (i.e., PBS as the lubricant) and could be retained in the rat joint for at least 72 hours, much longer than hyaluronan alone. Importantly, in osteoarthritic cartilage explants, high concentration of hyaluronan in the testing solution did not

reduce friction coefficients relative to the hyaluronan-binding system applied to the same tissue type, indicating that even low levels of hyaluronan, when bound to a surface, can improve lubrication properties.[343] Samples in this study were tested in a pin-on-disc (in this case, tissue-on-tissue) configuration within the boundary lubrication regime.

There are already clinically available hyaluronan-based biolubricants, or viscosupplements, such as Artz®, Healon®, Hyalgan®, Opegan®, Opelead®, Orthovisc®, and Synvisc-One®.[299,311] While some patients experience a transient improvement in their osteoarthritis symptoms after treatment, evidence is lacking to demonstrate the clinical efficacy and disease-modifying ability of these injections.[344] In a similar context, modified, recombinant SZP as an intra-articular injection has been investigated preclinically in a rat osteoarthritis model.[345] 1 week following osteoarthritis induction, SZP injections were administered for 4 weeks before animal sacrifice, significantly improving total joint scores and reducing cartilage degeneration. Like hyaluronan viscosupplementation, however, the long-term clinical efficacy of SZP injections remains to be elucidated.

In another study, a poly(glutamic acid) backbone (PGA) was modified with poly(2-methyl-2 oxazoline) (PMOXA) and hydroxybenzaldehyde (HBA) to create a graft copolymer (PGA-PMOXA-HBA) that mimics the boundary lubrication properties of SZP and hyaluronan.[346] PGA-PMOXA-HBA is designed to bind to damaged articular cartilage to provide a boundary lubrication layer and prevent cytokine penetration into the tissue. Tested in a rolling-ball-on-disc configuration within the boundary lubrication regime, certain PGA-PMOXA-HBA formulations were able to reduce friction coefficients of damaged articular cartilage (around 0.14) to levels exhibited by healthy articular cartilage (less than 0.06).[347] Furthermore, PGA-CPMOXA-HBA prevented chondroitinase ABC-mediated and collagenase-mediated digestion of GAGs and collagen, respectively.[346] Another technique involved an interpenetrating polymer network (IPN) designed to mimic GAGs lost during osteoarthritis progression. IPN includes a GAG-inspired zwitterionic polymer 2-methacryloyloxyethyl phos-phorylcholine (pMPC) that is photopolymerized *in situ* and

decreased friction coefficients in bovine articular cartilage by 24% relative to untreated controls in a pin-on-disc configuration under fluid-film lubrication mode.[348] These and other lubricants can reduce friction at the cartilage interface, however comparing absolute values from each study is difficult because the testing modality and lubrication mode vary broadly. Furthermore, it is possible that achieving a clinically effective strategy may require an approach that focuses more specifically on boundary lubrication of articular cartilage.

Scaffolds

Articular cartilage synthetic scaffold design criteria tend to focus on mechanical properties; however, some scaffolds have been developed with greater emphasis on improving tribological properties (Table 4-2). In one study, biodegradable polyvinyl alcohol (PVA) polymer hydrogels were functionalized with a carboxylic acid derivative boundary lubricant molecule and reduced friction coefficients up to 70% relative to unfunctionalized PVA scaffolds.[340] Furthermore, functionalized PVA hydrogels demonstrated friction coefficients that resembled those of native cartilage. Friction tests were conducted in a ball-on-disc configuration within the boundary lubrication mode. PVA/polyvinyl pyrrolidone (PVP) blend hydrogels have also been tested against articular cartilage across lubrication modes and demonstrated average coefficients of friction between 0.12 and 0.14, which were close to cartilage-on-cartilage interaction (0.03) and much lower than cartilage-on-stainless steel articulation (0.46).[349] Interestingly, increasing hydrogel compressive modulus was highly correlated to coefficient of friction, likely due to lower congruence in stiffer hydrogels.

In a combinatorial approach, infiltration of a 3D-woven polycaprolactone scaffold with an alginate/polyacrylamide hydrogel created a composite scaffold that significantly reduced the boundary lubrication coefficient of friction from 0.64 for the scaffold alone to 0.28.[350] A tissue-engineered cartilage implant that replicates NeoCart® demonstrated a decreasing boundary mode coefficient of friction throughout 7 weeks of culture (0.40 at week 0 to 0.24 at week 7).[296]

The coefficient of friction of constructs from week 3 of culture onward was not statistically different than healthy human cartilage (0.22) tested in the same pin-on-plate configuration using PBS as the test solution. This study is one of the first to assess the *in vitro* boundary lubrication tribological properties of an engineered articular cartilage product that has been investigated in a clinical trial. These characterizations are imperative for articular cartilage scaffolds that will be used *in vivo*.

Studying tribological properties for meniscal replacements is also of paramount importance. While hyaline articular cartilage has generally been a focus for scaffold strategies to improve diarthrodial joint lubrication, some scaffolds for meniscus replacement have also incorporated tribological properties as design criteria. Toward engineering lubrication in menisci, a silk fibroin scaffold that could potentially be used for meniscus replacement was developed. The friction coefficients of the scaffold tested against femoral cartilage (0.056) were significantly higher than native articular cartilage (0.014) and meniscus (0.021) controls tested against femoral articular cartilage.[305]

According to requirements for meniscus replacements described previously,[351] a coefficient of friction of 0.056 for the scaffold against femoral articular cartilage could be within the range of acceptable tribological properties for meniscus replacements.[305] It should be noted that these values are dependent upon many factors such as the experimental setup, thus any comparisons to native tissue should only be made within the same testing modality, lubrication mode, and tissue type.

One meniscus replacement that was tested *in vivo* consisted of a porous polyurethane scaffold implanted into sheep to augment meniscus repair after partial meniscectomy. After 6 months *in vivo*, the boundary lubrication mode coefficient of friction of engineered meniscus (~0.35), tested in a pin-on-plate configuration, was not significantly different from either contralateral or adjacent healthy meniscus tissue, suggesting that the polyurethane scaffold was able to promote biomimetic neotissue formation.[352] Biomaterial scaffolds have been developed with coefficient of friction as a design criterion, but it is difficult to compare them to each other due to varying testing

modalities. In general, the lack of meniscus tribology research is even more acute than for hyaline articular cartilage.

Bioactive factors

Bioactive factors, or molecules with an effect on cell behavior or extracellular matrix structure, that can enhance the tribological properties of native and engineered articular cartilages have been explored. Synoviocytes and superficial zone chondrocytes are known to endogenously produce SZP.[353] It has been demonstrated that TGF-β1 increased SZP secretion in superficial zone chondrocytes seeded in monolayer, identifying it as a bioactive factor of interest.[354] Combined treatment of synovium explants with TGF-β1 and bone morphogenetic protein 7 (BMP-7) further improved SZP secretion.[355]

An increase in SZP secretion does not always cause a decrease in tissue friction coefficients, as SZP must be retained at the cartilage surface to improve boundary lubrication.[356] To improve retention of SZP in engineered cartilage, native superficial zone cartilage extract, which likely contains binding macromolecules for SZP, was added to the culture media of self-assembled articular cartilage. Groups treated with a low concentration of extract demonstrated greater SZP staining and a boundary mode coefficient of friction of 0.03, which was significantly lower than the coefficient of friction of self-assembled cartilage cultured in the absence of superficial zone cartilage extracts (0.10).[356] Combining superficial zone extract with growth factors such as TGF-β1 and BMP-7 could further enhance tribological properties.

Another growth factor of interest is insulin-like growth factor I (IGF-1). IGF-1 led to SZP localization at the surface of a collagen I gel seeded with meniscal fibrochondrocytes after 20 days in culture. This treatment resulted in a boundary friction coefficient of 0.22, which was not statistically different from the native tissue value of 0.2. Gels not stimulated with IGF-1, however, had a coefficient of friction of 0.29, which was significantly greater than the native tissue value.[337] In another study, increasing the proportion of mesenchymal stem cells seeded with

fibrochondrocytes led to a dose-dependent increase in SZP deposition on collagen I gels, which was matched by a decrease in coefficients of friction.[357] The correlation between SZP deposition and coefficient of friction had an R^2 value of 0.80.

This suggests that MSCs not only produce SZP, but could produce SZP-binding factors that could be further investigated to improve SZP retention in native and engineered tissues. Bioactive factors to improve cartilage lubrication remain largely unexplored compared to bioactive factors used to improve other mechanical properties such as compressive moduli.

Table 4-2. Coefficients of friction (μ) for engineered articular cartilage and meniscus in the boundary lubrication regime

Construct type	Species	Modality	Substrate	Lubricant	μ*	Reference
cell-seeded AC scaffold (polyurethane)	bovine	ball-on-disc	glass	N/A	0.251-0.681	(Grad et al., 2012)
scaffold-free AC	bovine	pin-on-disc	glass	PBS	0.08-0.17	(Peng et al., 2014)
scaffold-free AC	bovine	pin-on-disc	glass	PBS	0.02-0.10	(Peng et al., 2016)
cell-seeded AC scaffold (collagen I)	human	pin-on-plate	glass	PBS	0.24	(Middendorf et al., 2017)
scaffold-free AC	leporine	pin-on-plate	glass	PBS	0.05-0.1	(Whitney et al., 2015)
scaffold-free AC	leporine	pin-on-plate	glass	PBS	0.05-0.38	(Whitney et al., 2017)
acellular AC construct (PCL scaffold with Alg/PAAm IPN hydrogel)	synthetic	pin-on-plate	stainless steel	PBS	0.28	(Liao et al., 2013)
acellular AC hydrogel (PVA/PVP)	synthetic	pin-on-plate	AC	FBS	0.12-0.14	(Kanca et al., 2018b)
acellular AC hydrogel (PVA)	synthetic	ball-on-disc	glass	N/A	0.27-0.93	(Blum and Ovaert, 2013)

cell-seeded meniscus scaffold (collagen I)	bovine	pin-on-plate	glass	PBS	0.21-0.48	(Bonnevie et al., 2014)
cell-seeded meniscus scaffold (collagen I)	bovine	pin-on-plate	glass	PBS	0.15-0.33	(Bonnevie et al., 2016)
Acellular meniscus scaffold (collagen I)	synthetic	pin-on-plate	glass	PBS	0.38	(Bonnevie et al., 2016)
acellular meniscus scaffold (silk)	synthetic	pin-on-plate	AC	BSF	0.056	(Warnecke et al., 2017)
acellular meniscus scaffold (silk)	synthetic	pin-on-plate	glass	BSF	0.446	(Warnecke et al., 2017)
in vivo meniscus scaffold (polyurethane)	synthetic	pin-on-plate	glass	PBS	0.35-0.45	(Galley et al., 2011)
in vivo meniscus scaffold (polyurethane)	synthetic	pin-on-plate	glass	ESF	0.12-0.18	(Galley et al., 2011)

Abbreviations. AC: articular cartilage; Alg/PAAm IPN: alginate polyacrylamide interpenetrating network; BSF: bovine synovial fluid; ESF: equine synovial fluid; PBS: phosphate buffered saline; PCL: polycaprolactone; PVA: polyvinyl alcohol; PVP: polyvinylpyrrolidone;
*Boundary lubrication, average, equilibrium, kinetic coefficient of friction (μ)

Mechanical stimulation

Mechanical stimulation, when applied at physiologic levels, has led to improvements in tissue-engineered cartilage lubrication. For example, a joint-mimicking loading system was applied to cell-seeded fibrin/hyaluronan composite gels. This biomimetic load increased SZP surface localization, suggesting enhancement of the construct surface, but quantitative tribological properties were not reported in this study.[358] In a separate study, chondrocyte-seeded polyurethane scaffolds were subjected to dynamic compression and sliding surface motion by a ceramic ball, which also led to SZP localization at the surface of the construct. Additionally, constructs subjected to both sliding and compression exhibited a reduced coefficient of friction

(0.251), compared to unloaded controls (0.681) and constructs only stimulated in compression (0.427).[339]

Hydrostatic pressure, known to increase collagen synthesis and tensile properties in self-assembled articular cartilage, has also been investigated as a mechanical stimulus to enhance cartilage tribological properties.[56] Self-assembled constructs treated with TGF-β1 and chondroitinase-ABC (C-ABC) were subjected to 10 MPa of continuous hydrostatic pressure from days 10 to 14 of culture for 1 hr per day. These constructs demonstrated increased SZP staining compared to constructs stimulated with TGF-β1 and C-ABC alone. Since coefficient of friction was not examined in this study, hydrostatic pressure as a method to improve tribological properties merits further investigation.

Supplementing culture media with factors found in synovial fluid, such as hyaluronan, can further replicate physiologic conditions during loading and have an impact on tribological properties. Indeed, mechanically stimulated, chondrocyte-seeded polyurethane scaffolds produced significantly more *PRG4* mRNA and SZP when culture medium was supplemented with hyaluronan.[359] This indicates that not only does hyaluronan have lubricating properties, but it also can regulate cellular behavior to promote better tribological properties. However, this study did not examine the functional impact of greater SZP content on construct tribological properties. These studies suggest that mechanical stimulation techniques should be further investigated toward improving lubrication of engineered constructs.

Perspectives

When articular cartilages are described, load-bearing capacity and nearly frictionless surfaces are presented as key characteristics. However, in many studies of tissue-engineered cartilages, mechanical properties are investigated while tribological properties are rarely explored. To augment the translatability of tissue-engineered cartilages, both mechanical and tribological functions should be considered as release criteria for cartilage implants. Because the FDA has

guidelines for mechanical testing of engineered articular cartilages, we suggest that analogous guidelines be created for tribological properties.

Tissue-engineered articular cartilages must exhibit biomimetic mechanical properties, otherwise they will likely fail under repeated loads. *In vivo* durability is also of concern; therefore, tribological properties of engineered articular cartilages are also crucial because poor lubrication contributes to tissue degeneration.[327-329,332] Indeed, if gross morphology, biochemical content, or mechanical properties are negatively impacted by insufficient lubrication, articular cartilages could degenerate in each of these aspects.

The tribological properties of native articular cartilages have yet to be defined, due to variability in testing conditions. A standardized tribological testing protocol, such as testing tissue bathed in PBS in a pin-on-plate configuration within the boundary lubrication regime, would be ideal to facilitate interlaboratory comparisons. If limitations exist that prevent adoption of this standardized assay, incorporating native tissue controls when performing tribological testing of engineered cartilages would provide a better indication of translational potential.

Of the two articular cartilages discussed in this review, the tribological properties of the knee meniscus remain relatively understudied, even though meniscus lubrication is vital for diarthrodial joint health. For example, a PubMed search for “knee meniscus tribology” returned 8 results, whereas a PubMed search for “articular cartilage tribology” returned 47 references. While this disparity is stark, both fields would benefit from increased research.

A well-defined understanding of the tribology of native cartilages can provide design criteria for tissue-engineering efforts. Using that understanding to engineer clinically applicable implants should be the aim of cartilage researchers. Achieving biomimetic tribological properties in engineered articular cartilages will be crucial to the translational success of these approaches.

CHAPTER 5 Chondroitinase ABC enhances integration of self-assembled articular cartilage, but its dosage needs to be moderated based on neocartilage maturity

Abstract

Objective: To enhance the *in vitro* integration of self-assembled articular cartilage to native articular cartilage using chondroitinase ABC. Design: To examine the hypothesis that chondroitinase ABC (C-ABC) integration treatment (C-ABC_{int}) would enhance integration of neocartilage of different maturity levels, this study was conducted in two phases. In Phase I, the impact on integration of two treatments, TCL (TGF-β1, C-ABC, and lysyl oxidase like 2) and C-ABC_{int}, was examined via a two-factor, full factorial design. In Phase II, construct maturity (two levels) and C-ABC_{int} concentration (three levels) were the factors in a full factorial design to determine whether the effective C-ABC_{int} dose was dependent on neocartilage maturity level. Neocartilages formed or treated per the factors above were placed into native cartilage rings, cultured for 2 weeks, and, then, integration was studied histologically and mechanically. Prior to integration, in Phase II, a set of treated constructs were also assayed to provide a baseline of properties. Results: In Phase I, C-ABC_{int} and TCL treatments synergistically enhanced interface Young's modulus by 6.2-fold ($p=0.004$) and increased interface tensile strength by 3.8-fold ($p=0.02$) compared to control. In Phase II, the interaction of the factors C-ABC_{int} and construct maturity was significant ($p=0.0004$), indicating that the effective C-ABC_{int} dose to improve integration Young's modulus is dependent on construct maturity. Construct mechanical properties were preserved regardless of C-ABC_{int} dose. Conclusions: Applying C-ABC_{int} to neocartilage is

Chapter published as: Link JM, Hu JC, and Athanasiou KA. Chondroitinase ABC Enhances Integration of Self-assembled Articular Cartilage, but its Dosage Needs to be Moderated Based on Neocartilage Maturity. Cartilage. (online ahead of print 2020)

an effective integration strategy with translational potential, provided its dose is calibrated appropriately based on implant maturity, that also preserves implant biomechanical properties.

Introduction

Translational cartilage tissue engineering aims to generate neotissue with biomimetic properties for the purpose of *in vivo* implantation. In addition to achieving biomimetic properties, one of the major impediments to cartilage regeneration is the inability of implants to integrate with adjacent, native tissue; this poses a serious, clinical problem.[360-363] Evaluating one of the salient standards of care shows that cartilage allografts suffer from incomplete integration, which hampers their long-term durability and efficacy.[364,365] Because tissue engineered cartilage is designed to be similar if not identical to native tissue, like with allografts, barriers to neocartilage integration are also anticipated.[277] Cartilage integration strategies are necessary for both native tissue repair and for deploying tissue-engineered cartilage in the clinical setting.

Cartilage has unique intrinsic properties that hinder integration, including: 1) lack of highly metabolic cells at the interface;[366] 2) repulsive negative charges induced by cartilage glycosaminoglycans (GAGs);[365] 3) a dense extracellular matrix (ECM);[367] and 4) a limited number of stabilizing crosslinks at the interface.[35] Chondroitin sulfate, an abundant ECM component in cartilage, contributes to the paucity of cells at the interface because it has been shown to impede migration of chondrocytes.[368] Chondroitin sulfate is also a negatively charged molecule that results in repulsion between engineered and native cartilage.[365,369] With regard to ECM, juvenile articular cartilage integrates better than adult tissue because fully mature cartilage contains denser ECM and chondrocytes that are less metabolically active, both factors that impede integration.[370] The maturation and development of articular cartilage has been modulated by removal of GAG and has been proposed as a method of improving collagen network interaction, and, therefore, crosslink development.[371-373] The observation that chondroitin sulfate and tissue maturity can hinder cartilage integration suggests that the four factors above can be targeted by

focusing on GAG-specific agents and tissue maturity in the development of cartilage integration strategies.

In terms of improving cartilage integration, chondroitinase ABC (C-ABC), a catabolic enzyme that digests chondroitin sulfate, and to a lesser degree other GAGs such as dermatan sulfate and hyaluronic acid,[374] has been explored previously for engineered cartilage integration because it could target each of the four integration hindrances described above.[363,375] For example, removal of chondroitin sulfate could encourage cell migration,[368] transiently decrease repulsive negative charge and physical ECM density,[371,373] and, due to decreased steric hindrance, lead to more collagen remodeling and pyridinoline (PYR) crosslinking at the interface.[55,372] A variety of cartilage integration strategies employing catabolic enzymes have been explored;[363,367,376-379] however, to the best of our knowledge, catabolic enzymes have not been used with biomimetic neocartilage. Furthermore, the effects of catabolic enzymes have not been quantified on neocartilage properties. For example, collagenase has been explored for cartilage integration and has shown promise.[376,377] However, digesting cartilage matrix at the implant edge using collagenase could also damage PYR crosslinks, which have been shown to enhance self-assembled cartilage properties and integration.[35,277] To avoid disrupting these beneficial crosslinks while still targeting integration hindrances, C-ABC could be used in lieu of collagenase. Self-assembled articular cartilage, which has been shown to have many properties on par with those of native articular cartilage, has the potential for more complete integration than scaffold-based cartilage constructs because it contains highly metabolic cells and a propensity for remodeling since it is composed strictly of ECM formed from its own cells.[18,380] C-ABC used for integration (C-ABC$_{int}$) in combination with these inherent properties could significantly enhance self-assembled articular cartilage integration, especially when combined with lysyl oxidase like 2 cocktail (LOXL2), an enzymatic treatment that mediates PYR crosslinking. C-ABC$_{int}$ dose would be selected to only affect the construct periphery, and, thus, would not compromise construct mechanical integrity.

Using both C-ABC$_{int}$ and bioactive agents, this study targeted the aforementioned integration hindrances in both immature and mature self-assembled articular cartilage. In Phase I of this study, it was hypothesized that a combination of C-ABC$_{int}$ and bioactive agents (TCL; TGF-β1, C-ABC, and LOXL2) applied to constructs could enhance integration between native and engineered articular cartilage. Because it has been shown previously that tissue maturation influences cartilage integration, in Phase II, the combined effects of construct maturity and C-ABC$_{int}$ concentration were examined. In Phase II, it was hypothesized that the effective C-ABC$_{int}$ dosage would be higher for mature constructs and lower for immature constructs, but that no dose of C-ABC$_{int}$ would affect construct mechanical properties.

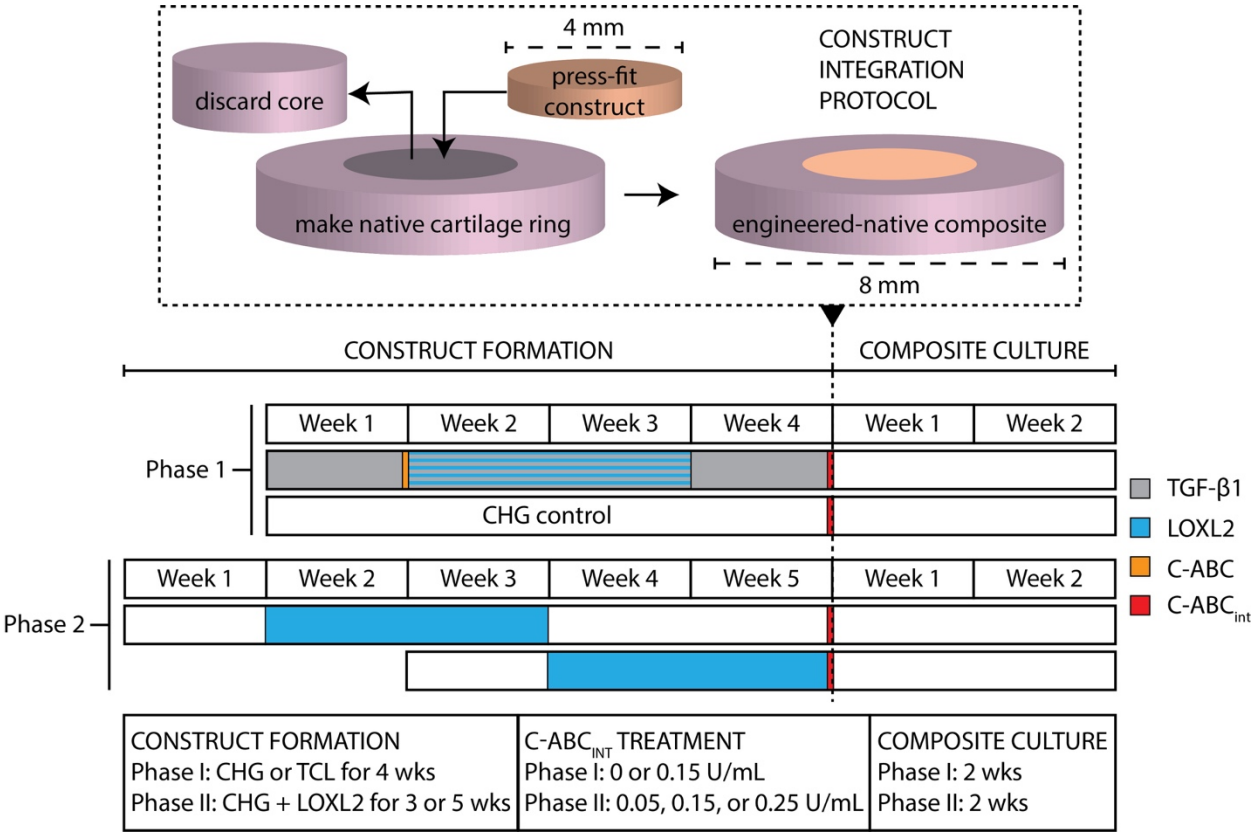

Figure 5-1. A schematic diagram describes the integration of engineered cartilage to native cartilage. Construct formation in phase I lasted for 4 weeks and involved either TCL or CHG, while in phase II, all constructs were formed with CHG and LOXL2, but were cultured for either 3 or 5 weeks prior to integration. The timeline depicts when these construct formation agents were applied. In phase I, C-ABC$_{int}$ was either applied at 0.15 U/ml or not at all directly before integration, whereas in phase II, 0.05 (low), 0.15 (medium), or 0.25 (high) U/ml was used. Engineered-native composite culture lasted 2 weeks for each phase before subsequent assays. TCL, transforming growth factor–β1 (TGF-β1), C-ABC, and lysyl oxidase like 2 (LOXL2); CHG, chemically defined chondrogenic medium; C-ABC$_{int}$, chondroitinase ABC integration treatment.

Methods

Cell and tissue harvest

Primary articular chondrocytes and articular cartilage explants were isolated in a sterile fashion from juvenile bovine stifle joints as previously described.[381] Briefly, juvenile bovine hind limbs were obtained from a commercial provider of animal specimens (Research 87, Boylston, MA). Subsequently, the stifle joints were dissected in a sterile fashion to reveal the articular cartilage surfaces of the distal femur. To obtain primary articular chondrocytes, articular cartilage from both the femoral condyles and trochlear groove was minced and digested in a 0.2% w/v collagenase type II solution (Worthington Biochemical Corporation, Lakewood, NJ). Osteochondral explants were isolated from the femoral condyles using an 8-mm dermal biopsy punch. These explants were then trimmed to 1.5 mm such that only the most superficial articular cartilage remained.

Construct formation and culture

Chondrocytes were seeded at a high density ($4.5x10^6$ cells/100 µL medium) in chemically defined chondrogenic media (CHG; Dulbecco's modified Eagle's medium with high glucose/GlutaMAX [Life Technologies, Grand Island, NY], 1% penicillin-streptomycin-fungizone [Lonza, Basel, Switzerland], 1% nonessential amino acids [Life Technologies], 1% ITS+ Premix [BD Biosciences, San Jose, CA], 50 µg/ml ascorbate-2-phosphate [Sigma-Aldrich, St. Louis, MO], 40 µg/ml L-proline [Sigma], 100 µg/ml sodium pyruvate [Sigma], and 100 nM dexamethasone [Sigma]) into 5 mm non-adherent agarose wells to form self-assembled cartilage constructs as previously described.[381] Construct media was changed once daily until they were unconfined from the agarose wells after five days of culture, after which media was changed every other day. In Phase I, neocartilage constructs were maintained with CHG (CHG group) or TCL (continuous 10 ng/mL transforming growth factor-β1 [TGF-β1] [Peprotech, Rocky Hills, NJ], 2 U/mL C-ABC [Sigma] for 4 hours at the end of week 1 of culture, and lysyl oxidase like 2 treatment cocktail [LOXL2] during weeks 2 and 3 of culture [0.15 µg/mL lysyl oxidase like 2 (SignalChem, Richmond, British

Columbia, Canada), 0.146 mg/mL hydroxylysine (Sigma), and 1.6 μg/mL copper sulfate (Sigma)] (TCL group). Phase I constructs were cultured for 4 weeks prior to integration. Directly prior to integration, Phase I constructs were treated with C-ABC$_{int}$ and combined with native tissue as described below. In Phase II, constructs were seeded in the same fashion, but were cultured for either 3 weeks or 5 weeks before C-ABC$_{int}$ treatment and subsequent integration. All constructs in Phase II were fed with CHG and treated with LOXL2 during week 2 and 3 of culture. TGF-β1 and C-ABC were not used for construct culture in Phase II. Additionally, in this phase, prior to being placed in the rings, a set of treated neocartilage constructs were also assayed to provide a baseline of properties.

Construct integration

Using a sterile dermal biopsy punch, 4 mm discs were taken from constructs, which were then treated with C-ABC$_{int}$ for 2 hours. Experiments were carried out in two phases. In Phase I, a two factor, full factorial study was conducted with 4-week constructs of two culture conditions (CHG or TCL) and C-ABC$_{int}$ (none or 0.15 U/mL). For Phase II, a two factor, full factorial study was conducted with constructs of two different maturities (3-week or 5-week) and three C-ABC concentrations (0.05 [low], 0.15 [medium], and 0.25 [high] U/mL). Following treatment, C-ABC$_{int}$ activity was quenched with zinc sulfate (1 mM) for 10 minutes, and elimination of residual, inactive enzyme was achieved by sequentially washing constructs with medium. Subsequently, neocartilage discs were press-fit into native bovine articular cartilage explant rings with an 8 mm outer diameter, 4 mm inner diameter, and 1.5 mm thickness, thus, creating engineered-native composites (Figure 5-1). In both phases, engineered-native composites were cultured in CHG for an additional 2 weeks on an orbital shaker (20 RPM for week 1 and 50 RPM for week 2) and then processed for subsequent assays.

Histology of constructs and composites

Self-assembled constructs and engineered-native composites were fixed in 10% neutral-buffered formalin for histological evaluation. Fixed samples were processed, embedded in paraffin, and sectioned at a thickness of 5 μm. Sections were then stained with hematoxylin and eosin (H&E), Safranin O/Fast Green (Saf-O), and picrosirius red as previously described.[164] Sections stained with Saf-O were also rehydrated and stained with additional Fast Green counterstain for 10 minutes to determine GAG diffusion from the sections.

Biochemical analyses of constructs

Self-assembled constructs were weighed before and after lyophilization, and then digested in papain. DNA content was measured with PicoGreen (Thermo Fisher Scientific, Waltham, MA), total collagen content was measured via a modified hydroxyproline assay as previously described,[381] and GAG content was determined using a dimethylmethylene blue dye-binding assay kit (Biocolor, Newtownabbey, Northern Ireland). PYR collagen crosslink quantification was performed via a liquid chromatography mass spectrometry (LCMS) assay.[382] Samples were hydrolyzed in 6N HCl at 105°C for 18 hours, after which acid was removed using centrifugal evaporation. Dried hydrolysates were resuspended in 25% (v/v) acetonitrile and 0.1% (v/v) formic acid in water, centrifuged at 15,000g for 5 min, and supernatant was transferred to a vial compatible with the LCMS system. Liquid chromatography was performed on a Cogent Diamond Hydride HPLC Column (2.1 mm x 150 mm, particle size 2.2 μm, pore size 120 Å, MicroSolv, Leland, NC). The elution gradient used 0.1% (v/v) formic acid in water as solvent A and 100% acetonitrile as solvent B. The 5-minute elution gradient ran at 300 μL/min (0 min 25% B, 2 min 25% B, 2.2 min 5% B, 3 min 25% B). Mass spectrometry was performed on a Quadrupole Mass Detector (ACQUITY QDa, Waters, Milford, MA) in ESI+ MS scan mode. The quadrupole range was set to 150-450 m/z with cone voltage 12.5 V. MassLynx software version 4.1 with TargetLynx was used to quantify PYR in 10 μL injections of self-assembled construct hydrolysate by

integrating the extracted ion chromatogram of double-charged PYR (m/z=215.1) and comparing to a PYR standard (BOC Sciences, Shirley, NY) prepared and run in the same fashion.

Construct and composite mechanical testing

Tensile testing was conducted on dog-bone-shaped construct specimens as previously described.[277] To test the integration, engineered-native composites were trimmed into strips containing engineered tissue on one side and native tissue on the other. The ends of each strip were then glued to paper tabs, which were then gripped by a uniaxial testing machine (Instron 5565, Norwood, MA). A pull-to-failure test was conducted at a rate of 1% strain per second. From this experimental data, Young's Modulus (E_y) and ultimate tensile strength (UTS) values were determined for both constructs and for the engineered-native composite interface of composites. Creep indentation compressive tests were conducted on self-assembled constructs using a flat, porous indenter tip and a constant load as previously described.[383] A linear biphasic model and finite element analysis were used to obtain the aggregate modulus, permeability, and Poisson's ratio from the experimental creep curves.[384,385]

Statistics

All statistical analyses were performed using Prism 8 (GraphPad Software, San Diego, CA). Quantitative data were assessed using a two-way ANOVA with a *post hoc* Tukey's HSD test at a significance level of $\alpha=0.05$. Significance of ANOVA factors is denoted with Greek characters. Two-way ANOVA factor interactions were analyzed to determine if the effect of one factor is dependent upon the level of the other. Significance among particular groups is illustrated by a connecting letters report with Latin characters (i.e., bars that do not share the same Latin character(s) are statistically significant). Synergism of factors was defined as the case in which the combined application of two factors led to a greater increase in a property than the sum of the effects of those two treatments individually.

Results

Phase I: C-ABC$_{int}$ and TCL enhanced cartilage integration synergistically

C-ABC$_{int}$ improved visible congruence of engineered constructs to native tissue, both in terms of gross morphology and H&E staining (Figure 5-2A-B). Gaps between the native cartilage and neocartilage were visible in control composites (Figure 5-2A), but not in composites treated with C-ABC$_{int}$ (Figure 5-2B). As an individual factor, the effect of C-ABC$_{int}$ significantly enhanced interface E_y ($p=0.0009$) and interface UTS ($p=0.0001$), but TCL was not a significant factor for interface E_y ($p=0.05$) or UTS ($p=0.98$) (Figure 5-2C-D). For the CHG group, C-ABC$_{int}$ increased E_y from 0.20±0.21 to 0.69±0.13 MPa ($p=0.2$) and significantly increased UTS from 0.057±0.046 to 0.24±0.080 MPa ($p=0.004$). Similarly, for the TCL group, C-ABC$_{int}$ significantly improved E_y from 0.36±0.39 to 1.25±0.78 MPa ($p=0.2$) and UTS from 0.076±0.090 to 0.22±0.090 MPa ($p=0.04$). The combined, beneficial effect of TCL and C-ABC$_{int}$ on interface E_y (1.05 MPa) was greater than the sum of the individual effects of those factors (0.65 MPa). Thus, TCL and C-ABC$_{int}$ synergistically increased interface E_y.

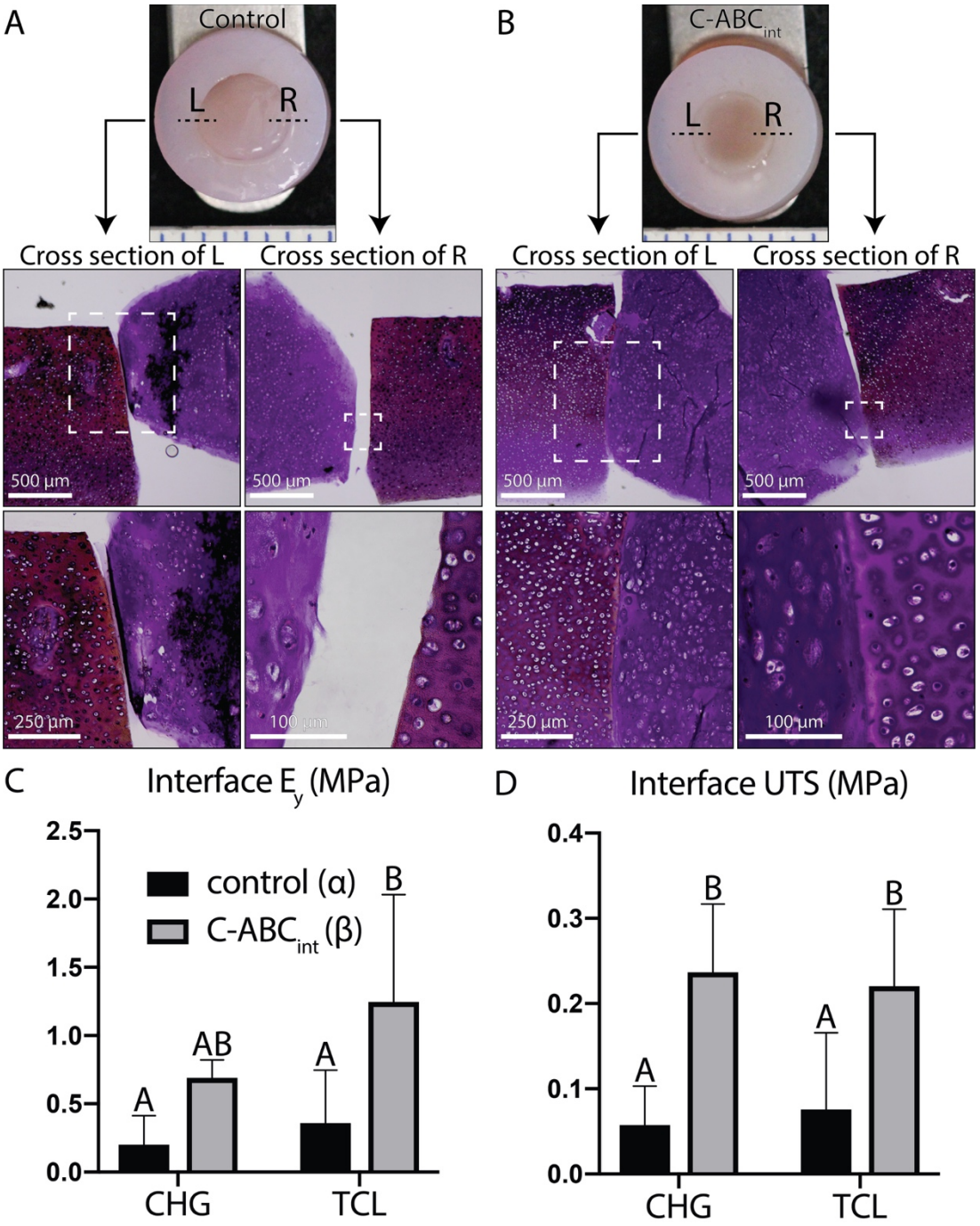

Figure 5-2. C-ABC$_{int}$ and TCL synergistically enhanced cartilage integration (Phase I). A) Gross morphology (1-mm tick marks) and histology (H&E) of interface for control group showed limited integration. White dashed boxes correspond to regions shown at higher magnification. B) Gross morphology (1-mm tick marks) and histology (H&E) of interface for groups treated with C-ABC$_{int}$ demonstrated cartilage integration. White dashed boxes correspond to regions shown at higher magnification. C) Interface E$_y$ was synergistically improved by the combination of C-ABC$_{int}$ and TCL. D) Interface UTS significantly improved with the addition of C-ABC$_{int}$. Latin alphabet letters denote significant differences according to Tukey's HSD. Greek letters indicate that C-ABC$_{int}$ is a significant factor according to a two-way ANOVA for both interface E$_y$ and UTS. C-ABC$_{int}$, chondroitinase ABC integration treatment; TCL, transforming growth factor–β1 (TGF-β1), C-ABC, and lysyl oxidase like 2 (LOXL2); H&E, hematoxylin and eosin; E$_y$, Young's modulus; UTS, ultimate tensile strength.

Phase II: Construct mechanical properties were preserved regardless of C-ABC$_{int}$ concentration, but local, histologic effects of C-ABC$_{int}$ were observed for both immature and mature constructs

For constructs assayed prior to integration, C-ABC$_{int}$ as a factor did not significantly affect any quantitative morphological, biochemical, or mechanical properties of constructs. C-ABC$_{int}$ did affect construct histological properties, however (Figure 5-3). Saf-O staining intensity in general was lower for 3-week constructs than 5-week constructs. Both construct maturity levels demonstrated a reduction in Saf-O at the neocartilage edge as C-ABC$_{int}$ concentration increased from the low dose to the high dose. Picrosirius red staining was not affected by C-ABC$_{int}$ at any concentration, but was more intense at the edge of 5-week constructs in comparison to 3-week constructs.

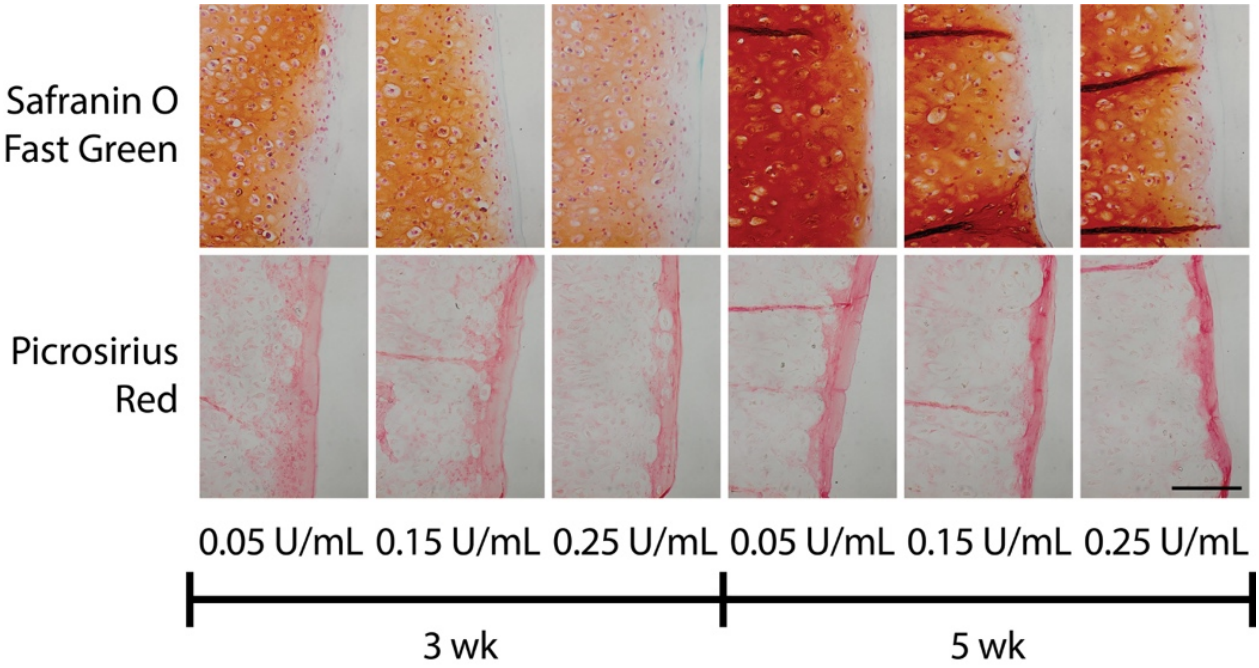

Figure 5-3. A higher C-ABC$_{int}$ dose is required for local GAG depletion in 5-week constructs due to increased collagen density at the edge (Phase II). Histology of constructs demonstrated differences in construct staining intensity and distribution based on construct maturity and C-ABC$_{int}$ dose. Safranin O/Fast Green staining of constructs illustrated local effects of higher doses of C-ABC$_{int}$ at the edge of both immature and mature constructs. Picrosirius red staining demonstrated higher intensity staining of collagen at the edge of 5-week constructs. The scale bar represents 100 μm and applies to all images. C-ABC$_{int}$, chondroitinase ABC integration treatment; GAG, glycosaminoglycan.

As a factor, greater construct maturity (i.e., 5-week constructs versus 3-week constructs) significantly increased construct wet weight (WW) ($p<0.0001$) and construct thickness ($p<0.0001$)

(Table 5-S1). Increased construct maturity did not lead to differences in biochemical contents per WW or per DW (Table 5-S1), but caused collagen/DNA ($p=<0.0001$), GAG/DNA ($p=<0.0001$), and PYR/DNA ($p=0.002$) to significantly increase (Figure 5-4A-C). Qualitatively, increased Saf-O (GAG) and picrosirius red (collagen) staining intensity for 5-week constructs versus 3-week constructs correspond to these biochemical data (Figure 5-3). For all constructs, picrosirius red staining was primarily localized to the edge of the construct. Construct maturity as a factor significantly influenced E_y ($p=0.013$), as 3-week constructs had an E_y of 1.70±0.24, 1.91±0.46, 1.59±0.34 MPa, and 5-week constructs had an E_y of 2.21±0.53, 2.22±0.31, 2.20±0.70 MPa (low, medium, and high doses of C-ABC_{int}, respectively) (Figure 5-4D). There were no significant differences between individual groups, however. Similarly, construct maturity as a factor significantly affected UTS ($p=0.049$) (Figure 5-4E). While tensile properties were significantly affected by construct maturation, aggregate modulus was not affected over the levels of maturities examined ($p=0.25$) (Figure 5-4F). Comprehensive construct properties can be found in Table 5-S1.

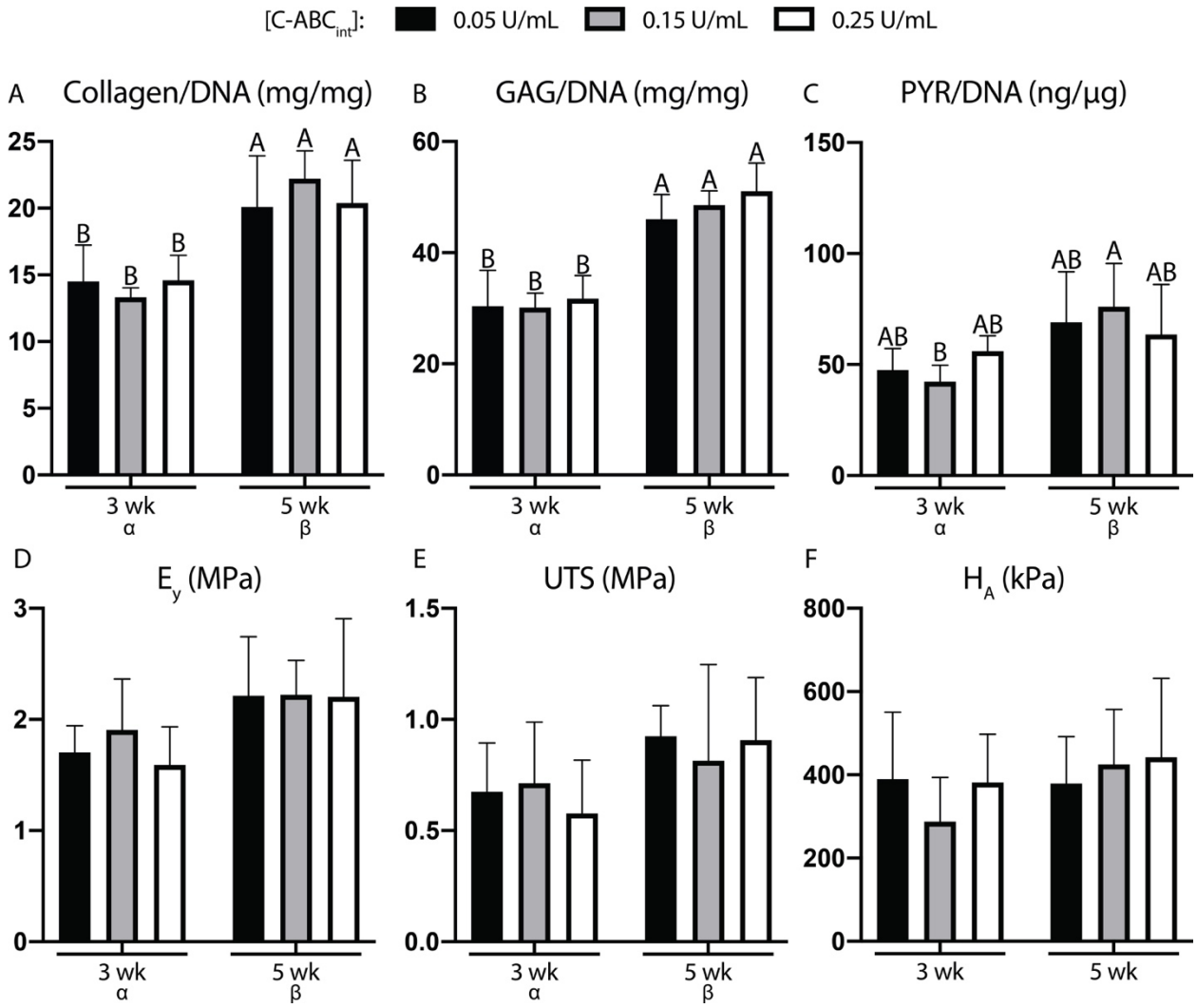

Figure 5-4. Properties of engineered constructs were found to be preserved regardless of C-ABC$_{int}$ dose (Phase II). Biochemical contents A) Collagen/DNA, B) GAG/DNA, and C) PYR/DNA increased in 5-week constructs compared to 3-week constructs. In terms of biomechanical properties, D) E_y of constructs increased with construct maturity, while E) aggregate modulus (H_A) did not. Latin alphabet letters denote significant differences between groups. Greek alphabet letters denote significance of factors as determined by two-way ANOVA. C-ABC$_{int}$, chondroitinase ABC integration treatment; GAG, glycosaminoglycan; PYR, pyridinoline; E_y, Young's modulus; UTS, ultimate tensile strength; H_A, aggregate modulus

Phase II: Effective C-ABC$_{int}$ dose to enhance cartilage integration is greater for mature constructs than for immature constructs

Saf-O and picrosirius red staining of the interface indicate that for 3-week constructs treated with either the low or medium dose of C-ABC$_{int}$ and for 5-week constructs treated with either the medium or high dose of C-ABC$_{int}$, the native tissue and neotissue are in apposition (interface is closed), and this interface stains for both collagen and GAG (Figure 5-5). Conversely, in the 3-week construct maturity and high C-ABC$_{int}$ dose group, Saf-O and picrosirius red staining indicate

a discontinuity at the interface. Flattened cells are also present at this interface as observed in the Saf-O stain. In the 5-week construct and low C-ABC$_{int}$ dose group, there is a distinct gap between the native and engineered tissue illustrating a lack of integration.

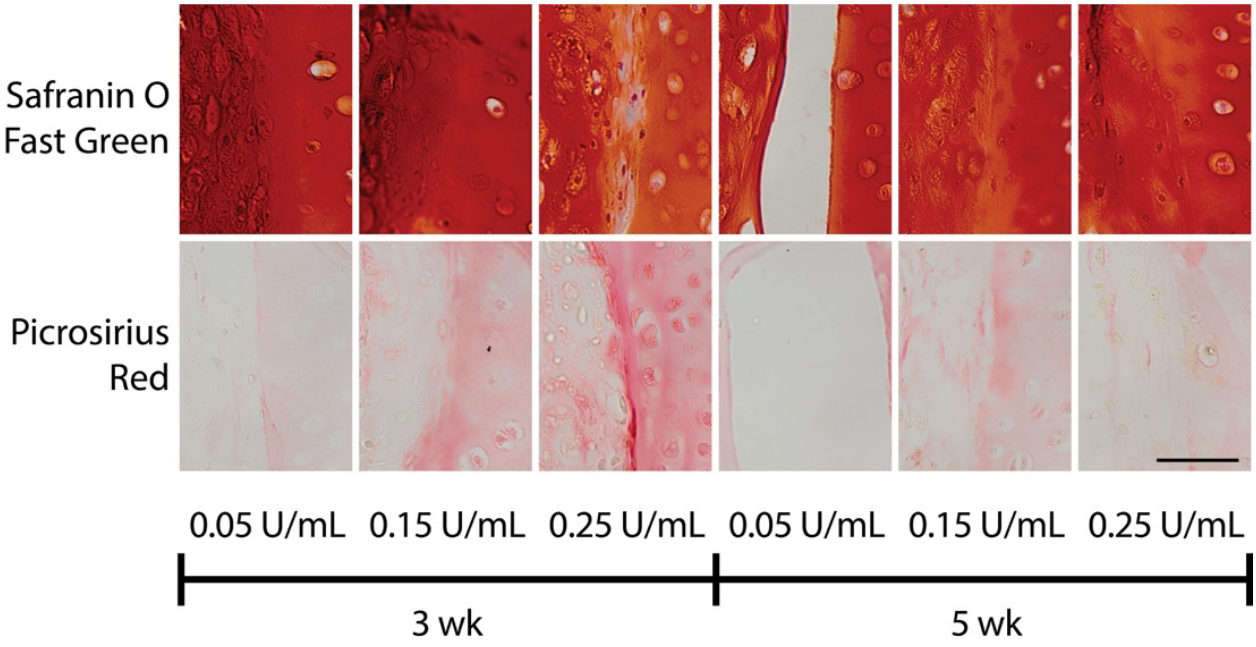

Figure 5-5. Effective C-ABC$_{int}$ dose to achieve integration for immature constructs is lower than for mature constructs (Phase II). Histology of the engineered-native composites showed GAG content (Safranin O/Fast Green) and collagen content (picrosirius red) at the interface. In each image, the engineered construct is on the left and the native tissue is on the right. Staining illustrated tissue apposition and development of matrix across the interface in groups with 3 wk constructs treated with either 0.05 (low) U/mL or 0.15 (medium) U/mL C-ABC$_{int}$ and groups with 5 wk constructs treated with either 0.15 (medium) U/mL or 0.25 (high) U/mL C-ABC$_{int}$. The scale bar represents 50 μm and applies to all images. GAG, glycosaminoglycan.

The interface E_y and UTS of engineered-native composites in Phase II were significantly dependent upon the interaction between the factors of construct maturation and C-ABC$_{int}$, as the *p* values for the two-way ANOVA interaction term were 0.0004 and 0.003, respectively (Figure 5-6A-B). As individual factors, neither construct maturation nor C-ABC$_{int}$ concentration had a significant effect on interface E_y or UTS. For 3-week construct maturity, the low and medium doses of C-ABC$_{int}$ showed trends of increased interface E_y by 4.5-fold (p=0.08) and 4.3-fold (p=0.08), respectively, relative to the high dose of C-ABC$_{int}$ (Figure 5-6A). For 5-week construct maturity, the medium and high doses of C-ABC$_{int}$ increased interface E_y 10.5-fold (p=0.04) and 11.4-fold (p=0.01), respectively, over the low dose of C-ABC$_{int}$. Interface E_y for 3-week construct maturity

combined with the low dose of C-ABC$_{int}$ was 1.02±0.46 MPa. Interface E_y for 5-week construct maturity combined with the high dose of C-ABC$_{int}$ was 1.07±0.36 MPa. These two groups demonstrated the best interface E_y. Across all groups, 3-week construct maturity treated with the low dose of C-ABC$_{int}$ led to the highest interface UTS (0.20±0.11 MPa), which was significantly greater than the UTS of 3-week constructs treated with the high dose of C-ABC$_{int}$ ($p=0.02$), and 5-week constructs treated with the low dose of C-ABC$_{int}$ ($p=0.01$) (Figure 5-6B). Gross morphologically (Figure 5-6C), gaps were not present between neocartilage and native cartilage in groups that integrated effectively, but existed for the 3-week construct maturity and high C-ABC$_{int}$ dose group as well as the 5-week construct and low C-ABC$_{int}$ dose group (shown with arrows).

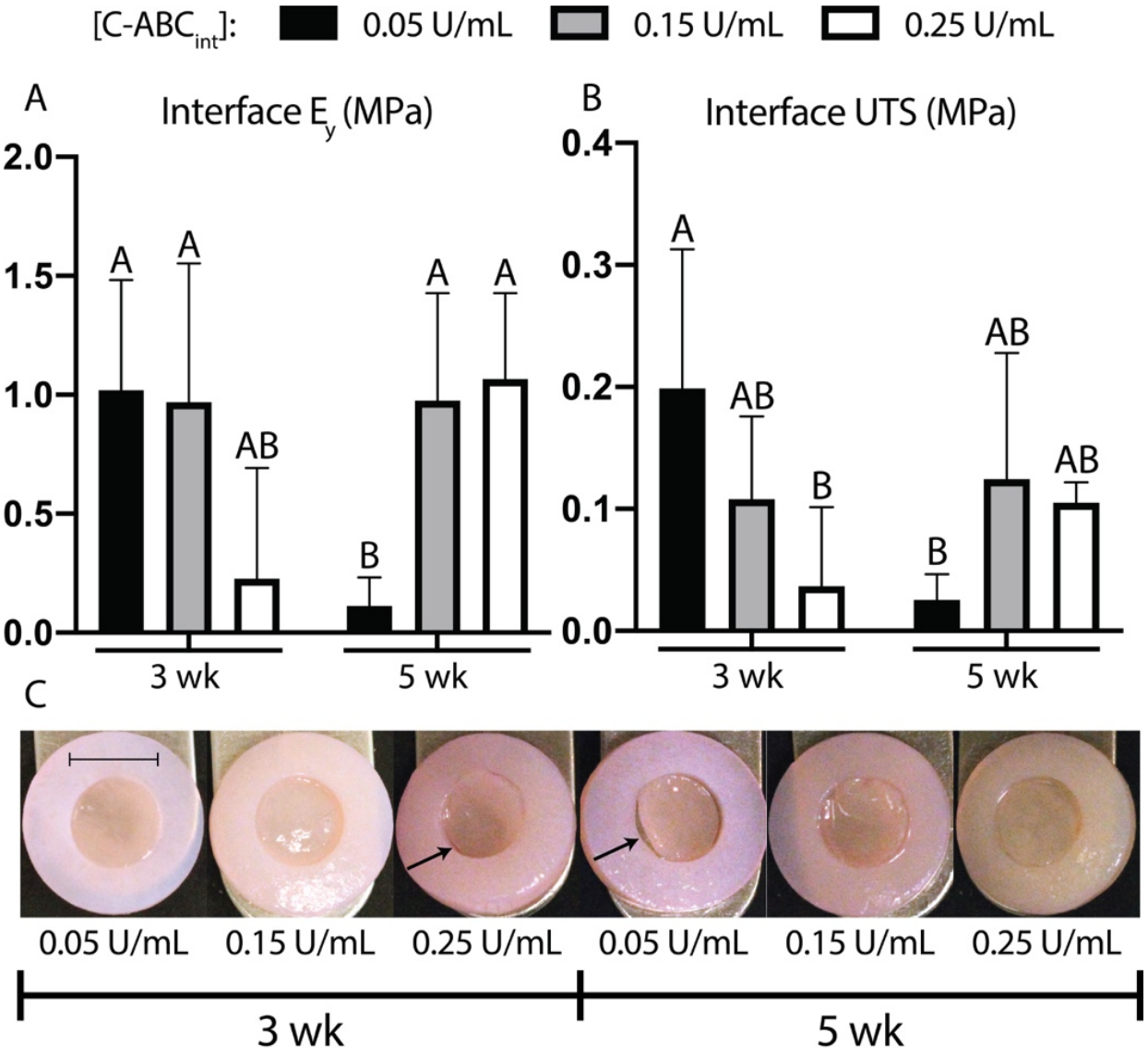

Figure 5-6. C-ABC$_{int}$ dose required for enhanced mechanical integration is higher for mature constructs than for immature constructs (Phase II). Interface mechanical properties and gross morphology demonstrated the dependence of C-ABC$_{int}$ dose on construct maturity. A) Interface E$_y$ depended on the interaction between the factors of construct maturity and C-ABC$_{int}$ concentration (p=0.0004). B) Interface UTS also depended on the interaction between construct maturity and C-ABC$_{int}$ concentration (p=0.003). C) Gross morphology of composites demonstrated poor integration in groups that had low interface E$_y$ and UTS (shown with arrows). All other groups appear to have integrated effectively. The scale bar represents 4 mm and applies to all images. English alphabet letters denote significant differences between groups. C-ABC$_{int}$, chondroitinase ABC integration treatment; E$_y$, Young's modulus; UTS, ultimate tensile strength.

Discussion

Toward restoring load bearing function of articular cartilage, strides have been made in enhancing the mechanical properties of tissue-engineered neocartilage. While both the compressive and

tensile properties of self-assembled articular cartilage have approached those of native tissue,[5,6] an effective cartilage integration strategy is still lacking. For either new or existing cartilage therapies, cartilage-to-cartilage integration is crucial to the *in vivo* function, durability, and, ultimately, translational success of implants. An integration strategy that employs a catabolic agent should be designed to integrate cartilage as quickly as possible while using a minimal amount of that agent to avoid damaging implant properties. This study examined the ability of C-ABC_{int} to enhance the integration of neocartilage to native cartilage in an *in vitro* defect model. C-ABC_{int} dosages and neotissue maturation levels were modulated with the intent of identifying effective treatments that do not affect implant mechanical properties and, yet, are effective toward enhancing neotissue integration to native cartilage explants. In Phase I, the hypothesis that C-ABC_{int} combined with TCL would enhance the integration of self-assembled cartilage to native cartilage was confirmed. Indeed, TCL and C-ABC_{int} together increased cartilage integration synergistically. In Phase II, the hypothesis that C-ABC_{int} at a lower dose would improve integration of immature self-assembled cartilage, but that a higher dose would be required for more mature constructs, was also supported. C-ABC_{int} at a low dose enhanced the integration of immature constructs by up to 4.5-fold, while at a high dose, it improved mature self-assembled cartilage integration by up to 11.4-fold. Furthermore, it was confirmed that C-ABC_{int} did not affect implant mechanical properties at any of the doses selected for testing. Ultimately, the results from this study demonstrate that C-ABC_{int} can enhance both immature and mature self-assembled construct integration without compromising construct integrity.

C-ABC_{int} demonstrated the capacity to enhance the integration of immature self-assembled articular cartilage. Specifically, 3-week constructs treated with either low or medium doses of C-ABC_{int} experienced better integration than the high dose. It has been shown that that there is a positive correlation (R^2=0.7773) between normalized integration strength and rate of change of equilibrium modulus of MSC-seeded, hydrogel cartilage constructs, supporting the notion that tissues which are still developing, and therefore are more immature, integrate more

effectively.[386] However, since 3-week constructs are less mature and still developing, if they are treated with a high dose of C-ABC$_{int}$, they do not integrate effectively. This finding is likely due to excessive GAG removal by C-ABC$_{int}$, and an inability for that GAG to recover within 2 weeks. Indeed, GAG content and compressive properties following a 2 U/mL C-ABC treatment have been shown to require at least 2 weeks to recover in self-assembled cartilage constructs.[373] Thus, for the purpose of cartilage integration within a short timeframe, using a minimal amount of C-ABC$_{int}$ is desired.

C-ABC$_{int}$ also demonstrated the capacity to enhance the integration of mature self-assembled articular cartilage, provided that a higher concentration of C-ABC$_{int}$ is applied to the neocartilage. Greater maturity and mechanical robustness of engineered tissue appears not to inhibit self-assembled articular cartilage integration. In other words, a more biomimetic self-assembled construct can be implanted with C-ABC$_{int}$. It is well established that mature cartilage does not integrate effectively,[365] and success has been elusive for mature tissue-engineered cartilage implants as well.[35,363,365,367] For example, it has been shown that cartilage constructs cultured for 5 days integrate more effectively than those cultured for 5 weeks.[387] Conversely, other studies have shown that construct maturity does not affect cartilage integration[388] or that precultured (i.e., mature) cartilage hydrogel constructs integrate more effectively than hydrogel constructs formed *in situ*.[389] We found that by increasing C-ABC$_{int}$ dosage, mature self-assembled cartilage constructs could be integrated as well. Indeed, a low dose of C-ABC$_{int}$ led to minimal GAG removal, likely due to increased collagen density at the construct edge (Figure 5-3). The medium and high doses, however, allowed for greater C-ABC$_{int}$ diffusion into the neotissue, and, therefore, more efficient GAG removal (Figure 5-3). Catabolic enzymes like C-ABC have been shown to improve tensile characteristics of engineered and native articular cartilage by removing ECM components like chondroitin sulfate that could interfere with the collagen network's ability to remodel and develop.[371,373] A similar mechanism is possibly responsible for enhancing interface tensile properties in engineered-native composites, provided the dose of C-ABC$_{int}$ is high enough

to remove sufficient GAG. Given this capacity to improve integration of mature self-assembled cartilage constructs, C-ABC$_{int}$ dosage could be tailored to enhance the integration of a variety of engineered cartilage constructs, such as highly biomimetic cartilage implants.

C-ABC$_{int}$ was able to enhance cartilage integration without affecting whole construct properties. Other groups have shown that catabolic enzymes like C-ABC can be used to improve engineered cartilage integration,[363,367,377-379] however this study illustrates how it can enhance cartilage integration without diminishing construct properties. No dose of C-ABC$_{int}$ evaluated in this study affected any construct mechanical properties (Figure 5-4). Construct mechanical integrity must remain intact if it is to withstand the loads present within a synovial joint and subsequently integrate.[2] C-ABC at high concentrations is known to decrease compressive properties of constructs transiently,[373,380] but many studies investigating catabolic enzymes as cartilage integration agents have not assessed implant mechanical properties following treatment.[363,367,377-379] This lack of data hampers evaluation of the translational potential of these strategies. This study identified C-ABC$_{int}$ as an effective integration treatment that does not adversely affect self-assembled construct properties.

C-ABC$_{int}$ and TCL synergistically improved the integration of self-assembled cartilage constructs to native tissue. C-ABC$_{int}$ treatment increased the interface E_y and UTS relative to untreated controls by more than 6-fold and 4-fold, respectively, and worked synergistically with TCL. Notably, the interface E_y of TCL- and C-ABC$_{int}$-treated engineered-native composites reached levels more than 5-fold higher than previously shown by our group,[277] while the interface UTS was on par with other integration models that extended composite culture from 2 weeks to 4 weeks.[367,390] Additionally, the best integration E_y values shown in this study are approaching the E_y of self-assembled articular cartilage shown in this study and others,[6,391] indicating a developing, mechanically stiff interface. The reduction of GAG-induced steric hindrance at the periphery of implants via C-ABC$_{int}$ possibly enabled more effective interfacial collagen crosslinking due to increased collagen network remodeling and interaction,[372] which would explain the discrepancy

between interface E_y and UTS values in groups receiving TCL but with or without C-ABC$_{int}$ treatment. Prior work has demonstrated the beneficial effect of LOXL2 alone on integration of self-assembled articular cartilage,[35] and this effect is enhanced with the addition of C-ABC$_{int}$. In addition to TCL, C-ABC$_{int}$ could potentially be combined with a variety of cartilage construct treatments to further improve integration to native articular cartilage.

Another mechanism through which C-ABC$_{int}$ could enhance integration of self-assembled articular cartilage is by encouraging chondrocyte migration via reduction of GAG negative charge density at the construct edge.[368,369] C-ABC-mediated chondroitin sulfate removal has been shown to increase chondrocyte migration *in vitro*.[368] Importantly, in that study, migrating chondrocytes regained their rounded, chondrocytic phenotype once they had migrated into adjacent tissue. The hypercellularity of self-assembled neocartilage would provide a substantial number of potentially migratory cells that could be released following C-ABC$_{int}$ treatment. Trypsin has also been investigated as a GAG-depleting, integration enhancer.[367] However, trypsin pre-treatment of chondrocyte-seeded hydrogels only improved integration strength when it was used in concert with HB-IGF-1, which can effect both chondrocyte motility and anabolism.[367,392] Self-assembled constructs subjected to C-ABC$_{int}$ did not require a motility agent for improved integration strength, suggesting that the cells within this neotissue could have greater migration potential than those in a hydrogel. It is possible that certain, inherent characteristics of self-assembled constructs, such as hypercellularity,[393] and metabolic activity of juvenile bovine ACs,[6,370] led to C-ABC$_{int}$ being a more effective enhancer of integration than if it were applied to native articular cartilage or scaffold-based cartilage constructs in the same way. Furthermore, enzymatic treatment of the native tissue ring was not necessary to facilitate integration, suggesting that the properties of self-assembled constructs treated with C-ABC$_{int}$ are sufficient for enhanced cartilage integration. Ultimately, the characteristics of self-assembled articular cartilage lend themselves to transient, small-scale depletion of GAG via C-ABC$_{int}$ to facilitate cartilage integration, as the implant has

demonstrated the capacity to secrete collagen at the wound interface and recover GAG content subsequently, suggesting the development of a homogeneous, contiguous interface.

While promising, the results of this study could be further enhanced in a variety of ways. In general, *in vitro* methods of cartilage integration have yet to produce cartilage integration strength that approaches the UTS of native, intact articular cartilage. Additional culture time after forming the composites of engineered and native tissue beyond the 2 weeks examined in this experiment could further enhance integration. Our group is interested in extending *in vitro* composite culture duration in future integration studies to assess longer-term effects of treatments since previous work has shown temporal differences in *in vitro* integration.[386] Also, for Phase II, LOXL2 and 0.15 U/mL C-ABC$_{int}$ treatment were carried forward due to their positive effect on cartilage integration in Phase I. TGF-β1 and C-ABC as bioactive factors were omitted to more closely examine the effects of construct maturation time and varying concentrations of C-ABC$_{int}$ had on both interfacial and construct properties. However, it would be interesting to explore the effect of modulating C-ABC$_{int}$ dose on constructs treated with TCL or other bioactive stimuli, since additional combinations could further enhance interface properties. Additionally, measuring specific ECM components present at the interface, through LCMS techniques, for example, could verify the presence of cartilaginous repair tissue and exclude the possibility that fibrocartilage instead has formed at the interface.

Other methods of enhancing cartilage integration, such as additional enzymatic treatments,[372,378] chondrocyte motility agents,[367] or other bioactive factors,[390] could also yield improved *in vitro* cartilage integration strength. However, we expect that the *in vivo* environment and associated stimuli are required to elicit the integration strength desired for stability, durability, and long-term efficacy of an implant.[379] Ectopic *in vivo* implantation has been shown to improve integration strength by 230% between native and engineered cartilage relative to *in vitro* controls.[277] In particular, mechanical stimulation could further enhance integration. Fluid-induced shear stress has previously been shown to enhance cartilage integration by 1.89-fold.[394]

Composites in this study were subjected to fluid-induced shear stress since they were placed on an orbital shaker during culture, but this stimulus could be rigorously investigated further to determine its impact on *in vitro* self-assembled cartilage integration. Due to joint articulation, the orthotopic, *in vivo* environment would provide this, as well as other, mechanical stimuli that could further enhance integration, so long as the implant is protected sufficiently until it is stable within a defect. In this study, interface E_y approached those of intact self-assembled constructs within 2 weeks of *in vitro* composite culture. Thus, upon *in vivo* implantation, a period of 2 weeks or less may be sufficient for construct stability within the host articular cartilage environment. We are interested in testing this strategy in an orthotopic, large animal, *in vivo* defect model as this model would be more representative of the integration potential of self-assembled articular cartilage treated with C-ABC_{int}, and would represent progress toward the clinical translation of self-assembled articular cartilage.

In this study, C-ABC_{int} enhanced integration of both immature and mature self-assembled articular cartilage to native tissue. While its potential is promising, C-ABC_{int} could be combined with other treatments, such as additional growth factors, motility agents, or catabolic factors to further enhance its integration capacity. Ultimately, the straightforward nature of applying a GAG-removal agent at the periphery of a self-assembled articular cartilage implant could be readily implemented into a clinical setting and should be investigated further as this type of neocartilage construct nears clinical translation.

Supplementary material

Table 5-S1. Self-assembled articular cartilage construct properties prior to integration

	3-week construct maturity			5-week construct maturity			Two-way ANOVA *p* values		
	0.05 U/mL C-ABC$_{int}$	0.15 U/mL C-ABC$_{int}$	0.25 U/mL C-ABC$_{int}$	0.05 U/mL C-ABC$_{int}$	0.15 U/mL C-ABC$_{int}$	0.25 U/mL C-ABC$_{int}$	CM	C-ABC$_{int}$	αβ
Construct thickness (mm)	0.43±0.03^{B}	0.44±0.02^{B}	0.45±0.02^{B}	0.57±0.06^{A}	0.57±0.01^{A}	0.57±0.03^{A}	<0.001	0.9	0.7
Construct diameter (mm)	5.99±0.14	5.95±0.15	5.93±0.16	6.01±0.22	6.21±0.07	6.04±0.23	0.1	0.5	0.3
Construct WW (mg)	13.63±0.35^{B}	13.07±1.40^{B}	13.17±1.19^{B}	16.84±3.01^{A}	18.76±2.14^{A}	17.11±1.53^{A}	<0.001	0.6	0.3
Hydration (%)	0.81±0.01	0.81±0.02	0.81±0.01	0.82±0.03	0.81±0.02	0.82±0.02	0.3	0.9	0.6
Collagen/WW (mg/mg)	0.031±0.004	0.030±0.003	0.031±0.001	0.028±0.004	0.031±0.006	0.029±0.003	0.2	0.7	0.6
Collagen/DW (mg/mg)	0.16±0.02	0.16±0.01	0.16±0.01	0.15±0.01	0.16±0.01	0.16±0.02	0.5	0.7	0.98
Collagen/DNA (mg/mg)	14.50±2.74^{B}	13.33±0.71^{B}	14.60±1.87^{B}	20.10±3.84^{A}	22.21±2.08^{A}	20.39±3.21^{A}	<0.001	0.9	0.3
GAG/WW (mg/mg)	0.06±0.01	0.07±0.01	0.07±0.01	0.06±0.01	0.07±0.01	0.07±0.01	0.9	0.4	0.9
GAG/DW (mg/mg)	0.33±0.05	0.36±0.02	0.36±0.02	0.36±0.03	0.35±0.02	0.40±0.02	0.1	0.1	0.1
GAG/DNA (mg/mg)	30.40±6.42^{B}	30.10±2.63^{B}	31.74±4.15^{B}	46.01±4.44^{A}	48.58±2.56^{A}	51.09±5.01^{A}	<0.001	0.3	0.7
PYR/WW (ng/µg)	0.10±0.02	0.10±0.02	0.12±0.03	0.09±0.02	0.10±0.02	0.09±0.03	0.2	0.7	0.1
PYR/DW (ng/µg)	0.52±0.09	0.51±0.104	0.64±0.12	0.52±0.15	0.54±0.112	0.491±0.146	0.4	0.7	0.3
PYR/DNA (ng/µg)	47.61±9.55	42.32±7.41	56.11±6.85	69.02±22.78	76.04±19.56	63.58±22.50	0.002	0.98	0.2
DNA/WW (ng/µg)	2.14±0.19^{A}	2.28±0.13^{A}	2.19±0.34^{A}	1.42±0.36^{B}	1.39±0.30^{B}	1.42±0.26^{B}	<0.001	0.9	0.8
DNA/DW (ng/µg)	11.06±1.18^{A}	12.10±0.80^{A}	11.33±1.23^{A}	7.79±1.10^{B}	7.17±0.70^{B}	7.82±0.52^{B}	<0.001	0.9	0.2
E_Y (MPa)	1.70±0.24	1.91±0.46	1.59±0.34	2.21±0.53	2.22±0.31	2.20±0.70	0.01	0.7	0.8

UTS (MPa)	0.68±0.22	0.71±0.28	0.58±0.24	0.92±0.14	0.81±0.43	0.91±0.28	0.049	0.9	0.7
H_A (kPa)	389.6±160.6	287.6±106.3	381.4±116.2	379.3±112.7	425.0±132.0	442.5±189.4	0.3	0.7	0.5
Permeability (10^{-14} $m^4/N{\cdot}s$)	1.88±0.99	1.94±1.52	1.66±1.38	2.76±3.24	1.50±7.23	2.05±1.73	0.7	0.7	0.7
Poisson's ratio	0.20±0.11	0.20±0.10	0.26±0.10	0.17±0.10	0.19±0.08	0.31±0.08	0.9	0.1	0.6

Superscripted letters indicate significance ($p<0.05$) between individual groups according to a connecting letters report. Gray shading indicates significance of a two-way ANOVA factor.

Abbreviations: CM, construct maturity; αβ, two-way ANOVA interaction factor; WW, wet weight; DW, dry weight; GAG, glycosaminoglycan; PYR, pyridinoline; E_y, Young's modulus; UTS, ultimate tensile strength; H_A, aggregate modulus

CHAPTER 6 Bioactive factors confer protection to self-assembled cartilage against macrophage challenge in a novel co-culture system

Abstract

Tissue-engineered cartilage implants must be able to withstand the *in vivo* environment for successful long-term repair of defects. In addition to joint loading, neocartilage's ability to tolerate a potential immune or inflammatory response can affect its *in vivo* durability. However, the interactions between factors involved in the immune response, such as macrophages, and neocartilage remain underexplored. Thus, the objectives of this work were to develop a novel, direct cartilage-macrophage co-culture system and subsequently characterize interactions between self-assembled neocartilage and differentially stimulated macrophages. In Study 1, it was hypothesized that stiff, neocartilage constructs would enhance the pro-inflammatory response of macrophages, and, as a result, would experience a decrease in mechanical properties after co-culture. In Study 2, it was hypothesized that bioactive factors (i.e., TCL: transforming growth factor beta-1 (TGF-β1), chondroitinase ABC (C-ABC), and lysyl oxidase like 2 (LOXL2)) would protect neocartilage properties during macrophage co-culture. Also, it was hypothesized that interleukin 10 (IL-10)-stimulated macrophages would improve neocartilage mechanical properties compared to lipopolysaccharide (LPS)-stimulated macrophages. Stiffer neocartilage did elicit a heightened proinflammatory macrophage response, but, interestingly, this response did not adversely affect construct properties. Additionally, TCL protected constructs from macrophage challenge, whereas IL-10 did not improve neocartilage properties, although stiff constructs appeared to bolster the anti-inflammatory nature of IL-10-stimulated macrophages. In

Authors: Link JM*, Donahue RP*, Meli VM, Hu JC, Liu WF, and Athanasiou KA. (*authors contributed equally to this work)

conclusion, neocartilage stiffness can mediate macrophage behavior, but stiffness and bioactive factors prevent macrophage-induced degradation. Ultimately, this co-culture system could be utilized for many additional studies to develop the burgeoning field of cartilage mechano-immunology.

Introduction

Cartilages such as hyaline articular cartilage, the knee meniscus, and the temporomandibular joint (TMJ) disc lack innate capability to heal.[2,395,396] Small defects that may emanate from wear-and-tear or traumatic injury can lead to inflammation and often result in osteoarthritis (OA), leading to pain and loss of joint function.[397,398] According to the Centers for Disease Control, OA affects over 32 million in the U.S.A.,[399] and the number is projected to rise up to 60% in the next two decades.[400] To prevent degenerative changes and induce repair, these defects are often targets for surgical treatment.[2] However, clinically-available surgical approaches for repair of cartilage defects often do not provide long-term solutions in part because of the development of mechanically-inferior repair tissue, and, therefore, can be improved.[2] Furthermore, inflammation within injured or diseased joints can cause chondrocyte apoptosis and hypertrophy, as well as immune cell activation, all of which could impede healing induced by current surgical approaches.[397] To that end, it is the aim of cartilage tissue engineering to develop durable, biomimetic implants that can withstand the stresses and inflammation present in the *in vivo* environment and provide a long-term solution to healing cartilage defects.

Recent cartilage tissue engineering approaches have utilized allogeneic cell sources to overcome donor site morbidity and cell-sourcing issues associated with autologous approaches.[9,41] However, an allogeneic approach increases the risk of an immune response,[401] although various cartilages have been cited as immunoprivileged.[41,395,396] For example, recent work toward regeneration of the TMJ disc has shown that an allogeneic approach is feasible and

effective;[9] allogeneic neocartilage constructs induced healing in disc thinning defects that was mechanically superior to empty defect repair tissue.[9] While this allogeneic approach seems promising and appeared to be safe as it did not elicit a systemic immune response, some positive staining for T cells, B cells, and macrophages indicated the presence of a minor local immune response, which could affect the mechanical integrity of the tissue-engineered construct implanted into the disc. Thus, other factors apart from the allogeneic nature of the implant may drive the immune response. Within the field of cartilage tissue engineering, these potential interactions between neocartilage and components of the immune system has not been extensively studied.

Key initial mediators of the immune system are macrophages, which orchestrate the inflammatory and healing processes in response to injury or infection.[402] Depending on the healing or disease state, the spectrum of macrophage behavior and phenotype can polarize toward an proinflammatory (referred to as M1 phenotype) or anti-inflammatory (referred to as M2 phenotype) state.[403] It is well-established that macrophages have a differential response to various biochemical signals in the body.[404-406] For example, proinflammatory cytokines (e.g., tumor necrosis factor alpha or TNF-α) and lipopolysaccharide (LPS), an outer membrane component of Gram negative bacteria, can activate macrophages toward a proinflammatory phenotype.[402,406] In native cartilages, this macrophage phenotype has been shown to enhance cartilage inflammation and degeneration.[10] Conversely, interleukin 10 (IL-10) or a combination of IL-4 and IL-13 can drive macrophages toward an anti-inflammatory phenotype,[407],[404] which has been shown to prevent extracellular matrix degradation and promote healing in cartilage.[408,409] Characterizations of macrophage behavior in the context of engineered neocartilages is limited, however.

More recently, the effect of biophysical cues, such as material topography, applied mechanical forces, and ECM stiffness, on macrophages has been explored.[410-412] Within the context of cartilage tissue engineering, ECM stiffness is of particular interest because cartilage tissue engineers aim to create stiff neocartilages that mimic the properties of native tissue to

withstand repeated loading.[3] Macrophage behavior may function at odds with the goal of engineering functional implants because matrix stiffness has been previously shown to positively correlate with macrophage-induced inflammatory responses.[413] Thus, stiffer neocartilage tissues desirable for implantation may be subject to increased macrophage-induced inflammation *in vivo*, resulting in breakdown of the stiff ECM.[10] Ultimately, characterization of the interactions between macrophages and biomimetic neocartilages *in vitro* would inform strategies for more effective *in vivo* cartilage repair.

In this study, a novel, direct co-culture system to explore the interaction between self-assembled neocartilage and macrophages is described. The global objective of implementing this system was to characterize the interaction between neocartilage constructs formed under a variety of conditions and macrophages in differentially activated states. In particular, the objective of Study 1 was to investigate the stiffness-mediated inflammatory response of macrophages. It was hypothesized that stiffer constructs would result in polarization of macrophages toward an inflammatory phenotype, and, thus, would cause a decrease in the mechanical properties of the constructs. Study 2 aimed to determine the protective effects of various bioactive factors. It was hypothesized that neocartilage-specific bioactive factors (i.e., TCL: transforming growth factor beta-1 (TGF-β1), chondroitinase ABC (C-ABC), and lysyl oxidase like 2 (LOXL2)) would confer protection to neocartilage during macrophage co-culture. Also, it was hypothesized that co-culture with IL-10-stimulated macrophages would result in improved neocartilage mechanical properties compared to constructs exposed to LPS-stimulated macrophages.

Methods

Isolation, expansion, and aggregate redifferentiation of chondrocytes

Costal cartilage from Yucatan minipigs between 5 and 8 months (n = 3, Premier BioSource) were obtained within 48 hours postmortem. The cartilage was obtained from the entirety of the rib cage, minced into 1 mm^3 pieces, and digested using 0.4% w/v pronase (Sigma Aldrich) supplemented

with 3% fetal bovine serum (FBS) (R&D Systems) for 1 hour at 37°C followed by 0.2% w/v collagenase type II (Worthington Biochemical) supplemented with 3% FBS for 18 hours at 37°C. Cells were filtered, counted, treated with ammonium-chloride-potassium (ACK) lysing buffer,[414] washed with phosphate buffered saline (PBS), and subsequently cultured in chemically defined culture (CHG) medium composed of Dulbecco's modified Eagle's medium (DMEM), high glucose, GlutaMAX supplement (Gibco), 1% penicillin-streptomycin-fungizone (Lonza), 1% insulin, transferrin, and selenous acid (ITS+) premix (Corning), 1% nonessential amino acids (Gibco), 100 nM dexamethasone (Sigma Aldrich), 50 µg/mL ascorbate-2-phosphate (Sigma Aldrich), 40 µg/mL L-proline (Sigma Aldrich), and 100 µg/mL sodium pyruvate (Sigma Aldrich) supplemented with 2% FBS at a density of 2.5 million cells per T-225 flask. During monolayer expansion, cells were further supplemented with 1 ng/mL TGF-β1 (PeproTech), 5 ng/mL basic fibroblastic growth factor (bFGF) (PeproTech), and 10 ng/mL platelet derived growth factor (PDGF) (PeproTech) (termed TFP), which has been previously shown to increase proliferation and postexpansion chondrogenic potential.[29] Medium was exchanged every 3-4 days. Upon 90% confluence, cells were lifted and digested using 0.05% Trypsin-EDTA (Gibco) followed by 0.2% w/v collagenase type II supplemented with 3% FBS for 40 minutes and frozen at passage 1 for downstream use. Cells were thawed for each experiment and expanded to passage 6 in CHG supplemented with TFP as described above. At passage 6, cells were placed into aggregate culture with CHG containing 10 ng/mL TGF-β1, 100 ng/mL growth differentiation factor 5 (GDF-5) (PeproTech), and 100 ng/mL bone morphogenetic protein 2 (BMP-2) (PeproTech) (termed TGB), which has been previously shown to promote redifferentiation of cells toward a chondrogenic phenotype.[30] Cells were plated on 1% agarose-coated plates at a density 750,000 per mL with medium changes every 3-4 days. Plates were kept on an orbital shaker at 50 RPM for 24 hours. After 14 days of aggregate culture, cells were digested with 0.05% Trypsin-EDTA for 45 minutes followed by 0.2% w/v type II collagenase supplemented with 3% FBS for 2 hours. Cells were passed through a 70 µm filter to ensure a single cell suspension for subsequent self-assembly.

Isolation of bone marrow-derived monocytes and differentiation into macrophages

Pelvises from Yucatan minipigs between 5 and 8 months (n = 3, Premier BioSource) were obtained within 6 hours postmortem. These animals were different donors from the costal cartilage donors. Bones were cleaned of muscle and other soft tissues. Using a sterile chisel and hammer, the bone marrow was exposed and rinsed from the bone cavity of pelvis using RPMI-1640 (Gibco). Cells were passed through a 70 μm filter, spun down, and rinsed with PBS. Cells were treated with ACK lysing buffer to remove any red blood cells and subsequently washed with PBS. Cells were plated at approximately 10 million cells per 100 x 25 mm petri dishes in a chemically defined macrophage culture medium (MΦ) composed of RMPI-1640, L-glutamine, and 1% penicillin-streptomycin, supplemented with 10% FBS and 20 ng/mL granulocyte-macrophage colony-stimulating factor (GM-CSF) (R&D Systems) to differentiate cells to bone marrow-derived macrophages. Cells were fed every 3-4 days and lifted after 7 days and frozen for downstream use.

Formation of self-assembled cartilage constructs

After expansion and aggregate redifferentiation, cells underwent the self-assembling process. Prior to seeding, non-adherent agarose wells were formed using 2% agarose and a negative mold to form the shape of 5 mm cylindrical constructs, and CHG was exchanged on the wells 3 times prior to seeding. Cells were subsequently seeded at 2 million per well in 100 μL of CHG. Four hours after seeding, wells were topped off with another 400 μL of CHG. Medium was exchanged every day until day 3 when constructs were unconfined from agarose wells, transferred to untreated dishes, and fed with 2 mL every other day up to 27 days. Study 1 consisted of CHG medium only. Study 2 consisted of CHG coupled with TGF-β1 continuously, C-ABC (Sigma Aldrich) on day 7 for four hours, and LOXL2 (SignalChem) from days 14-27, as previously described.[415] Briefly, C-ABC (2 U/mL) consisted of activation with 50 mM sodium acetate (Sigma Aldrich) and quenching with 1 mM zinc sulfate. LOXL2 treatment consisted of 0.15 μg/mL coupled

with 0.146 mg/mL hydroxylysine (Sigma Aldrich) and 1.6 μg/mL copper sulfate (Sigma Aldrich). TCL treatment has been previously shown to enhance the functional properties of neocartilage.[277]

Co-culture of macrophages and self-assembled cartilage constructs

After the self-assembling process, co-culture was initiated according to the steps illustrated in Figure 6-1. First, constructs were treated with C-ABC to modulate compressive stiffness via depletion of glycosaminoglycan (GAG) content. On day 27, constructs were treated with 0.0, 0.5, or 1.0 U/mL (1 mL/construct) of C-ABC for 2 hours. Macrophages were also thawed and cultured in MΦ medium overnight. On day 28, constructs were placed at the bottom of 2% agarose wells in 50 μL CHG medium. Subsequently, macrophages were seeded at a density of 25,000 in 50 μL MΦ medium on top of constructs inside the agarose well to confine macrophages to the construct surface. After 4 hours, a 1:1 mixture of the formulations of CHG and MΦ mediums described above was added to the co-culture system to sustain cell and tissue viability. Stimulation occurred the following day with 0.1 ng/mL of lipopolysaccharide (LPS) in Study 1 and 1.0 ng/mL LPS or 10 ng/mL IL-10 in Study 2. Medium was exchanged every 3 days and co-culture continued for 2 weeks. Both studies also included constructs cultured in 1:1 CHG:MΦ medium within agarose wells in the absence of macrophages (i.e., construct-only control), as well as 25,000 macrophages cultured in 1:1 CHG:MΦ within agarose wells without constructs (i.e., macrophage-only control).

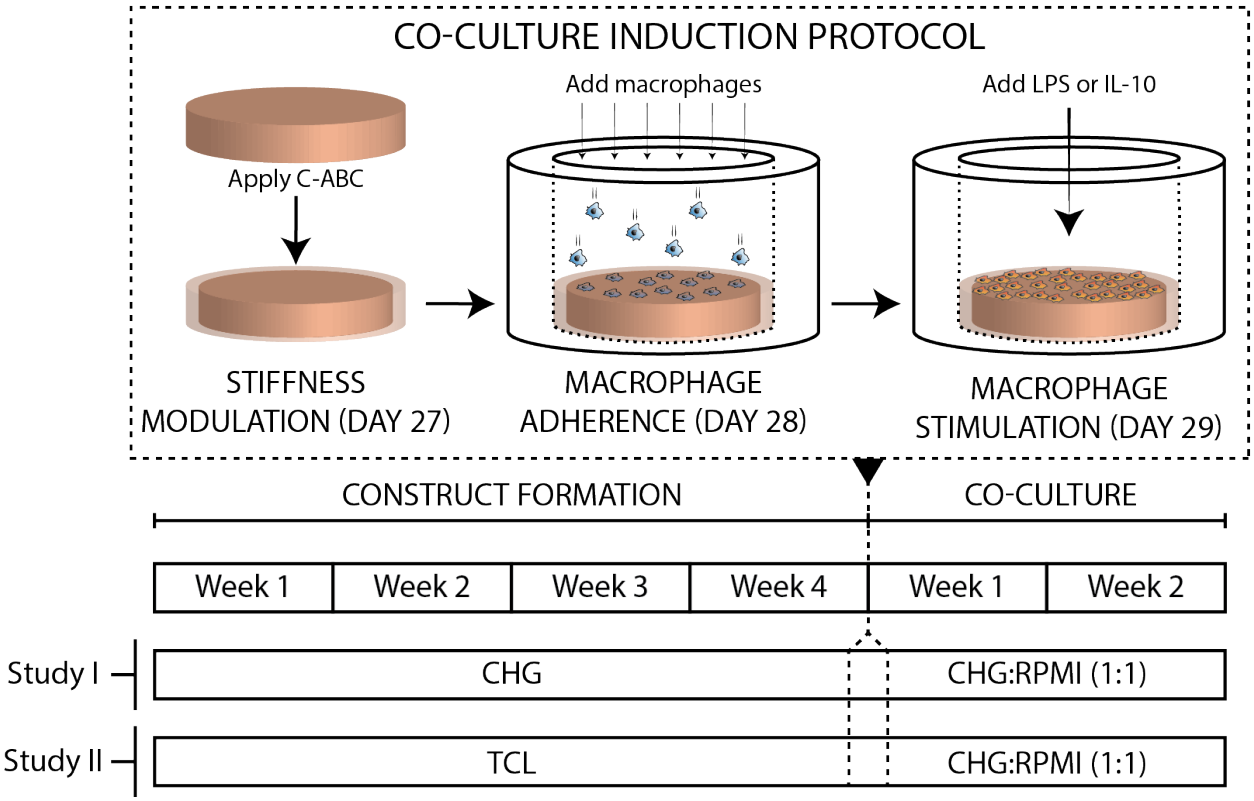

Figure 6-1. A schematic representation of the co-culture system. Constructs were cultured in either CHG only or with TCL treatment. After 27 days, compressive stiffness was modulated through C-ABC application. Constructs were assayed for baseline properties (t=0). The next day, macrophages were adhered and cultured in a 1:1 mix of CHG and MΦ mediums, then stimulated with LPS in Study 1 and LPS or IL-10 in Study 2. Unstimulated macrophage controls, construct-only controls, and macrophage-only controls were also included. After two weeks of co-culture, constructs were assayed again (t=2 weeks). C-ABC, chondroitinase ABC, IL-10, interleukin 10, LPS, lipopolysaccharide, TCL, transforming growth factor beta 1/chondroitinase ABC/lysyl oxidase like 2.

Sample processing and biochemical analyses

Following culture, construct samples were weighed before and after lyophilization, and subsequently digested in papain for biochemical analysis. Total collagen (Col) content was measured via a modified hydroxyproline assay as previously described.[381] GAG content was measured by a dimethylmethylene blue dye-binding assay kit (Biocolor). DNA content was measured via PicoGreen assay (ThermoFisher Scientific). Pyridinoline crosslink (PYR) quantification was conducted using a liquid chromatography–mass spectrometry (LCMS) assay as described previously.[4] Samples were hydrolyzed in 6 N HCl at 105°C for 18 hours, after which acid was evaporated in a fume hood. Dried hydrolysates were resuspended in 25% (v/v)

acetonitrile and 0.1% (v/v) formic acid in water, centrifuged at 15,000 × g for 5 minutes, and the supernatant was transferred to an LCMS-compatible vial. Liquid chromatography was performed on a Cogent Diamond Hydride HPLC Column (2.1 mm × 150 mm, particle size 2.2 µm, pore size 120 Å) (MicroSolv). The elution gradient used 0.1% (v/v) formic acid in water as solvent A and 100% acetonitrile as solvent B. The 5-minute elution gradient ran at 300 µL/min (0 minutes 25% B, 2 minutes 25% B, 2.2 minutes 5% B, 3 minutes 25% B). Mass spectrometry was performed on a Quadrupole Mass Detector (ACQUITY QDa, Waters) in ESI+ MS scan mode. MassLynx software version 4.1 with TargetLynx was used to quantify PYR in 10 µL injections of sample by integrating the extracted ion chromatogram of double-charged PYR (m/z = 215.1) and comparing to a PYR standard (BOC Sciences) prepared and run in the same fashion.

Mechanical testing

Constructs were analyzed under creep indentation and uniaxial tension. As previously described,[277] construct segments were trimmed into dog bone-shaped specimens and glued to paper tabs which were gripped to a uniaxial testing machine (Instron 5565). A pull-to-failure test was performed at 1% strain per second. Tensile Young's modulus and ultimate tensile strength (UTS) were determined using the force-displacement curves from a custom MATLAB (MathWorks) code. Creep indentation was performed on cylindrical pieces of construct as previously described.[383] Briefly, self-assembled cartilage constructs were indented with a flat, porous tip under a constant load. A linear biphasic model and finite element analysis were used to obtain aggregate modulus, permeability, and shear modulus from experimental curves.[385]

Histology

Construct samples were fixed in 10% neutral-buffered formalin for histological evaluation. Samples were subsequently processed, embedded in paraffin, and sectioned at 5 µm thickness. Samples were stained with hematoxylin and eosin (H&E) to show morphology and Safranin O/Fast Green (Saf O) to visualize GAG content.

ELISA cytokine analysis

Medium for enzyme-linked immunosorbent assays (ELISAs) was collected from sample wells either 24 or 48 hours after stimulation. Kits for TNF-α were purchased and used per the manufacturer's instructions (R&D Systems).

Statistics

All statistical analyses were performed using Prism 8 (GraphPad Software). Quantitative data including more than two groups were assessed using either a one-way or two-way analysis of variance (ANOVA) with a *post hoc* Tukey's HSD (honestly significant difference) test at a significance level of $\alpha = 0.05$. Two-way ANOVA factors and interactions were analyzed to determine the individual factor effects as well as any interactions between those factors. P-values for ANOVA factors are capitalized. Significance among particular groups is illustrated by a connecting letters report with Latin characters (i.e., bars that do not share the same Latin character(s) are statistically significant), and p-values for post hoc tests are lower case. For two-way ANOVAs, *post hoc* Tukey's HSD tests were only used to compare groups within the dotted lines. For each set of quantitative data that only included two groups, a student's t-test was performed at a significance level of $\alpha = 0.05$.

Results

Study 1: C-ABC modulates compressive stiffness in CHG-treated constructs

C-ABC was used at a concentration of 0.0 U/mL (stiff), 0.5 U/mL (medium), or 1.0 U/mL (soft) to modulate compressive stiffness. Directly following this treatment, constructs were evaluated to establish a baseline of properties. Application of 1.0 U/mL (soft) and 0.5 U/mL (medium) of C-ABC significantly decreased soft ($p = 0.0008$) and medium ($p = 0.03$) group WWs compared to the stiff group (Figure 6-2A). Similarly, GAG/WW significantly decreased by 28% in the soft group compared to the stiff group ($p = 0.006$), but was not significantly different from the medium group

(p = 0.2) (Figure 6-2B). As expected this led to a subsequent decrease in aggregate moduli from 133.7 ± 67.2 kPa for soft (p = 0.009) and 182.7 ± 22.4 kPa for medium (p = 0.03) groups compared to 341.7 ± 65.6 kPa for the stiff group (Figure 6-5A), however there was no significant difference between soft and medium groups (p = 0.6). Tensile Young's modulus and UTS did not differ significantly between the groups (Figure 6-5A).

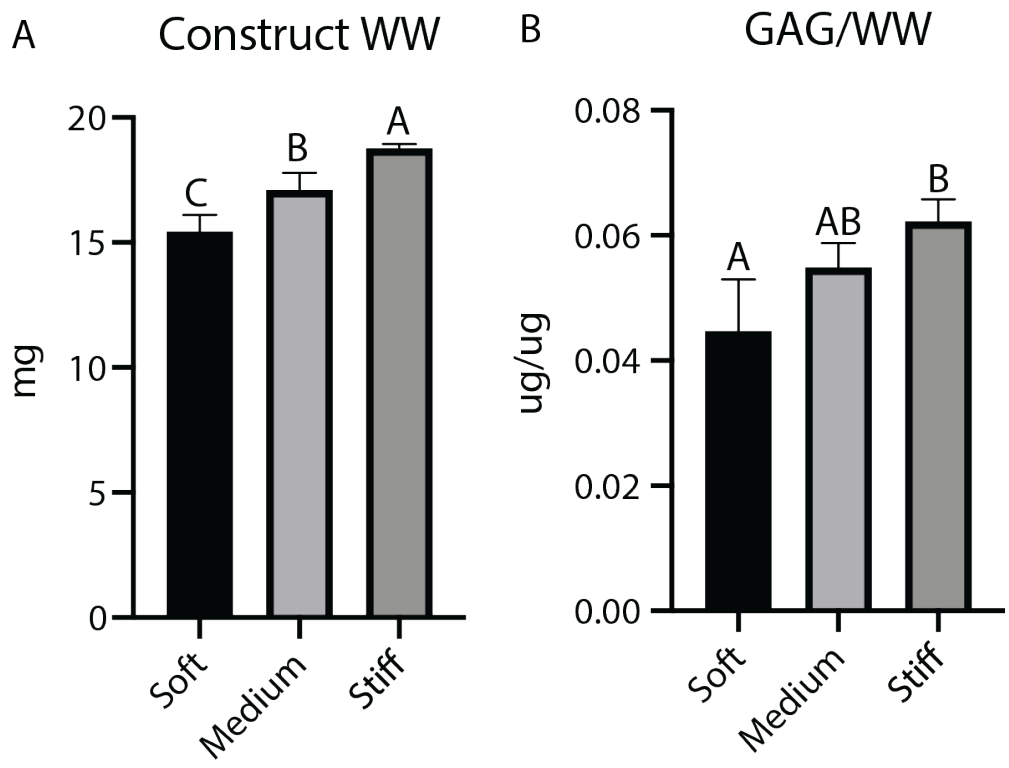

Figure 6-2. C-ABC application modulates CHG-treated construct biochemical properties. A) At t=0, construct WW was significantly different in all groups, indicating more matrix depletion with increasing C-ABC concentration. B) GAG/WW at t=0 trended similarly to Construct WW, increasing with stiffness and decreasing with C-ABC application. GAG, glycosaminoglycan, WW, wet weight.

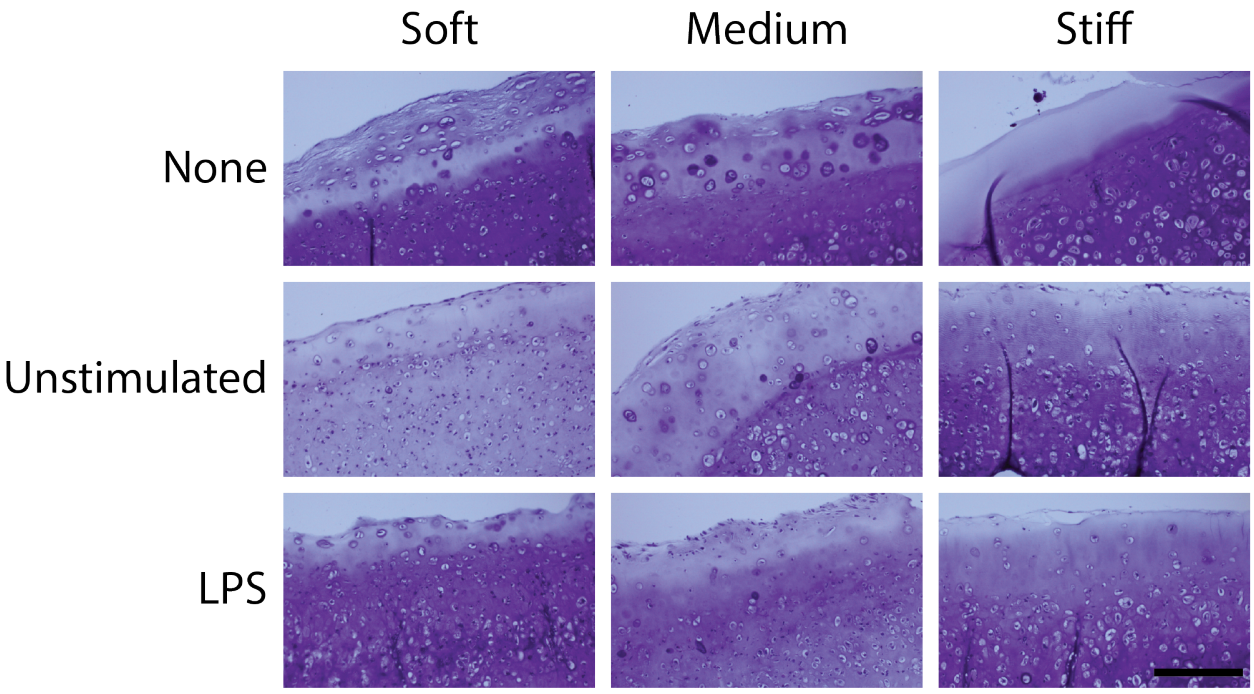

Figure 6-3. H&E from CHG-treated constructs following 2 weeks of co-culture. Stiff constructs appear to maintain cell morphology and tissue staining intensity in co-culture groups more than the soft and medium groups. LPS, lipopolysaccharide. Scale bar = 200 μm.

Study 1: Stiff, CHG-treated constructs are protected from macrophage inflammatory challenge even in the presence of an elevated proinflammatory response

CHG-treated neocartilage cultured for 2 weeks in the presence of macrophages demonstrated differences in tissue morphological characteristics according to construct stiffness (Figure 6-3). For example, the soft, unstimulated group demonstrated fewer chondrocytes with intact lacunae structure than the stiff, unstimulated group. Also, both co-culture groups for the stiff group did not appear to lose as much staining intensity relative to its corresponding construct-only control compared to the soft and medium group. Additionally, stiff construct-only constructs did not exhibit cells near the construct edge, unlike the other construct-only control groups. The factor of macrophage co-culture significantly affected construct WW across all stiffnesses ($P < 0.0001$) (Figure 6-4A). Similarly, the macrophage co-culture factor was also significant ($P = 0.01$) for GAG/WW, but only showed significant differences in the medium stiffness between the construct-only control (none) (0.066 ± 0.007 ug/ug) and LPS-stimulated macrophage co-culture (0.035 ±

0.018 ug/ug) ($p = 0.01$) (Figure 6-4B). Col/WW did not significantly differ between groups within any stiffness (Figure 6-4C), but, as a factor, stiffness was significant ($P = 0.001$).

Aggregate modulus values trended, as expected, with GAG/WW (Figure 6-4B, Figure 6-5B). Interestingly, aggregate modulus for soft ($p = 0.04$) and medium ($p = 0.001$) groups decreased from 160.33 ± 15.28 kPa and 180.50 ± 36.06 kPa to 91.20 ± 60.10 kPa and 57.80 ± 17.74 kPa, respectively, when co-cultured with LPS-stimulated macrophages (Figure 6-5B). Significant changes in aggregate modulus for soft ($p = 0.02$) and medium ($p = 0.02$) groups also occurred when comparing construct-only controls to unstimulated macrophage co-culture groups, decreasing by 59.9% and 46.4%, respectively (Figure 6-5B). Construct-only controls (159.67 ± 47.18 kPa) in the stiff group did not differ from unstimulated (134.50 ± 44.75 kPa) ($p = 0.6029$) or LPS-stimulated (123.83 ± 32.85 kPa) ($p = 0.4$) co-culture groups (Figure 6-5B).

After 48 hours of stimulation, TNF-α levels significantly increased by 547% in the stiff group when stimulated with LPS compared to construct-only controls ($p=0.01$), but there were no significant differences when comparing either of those groups to unstimulated co-culture groups, although TNF-α levels in the LPS group trended 1.6-fold higher than the unstimulated group ($p = 0.2$) (Figure 6-5C). Interestingly, the soft and medium groups did not differ significantly in TNF-α levels between macrophage conditions (Figure 6-5C), but did have significant decreases in aggregate modulus (Figure 6-5B). Conversely, the stiff group did not experience significant decreases in aggregate modulus compared to construct-only control (Figure 6-5B), indicating that stiff constructs are protected from increased levels of inflammatory cytokines (i.e., TNF-α).

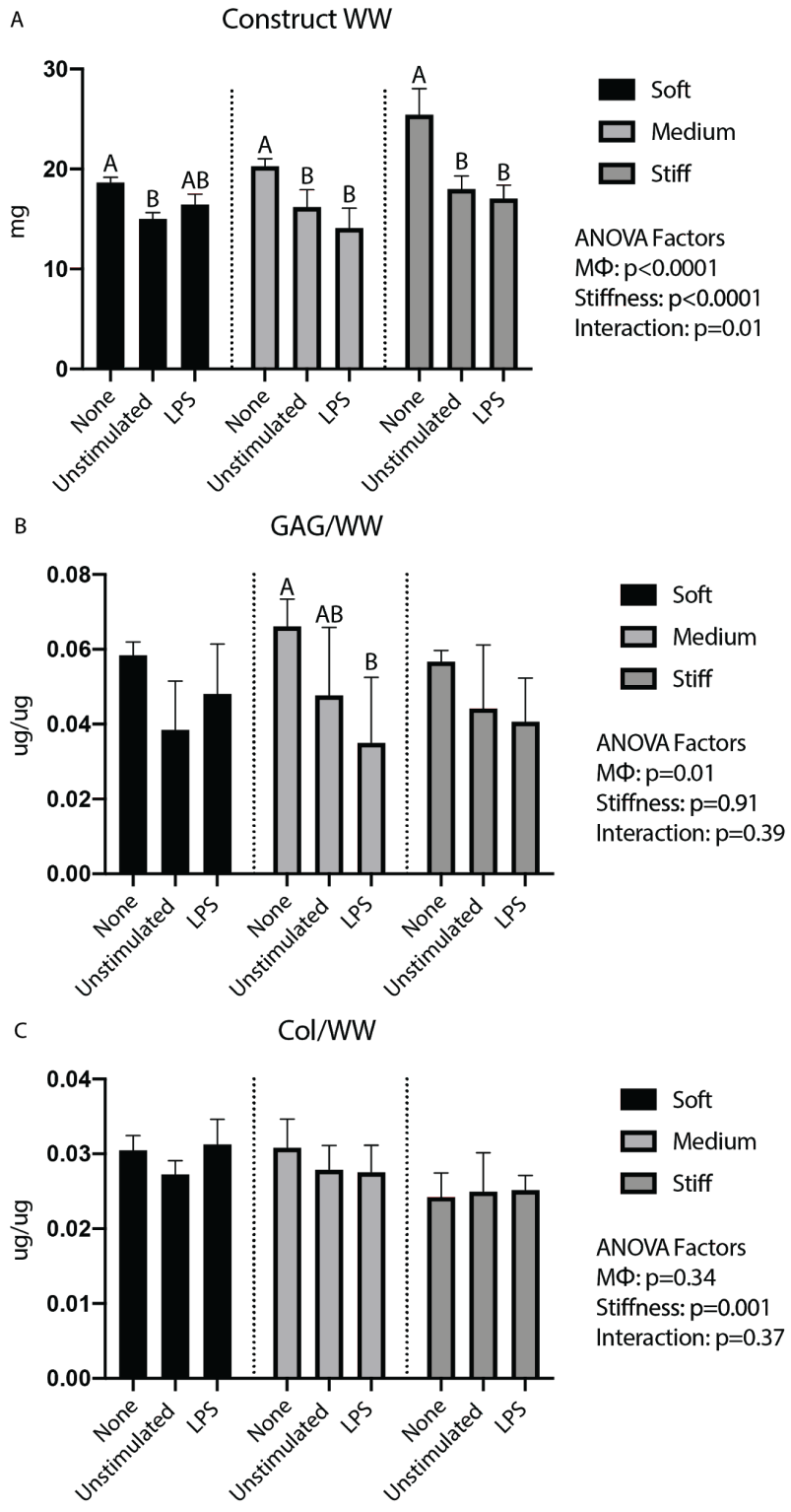

Figure 6-4. CHG-treated construct biochemical properties after 2 weeks of macrophage co-culture. A) Construct WW was significantly affected by the factor of macrophage condition (MΦ), indicating a general decrease in WW when adding macrophages to constructs. B) GAG/WW was also significantly affected by the factor MΦ. C) Col/WW was not affected by macrophage addition, but was affected by the stiffness factor. GAG, glycosaminoglycan, Col, collagen, LPS, lipopolysaccharide, MΦ, macrophage, WW, wet weight.

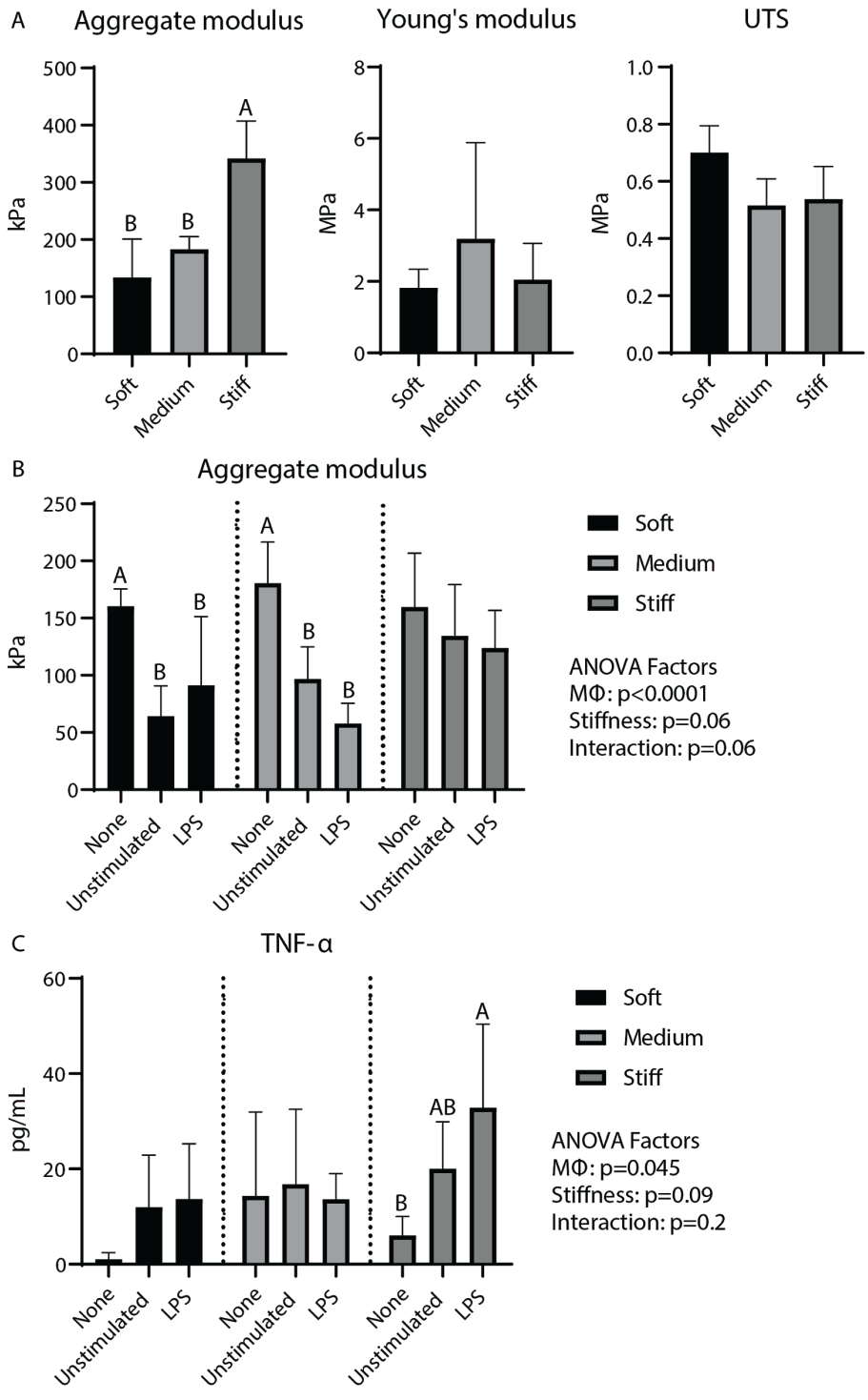

Figure 6-5. Mechanical properties and inflammatory cytokine data for CHG-treated constructs. A) Aggregate modulus decreased with C-ABC application at t=0, while tensile properties were not affected. B) After 2 weeks of co-culture, when comparing to their corresponding construct-only control, aggregate modulus significantly decreased in soft and medium groups, but not in the stiff group. C) After 48 hours of stimulation, TNF-α increased in the stiff group relative to control, but did not in other groups. LPS, lipopolysaccharide, MΦ, macrophage, TNF-α, tumor necrosis factor alpha, UTS, ultimate tensile strength.

Study 2: C-ABC modulates compressive stiffness in TCL-treated constructs

Directly following C-ABC treatment, TCL-treated constructs were evaluated to establish a baseline of properties. As shown in Figure 6-6, the soft group, which was treated with 1.0 U/mL C-ABC, had reduced extracellular matrix and GAG content at the periphery of the construct. Conversely, the stiff group exhibited intense matrix and GAG content all the way to the edge of the construct. GAG/WW was not significantly different between the two stiffnesses (Figure 6-8A), but aggregate modulus for the stiff group (165.6 ± 20.7 kPa) was significantly higher ($p < 0.0001$) than the soft group (76.8 ± 18.6 kPa). Thus, although C-ABC did not change GAG/WW between the soft and stiff groups, it still had a significant effect on aggregate modulus.

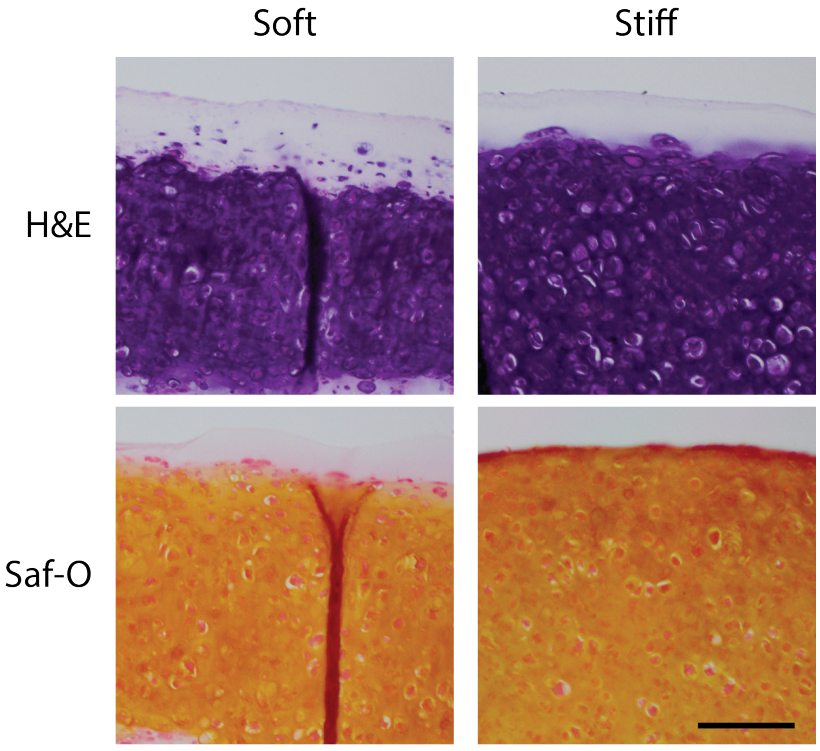

Figure 6-6. Histology of TCL-treated constructs after C-ABC application at t=0. Soft constructs show less intense Saf-O and H&E staining due to C-ABC application and only peripheral loss of GAG. Also, some cells are visible near the soft construct edge. Conversely, stiff constructs show intense Saf-O staining at the periphery indicating high GAG content, and cells are not present at the periphery of the construct. H&E, hematoxylin and eosin, Saf-O, Safranin O. Scale bar = 100 µm.

Study 2: TCL-treated constructs can withstand macrophage challenge regardless of stimulation and stiffness

Saf O staining of constructs illustrates variability in GAG content across macrophage donors as well as within the construct-only control (Figure 6-7). Compared to other conditions within stiffnesses, it appears as though staining intensity is slightly diminished in the LPS-stimulated group. In the soft group, relative to the construct construct-only control, GAG/WW significantly decreased by 0.74-fold ($p = 0.02$), 0.66-fold ($p = 0.002$), and 0.68-fold ($p = 0.004$) for the unstimulated, LPS-stimulated, and IL-10-stimulated groups, respectively (Figure 6-8B). For the stiff group, no condition caused GAG/WW to change. In terms of aggregate modulus (Figure 6-8C), in the soft group, only the LPS-stimulated group and construct-only control were significantly different from each other ($p = 0.04$), as the LPS group had an aggregate modulus that was 44% of the construct-only control. The unstimulated group and IL-10 group had aggregate moduli that were 77% and 49% of the construct-only control, but these trends were not statistically significant. For the stiff group, there were no significant differences in aggregate modulus, which were 186.0 ± 91.4 kPa, 173.0 ± 56.3 kPa, 144.0 ± 82.0 kPa, and 160.5 ± 65.3 kPa for the construct-only, unstimulated, LPS-stimulated, and IL-10-stimulated conditions, respectively.

Study 2: TCL-treated constructs diminish TNF-α production, and increased stiffness enhances the anti-inflammatory effect of IL-10-stimulated macrophages

In terms of TNF-α production (Figure 6-8D), 24 hours after the stimulation time point, unstimulated macrophages secreted 16.0 ± 4.6 pg/mL TNF-α. In comparison to the unstimulated macrophage-only control, the presence of soft constructs significantly reduced TNF-α levels to 4.8 ± 2.4 pg/mL ($p = 0.001$) for unstimulated macrophages, whereas stiff constructs did not have an effect. LPS-stimulated macrophages produced 117.6 ± 18.0 pg/mL TNF-α. Both soft and stiff constructs caused a significant 81% ($p < 0.0001$) and 76% ($p < 0.0001$) reduction in TNF-α levels compared to the LPS-stimulated macrophage-only control. IL-10-stimulated macrophages secreted 15.6 ± 1.3 pg/mL TNF-α. While soft constructs did not cause a significant difference in TNF-α levels

compared to the IL-10-stimulated macrophage-only control, stiff constructs significantly reduced the TNF-α concentration to 4.6 ± 2.9 pg/mL ($p = 0.005$).

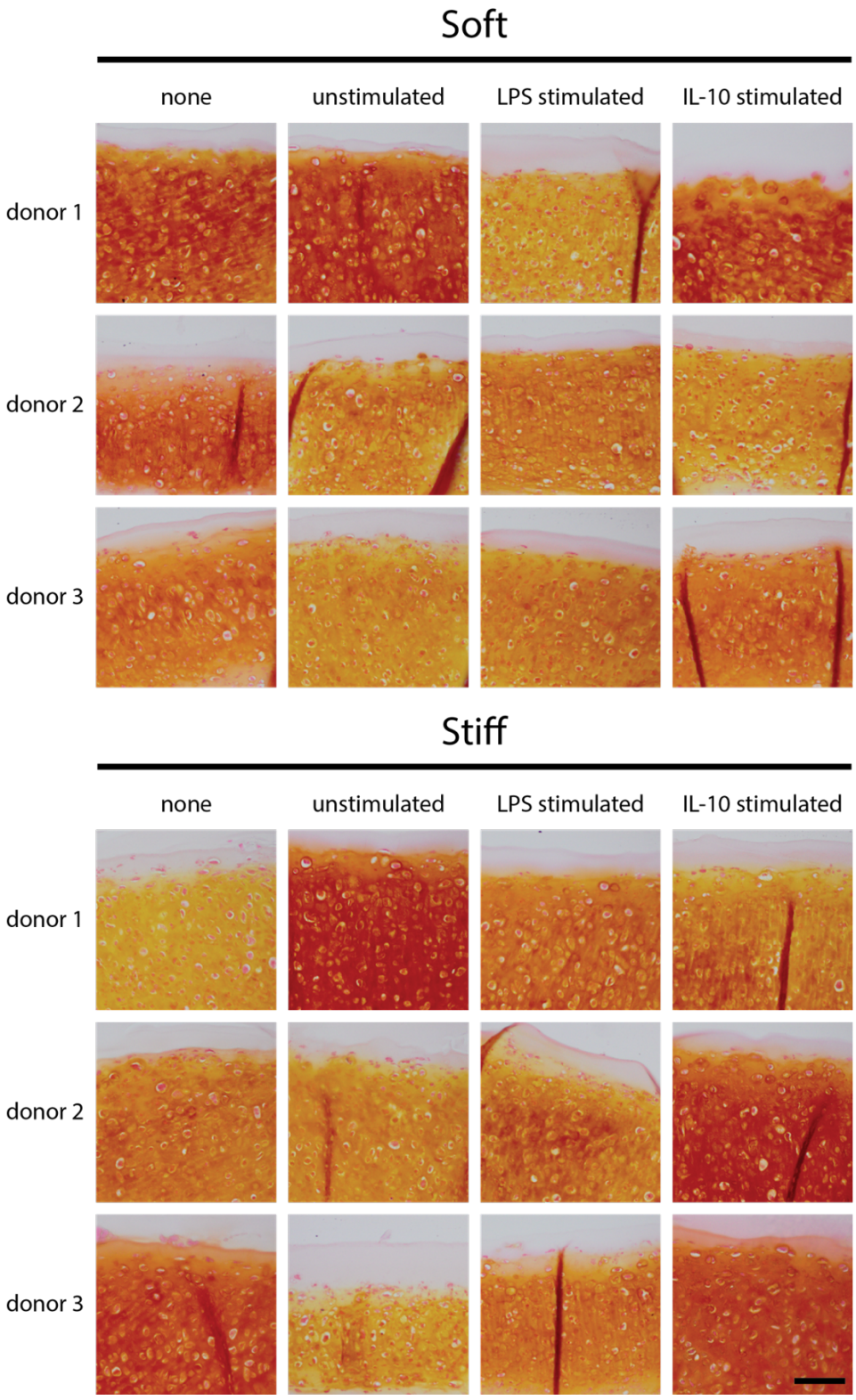

Figure 6-7. Saf O staining of TCL-treated constructs after two weeks of macrophage co-culture. Both construct-only controls and co-culture groups show variability between donors. However, staining, on average, seems to appear diminished in LPS stimulated groups. IL-10, interleukin 10, LPS, lipopolysaccharide. Scale bar = 100 μm.

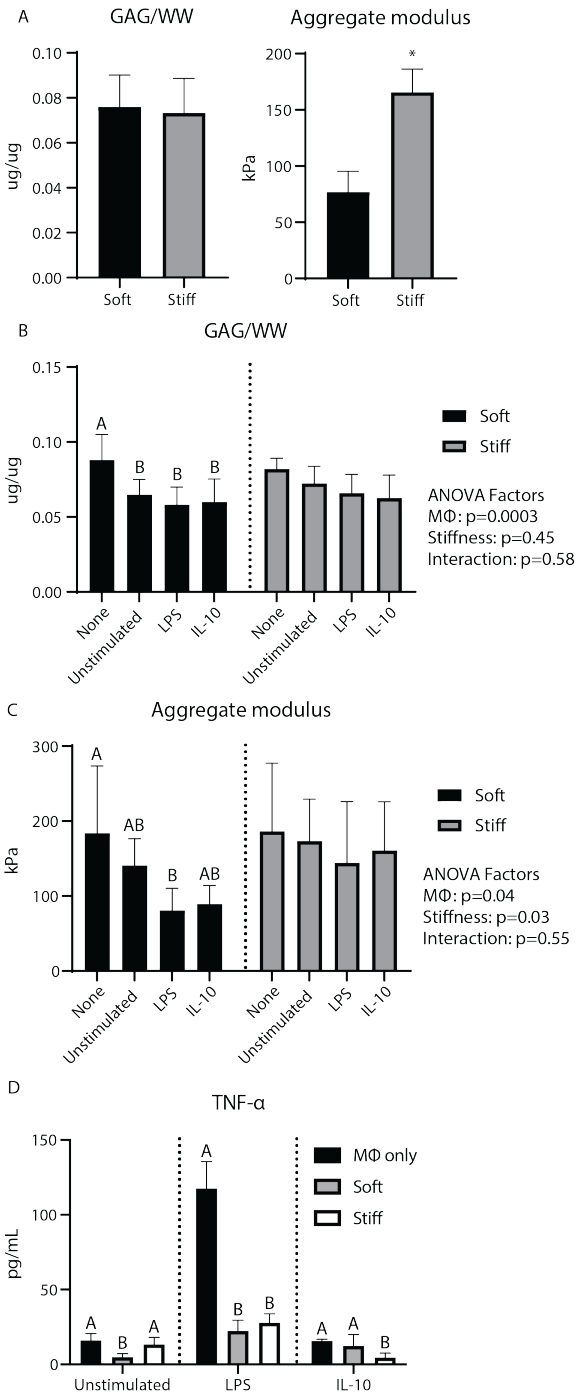

Figure 6-8. Biochemical, mechanical, and cytokine data for TCL-treated constructs. A) While GAG/WW does not differ significantly for TCL-treated constructs at t=0, aggregate modulus significantly decreases with application of C-ABC. B) GAG/WW after 2 weeks of co-culture significantly decreases with macrophage application in soft, but not stiff groups. C) Aggregate modulus also trends downward for the soft group when co-cultured with macrophages, but only the LPS stimulated co-culture group is significantly different from the construct-only control. Stiff group aggregate moduli were largely unaffected by macrophage treatment. D) After 24 hours of stimulation, within each macrophage condition, TNF-α concentration in media had significantly decreased compared to the corresponding MΦ only controls for the soft, unstimulated condition, soft and stiff LPS condition, and the stiff IL-10 condition. GAG, glycosaminoglycan, IL-10, interleukin 10, LPS, lipopolysaccharide, MΦ, macrophage, TNF-α, tumor necrosis factor alpha, WW, wet weight.

Discussion

Substantial progress has been made toward tissue engineered cartilages with properties approaching or on par with native tissue.[4-6,29] While achieving these biomimetic properties should be a part of the translational tissue engineering process, other factors must be considered to evaluate the potential success of a neocartilage implant in an *in vitro* setting. For example, as part of the innate immune response to surgical trauma, cells such as macrophages migrate to the treated area and would likely interact with the implant.[416] Due to the potentially deleterious effect these processes could have on the engineered tissue *in vivo*, the objective of this study was to develop a novel, *in vitro* direct co-culture model to study the interactions between differentially stimulated macrophages and self-assembled neocartilage. Two separate studies were conducted. Study 1 investigated the inflammatory response of macrophages to neocartilage of varying stiffnesses. The hypothesis that stiffer constructs would polarize macrophages toward a proinflammatory phenotype was confirmed, but, interestingly, this response did not cause a reduction in stiff construct mechanical properties. In Study 2, the potential protective effects of various bioactive factors against macrophage challenge were examined. While IL-10 stimulation of macrophages did not improve neocartilage mechanical properties compared to LPS-stimulation, the defined regimen of bioactive factors (i.e., TCL) prevented neocartilage mechanical degradation over time, regardless of macrophage stimulation condition or construct stiffness.

Increasing neocartilage stiffness drives polarization of macrophages to an enhanced proinflammatory phenotype, but that stiffness may also protect neocartilage from losing mechanical robustness. Specifically, in Study 1, LPS-stimulated macrophages co-cultured with stiff constructs secreted 2.4-fold more TNF-α than identically stimulated macrophages cultured on either soft or medium constructs 48 hours after stimulation. Also, macrophages co-cultured with soft or medium constructs did not produce TNF-α levels above those of their corresponding construct-only controls. Interestingly, this stiffness-mediated augmentation of macrophage phenotype was not limited to proinflammatory macrophages. In Study 2, IL-10-stimulated

macrophages co-cultured with stiff constructs had significantly lower TNF-α levels compared to soft constructs exposed to the same co-culture condition. This apparent stiffness-dependent macrophage behavior has been well documented on less complex substrates such as hydrogels.[417] For example, it has been observed that when LPS-stimulated macrophages were seeded on polyethylene glycol (PEG) hydrogels of increasing stiffness, TNF-α and IL-1β expression increased alongside stiffness.[418] Interestingly, however, while these proinflammatory cytokines are known to have catabolic effects on native articular cartilage mechanical properties,[10] stiff, self-assembled neocartilage did not experience a drop in properties relative to its corresponding construct-only control at 2 weeks. However, this is possibly due to the fact that after 2 weeks in CHG:RPMI medium, the stiff construct-only group lost 51% of its aggregate modulus. While the mechanism for this behavior is unclear, it can be concluded that the addition of macrophages to these stiff constructs did not further damage properties during the co-culture period, which was not the case for the other two stiffnesses.

In addition to stiffness, TCL prevents constructs from reductions in mechanical properties experienced by CHG-only treated neocartilage subjected to macrophage challenge. All groups except for the soft, TCL-treated constructs exposed to LPS-stimulated macrophages did not significantly differ from their corresponding construct-only controls after 2 weeks. Additionally, TCL-treated constructs co-cultured with macrophages in study 2 either maintained or increased their aggregate modulus compared to baseline values prior to co-culture. For example, the stiff construct co-cultured with unstimulated macrophages increased by 1.04-fold, and the soft construct co-cultured with unstimulated macrophages increased by 1.05-fold. This is in stark contrast to CHG-treated constructs co-cultured with macrophages, which all experienced a reduction in aggregate modulus ranging from 37-70% of the corresponding aggregate modulus value at t=0. Since the medium CHG-only group experienced such a marked drop in properties from baseline (30-57% of 180.5 ± 36.1 kPa), whereas the stiff TCL group did not (87-104% of 165.6 ± 20.7 kPa), this suggests that an effect inherent to TCL confers protection to constructs

because their baseline aggregate moduli corresponded to one another. Further exploration would be necessary to determine the mechanism responsible for this behavior.

TCL-treatment has been shown to enhance extracellular matrix content and collagen crosslinking in self-assembled cartilage constructs,[4-6,55,278] which could make TCL-treated constructs more durable and, in turn, less susceptible to macrophage infiltration compared to CHG-treated constructs. It is also possible that TCL treatment causes chondrocytes within self-assembled constructs to respond to macrophage-secreted cytokines more favorably in terms of maintenance of properties in comparison to cells that were not exposed to bioactive factors.[419] In other words, TCL treatment could reduce chondrocyte production of catabolic factors that might otherwise be produced in the presence of macrophages and associated cytokines. Alternatively, it is possible that alterations in construct surface topology and extracellular matrix contents driven by TCL treatment alters the behavior and phenotype of macrophages.[417] The fact that LPS-stimulated macrophage TNF-α production was reduced by more than 4-fold when co-cultured with either soft or stiff TCL-treated constructs suggests that TCL-treated constructs have an anti-inflammatory effect on macrophage phenotype. Ultimately, due to their stability and robustness, TCL-treated constructs should be used for future cartilage mechano-immunology studies.

While some of the results and conclusions of this study are promising, this study could have been improved in a variety of ways. Macrophage behavior varies substantially from donor to donor; thus, it is important to include macrophages from multiple donors. In Study 2, two replicates from a total of three donors were used to account for this variability. However, this variability could convolute the relationship between differentially stimulated macrophages and constructs, which also exhibit variability in properties. Because absolute levels of TNF-α secreted by macrophages from different donors exposed to the same controlled conditions can vary so much,[410,412] it may be worthwhile limiting future studies to one donor or expanding the sample number to uncover clearer relationships between macrophage behavior and construct stiffness, for example. Another downside to this study is the manner in which stiffness was modulated. C-

ABC decreases aggregate modulus by depleting constructs of GAG; thus, GAG content at the construct periphery could contribute to changes in macrophage behavior. For example, it has been shown that individual GAGs, such as chondroitin sulfate, can modulate macrophage phenotype by eliciting production of nitric oxide.[420] Because self-assembled neocartilage is a complex biological tissue, it would be challenging, but potentially worthwhile to develop a way to decouple changes in stiffness from changes in ECM content and construct surface topology.

Nevertheless, despite some of the drawbacks of this study, the novel, direct co-culture model developed in this study sets the stage for future investigations and will foster the development of the nascent field of cartilage mechano-immunology. Future studies could take the shape of disease or injury modeling, prohealing macrophage-assisted cartilage tissue engineering, or elucidation of biomolecular pathways that drive macrophage polarization and chondrocyte behavior. These *in vitro* studies could inform the development of relevant mechano-immunologic animal models to better understand disease and engineer neocartilage implants with immunomodulatory or immunoprotective effects. In conclusion, through the development of a novel, porcine, *in vitro* co-culture system, this study demonstrated that variable neocartilage stiffness can alter macrophage behavior, but that stiffness, as well as the bioactive factor treatment TCL, can protect construct integrity in the presence of proinflammatory factors.

CHAPTER 7 Establishing the safety of self-assembled articular cartilage implants in the Yucatan minipig

Abstract

For 250,000 Americans every year, the only clinical options for articular cartilage lesion repairs are microfracture, chondroplasty, mosaicplasty, and autologous chondrocyte implantation, which are unreliable and produce inconsistent results. The translation of tissue-engineered neocartilage is a significant clinical need that has the potential to provide consistent and long-term articular cartilage repair. However, before the translation of efficacious tissue-engineered technologies can be conceived, the FDA requires that preclinical studies demonstrate both local and systemic safety. Therefore, the objective of this study was to evaluate the preclinical safety of allogeneic, neocartilage implants using the Yucatan minipig as an animal model. The allogeneic, neocartilage implants were created using the scaffold-free, self-assembling process, which does not have the typical detriments associated with scaffold-based approaches, such as scaffold degradation byproducts. It was hypothesized that the self-assembled, allogeneic, neocartilage implants would not cause adverse local or systemic responses in minipigs. The local immune response was investigated in Surgical Set #1, where every minipig received multiple implants that were fixed within cartilage defects using three different strategies (microfracture, fibrin, or superficial fibrin). In Surgical Set #2, the systemic immune response was examined using three minipigs which received neocartilage implants, and two minipigs which served as empty defect, negative control animals. The results of this study indicate that allogeneic, self-assembled, neocartilage implants are safe for use in the Yucatan minipig model, suggesting that an analogous approach in the human would also be safe.

Authors: Link JM*, Salinas EY*, Hu JC, and Athanasiou KA. (*authors contributed equally to this work)

Introduction

Of the issues facing articular cartilage tissue engineering, one of the most pressing is the translation of these technologies into the clinic. Annually in the U.S., about 250,000 articular cartilage repair surgeries (i.e., microfracture, chondroplasty, mosaicplasty, and autologous chondrocyte implantation) are performed, indicating a significant clinical need for a reliable repair strategy.[421] The current treatment options for articular cartilage lesions are inadequate because of their inconsistency in producing hyaline cartilage, integrating with native tissue, and even filling the entire lesion.[422] Articular cartilage tissue-engineered constructs are a promising option for the repair of cartilage lesions because they can be designed and manipulated *in vitro* to enhance biochemical and biomechanical properties, completely fill cartilage lesions, and integrate with surrounding native tissue. However, even before the translation of efficacious technologies can be conceived, the safety of implanting allogeneic, tissue-engineered implants should be demonstrated.

Although articular cartilage is largely considered to be immune-privileged because of its avascularity and isolated encapsulation by the synovial membrane,[41,423,424] the FDA still requires that preclinical studies demonstrate both local and systemic safety.[12] The local safety of a neocartilage implant may first be assessed by looking at resulting gross morphological changes, such as the deterioration of native tissue surrounding the implant. Locally, the safety of a neocartilage implant may also be determined at the microscopic level by using histological staining to evaluate the level of tissue fibrosis and cellular infiltration. Determining the local response to an implant may be done with a small number of animals by also including an empty defect control in the same synovial joint. On the other hand, the evaluation of a systemic response necessitates control specimens that do not receive implants. Assessing a systemic response to neocartilage implants may involve the collection of hematology samples for the completion of complete blood counts and blood phenotyping chemistry panels. In this study, both local and

systemic responses were investigated to determine the safety of allogeneic, tissue-engineered, neocartilage implants.

Using the self-assembling process, the creation of robust, scaffold-free, neocartilage implants has been achieved.[30,56,393] The self-assembling process has several advantages over traditional tissue engineering systems in that it does not rely on the use of scaffolds for robust biomechanical properties, which have been shown to contribute to an immune response following implantation.[14] Conversely, scaffold-free, self-assembled neocartilage, formed via cell-to-cell interactions to recapitulate the native developmental conditions of cartilage,[18] does not have the typical detriments associated with scaffold-based approaches, such as scaffold degradation byproducts.[14] Additionally, the use of biochemical and biomechanical stimuli during the tissue culture process results in neocartilage with functional properties on par with native tissue.[6,277,425-427] In particular, for this study, bioactive factors (TGF-β1, LOXL2, C-ABC, and C-ABC$_{int}$) and mechanical stimulation (fluid-induced shear stress) were used to create self-assembled neocartilage with robust mechanical properties for implantation in a Yucatan minipig animal model.

Yucatan minipig costal cartilage cells present a favorable cell source and species for preclinical studies of neocartilage implants. Costal cartilage cells allow for autologous and allogeneic chondrocyte harvest without further damaging the affected joint. Although costal cartilage does not articulate, costal cartilage cells produce hyaline cartilage when used in the self-assembling process to create neocartilage implants.[428] Additionally, costal cartilage cells are advantageous over other alternative cell sources, such as stem cells, because they are able to regain their chondrogenic phenotype after expansion and aggregate redifferentiation, and they generate a more stable, homogeneous cell population.[29] The Yucatan minipig in particular, is considered a suitable animal model for most preclinical work geared toward safety because of its similarity to humans in terms of anatomy, weight, immunology, physiology, and bone biology.[429-433] When considering Yucatan minipigs specifically for use in articular cartilage repair, they also

have similar histologic features in terms of glycosaminoglycans and collagen type II.[428,433,434] Because of these advantages, costal cartilage cells from Yucatan minipigs present a feasible and efficient cell source and species for use in the laboratory and in translational articular cartilage repair studies.

The objective of this study was to evaluate the preclinical safety of allogeneic, neocartilage implants using the Yucatan minipig as an animal model. The neocartilage implants were created according to the self-assembling process using allogeneic, passaged costal cartilage cells, then enhanced with bioactive factors and mechanical stimulation, and, finally, primed for integration with the native tissue using C-ABC$_{int}$. To assess both the local and systemic safety profiles of the minipig response to neocartilage implants, two separate surgical sets were conducted. In Surgical Set #1, every minipig received multiple implants that were engineered in the same fashion, but were fixed within cartilage defects using three different strategies (microfracture, fibrin, or superficial fibrin). It was hypothesized that implants that remain in place for the duration of the study would not lead to a local immune or inflammatory response. In Surgical Set #2, three minipigs received neocartilage implants (implant group), while two minipigs served as empty defect, negative control animals (empty defect group). For Surgical Set #2, it was hypothesized that the animals that received implants would not present with a systemic immune response different to that of the negative control animals. Overall, the results from these two surgical sets should provide evidence to support the notion that self-assembled, allogeneic, neocartilage implants are safe and do not lead to adverse local or systemic reactions.

Materials and Methods

Fabrication of tissue engineered implants

Chondrocyte procurement and expansion

Costal chondrocytes were obtained from 6-month-old Yucatan mini pigs. The costal cartilage was removed from the rib cage and the perichondrium was removed. The remaining cartilage was

minced into pieces about 1 mm^3, and subsequently digested in a 0.2% weight/volume collagenase solution with 3% FBS for 18 hr. The liberated cells were then strained, washed, and plated in tissue culture flasks. The chondrocytes were seeded at 2 million cells per T225 flasks with 30 ml of expansion media consisting of chondrogenic media at 2% FBS and additional growth factors growth factors (1 ng/ml TGF-β1, 10 ng/ml PDGF, and 5 ng/ml bFGF).

The chondrocytes were passaged every two weeks or until cells were confluent as described previously.[30,56] To passage, chondrocytes were lifted from the flask using 0.05% Trypsin-EDTA. After quelling the Trypsin-EDTA reaction with wash media at 10% FBS, the cells were spun down and resuspended in a 0.2% weight/volume collagenase solution at 3% FBS for about 2 hr at 37°C. This cell suspension was agitated with a serological 25 mL pipette every 15 minutes. Finally, the cell suspension was spun down, washed, and resuspended in expansion media to be plated again.

After the chondrocytes were expanded to passage 3, they were placed into aggregate redifferentiation as described previously. [56] The aggregates were seeded in a dropwise fashion into an agarose coated petri dish at a density of 22.5 million cells per 30 ml of redifferentiation media. Redifferentiation media consisted of chondrogenic media and growth factors (10 ng/ml TGF-β1, 100 ng/ml GDF5, and 100 ng/ml BMP-2). The petri dishes were then placed on an orbital shaker at a speed of 50 RPM for 24 hr. After 24 hr the cell suspension was removed from the orbital shaker and fed redifferentiation media every 3-4 days for 2 weeks. After 2 weeks, the cell suspension was resuspended in 0.05% Trypsin for 45 minutes, washed and resuspended in 0.2% w/v collagenase for 2 hr, and strained. The remaining cells were used to create the neocartilage constructs.

Self-assembling process

Neocartilage implants were created using the self-assembling method as described previously. [277,393] Briefly, 5 mm diameter molds were used to create 2% agarose wells in a 48 well plate. Chondrogenic media was exchanged 2-3 times to saturate the wells before cell seeding.

Chondrocytes were seeded at 2 million cells per well in 100 µl of chondrogenic media. After 4 hr, the cells were fed with 500 µl of chondrogenic media and additional growth factors (10 ng/ml TGF-β1). 3 days after seeding, the neocartilage constructs were removed from the wells, and after 7 days they were treated with C-ABC as described previously.[277] Finally, the constructs were treated with LOXL2 as described previously.[435]

Shear stress stimulation

Neocartilage constructs were stimulated with fluid-induced shear stress from days 14-21 of tissue culture as described previously.[436] Briefly, the fluid-induced shear stress device was created using a mold, 3% agarose, and a petri dish. The mold was placed into the petri dish containing 3% agarose, producing small protruding agarose poles that hold the neocartilage in place. The neocartilage constructs were placed in the fluid-induced shear stress device, and 15 ml of chondrogenic media and additional growth factors were added. The device was then placed on an orbital shaker and set to 50 RPM. As the orbital shaker rotated, the chondrogenic media flowed over the constructs subjecting them to a fluid induced shear stress range of 0.045-0.021 Pa. Chondrogenic media was replaced every 2-3 days, and after day 21 of culture, the neocartilage constructs were removed from the device and placed into 24-well plates until the end of culture.

C-ABC integration treatment

Directly prior to surgical implantation, using a sterile dermal biopsy punch, 4- and 5-mm discs were taken from implants, which were then treated with chondroitinase ABC for integration (C-ABC_{int}; 0.15 U/ml for 2 hr).[415] Following treatment, C-ABC_{int} activity was quenched with zinc sulfate (1 mM) for 10 minutes, and elimination of residual, inactive enzyme was achieved by sequentially washing constructs with medium. Subsequently, implants were placed in CHG containing HEPES buffer (25 mM) for transport to UCI medical center.

Quality control of engineered implants

Mechanical testing of engineered constructs

Constructs were mechanically tested prior to implantation to generate a baseline of properties and were also tested at the end of the study to provide in vitro control data. Tensile testing was conducted on dog-bone-shaped specimens as previously described.[428] Briefly, these samples were glued to paper tabs, which were then gripped by a uniaxial testing machine (Instron 5565, Norwood, MA), and a pull-to-failure test was conducted at a rate of 1% strain per second. From these experimental data, Young's modulus and ultimate tensile strength values were determined for the constructs. Creep indentation compressive tests were conducted on constructs using a flat, porous indenter tip and a constant load as previously described.[437] A linear biphasic model and finite element analysis were used to obtain the aggregate modulus, permeability, and Poisson's ratio from the experimental creep curves.[437] These data can be found in the supplementary material (Figure 7-S1).

In vitro toxicology

On the day of implantation for both surgery sets, media samples were taken from tissue culture wells containing constructs to be implanted and stored at -20°C for subsequent analysis. For each surgery set, aliquots were taken from each sample, pooled, and sent to the UC Davis Comparative Pathology Lab (CPL), where they were tested for mycoplasma, bacterial, and fungal contamination.

Acquisition of Yucatan minipigs

Skeletally mature (~18 months old) Yucatan minipigs were obtained from LoneStar Laboratory Swine, a commercial provider of laboratory-grade swine (LoneStar Laboratory Swine, Exemplar Genetics, Sioux Center, IA, USA). These minipigs came from a closed herd, and their health was verified prior to shipment to the UCI Medical Center (UCIMC) University Laboratory Animal Resources (ULAR) facility.

Surgical set #1

Surgical approach

The surgical preparation, which included the administration of anesthesia, was performed with assistance by ULAR Veterinary Services. The initial induction was performed with an intramuscular (IM) injection of Telazol (Tiletamine + Zolazapam at 10 mg/kg) and xylazine (2 mg/kg). Dosages were subject to the discretion of the veterinarian. An intravenous (IV) catheter was placed in the ear vein for the administration of intravenous fluids (LRS 5-10 ml/kg/hr), and a mask was used to deliver isoflurane during this induction period. Once the minipig was sufficiently unconscious, they were intubated, and general anesthesia was maintained with isoflurane (1-3%) accompanied with mechanical ventilation. Preemptive analgesia was delivered with meloxicam 0.4 mg/kg IM as well as buprenorphine at 0.2 mg/kg subcutaneously. Vitals monitoring was achieved with capnography, a thermometer, and pulse oximeter, and the pigs were kept at a temperature of 37-38°C with heated water blankets.

Under general anesthesia, the knees were surgically prepared and draped. With the minipig in dorsal recumbency, a craniolateral parapatellar approach was taken to access the knee joint. The patella and patellar tendon were not distracted and cruciate ligaments, and joint surface cartilage integrity was maintained. The digital extensor tendon that runs along the lateral condyle was removed in 2 out of 3 of the mini pigs to better access the condyles (the minipig that received superficial fibrin glue treatment did not have the digital extensor tendon removed). A 5 mm diameter biopsy punch was used to uniformly mark circular defects on the femoral condyles. A map of the defects created, and their corresponding treatments is found in Figure 7-1. A ring curette and Midex Rex drill were used to delicately remove all of the articular cartilage in the defect until a full thickness chondral defect with perpendicular walls was created. Implants were placed and fixed according to the defect maps shown in Figure 7-1, and then fixation was tested by articulating the knee joint multiple times and ensuring the implants were still in place. To conclude

the procedure, the joint capsule, subcutaneous tissue, and skin were individually sutured in a simple interrupted fashion.

Post-operative animal care

Post-operative analgesia included the administration of Meloxicam 0.4 mg/kg IM or Banamine (Flunixin) 2.2 mg/kg once daily for 3 days and then as needed per ULAR vet services' recommendation. An additional dosage of buprenorphine was given 2-3 days postoperatively if needed.

Euthanasia

The minipigs in Surgical Set #1 were euthanized 4 weeks after implantation with an IM injection of Telazol/Xylazine followed by an IV injection of pentobarbital (Euthasol) at a dose of 1 ml (390mg/4.5kg). Both knee joints were removed en bloc and transported to the lab to be processed for safety assessments.

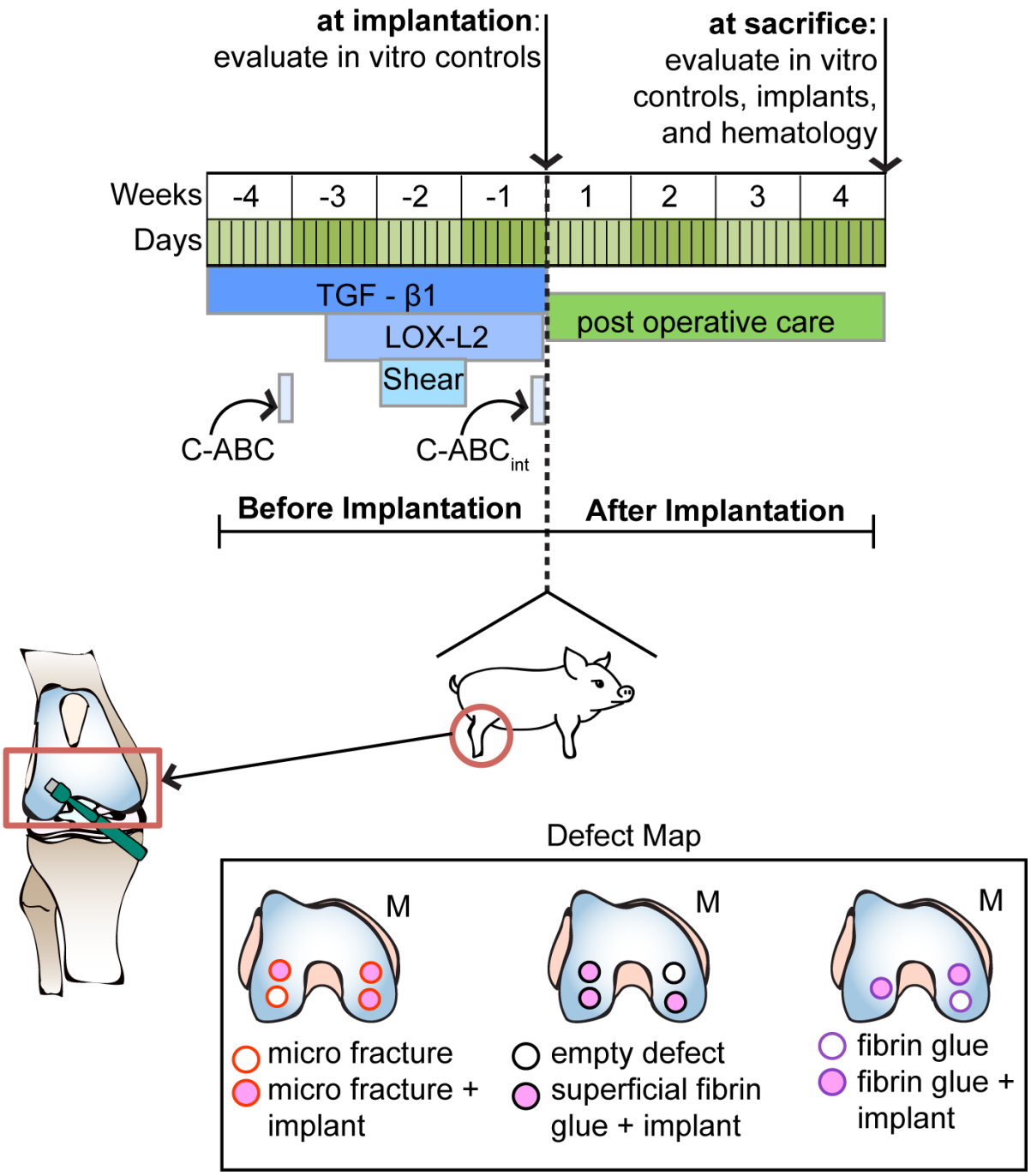

Figure 7-1. Surgical set #1 timeline and surgical approach: A schematic depicting a timeline for the creation of the tissue engineered neocartilage implants, to implantation and sacrifice. The timeline at the top of the figure shows the tissue engineering strategy used to create the implants. Neocartilage implants were treated with TGF-β1 for the entire duration of culture, C-ABC for 4 hr at day 7, LOX-L2 from days 10-28, and shear stress from days 14-21. Finally, on the day before surgery, C-ABC$_{int}$ treatment was applied. The day of the surgery, *in vitro* control constructs were evaluated. The implants remained in the minipigs for 4 weeks, at which point they were sacrificed. On the day of sacrifice, the implants were evaluated, and blood was collected for hematology assays. The bottom half of the figure depicts the surgical approach for surgical set #1. A total of 3 minipigs were operated on, all on their right knee, and a biopsy punch was used to create all defects (shown in the defect map).

Surgical set #2

Surgical approach

Preparation for surgery, including the administration of anesthesia, was performed with assistance by ULAR Veterinary Services. Initial induction was with Telazol 10 mg/kg IM injection with addition of xylazine 2 mg/kg IM. Dosages were subject to the discretion of the veterinarian An IV catheter was placed in the ear vein and was used for administration of IV fluids (LRS 5-10 ml/kg/hr). In addition, isoflurane delivered by mask was used during the IV catheter and induction period. Once in the appropriate depth of anesthesia, the minipig was intubated; general anesthesia was maintained with isoflurane (1-3%) accompanied with mechanical ventilation. Pre-emptive analgesia was delivered with Meloxicam 0.4 mg/kg IM as well as sustained release buprenorphine at 0.2 mg/kg subcutaneously. Vitals monitoring was achieved with capnography, a thermometer, and pulse oximetry. A heated water pad was used to keep the pigs at a temperature of 37-38 degree Celsius. Once the minipig was anesthetized, 2-4 ml of blood was collected for analysis of complete blood count (CBC) and blood phenotyping chemistry panel (BPCP) to establish a baseline of properties for all minipigs. Additional blood samples for CBC and the BPCP were collected for each animal directly prior to euthanasia in order to determine the possible systemic effect of the implant.

Under general anesthesia, the animals had their knees surgically prepared and draped. A craniolateral parapatellar approach to the knee joint with a scalpel blade was performed with the minipig in dorsal recumbency. The patella or patellar tendon was not distracted, and the digital extensor tendon that runs along the lateral condyle was preserved in all cases. Additionally, cruciate ligaments and joint surface cartilage integrity were maintained. A 5 mm diameter biopsy punch was used to uniformly mark two circular sections on the medial femoral condyle. A map of the defects created, and their corresponding treatments is found in Figure 7-2. A ring curette and Midex Rex drill were used to delicately remove all of the articular cartilage in the defect until a full thickness chondral defect with perpendicular walls was created. Then, for three minipigs, tissue-

engineered constructs were placed in the defect sites and secured with fibrin glue. Implant fixation was tested by articulating the knee joint multiple times and ensuring the implants were still in place. For the other two minipigs, the defect sites were left empty. To conclude the procedure, the joint capsule, subcutaneous tissue, and skin were individually sutured in a simple interrupted fashion.

Postoperative animal care

For Surgical Set #2, minipigs were placed in a custom-made, IACUC-approved, sling immediately after surgery to prevent the minipig from injuring itself while coming out of anesthesia, as well as to prevent the immediate loading of the operated knee joint (Figure 7-3). The sling was made of vinyl fabric and had four holes for the limbs which were equipped with padding. Double-layer reinforcements were included to support the weight of the mini pigs. Plywood was used to transport the sling while holding the minipig. Rotation of the plywood unrolled the sling, giving it an adjustable height feature and allowing the minipig to be gently placed on the bottom of the cage 3-4 hr after surgery, once the minipig was sufficiently awake to walk and load the knee joint normally. The cage in which the minipigs were placed while in the sling was also equipped with additional cage padding to prevent the minipig from injuring itself in its semi-conscious postoperative state.

In terms of postoperative analgesia, animals received Meloxicam 0.4 mg/kg IM or Banamine (Flunixin) 2.2 mg/kg once daily for 3 days and then as needed per ULAR vet services' recommendation. An additional dosage of buprenorphine was given 2-3 days postoperatively if needed. Also, two minipigs were selected for midpoint arthroscopy at 4 weeks to ensure that there was no synovial tissue damage or gross evidence of an immune response.

Euthanasia

The minipigs in Surgical Set #2 were euthanized 8 weeks after implantation with an intramuscular injection of Telazol/Xylazine followed by an IV injection of pentobarbital (Euthasol) at a dose of 1

ml (390 mg/4.5 kg). Both knee joints were removed en bloc and transported to the lab to be processed for safety assessments.

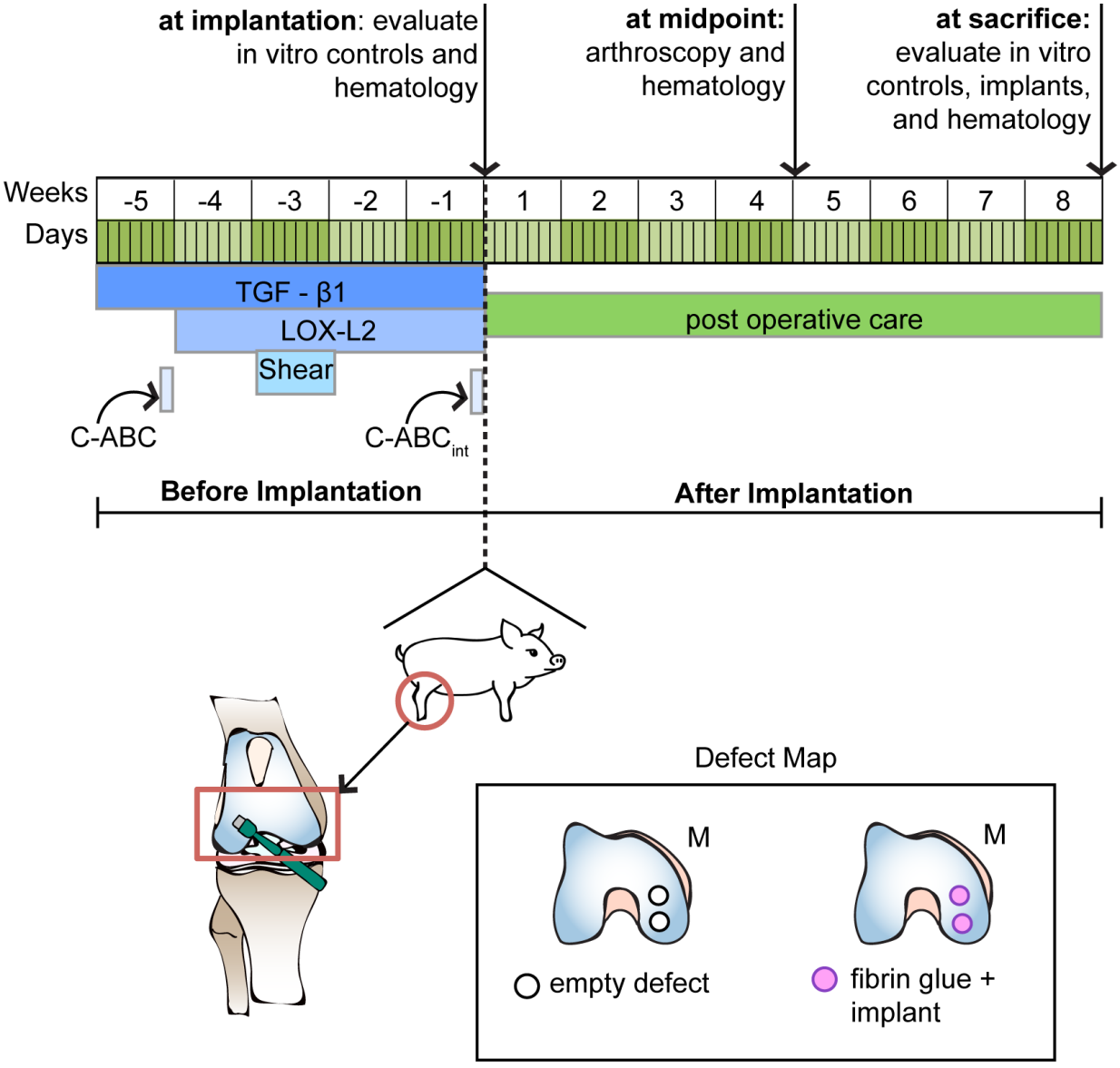

Figure 7-2. Surgical set #2 timeline and surgical approach: A schematic depicting a timeline from the creation of the tissue engineered neocartilage implants, implantation, and sacrifice. The timeline at the top of the figure shows the tissue engineering strategy used to create the implants. Neocartilage implants were treated with TGF-β1 for the entire duration of culture, C-ABC for 4h at day 7, LOX-L2 from days 10-28, and shear stress from days 14-21. Finally, on the day before surgery C-ABC$_{int}$ treatment was applied. The bottom half of the figure depicts the surgical approach for surgical set #2. A total of 5 minipigs were operated on the right knee. 3 of these minipigs received implants, and 2 did not. At implantation, *in vitro* control constructs were evaluated for their mechanical properties, and a sample of blood was collected from each minipig for hematology assays. At 4 weeks post-operatively, 2 of the minipigs that had neocartilage implanted underwent arthroscopy, and a sample of their blood was collected for hematology assays. At sacrifice, control constructs that were left in *in vitro* culture for 8 weeks were evaluated for their mechanical properties, the condyles of the minipigs were processed, and blood samples and synovial fluid were collected from all minipigs for hematology and cytology assays, respectively.

Safety assessments

Gross morphology

Immediately after euthanasia, the hind limbs were removed at the hip joint, keeping the knee joint intact, and transported to the laboratory for dissection. The hind limbs were then dissected to expose the knee joint, and the femur was separated from the tibia and patella. All femoral condyles, including non-operated joints and condyles were measured, and their appearance was documented via photographs.

Lameness scale and animal wellness observations

The minipigs were evaluated for lameness 2 weeks after undergoing surgery. The stance and gait of the minipigs was graded using a scale from 0 to 5.[438] Minipigs were given grades as follows: 0 - full weight bearing stance with no apparent lameness while walking; 1 - mild lameness while walking; 2 - mid weight bearing stance with apparent lameness; 3 - stands toe-touching only with significant lameness while walking; 4 - stands holding leg up with significant lameness; and 5 - non weight bearing. Additionally, animal wellness was observed with the help from veterinary staff and animal husbandry at ULAR on a daily basis. The minipigs were monitored for their activity, eating, weight-gain, and engagement with the staff and researchers.

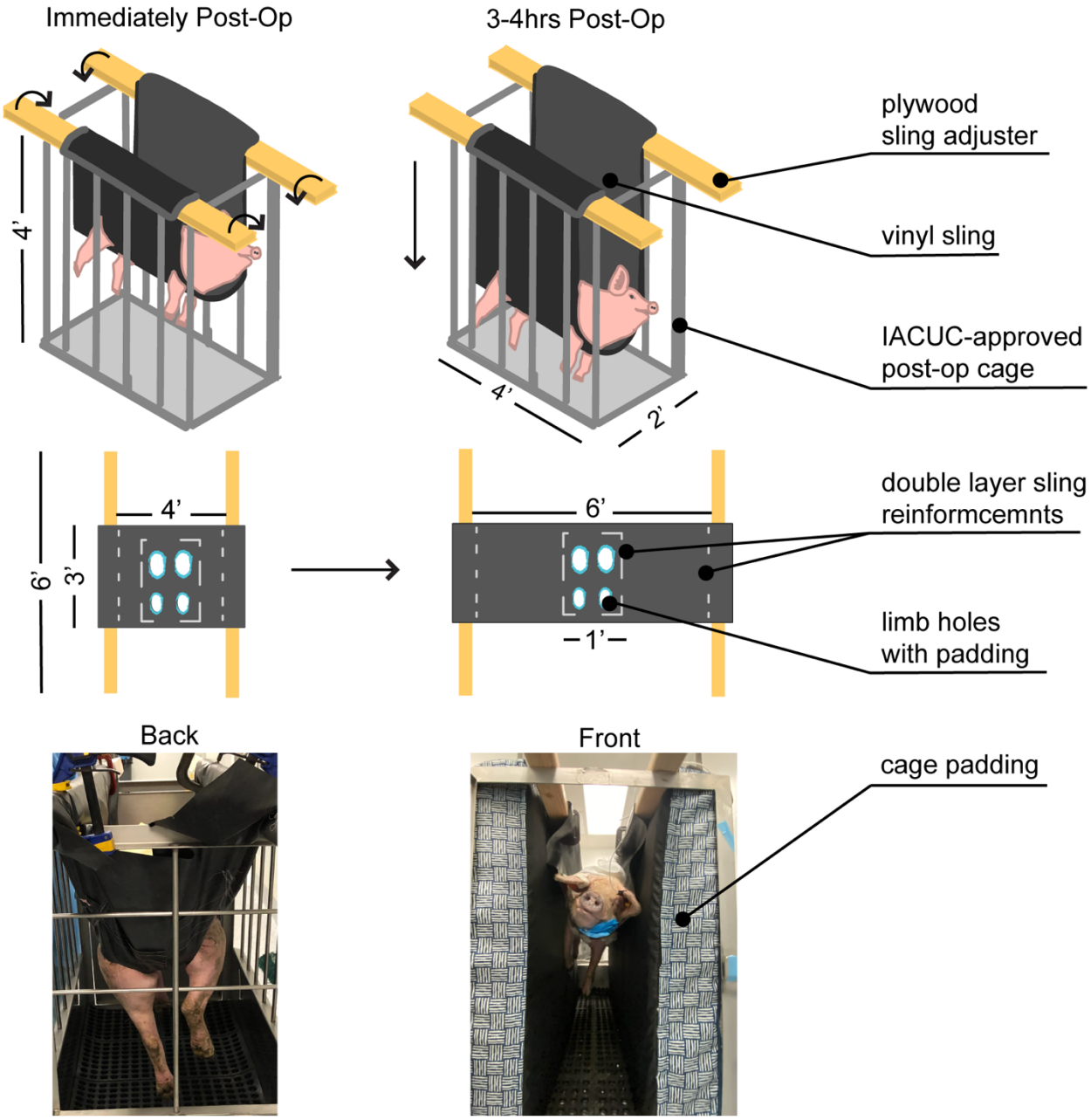

Figure 7-3. Surgical set #2 post-operative care: Immediately after surgery, minipigs were placed in a custom-made, IACUC-approved, sling. The sling is made of vinyl and has 4 holes for the limbs, which were equipped with padding. Double-layer reinforcements were included to support the weight of the minipigs. Plywood was used to transport the sling while holding the minipig. Rotation of the plywood unrolls the sling, giving it an adjustable height feature and allowing the minipig to be gently placed on the bottom of the cage 3-4 hrs post-operatively. The cage was also equipped with additional cage padding to prevent the minipig from injuring itself in its semi-conscious, post-op state.

Histopathology

Condyles were removed from the distal femur using an oscillating saw and then fixed in 10% neutral-buffered formalin for ~1 month. Subsequently, the condyles were decalcified in a 10-20%

EDTA solution for ~1 month.[439] Decalcification solution was changed 2-3 times per week. Once samples were fully decalcified, the condyles were trimmed to contain only the defect site and 1-2 mm of adjacent, native tissue. Then, these samples were processed, embedded in paraffin, and sectioned at a thickness of 5 μm. Finally, these sections were stained with hematoxylin and eosin (H&E) as previously described and evaluated for evidence of a local immune response and tissue abnormality.[9]

UC Davis CPL assays

Blood samples taken from minipigs pre- and post-operatively were shipped overnight to the UC Davis Comparative Pathology Laboratory (UCD CPL), where they were subjected to a CBC and a BPCP. Additionally, synovial fluid was collected post-mortem from each minipig and subjected to a synovial fluid cytology exam performed by a trained veterinary pathologist. Finally, cell-culture media samples that contained constructs that were implanted were collected from each surgical set, pooled, and sent to the UCD CPL for microbial contamination testing (e.g., mycoplasma and bacterial).

Statistics

Using GraphPad Prism, a Student's t-test was run for each CBC and BPCP output. Data was grouped in two ways. First, data were grouped according to treatment (i.e., empty defect or implant) and compared to assess differences between the treatments. Second, within treatment groups, presurgical values were compared to endpoint values to assess change within groups over time.

Results

Surgical set #1

Lameness scale and animal wellness observations

Two weeks after the surgery, the stance and gait of the minipigs were evaluated using a scale from 0 to 5. A score of 0 was given to minipigs that did not exhibit lameness and a score of 5 was given to minipigs that were non-weight bearing. The minipig that received 4 defects and treated with implants fixed with superficial fibrin glue was given a score of 1, indicating a full-weight bearing stance and mild lameness while walking. The minipig that received the microfracture treatment was evaluated as a 2, meaning that the minipig stood with mild weight-bearing and there was lameness noted while walking. The minipig that received 3 defects and was treated with fibrin glue was also evaluated as a 2.

Animal wellness throughout the implantation period was also documented. The ULAR staff determined that eating, drinking water, and weight gain was normal in all minipigs. The minipigs were moderately subdued for 24-48 hr immediately after the surgery. Once recovered from the immediate effects of surgery, the minipigs regained a keen engagement in their surroundings. Additionally, the ULAR veterinary and husbandry staff noted moderate interest and normal interaction with the minipigs.

Gross morphology

The gross morphology of the condyles was observed and documented about 6 hr after sacrifice. The photos in Figure 7-4 show the gross morphology of the constructs and the corresponding defect maps. All defects were created with a biopsy punch, and one control defect was included in each operated knee in which no implants were placed. In the minipig that received the microfracture treatment, the resulting gross morphology at 4 weeks post-op shows little to no repair tissue in all of the defects and no implant retention. In the minipig that received implants held in place with fibrin glue covering the top of the defect, the resulting gross morphology at 4

weeks post-op showed no repair tissue and no implant retention in the anterior-lateral and posterior-medial defects. Some repair tissue was evident in the posterior-lateral defect as well as in the anterior-medial defect. In the minipig that received implants fixed with fibrin glue along the bottom, sides, and top of the defect, the gross morphology at 4 weeks post op showed implant retention and repair in the anterior-medial defect. The posterior-medial defect and the defect on the lateral condyle showed the formation of repair tissue. These results indicate that the use of microfracture and an implant are not an effective option for tissue repair and implant retention. Fibrin glue is a more effective tool for implant retention; thus, this treatment strategy was carried into surgical set #2.

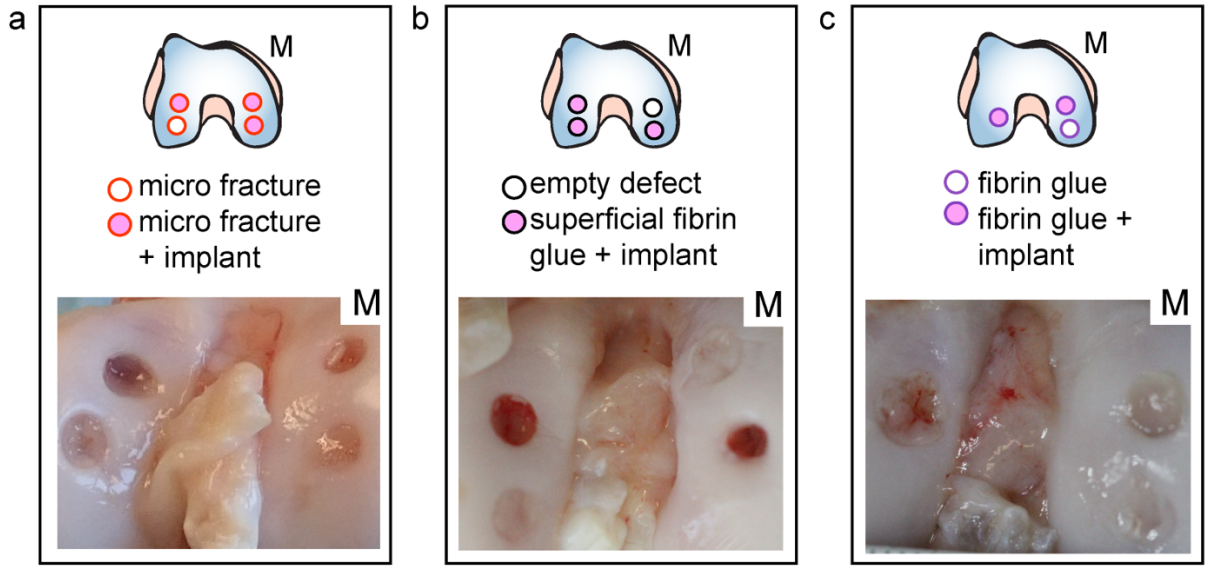

Figure 7-4. Surgical set #1 defect maps and resulting gross morphology: Defect maps for all three minipigs are presented at the top of each panel and depict the location of defects made and their corresponding conditions. All defects were created with a biopsy punch. 1 control defect was included in each operated knee in which no implants were placed. a) All 4 defects created were treated with microfracture, 3 of which also received an implant. The resulting gross morphology at 4 weeks following surgery shows little to no repair tissue in all of the defects and no implant retention. b) 4 defects were created, and 3 of these received an implant. The implants were held in place with fibrin glue covering the top of the defect. The fourth defect was left empty. The resulting gross morphology at 4 weeks after surgery shows no repair tissue and no implant retention in the anterior lateral and posterior medial defects. Some repair tissue is evident in the posterior lateral defect, as well as in the anterior medial defect. c) 3 defects were created, 2 of which received an implant. The implants were held in place with fibrin glue along the bottom, sides, and top of the defect. The third defect was filled with fibrin glue only. The gross morphology at 4 weeks following surgery shows implant retention and repair in the anterior medial defect. The posterior medial defect and the defect on the lateral condyle show the formation of repair tissue.

Histopathology

Hematoxylin and eosin staining of the implant that remained in place for the duration of the study demonstrated hematoxylin staining that appeared similar in intensity to the adjacent native tissue (Figure 7-5). Cells were retained within the implant and exhibited chondrocyte morphology (e.g., rounded shape and lacunae structure) (Figure 7-5, inset A). Some cells near a portion of the surface of the implant, which stained less intensely for hematoxylin, appeared to be more fibroblastic (Figure 7-5, inset B). However, there was no indication of the presence of immune cells such as macrophages or foreign body giant cells, nor did a fibrous, collagen capsule form around the periphery of the implant. Within the bone, which appears to have undergone some remodeling, osteocytes were visible within trabeculae, while osteoclasts and osteoblasts appeared to have occupied the space between trabeculae (Figure 7-5, inset C).

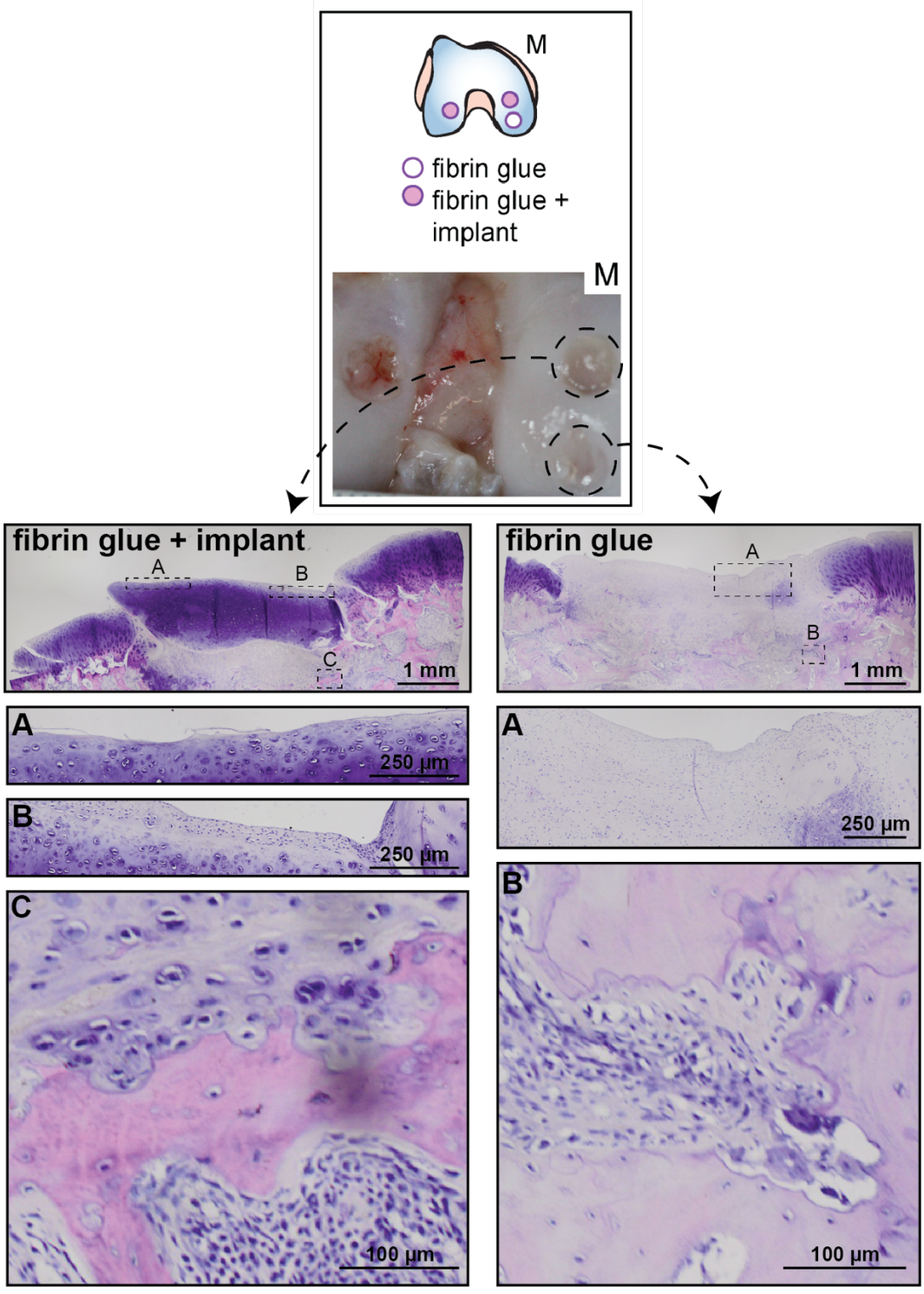

Figure 7-5. Histopathology of graft sites from the fibrin minipig. The fibrin glue + implant graft site did not illustrate any evidence of a local immune response to the implant at the surface (A and B) or in the bone (C). In general, chondrocyte phenotype and matrix integrity were retained at the surface of the implant (A), but some cells took on a more fibroblastic phenotype (B). Basic multicellular units, bone remodeling compartments, and osteocytes within lacunae were present in the bone (C). The fibrin glue graft site filled with what appears to be fibrous repair tissue (A), while the bone also exhibited signs of remodeling and healthy osteocyte structure (B).

Cell culture media contamination testing

The pooled cell culture media sample was negative for all testable contaminants including fungus, bacteria, and mycoplasma.

Surgical set #2

Lameness scale and animal wellness observations

As in surgical set #1, the stance and gait of the minipigs were evaluated using a scale from 0 to 5 about 1 week after the surgery. A score of 0 was given to minipigs that did not exhibit lameness and a score of 5 was given to mini pigs that were non-weight bearing. The three minipigs that received two defects each and were treated with implants were given scores of 1, 1, and 2. The two minipigs that received two defects each, but were not treated with implants were given scores of 1. A score of 1 indicated a normal stance with mild lameness while walking, and a score of 2 indicated that the minipig stood with mild weight-bearing and there was lameness noted while walking.

Animal wellness throughout the implantation period was also documented. The ULAR staff determined that eating, drinking water, and weight gain was normal in all minipigs. The minipigs were moderately subdued for 24-48 hr immediately after the surgery. Once recovered from the immediate effects of surgery, the minipigs regained a keen engagement and interest in their surroundings, as well as normal interaction.

Gross morphology

As in surgical set #1, the gross morphology of the condyles was observed and documented about 6 hr after sacrifice. The photos in Figure 7-6 show the gross morphology of the constructs and the corresponding defect maps from surgical set #2. All defects were created with a biopsy punch. The defects were left empty in 2 minipigs, whereas 3 minipigs received 2 implants each. The gross morphology of the mini pigs that received no implants demonstrated little to no repair tissue in the defects at 8 weeks postoperatively. The gross morphology of the mini pigs that received implants showed repair tissue in 2 of the 3 mini pigs, but no implant retention. This indicates that

a fixation strategy with only the use of fibrin glue is not effective in keeping the implants in the defect after surgery. The repair tissue and lack of gross pathology, however, provides evidence that the implants are safe to use and don't produce a local immune response.

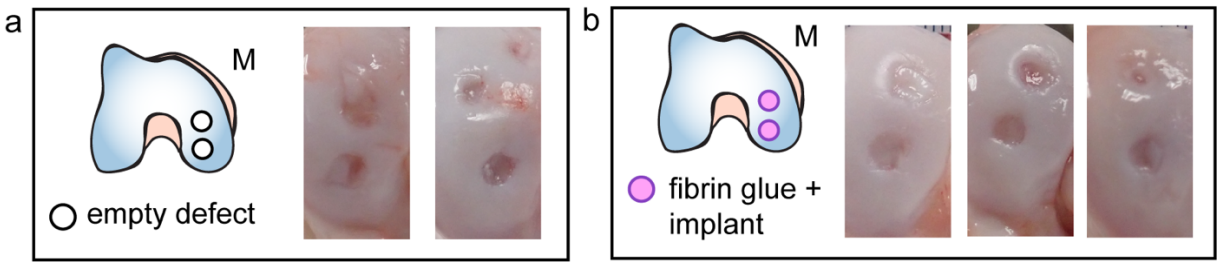

Figure 7-6. Surgical set #2 results: Defect maps for control (a) and treated (b) minipigs are presented and depict the location of defects made and their corresponding treatment. All defects were created with a biopsy punch. a) The gross morphology of the minipigs that received no implants show little to no repair tissue in the defects at 8 weeks following surgery. b) The gross morphology of the minipigs that received implants show no implant retention in all three minipigs 8 weeks after surgery. However, repair tissue was evident in 2 of the 3 minipigs.

Complete blood count (CBC)

For comparison between the implant and empty defect groups, all endpoint CBC values were normalized to their corresponding presurgical values. No CBC values for the implant group were significantly different from the empty defect group (Figure 7-7). For assessment of changes within groups over time, absolute CBC values at t=0 and t=8 weeks were compared using a student's t-test. 18 out of 20 CBC values remained stable throughout the duration of the study for the implant group. Red blood cell count was significantly higher (5.40 ± 0.49 M/μL vs. 4.24 ± 0.26 M/μL; $p = 0.02$) at t=8 weeks than t=0 for the implant group, as was the red blood cell distribution width (RDW) (18.20 ± 0.10% vs. 17.57 ± 0.25%; $p = 0.02$). One minipig demonstrated substantially elevated monocyte levels, but this was due to a skin infection unrelated to the experimental treatment. All CBC values remained stable over the course of the study for the empty defect group.

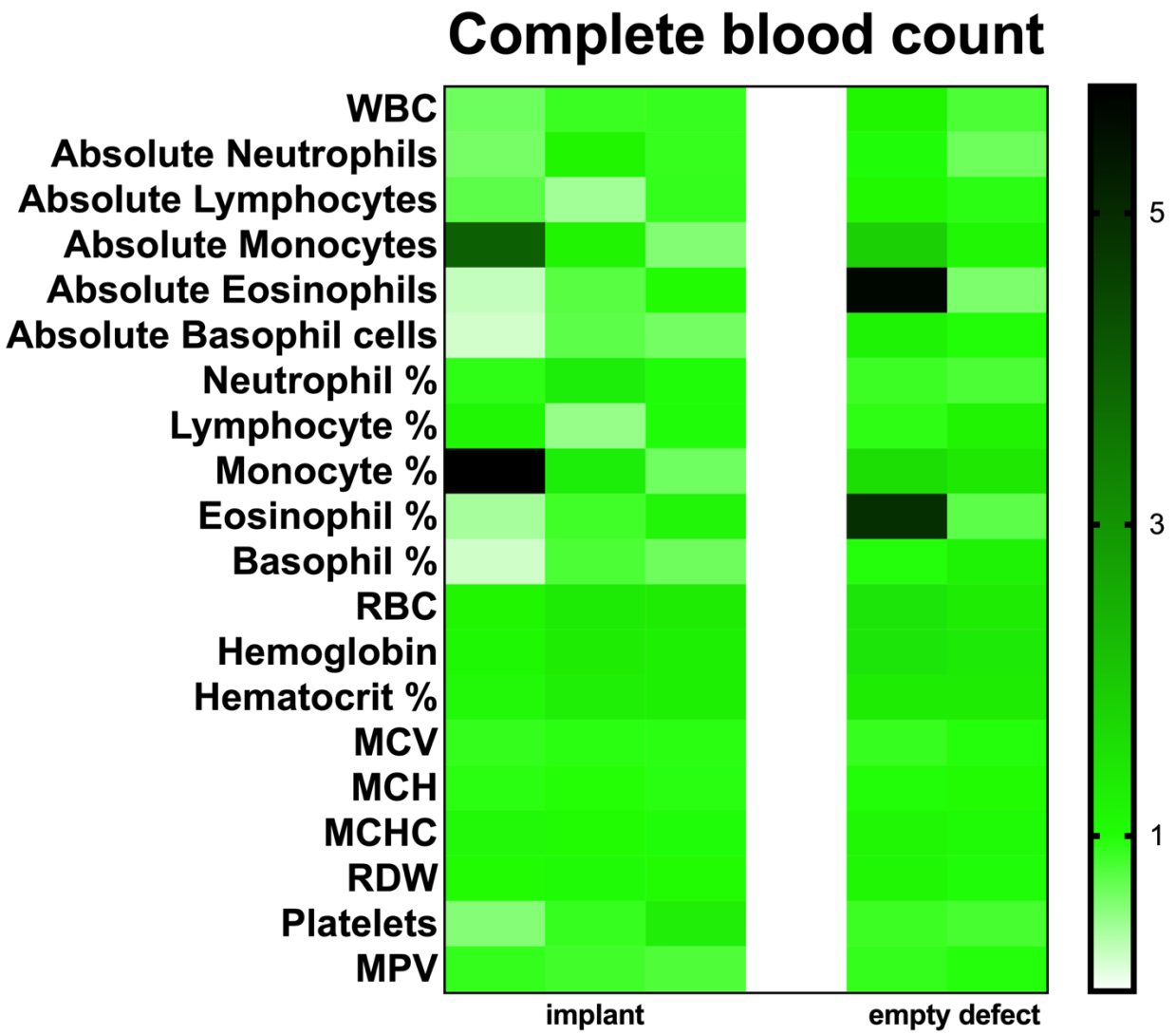

Figure 7-7. Surgical set #2 8-week endpoint complete blood count normalized to presurgical values. For each complete blood count measure, there were no significant differences between the implant group and the empty defect group. Abbreviations: WBC, white blood cells; RBC, red blood cells; MCV, mean corpuscular volume, mean corpuscular hemoglobin; MCHC, mean corpuscular hemoglobin concentration; RDW, red cell distribution width; MPV, mean platelet volume

Blood phenotyping chemistry panel (BPCP)

For comparison between the implant and empty defect groups, all endpoint BPCP values were normalized to their corresponding presurgical values. No BPCP values for the implant group were significantly different from the empty defect group (Figure 7-8). For assessment of changes within groups over time, absolute BPCP values at t=0 and t=8 weeks were compared using a student's t-test. 14 out of 15 BPCP values remained stable for the duration of the study in the implant group.

Alkaline phosphatase significantly increased from t=0 to t=8 weeks (43.70 ± 4.77 U/L vs. 56.00 ± 4.93 U/L; p = 0.04). 14 out of 15 values were unchanged for the empty defect group. Blood urea nitrogen significantly increased from t=0 to t=8 weeks (14.15 ± 0.64 mg/dl vs. 19.70 ± 1.24 mg/dl; p = 0.03).

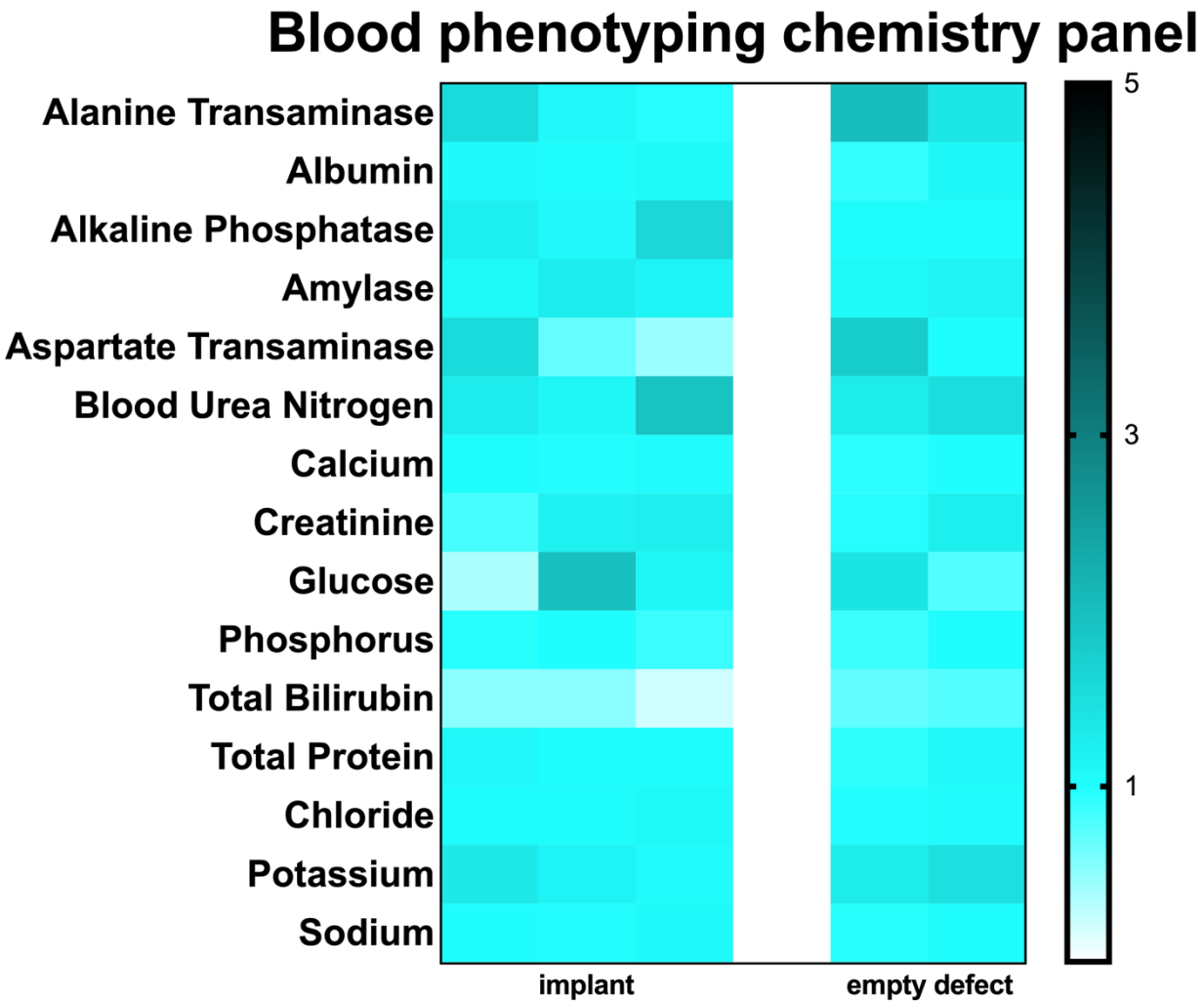

Figure 7-8. Surgical set #2 8-week endpoint blood phenotyping chemistry panel normalized to presurgical values. For each blood phenotyping chemistry measure, there were no differences between the implant group and the empty defect group.

Synovial fluid cytology

Qualitative synovial fluid cytology detected slightly elevated numbers of large non-reactive macrophages and erythrocytes in both implant and empty defect groups. A small number of lymphocytes were also detected in both groups. One minipig in the implant group presented with

markedly elevated numbers of large non-reactive macrophages and neutrophils, but this was not observed in the other two minipigs from this group.

Cell culture media contamination testing

The pooled cell culture media sample was negative for all testable contaminants including fungus, bacteria, and mycoplasma.

Discussion

Toward the clinical translation of allogeneic, tissue-engineered neocartilage implants, it is imperative to demonstrate their biocompatibility and safety in preclinical animal models. While it is generally accepted that articular cartilage is an immune-privileged tissue,[41,423,424] rigorous, preclinical evaluation of the both the local and systemic safety profiles of allogeneic, biologic implants is required by the FDA before proceeding with human clinical trials.[12] Since the ultimate goal of our laboratory is clinical translation of neocartilage implants, the objective of this study was to evaluate the preclinical safety of allogeneic, self-assembled neocartilage implants using the Yucatan minipig animal model. The study was conducted in two separate surgical sets. In surgical set #1, all minipigs received multiple implants that were engineered in the same fashion, but were fixed within cartilage defects using three different strategies (microfracture, fibrin, or superficial fibrin). For this set, the hypothesis that implants that remain in place for the duration of the study would not lead to a local immune or inflammatory response was supported by gross morphologic and histopathologic evaluation. In surgical set #2, three minipigs received cartilage implants (implant group), while two minipigs served as empty defect, negative control animals (empty defect group). The implant group did not experience a systemic immune response that developed over time, and measures of systemic health did not differ from the empty defect group. The results from these two surgical sets support the notion that self-assembled neocartilage implants are safe and do not lead to adverse local or systemic immune reactions.

The allogeneic neocartilage implants used in this study did not appear to lead to a local immune response in the distal femur articular cartilage of the Yucatan minipig. The integrity of extracellular matrix (ECM) in the implant was retained, suggesting that there was no degradation of ECM by an immune response and associated catabolic inflammation.[440] The chondrocytic phenotype of cells within the implant was largely maintained, indicating that cells had not dedifferentiated, a process that can be initiated by cytokines released during an immune response.[441,442] While it appears as though there are some fibroblastic cells on the surface of the implant, the change in phenotype of these cells was likely caused by the presence of fibrin glue used to initially fix this implant in place. Fibrin glue has been shown to lead to dedifferentiation of chondrocytes *in vivo*.[419] Additionally, since these fibroblastic cells were not present around the entirety of the implant, there is no indication of fibrous capsule or foreign body giant cell formation, suggesting that there was no foreign body response.[440,442] Cells in bone between trabeculae appear to be “basic multicellular units” (BMUs) of osteoclasts and osteoblasts within bone remodeling compartments. This is indicative of normal remodeling following bone injury,[443] which was likely caused during the initial formation of the defect and not by the implant, since BMUs and bone remodeling compartments are visible near the fibrin-only defect site as well as the implant site. Future preclinical work should consider limiting defect depth to the chondral layer to mitigate subchondral bone remodeling. Osteocyte nuclei within lacunae are also clearly visible in trabeculae near both defect sites, suggesting that these cells have not apoptosed nor has the tissue necrosed.[444,445] Altogether, the integrity of the implant ECM and lack of evidence of a foreign body response suggest that the implants used in this study are safe and do not cause a local immune response.

The implants in this study did not cause a systemic immune response that negatively impacted the health and well-being of the minipigs. In addition to there being no notable differences between the implant and empty defect groups in terms of gait and wellness as evaluated by ULAR veterinary and husbandry staff, there were no significant differences between

these two groups for any CBC or BPCP output value. This suggests that the implants did not cause a chronic, adverse condition in the minipigs. 18 out of 20 complete blood count outcome measures did not significantly change over time for the implant group. For both the implant group and empty defect group, red blood cell content (RBC) and red blood cell distribution width (RDW) increased. For the implant group, RBC and RDW significantly increased by 1.27-fold and 1.04-fold, respectively, while for the empty defect group, RBC and RDW also trended higher by 1.40-fold and 1.06-fold, respectively. This comparable trend suggests that consistent environmental factors that affected both groups of pigs, rather than the implants, were responsible for these changes. In terms of the BPCP results, 14 out of 15 output values did not significantly change over time for the implant group. Alkaline phosphatase levels in the blood did significantly increase by 1.28-fold from t=0 to t=8 weeks, but at both timepoints, alkaline phosphatase levels were below the reference value range provided by Exemplar Genetics (43.70 ± 4.77 U/L at t=0, 56.00 ± 4.93 U/L at t= 8 weeks, reference range: 75-167 U/L). Since low alkaline phosphatase levels can be caused by malnutrition,[446,447] it is possible that the observed temporal increase can be attributed to a recovery following the multiple day transportation time from LoneStar Laboratory Swine to UCIMC. In a similar fashion to the CBC and BPCP, the synovial fluid cytology exam did not demonstrate any appreciable, consistent differences between synovial fluid samples from each group, which would have been present in the case of an adverse response within the joint.[448] Ultimately, minipigs that received implants exhibited no concerning systemic changes over time or relative to the empty defect control group.

In conclusion, allogeneic, self-assembled neocartilage implants appear to be safe for use in the Yucatan minipig model, suggesting that an analogous approach in the human would also be safe. Therefore, future preclinical studies conducted by our lab should focus on the efficacy of this approach. First and foremost, a reliable implant fixation strategy is crucial to assessing the efficacy of engineered cartilage implants and must be carefully developed. Secondarily, while the sling immobilization strategy deployed for surgical set #2 seemed to improve minipig recovery

from anesthesia, a longer-duration immobilization strategy could work in conjunction with a cartilage fixation strategy to ensure implant retention. Securely fixing the implant and protecting it from mechanical stimuli initially could also allow the C-ABC$_{int}$ treatment to promote long-term integration, stability, and durability.[415] In the end, a study confirming the safety of allogeneic neocartilage implants such as this one was necessary to serve as a foundation for efficacy studies moving forward.

Supplementary Material

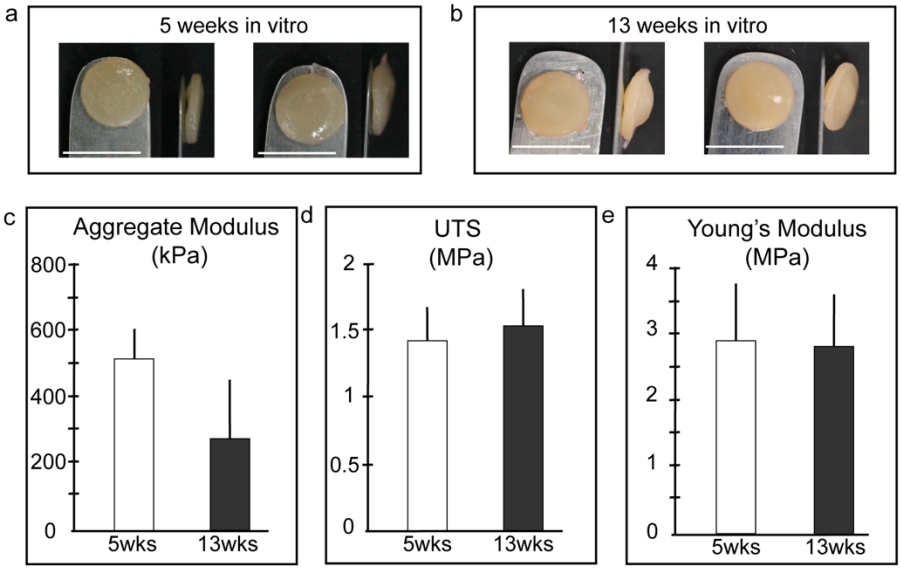

Figure 7-S1. Gross morphology and mechanical properties of self-assembled articular cartilage constructs after 5 weeks and 13 weeks of *in vitro* culture are depicted from surgical set #2. a) Thick, robust constructs had formed by 5 weeks of *in vitro* culture. b) Constructs had developed cysts and abnormal shape by 13 weeks of *in vitro* culture. c) Directly prior to implantation (i.e., after 5 weeks of *in vitro* culture), constructs had robust aggregate moduli, but that diminished during further *in vitro* culture. d,e) Tensile properties did not change during prolonged *in vitro* culture.

CONCLUSIONS AND FUTURE DIRECTIONS

The field of cartilage tissue engineering has made strides toward creating functional tissues to replace those damaged by disease, trauma, or age. Specifically, self-assembled neocartilage, which has been engineered with mechanical properties on par or approaching those of native tissue, has the potential to be a transformative therapy to repair and regenerate articular cartilage defects and halt osteoarthritis progression. In this work, first the self-assembling process as it relates to functional, translational tissue engineering as a whole was described. Techniques to measure structural components, such as collagen, were provided. Structure-function relationships, unmet clinical needs, and tissue-engineering strategies to address those needs were discussed in the context of the facet joint and articular cartilage tribology. These discussions established a roadmap for developing translational tissue-engineered solutions toward solving a variety of clinical problems. To that end, a method to enhance the integration of engineered neocartilage and native articular cartilage was developed, which will help overcome a longstanding barrier to more effective cartilage repair *in vivo*. Also, since inflammatory processes driven by cells such as macrophages can be harmful to implants *in vivo*, this work investigated and described the protective effect bioactive stimuli have on neocartilage constructs subjected to differentially stimulated macrophages using a direct, *in vitro* co-culture system. These protective bioactive factors may improve durability of neocartilage *in vivo*, which bodes well for future animal studies. Finally, the preclinical safety of allogeneic implants formed using the *in vitro* tissue-engineering strategies developed in this work was studied in the Yucatan minipig. These implants did not generate a local or systemic immune response in the minipig and can therefore be investigated further for their efficacy in healing cartilage defects. Ultimately, this work represents progress toward enhancing the durability and integration of engineered articular cartilage for the purpose of clinical translation.

Articular cartilage has several properties that hinder integration to an implant at a defect interface. These impediments include: 1) a lack of highly metabolic cells near the interface; 2) repulsive negative charges induced by cartilage glycosaminoglycans (GAGs); 3) dense extracellular matrix (ECM); and 4) a minimal number of stabilizing crosslinks that can form at the interface. Chondroitin sulfate, a GAG found within articular cartilage, and tissue maturity contribute to these properties. Additionally, bioactive factors could target the minimal number of interfacial crosslinks. Therefore, the GAG-specific treatment C-ABC$_{int}$, tissue maturity, and bioactive factors (i.e., TCL) were investigated as factors to enhance cartilage integration. Ultimately, C-ABC$_{int}$ and bioactive factors synergistically enhanced interface stiffness by 6.2-fold, and it was found that C-ABC$_{int}$ dose can be tailored to enhance integration of both immature and mature constructs. Importantly, and in spite of its catabolic potential, C-ABC$_{int}$ did not affect construct mechanical properties since its effects were localized to the periphery. Since C-ABC$_{int}$ is a simple, adaptable strategy that preserves biomimetic properties of neocartilage constructs, it could be readily deployed in a clinical setting for various cartilage implants, including self-assembled neocartilage.

Nevertheless, improvement of this integration strategy is possible and should be investigated further since *in vitro* methods of cartilage integration have yet to produce cartilage integration strength that approaches the UTS of native, intact articular cartilage. For example, it would be interesting to explore combinations of C-ABC$_{int}$ and other bioactive stimuli not examined in this work, since additional factors could more efficiently target obstacles to integration. On the other hand, stimuli present in the *in vivo* environment might obviate the need to further develop *in vitro* techniques. Thus, studying the *in vivo* maturation of the cartilage interface, whether ectopically or orthotopically, could further elucidate the performance of this approach. Finally, measuring specific ECM components present at the interface, through LCMS techniques, for example, could verify the presence of cartilaginous repair tissue and exclude the possibility that

fibrocartilage instead has formed at the interface. Further refinement of a cartilage integration approach may be necessary for cartilage implants to effectively heal defects *in vivo*.

In addition to working toward better cartilage integration, this thesis laid the foundation for and contributed to research at the nexus between cartilage tissue engineering and immunology, or cartilage mechano-immunology. The co-culture model developed in this work enabled assessment of the direct effects between differentially stimulated macrophages and neocartilage constructs. The initial objectives of using this system were to determine if neocartilage stiffness affects macrophage behavior and to establish the potential protective effect of neocartilage specific bioactive factors (i.e., TCL). As hypothesized, it was discovered that neocartilage stiffness can elicit a heightened inflammatory response in macrophages. However, unexpectedly, in the absence of bioactive factors, increased stiffness alone can protect neocartilage from catabolic degradation. However, bioactive factors were shown to protect the integrity of neocartilage constructs in a manner superior to stiffness alone, supporting the hypothesis that bioactive factors are chondroprotective. The mechanisms that drive this protection should be investigated in future studies and harnessed to advance translational tissue engineering efforts. For example, it is possible that treatment with bioactive factors causes expression or epigenetic level changes in the chondrocytes within the neocartilage that counteract macrophage-secreted cytokines. Alternatively, the topology or surface characteristics of a construct treated with TCL could sufficiently alter macrophage phenotype. Ultimately, this model and initial work will catalyze many future investigations (e.g., cartilage inflammatory disease modeling or macrophage-assisted cartilage tissue engineering) and foster the development of the emerging field of cartilage mechano-immunology.

To proceed along the clinical translational paradigm, the best strategies developed and examined *in vitro* were combined and carried forward for evaluation of their safety *in vivo*. The FDA has two main criteria for assessing new therapies such as biologic neocartilage implants. These criteria are safety and efficacy. Due to the unknown safety profile of allogeneic neocartilage

implants engineered according to the methods developed in this work, it was necessary and responsible to establish the safety of this approach on a small scale before proceeding to larger, statistically driven efficacy studies. The results from the preclinical safety studies in the Yucatan minipig support the notion that these implants are safe, as they did not elicit a local or systemic immune response. Due to the similarities between minipigs and humans, this finding suggests that an analogous approach in the human would also be safe, but preclinical safety studies would have to be performed under good laboratory practice conditions (GLP) prior to advancing to studies assessing safety in humans. Nevertheless, future, non-GLP preclinical studies, which are less expensive and more accessible to academic research laboratories, should focus on the efficacy of self-assembled neocartilage implants in repairing cartilage defects to add evidence in support of moving this therapy into human clinical trials. To achieve this, first and foremost, a reliable implant fixation strategy must be developed. Implant retention is crucial in evaluating the efficacy of engineered cartilage implants and could also allow the C-ABC$_{int}$ treatment to foster long-term integration and durability.[415] The fact that the one implant retained throughout the duration of the *in vivo* study did not elicit a local or systemic immune response, and also retained its extracellular matrix content, provides hope that once a fixation strategy is developed, the efficacy of the approach will be demonstrated *in vivo*.

Collectively, the work described in this thesis aimed to bolster the translational potential of self-assembled neocartilage by targeting *in vitro* cartilage integration, *in vitro* cartilage mechano-immunology, and preclinical implant safety separately. Moving forward, it is possible that the individual strategies could be combined to improve their effects synergistically. For example, while macrophages can exhibit proinflammatory qualities, they also have prohealing potential that could be harnessed to enhance cartilage integration in conjunction with C-ABC$_{int}$. The integration model and approach developed in Aim 1 could be combined with the co-culture model from Aim 2 to investigate how macrophages may affect or even improve cartilage integration, which could have implications for the design of future animal studies. Also, although

not specifically addressed experimentally, the importance of lubrication for the function and maintenance of cartilage was well-documented in Chapter 4 and should be measured in future studies on cartilage integration and mechano-immunology. Studies such as these could, for example, ensure that the tribological properties of neocartilage remain viable following C-ABC$_{int}$ treatment or elucidate relationships between cartilage lubrication and macrophage polarization state. Although further characterization and development of these concepts and methods would be beneficial to the field and would further refine the tissue-engineering approach described in this work, these *in vitro* studies should be conducted in parallel with future animal studies because the present tissue-engineering approach may be sufficient.

Ultimately, the objective of cartilage tissue engineering is to translate new and more efficacious treatments to the clinic to improve the quality of life of human and veterinary patients. That goal can only be achieved by rigorously establishing the preclinical safety and efficacy of the implant. Based on the mechanical robustness and integration potential of engineered neocartilage, the demonstrated safety of allogeneic implants, and the ability of an implant to retain its integrity orthotopically *in vivo*, there can be optimism that the efficacy of self-assembled neocartilage will be demonstrated in the near future.

REFERENCES

1 Link, J. M., Salinas, E. Y., Hu, J. C. & Athanasiou, K. A. The tribology of cartilage: Mechanisms, experimental techniques, and relevance to translational tissue engineering. *Clin Biomech (Bristol, Avon)*, 104880, doi:10.1016/j.clinbiomech.2019.10.016 (2019).

2 Kwon, H., Brown, W. E., Lee, C. A., Wang, D., Paschos, N., Hu, J. C. & Athanasiou, K. A. Surgical and tissue engineering strategies for articular cartilage and meniscus repair. *Nat Rev Rheumatol* **15**, 550-570, doi:10.1038/s41584-019-0255-1 (2019).

3 Lee, J. K., Link, J. M., Hu, J. C. Y. & Athanasiou, K. A. The Self-Assembling Process and Applications in Tissue Engineering. *Cold Spring Harb Perspect Med* **7**, doi:10.1101/cshperspect.a025668 (2017).

4 Gonzalez-Leon, E. A., Bielajew, B. J., Hu, J. C. & Athanasiou, K. A. Engineering self-assembled neomenisci through combination of matrix augmentation and directional remodeling. *Acta Biomater* **109**, 73-81, doi:10.1016/j.actbio.2020.04.019 (2020).

5 Kwon, H., O'Leary, S. A., Hu, J. C. & Athanasiou, K. A. Translating the application of transforming growth factor-beta1, chondroitinase-ABC, and lysyl oxidase-like 2 for mechanically robust tissue-engineered human neocartilage. *J Tissue Eng Regen Med* **13**, 283-294, doi:10.1002/term.2791 (2019).

6 Lee, J. K., Huwe, L. W., Paschos, N., Aryaei, A., Gegg, C. A., Hu, J. C. & Athanasiou, K. A. Tension stimulation drives tissue formation in scaffold-free systems. *Nature Materials* **16**, 864, doi:10.1038/nmat4917 (2017).

7 Oungoulian, S. R., Durney, K. M., Jones, B. K., Ahmad, C. S., Hung, C. T. & Ateshian, G. A. Wear and Damage of Articular Cartilage with Friction Against Orthopaedic Implant Materials. *J Biomech* **48**, 1957-1964, doi:10.1016/j.jbiomech.2015.04.008 (2015).

8 Makris, E. A., Gomoll, A. H., Malizos, K. N., Hu, J. C. & Athanasiou, K. A. Repair and tissue engineering techniques for articular cartilage. *Nat Rev Rheumatol* **11**, 21-34, doi:10.1038/nrrheum.2014.157 (2015).

9 Vapniarsky, N., Huwe, L. W., Arzi, B., Houghton, M. K., Wong, M. E., Wilson, J. W., Hatcher, D. C., Hu, J. C. & Athanasiou, K. A. Tissue engineering toward temporomandibular joint disc regeneration. *Sci Transl Med* **10**, doi:10.1126/scitranslmed.aaq1802 (2018).

10 Utomo, L., Bastiaansen-Jenniskens, Y. M., Verhaar, J. A. N. & van Osch, G. J. V. M. Cartilage inflammation and degeneration is enhanced by pro-inflammatory (M1) macrophages in vitro, but not inhibited directly by anti-inflammatory (M2) macrophages. *Osteoarthritis and Cartilage* **24**, 2162-2170, doi:https://doi.org/10.1016/j.joca.2016.07.018 (2016).

11 Haltmayer, E., Ribitsch, I., Gabner, S., Rosser, J., Gueltekin, S., Peham, J., Giese, U., Dolezal, M., Egerbacher, M. & Jenner, F. Co-culture of osteochondral explants and synovial membrane as in vitro model for osteoarthritis. *PLoS One* **14**, e0214709, doi:10.1371/journal.pone.0214709 (2019).

12 Preparation of IDEs and INDs for Products Intended to Repair or Replace Knee Cartilage. FDA (2012).

13 DuRaine, G. D., Brown, W. E., Hu, J. C. & Athanasiou, K. A. Emergence of scaffold-free approaches for tissue engineering musculoskeletal cartilages. *Ann Biomed Eng* **43**, 543-554, doi:10.1007/s10439-014-1161-y (2015).

14 Athanasiou, K. A., Eswaramoorthy, R., Hadidi, P. & Hu, J. C. Self-organization and the self-assembling process in tissue engineering. *Annu Rev Biomed Eng* **15**, 115-136, doi:10.1146/annurev-bioeng-071812-152423 (2013).

15 Shimizu, T., Akahane, M., Morita, Y., Omokawa, S., Nakano, K., Kira, T., Onishi, T., Inagaki, Y., Okuda, A., Kawate, K. & Tanaka, Y. The regeneration and augmentation of

bone with injectable osteogenic cell sheet in a rat critical fracture healing model. *Injury* **46**, 1457-1464, doi:10.1016/j.injury.2015.04.031 (2015).

16 Chaparro, F. J., Matusicky, M. E., Allen, M. J. & Lannutti, J. J. Biomimetic microstructural reorganization during suture retention strength evaluation of electrospun vascular scaffolds. *J Biomed Mater Res B Appl Biomater*, doi:10.1002/jbm.b.33493 (2015).

17 Hu, J. C. & Athanasiou, K. A. A Self-Assembling Process in Articular Cartilage Tissue Engineering. *Tissue Engineering* **12**, 969-979, doi:doi:10.1089/ten.2006.12.969 (2006).

18 Ofek, G., Revell, C. M., Hu, J. C., Allison, D. D., Grande-Allen, K. J. & Athanasiou, K. A. Matrix development in self-assembly of articular cartilage. *PLoS One* **3**, e2795, doi:10.1371/journal.pone.0002795 (2008).

19 DeLise, A. M., Fischer, L. & Tuan, R. S. Cellular interactions and signaling in cartilage development. *Osteoarthritis Cartilage* **8**, 309-334, doi:10.1053/joca.1999.0306 (2000).

20 Tavella, S., Raffo, P., Tacchetti, C., Cancedda, R. & Castagnola, P. N-CAM and N-cadherin expression during in vitro chondrogenesis. *Exp Cell Res* **215**, 354-362, doi:10.1006/excr.1994.1352 (1994).

21 Raghothaman, D., Leong, M. F., Lim, T. C., Toh, J. K., Wan, A. C., Yang, Z. & Lee, E. H. Engineering cell matrix interactions in assembled polyelectrolyte fiber hydrogels for mesenchymal stem cell chondrogenesis. *Biomaterials* **35**, 2607-2616, doi:10.1016/j.biomaterials.2013.12.008 (2014).

22 Krieg, M., Arboleda-Estudillo, Y., Puech, P. H., Kafer, J., Graner, F., Muller, D. J. & Heisenberg, C. P. Tensile forces govern germ-layer organization in zebrafish. *Nat Cell Biol* **10**, 429-436, doi:http://www.nature.com/ncb/journal/v10/n4/suppinfo/ncb1705_S1.html (2008).

23 Brodland, G. W. The Differential Interfacial Tension Hypothesis (DITH): a comprehensive theory for the self-rearrangement of embryonic cells and tissues. *J Biomech Eng* **124**, 188-197 (2002).

24 Manning, M. L., Foty, R. A., Steinberg, M. S. & Schoetz, E.-M. Coaction of intercellular adhesion and cortical tension specifies tissue surface tension. *Proceedings of the National Academy of Sciences of the United States of America* **107**, 12517-12522, doi:10.1073/pnas.1003743107 (2010).

25 Huey, D. J., Hu, J. C. & Athanasiou, K. A. Unlike bone, cartilage regeneration remains elusive. *Science* **338**, 917-921, doi:10.1126/science.1222454 (2012).

26 Ong, S. Y., Dai, H. & Leong, K. W. Inducing hepatic differentiation of human mesenchymal stem cells in pellet culture. *Biomaterials* **27**, 4087-4097, doi:10.1016/j.biomaterials.2006.03.022 (2006).

27 Gurkan, U. A., Kishore, V., Condon, K. W., Bellido, T. M. & Akkus, O. A scaffold-free multicellular three-dimensional in vitro model of osteogenesis. *Calcif Tissue Int* **88**, 388-401, doi:10.1007/s00223-011-9467-3 (2011).

28 Diekman, B. O., Christoforou, N., Willard, V. P., Sun, H., Sanchez-Adams, J., Leong, K. W. & Guilak, F. Cartilage tissue engineering using differentiated and purified induced pluripotent stem cells. *Proceedings of the National Academy of Sciences* **109**, 19172-19177, doi:10.1073/pnas.1210422109 (2012).

29 Murphy, M. K., Masters, T. E., Hu, J. C. & Athanasiou, K. A. Engineering a fibrocartilage spectrum through modulation of aggregate redifferentiation. *Cell transplantation* **24**, 235-245 (2015).

30 Murphy, M. K., Huey, D. J., Hu, J. C. & Athanasiou, K. A. TGF-beta1, GDF-5, and BMP-2 stimulation induces chondrogenesis in expanded human articular chondrocytes and marrow-derived stromal cells. *Stem Cells* **33**, 762-773, doi:10.1002/stem.1890 (2015).

31 Bhumiratana, S., Eton, R. E., Oungoulian, S. R., Wan, L. Q., Ateshian, G. A. & Vunjak-Novakovic, G. Large, stratified, and mechanically functional human cartilage grown in vitro by mesenchymal condensation. *Proc Natl Acad Sci U S A* **111**, 6940-6945, doi:10.1073/pnas.1324050111 (2014).

32 L'Heureux, N., Pâquet, S., Labbé, R., Germain, L. & Auger, F. A. A completely biological tissue-engineered human blood vessel. *FASEB J* **12**, 47-56 (1998).

33 Nishida, K., Yamato, M., Hayashida, Y., Watanabe, K., Maeda, N., Watanabe, H., Yamamoto, K., Nagai, S., Kikuchi, A., Tano, Y. & Okano, T. Functional bioengineered corneal epithelial sheet grafts from corneal stem cells expanded ex vivo on a temperature-responsive cell culture surface. *Transplantation* **77**, 379-385, doi:10.1097/01.TP.0000110320.45678.30 (2004).

34 Shimizu, T., Sekine, H., Yang, J., Isoi, Y., Yamato, M., Kikuchi, A., Kobayashi, E. & Okano, T. Polysurgery of cell sheet grafts overcomes diffusion limits to produce thick, vascularized myocardial tissues. *FASEB J* **20**, 708-710, doi:10.1096/fj.05-4715fje (2006).

35 Athens, A. A., Makris, E. A. & Hu, J. C. Induced collagen cross-links enhance cartilage integration. *PLoS One* **8**, e60719, doi:10.1371/journal.pone.0060719 (2013).

36 Vunjak-Novakovic, G., Martin, I., Obradovic, B., Treppo, S., Grodzinsky, A. J., Langer, R. & Freed, L. E. Bioreactor cultivation conditions modulate the composition and mechanical properties of tissue-engineered cartilage. *J Orthop Res* **17**, 130-138, doi:10.1002/jor.1100170119 (1999).

37 Avula, M. N., Rao, A. N., McGill, L. D., Grainger, D. W. & Solzbacher, F. Foreign body response to subcutaneous biomaterial implants in a mast cell-deficient Kit(w-Sh) murine model. *Acta Biomater* **10**, 1856-1863, doi:10.1016/j.actbio.2013.12.056 (2014).

38 Athanasiou, K. A., Responte, D. J., Brown, W. E. & Hu, J. C. Harnessing biomechanics to develop cartilage regeneration strategies. *J Biomech Eng* **137**, 020901, doi:10.1115/1.4028825 (2015).

39 Amini, A. R., Laurencin, C. T. & Nukavarapu, S. P. Bone Tissue Engineering: Recent Advances and Challenges. *Crit Rev Biomed Eng* **40**, 363-408 (2012).

40 Darling, E. M. & Athanasiou, K. A. Rapid phenotypic changes in passaged articular chondrocyte subpopulations. *J Orthop Res* **23**, 425-432, doi:10.1016/j.orthres.2004.08.008 (2005).

41 Arzi, B., DuRaine, G. D., Lee, C. A., Huey, D. J., Borjesson, D. L., Murphy, B. G., Hu, J. C., Baumgarth, N. & Athanasiou, K. A. Cartilage immunoprivilege depends on donor source and lesion location. *Acta Biomater* **23**, 72-81, doi:10.1016/j.actbio.2015.05.025 (2015).

42 Brittberg, M., Lindahl, A., Nilsson, A., Ohlsson, C., Isaksson, O. & Peterson, L. Treatment of deep cartilage defects in the knee with autologous chondrocyte transplantation. *N Engl J Med* **331**, 889-895, doi:10.1056/nejm199410063311401 (1994).

43 Bentley, G., Biant, L. C., Vijayan, S., Macmull, S., Skinner, J. A. & Carrington, R. W. J. Minimum ten-year results of a prospective randomised study of autologous chondrocyte implantation versus mosaicplasty for symptomatic articular cartilage lesions of the knee. *Journal of Bone & Joint Surgery, British Volume* **94-B**, 504-509, doi:10.1302/0301-620x.94b4.27495 (2012).

44 Tuan, R. S. A second-generation autologous chondrocyte implantation approach to the treatment of focal articular cartilage defects. *Arthritis Res Ther* **9**, 109, doi:10.1186/ar2310 (2007).

45 Lim, H.-C., Bae, J.-H., Song, S.-H., Park, Y.-E. & Kim, S.-J. Current Treatments of Isolated Articular Cartilage Lesions of the Knee Achieve Similar Outcomes. *Clinical Orthopaedics and Related Research* **470**, 2261-2267, doi:10.1007/s11999-012-2304-9 (2012).

46 McAllister, T. N., Maruszewski, M., Garrido, S. A., Wystrychowski, W., Dusserre, N., Marini, A., Zagalski, K., Fiorillo, A., Avila, H., Manglano, X., Antonelli, J., Kocher, A., Zembala, M., Cierpka, L., de la Fuente, L. M. & L'Heureux, N. Effectiveness of haemodialysis access with an autologous tissue-engineered vascular graft: a multicentre cohort study. *Lancet* **373**, 1440-1446, doi:10.1016/s0140-6736(09)60248-8 (2009).

47 L'Heureux, N., Dusserre, N., Konig, G., Victor, B., Keire, P., Wight, T. N., Chronos, N. A. F., Kyles, A. E., Gregory, C. R., Hoyt, G., Robbins, R. C. & McAllister, T. N. Human tissue-engineered blood vessels for adult arterial revascularization. *Nat Med* **12**, 361-365, doi:10.1038/nm1364 (2006).

48 Adkisson, H. D., Gillis, M. P., Davis, E. C., Maloney, W. & Hruska, K. A. In vitro generation of scaffold independent neocartilage. *Clin Orthop Relat Res*, S280-294 (2001).

49 McCormick, F., Cole, B. J., Nwachukwu, B., Harris, J. D., Adkisson Iv, H. D. & Farr, J. Treatment of Focal Cartilage Defects With a Juvenile Allogeneic 3-Dimensional Articular Cartilage Graft. *Operative Techniques in Sports Medicine* **21**, 95-99, doi:http://dx.doi.org/10.1053/j.otsm.2013.03.007 (2013).

50 Lu, Y., Adkisson, H. D., Bogdanske, J., Kalscheur, V., Maloney, W., Cheung, R., Grodzinsky, A. J., Hruska, K. A. & Markel, M. D. In vivo transplantation of neonatal ovine neocartilage allografts: determining the effectiveness of tissue transglutaminase. *The journal of knee surgery* **18**, 31-42 (2005).

51 Ma, D., Ren, L., Liu, Y., Chen, F., Zhang, J., Xue, Z. & Mao, T. Engineering scaffold-free bone tissue using bone marrow stromal cell sheets. *J Orthop Res* **28**, 697-702, doi:10.1002/jor.21012 (2010).

52 Akahane, M., Shigematsu, H., Tadokoro, M., Ueha, T., Matsumoto, T., Tohma, Y., Kido, A., Imamura, T. & Tanaka, Y. Scaffold-free cell sheet injection results in bone formation. *J Tissue Eng Regen Med* **4**, 404-411, doi:10.1002/term.259 (2010).

53 Pirraco, R. P., Iwata, T., Yoshida, T., Marques, A. P., Yamato, M., Reis, R. L. & Okano, T. Endothelial cells enhance the in vivo bone-forming ability of osteogenic cell sheets. *Lab Invest* **94**, 663-673, doi:10.1038/labinvest.2014.55 (2014).

54 Hildebrandt, C., Büth, H. & Thielecke, H. A scaffold-free in vitro model for osteogenesis of human mesenchymal stem cells. *Tissue Cell* **43**, 91-100, doi:10.1016/j.tice.2010.12.004 (2011).

55 Makris, E. A., Responte, D. J., Paschos, N. K., Hu, J. C. & Athanasiou, K. A. Developing functional musculoskeletal tissues through hypoxia and lysyl oxidase-induced collagen cross-linking. *Proc Natl Acad Sci U S A* **111**, E4832-4841, doi:10.1073/pnas.1414271111 (2014).

56 Murphy, M. K., DuRaine, G. D., Reddi, A., Hu, J. C. & Athanasiou, K. A. Inducing articular cartilage phenotype in costochondral cells. *Arthritis Res Ther* **15**, R214, doi:10.1186/ar4409 (2013).

57 Peng, G., McNary, S. M., Athanasiou, K. A. & Reddi, A. H. Surface Zone Articular Chondrocytes Modulate the Bulk and Surface Mechanical Properties of the Tissue Engineered Cartilage. *Tissue Eng Part A*, doi:10.1089/ten.TEA.2014.0099 (2014).

58 Kraft, J. J., Jeong, C., Novotny, J. E., Seacrist, T., Chan, G., Domzalski, M., Turka, C. M., Richardson, D. W. & Dodge, G. R. Effects of Hydrostatic Loading on a Self-Aggregating, Suspension Culture-Derived Cartilage Tissue Analog. *Cartilage* **2**, 254-264, doi:10.1177/1947603510383686 (2011).

59 Mohanraj, B., Farran, A. J., Mauck, R. L. & Dodge, G. R. Time-dependent functional maturation of scaffold-free cartilage tissue analogs. *Journal of Biomechanics* **47**, 2137-2142, doi:http://dx.doi.org/10.1016/j.jbiomech.2013.10.022 (2014).

60 Ando, W., Tateishi, K., Katakai, D., Hart, D. A., Higuchi, C., Nakata, K., Hashimoto, J., Fujie, H., Shino, K., Yoshikawa, H. & Nakamura, N. In vitro generation of a scaffold-free tissue-engineered construct (TEC) derived from human synovial mesenchymal stem cells: biological and mechanical properties and further chondrogenic potential. *Tissue Eng Part A* **14**, 2041-2049, doi:10.1089/ten.tea.2008.0015 (2008).

61 Hairfield-Stein, M., England, C., Paek, H. J., Gilbraith, K. B., Dennis, R., Boland, E. & Kosnik, P. Development of self-assembled, tissue-engineered ligament from bone marrow stromal cells. *Tissue Eng* **13**, 703-710, doi:10.1089/ten.2007.13.ft-339 (2007).

62 Ni, M., Rui, Y. F., Tan, Q., Liu, Y., Xu, L. L., Chan, K. M., Wang, Y. & Li, G. Engineered scaffold-free tendon tissue produced by tendon-derived stem cells. *Biomaterials* **34**, 2024-2037, doi:10.1016/j.biomaterials.2012.11.046 (2013).

63 Hoyer, M., Meier, C., Breier, A., Hahner, J., Heinrich, G., Drechsel, N., Meyer, M., Rentsch, C., Garbe, L.-A., Ertel, W., Lohan, A. & Schulze-Tanzil, G. In vitro characterization of self-assembled anterior cruciate ligament cell spheroids for ligament tissue engineering. *Histochem Cell Biol* **143**, 289-300, doi:10.1007/s00418-014-1280-4 (2015).

64 Theiss, F., Mirsaidi, A., Mhanna, R., Kümmerle, J., Glanz, S., Bahrenberg, G., Tiaden, A. N. & Richards, P. J. Use of biomimetic microtissue spheroids and specific growth factor supplementation to improve tenocyte differentiation and adaptation to a collagen-based scaffold in vitro. *Biomaterials* **69**, 99-109, doi:10.1016/j.biomaterials.2015.08.013 (2015).

65 Shimizu, T., Yamato, M., Akutsu, T., Shibata, T., Isoi, Y., Kikuchi, A., Umezu, M. & Okano, T. Electrically communicating three-dimensional cardiac tissue mimic fabricated by layered cultured cardiomyocyte sheets. *J Biomed Mater Res* **60**, 110-117 (2002).

66 Matsuura, K., Masuda, S., Haraguchi, Y., Yasuda, N., Shimizu, T., Hagiwara, N., Zandstra, P. W. & Okano, T. Creation of mouse embryonic stem cell-derived cardiac cell sheets. *Biomaterials* **32**, 7355-7362, doi:10.1016/j.biomaterials.2011.05.042 (2011).

67 Dilley, R. J. & Morrison, W. A. Vascularisation to improve translational potential of tissue engineering systems for cardiac repair. *Int J Biochem Cell Biol* **56**, 38-46, doi:10.1016/j.biocel.2014.10.020 (2014).

68 Seifu, D. G., Purnama, A., Mequanint, K. & Mantovani, D. Small-diameter vascular tissue engineering. *Nat Rev Cardiol* **10**, 410-421, doi:10.1038/nrcardio.2013.77 (2013).

69 Gwyther, T. A., Hu, J. Z., Billiar, K. L. & Rolle, M. W. Directed cellular self-assembly to fabricate cell-derived tissue rings for biomechanical analysis and tissue engineering. *J Vis Exp*, e3366, doi:10.3791/3366 (2011).

70 Zhao, J., Liu, L., Wei, J., Ma, D., Geng, W., Yan, X., Zhu, J., Du, H., Liu, Y., Li, L. & Chen, F. A novel strategy to engineer small-diameter vascular grafts from marrow-derived mesenchymal stem cells. *Artif Organs* **36**, 93-101, doi:10.1111/j.1525-1594.2011.01231.x (2012).

71 Ahn, H., Ju, Y. M., Takahashi, H., Williams, D. F., Yoo, J. J., Lee, S. J., Okano, T. & Atala, A. Engineered small diameter vascular grafts by combining cell sheet engineering and electrospinning technology. *Acta Biomater* **16**, 14-22, doi:10.1016/j.actbio.2015.01.030 (2015).

72 Norotte, C., Marga, F. S., Niklason, L. E. & Forgacs, G. Scaffold-free vascular tissue engineering using bioprinting. *Biomaterials* **30**, 5910-5917, doi:10.1016/j.biomaterials.2009.06.034 (2009).

73 Beachley, V., Kasyanov, V., Nagy-Mehesz, A., Norris, R., Ozolanta, I., Kalejs, M., Stradins, P., Baptista, L., da Silva, K., Grainjero, J., Wen, X. & Mironov, V. The fusion of tissue spheroids attached to pre-stretched electrospun polyurethane scaffolds. *J Tissue Eng* **5**, 2041731414556561, doi:10.1177/2041731414556561 (2014).

74 Gevaert, E., Dollé, L., Billiet, T., Dubruel, P., van Grunsven, L., van Apeldoorn, A. & Cornelissen, R. High throughput micro-well generation of hepatocyte micro-aggregates for tissue engineering. *PLoS One* **9**, e105171, doi:10.1371/journal.pone.0105171 (2014).

75 Ota, K., Saito, S., Fujisawa, K. & Tanaka, N. Xenotransplantation of spheroidal aggregate-cultured hepatocytes. *Transplant Proc* **29**, 912-913 (1997).

76 Wong, S. F., No, D. Y., Choi, Y. Y., Kim, D. S., Chung, B. G. & Lee, S.-H. Concave microwell based size-controllable hepatosphere as a three-dimensional liver tissue model. *Biomaterials* **32**, 8087-8096, doi:10.1016/j.biomaterials.2011.07.028 (2011).

77 Jun, Y., Kang, A. R., Lee, J. S., Jeong, G. S., Ju, J., Lee, D. Y. & Lee, S.-H. 3D co-culturing model of primary pancreatic islets and hepatocytes in hybrid spheroid to overcome

pancreatic cell shortage. *Biomaterials* **34**, 3784-3794, doi:10.1016/j.biomaterials.2013.02.010 (2013).

78 Ohashi, K., Yokoyama, T., Yamato, M., Kuge, H., Kanehiro, H., Tsutsumi, M., Amanuma, T., Iwata, H., Yang, J., Okano, T. & Nakajima, Y. Engineering functional two- and three-dimensional liver systems in vivo using hepatic tissue sheets. *Nat Med* **13**, 880-885, doi:10.1038/nm1576 (2007).

79 Sakai, Y., Yamanouchi, K., Ohashi, K., Koike, M., Utoh, R., Hasegawa, H., Muraoka, I., Suematsu, T., Soyama, A., Hidaka, M., Takatsuki, M., Kuroki, T. & Eguchi, S. Vascularized subcutaneous human liver tissue from engineered hepatocyte/fibroblast sheets in mice. *Biomaterials* **65**, 66-75, doi:10.1016/j.biomaterials.2015.06.046 (2015).

80 Ghezzi, C. E., Rnjak-Kovacina, J. & Kaplan, D. L. Corneal tissue engineering: recent advances and future perspectives. *Tissue Eng Part B Rev* **21**, 278-287, doi:10.1089/ten.TEB.2014.0397 (2015).

81 Nishida, K., Yamato, M., Hayashida, Y., Watanabe, K., Yamamoto, K., Adachi, E., Nagai, S., Kikuchi, A., Maeda, N., Watanabe, H., Okano, T. & Tano, Y. Corneal reconstruction with tissue-engineered cell sheets composed of autologous oral mucosal epithelium. *N Engl J Med* **351**, 1187-1196, doi:10.1056/NEJMoa040455 (2004).

82 Teichmann, J., Valtink, M., Gramm, S., Nitschke, M., Werner, C., Funk, R. H. W. & Engelmann, K. Human corneal endothelial cell sheets for transplantation: thermo-responsive cell culture carriers to meet cell-specific requirements. *Acta Biomater* **9**, 5031-5039, doi:10.1016/j.actbio.2012.10.023 (2013).

83 Madathil, B. K., Kumar, P. R. A. & Kumary, T. V. N-isopropylacrylamide-co-glycidylmethacrylate as a thermoresponsive substrate for corneal endothelial cell sheet engineering. *Biomed Res Int* **2014**, 450672, doi:10.1155/2014/450672 (2014).

84 Siegfried, M. Reticulin and collagen. *J Physiol* **28**, 319-324, doi:10.1113/jphysiol.1902.sp000919 (1902).

85 Tebb, M. C. Reticulin and collagen. *J Physiol* **27**, 463-472, doi:10.1113/jphysiol.1902.sp000885 (1902).

86 Nair, A. K., Gautieri, A. & Buehler, M. J. Role of intrafibrillar collagen mineralization in defining the compressive properties of nascent bone. *Biomacromolecules* **15**, 2494-2500, doi:10.1021/bm5003416 (2014).

87 Eleswarapu, S. V., Responte, D. J. & Athanasiou, K. A. Tensile properties, collagen content, and crosslinks in connective tissues of the immature knee joint. *PLoS One* **6**, e26178, doi:10.1371/journal.pone.0026178 (2011).

88 Rigozzi, S., Müller, R., Stemmer, A. & Snedeker, J. G. Tendon glycosaminoglycan proteoglycan sidechains promote collagen fibril sliding-AFM observations at the nanoscale. *J Biomech* **46**, 813-818, doi:10.1016/j.jbiomech.2012.11.017 (2013).

89 Miller, E. J. The structure of fibril-forming collagens. *Ann N Y Acad Sci* **460**, 1-13, doi:10.1111/j.1749-6632.1985.tb51152.x (1985).

90 Sherman, V. R., Yang, W. & Meyers, M. A. The materials science of collagen. *J Mech Behav Biomed Mater* **52**, 22-50, doi:10.1016/j.jmbbm.2015.05.023 (2015).

91 Loeser, R. F. Integrins and chondrocyte-matrix interactions in articular cartilage. *Matrix Biol* **39**, 11-16, doi:10.1016/j.matbio.2014.08.007 (2014).

92 Fang, M., Yuan, J., Peng, C. & Li, Y. Collagen as a double-edged sword in tumor progression. *Tumour Biol* **35**, 2871-2882, doi:10.1007/s13277-013-1511-7 (2014).

93 King Jr, T. E., Pardo, A. & Selman, M. Idiopathic pulmonary fibrosis. *The Lancet* **378**, 1949-1961, doi:http://dx.doi.org/10.1016/S0140-6736(11)60052-4.

94 Neuman, R. E. & Logan, M. A. The determination of hydroxyproline. *J Biol Chem* **184**, 299-306 (1950).

95 Prockop, D. J., Lindstedt, S. & Udenfriend, S. Simple Technique for Measuring Specific Activity of Labeled Hydroxyproline in Biological Materials. *Journal of Biological Chemistry* **236**, 1395-& (1961).

96 Kivirikko, K. I., Laitinen, O. & Prockop, D. J. Modifications of a specific assay for hydroxyproline in urine. *Analytical biochemistry* **19**, 249-255, doi:http://dx.doi.org/10.1016/0003-2697(67)90160-1 (1967).

97 Parekh, A. C. & Jung, D. H. An improved method for determination of total hydroxyproline in urine. *Biochemical Medicine* **4**, 446-456, doi:http://dx.doi.org/10.1016/0006-2944(70)90074-8 (1970).

98 Pødenphant, J., Larsen, N.-E. & Christiansen, C. An easy and reliable method for determination of urinary hydroxyproline. *Clinica Chimica Acta* **142**, 145-148, doi:http://dx.doi.org/10.1016/0009-8981(84)90110-4 (1984).

99 Reddy, G. K. & Enwemeka, C. S. A simplified method for the analysis of hydroxyproline in biological tissues. *Clin Biochem* **29**, 225-229, doi:10.1016/0009-9120(96)00003-6 (1996).

100 Colgrave, M. L., Allingham, P. G. & Jones, A. Hydroxyproline quantification for the estimation of collagen in tissue using multiple reaction monitoring mass spectrometry. *Journal of Chromatography A* **1212**, 150-153, doi:http://dx.doi.org/10.1016/j.chroma.2008.10.011 (2008).

101 Huszar, G., Maiocco, J. & Naftolin, F. Monitoring of collagen and collagen fragments in chromatography of protein mixtures. *Anal Biochem* **105**, 424-429, doi:10.1016/0003-2697(80)90481-9 (1980).

102 Stegemann, H. & Stalder, K. Determination of hydroxyproline. *Clin Chim Acta* **18**, 267-273, doi:10.1016/0009-8981(67)90167-2 (1967).

103 Junquiera, L. C., Junqueira, L. C. & Brentani, R. R. A simple and sensitive method for the quantitative estimation of collagen. *Anal Biochem* **94**, 96-99, doi:10.1016/0003-2697(79)90795-4 (1979).

104 Yasmin, H., Kabashima, T., Rahman, M. S., Shibata, T. & Kai, M. Amplified and selective assay of collagens by enzymatic and fluorescent reactions. *Sci Rep* **4**, 4950, doi:10.1038/srep04950 (2014).

105 *OSHA QUICK CARD: Hazard Communication Standard Pictogram | Occupational Safety and Health Administration*, <https://www.osha.gov/Publications/HazComm_QuickCard_Pictogram.html> (2016).

106 Maunder, M. J. d. F. A field test for hallucinogens: further improvements. *Journal of Pharmacy and Pharmacology* **26**, 637-638, doi:10.1111/j.2042-7158.1974.tb10677.x (1974).

107 Lin, L. I. A Concordance Correlation-Coefficient to Evaluate Reproducibility. *Biometrics* **45**, 255-268, doi:Doi 10.2307/2532051 (1989).

108 Lin, L., Hedayat, A. S., Sinha, B. & Yang, M. Statistical Methods in Assessing Agreement. *Journal of the American Statistical Association* **97**, 257-270, doi:10.1198/016214502753479392 (2002).

109 Kliment, C. R., Englert, J. M., Crum, L. P. & Oury, T. D. A novel method for accurate collagen and biochemical assessment of pulmonary tissue utilizing one animal. *International Journal of Clinical and Experimental Pathology* **4**, 349-355 (2011).

110 Ramshaw, J. A., Shah, N. K. & Brodsky, B. Gly-X-Y tripeptide frequencies in collagen: a context for host-guest triple-helical peptides. *J Struct Biol* **122**, 86-91, doi:10.1006/jsbi.1998.3977 (1998).

111 Etherington, D. J., Pugh, D. & Silver, I. A. Collagen degradation in an experimental inflammatory lesion: studies on the role of the macrophage. *Acta Biol Med Ger* **40**, 1625-1636 (1981).

112 Walsh, B. J., Thornton, S. C., Penny, R. & Breit, S. N. Microplate reader-based quantitation of collagens. *Anal Biochem* **203**, 187-190, doi:10.1016/0003-2697(92)90301-m (1992).

113 Junqueira, L. C., Bignolas, G. & Brentani, R. R. Picrosirius staining plus polarization microscopy, a specific method for collagen detection in tissue sections. *Histochem J* **11**, 447-455, doi:10.1007/bf01002772 (1979).

114 Bornstein, P. & Sage, H. Structurally distinct collagen types. *Annu Rev Biochem* **49**, 957-1003, doi:10.1146/annurev.bi.49.070180.004521 (1980).

115 Miller, E. J. & Rhodes, R. K. Preparation and characterization of the different types of collagen. *Methods Enzymol* **82 Pt A**, 33-64, doi:10.1016/0076-6879(82)82059-4 (1982).

116 Lareu, R. R., Zeugolis, D. I., Abu-Rub, M., Pandit, A. & Raghunath, M. Essential modification of the Sircol Collagen Assay for the accurate quantification of collagen content in complex protein solutions. *Acta Biomater* **6**, 3146-3151, doi:10.1016/j.actbio.2010.02.004 (2010).

117 Rennard, S. I., Berg, R., Martin, G. R., Foidart, J. M. & Robey, P. G. Enzyme-linked immunoassay (ELISA) for connective tissue components. *Analytical Biochemistry* **104**, 205-214, doi:http://dx.doi.org/10.1016/0003-2697(80)90300-0 (1980).

118 *Sigma-Aldrich*, <http://www.sigmaaldrich.com/catalog/search?interface=All&N=0+114333318&mode=partialmax&focus=product(=en&region=US> (2016).

119 Pal, G. P. & Routal, R. V. Transmission of weight through the lower thoracic and lumbar regions of the vertebral column in man. *Journal of Anatomy* **152**, 93-105 (1987).

120 Aarabi, B., Walters, B. C., Dhall, S. S., Gelb, D. E., Hurlbert, R. J., Rozzelle, C. J., Ryken, T. C., Theodore, N. & Hadley, M. N. Subaxial Cervical Spine Injury Classification Systems. *Neurosurgery* **72**, 170-186, doi:10.1227/NEU.0b013e31828341c5 (2013).

121 Crawford, N. R., Duggal, N., Chamberlain, R. H., Park, S. C., Sonntag, V. K. & Dickman, C. A. Unilateral cervical facet dislocation: injury mechanism and biomechanical consequences. *Spine (Phila Pa 1976)* **27**, 1858-1864; discussion 1864 (2002).

122 Dvorak, M. F., Fisher, C. G., Aarabi, B., Harris, M. B., Hurbert, R. J., Rampersaud, Y. R., Vaccaro, A., Harrop, J. S., Nockels, R. P., Madrazo, I. N., Schwartz, D., Kwon, B. K., Zhao, Y. & Fehlings, M. G. Clinical Outcomes of 90 Isolated Unilateral Facet Fractures,

Subluxations, and Dislocations Treated Surgically and Nonoperatively. *Spine* **32**, 3007-3013, doi:10.1097/BRS.0b013e31815cd439 (2007).

123 Li, J., Muehleman, C., Abe, Y. & Masuda, K. Prevalence of facet joint degeneration in association with intervertebral joint degeneration in a sample of organ donors. *Journal of Orthopaedic Research* **29**, 1267-1274 (2011).

124 Eubanks, J. D., Lee, M. J., Cassinelli, E. & Ahn, N. U. Prevalence of lumbar facet arthrosis and its relationship to age, sex, and race: an anatomic study of cadaveric specimens. *Spine (Phila Pa 1976)* **32**, 2058-2062, doi:10.1097/BRS.0b013e318145a3a9 (2007).

125 Suri, P., Hunter, D. J., Rainville, J., Guermazi, A. & Katz, J. N. Presence and extent of severe facet joint osteoarthritis are associated with back pain in older adults. *Osteoarthritis Cartilage* **21**, 1199-1206, doi:10.1016/j.joca.2013.05.013 (2013).

126 Genevay, S. & Atlas, S. J. Lumbar Spinal Stenosis. *Best practice & research. Clinical rheumatology* **24**, 253-265, doi:10.1016/j.berh.2009.11.001 (2010).

127 Weinstein, J. N., Lurie, J. D., Olson, P., Bronner, K. K., Fisher, E. S. & Morgan, M. T. S. United States trends and regional variations in lumbar spine surgery: 1992–2003. *Spine* **31**, 2707 (2006).

128 Newman, P. & Stone, K. The etiology of spondylolisthesis. *Journal of Bone & Joint Surgery, British Volume* **45**, 39-59 (1963).

129 Vanderpool, D. W., James, J. I. & Wynne-Davies, R. Scoliosis in the elderly. *J Bone Joint Surg Am* **51**, 446-455 (1969).

130 Lawrence, R. C., Felson, D. T., Helmick, C. G., Arnold, L. M., Choi, H., Deyo, R. A., Gabriel, S., Hirsch, R., Hochberg, M. C., Hunder, G. G., Jordan, J. M., Katz, J. N., Kremers, H. M. & Wolfe, F. Estimates of the prevalence of arthritis and other rheumatic conditions in the United States. Part II. *Arthritis Rheum* **58**, 26-35, doi:10.1002/art.23176 (2008).

131 Statistics, N. C. f. H. (National Center for Health Statistics, Hyattsville (2012), 2011).

132 Katz, J. N. *Lumbar Disc Disorders and Low-Back Pain: Socioeconomic Factors and Consequences*. Vol. 88 (2006).

133 Gaskin, D. J. & Richard, P. The Economic Costs of Pain in the United States. *The Journal of Pain* **13**, 715-724, doi:http://dx.doi.org/10.1016/j.jpain.2012.03.009 (2012).

134 Manchikanti, L., Pampati, V., Singh, V. & Falco, F. J. Assessment of the escalating growth of facet joint interventions in the medicare population in the United States from 2000 to 2011. *Pain Physician* **16**, E365-378 (2013).

135 Manchikanti, L., Pampati, S. & Cash, K. A. Making sense of the accuracy of diagnostic lumbar facet joint nerve blocks: an assessment of the implications of 50% relief, 80% relief, single block, or controlled diagnostic blocks. *Pain Physician* **13**, 133-143 (2010).

136 Manchikanti, L., Pampati, V., Singh, V., Beyer, C., Damron, K. & Fellows, B. Evaluation of the role of facet joints in persistent low back pain in obesity: a controlled, prospective, comparative evaluation. *Pain Physician* **4**, 266-272 (2001).

137 Manchikanti, L., Hirsch, J. A. & Pampati, V. Chronic low back pain of facet (zygapophysial) joint origin: is there a difference based on involvement of single or multiple spinal regions? *Pain Physician* **6**, 399-405 (2003).

138 Manchikanti, L., Singh, V., Pampati, V., Damron, K. S., Beyer, C. D. & Barnhill, R. C. Is there correlation of facet joint pain in lumbar and cervical spine? An evaluation of prevalence in combined chronic low back and neck pain. *Pain Physician* **5**, 365-371 (2002).

139 Manchikanti, L., Boswell, M. V., Singh, V., Pampati, V., Damron, K. S. & Beyer, C. D. Prevalence of facet joint pain in chronic spinal pain of cervical, thoracic, and lumbar regions. *BMC Musculoskeletal Disorders* **5**, 15-15, doi:10.1186/1471-2474-5-15 (2004).

140 Manchukonda, R., Manchikanti, K. N., Cash, K. A., Pampati, V. & Manchikanti, L. Facet joint pain in chronic spinal pain: an evaluation of prevalence and false-positive rate of

diagnostic blocks. *J Spinal Disord Tech* **20**, 539-545, doi:10.1097/BSD.0b013e3180577812 (2007).

141 Manchikanti, L., Manchukonda, R., Pampati, V., Damron, K. S. & McManus, C. D. Prevalence of facet joint pain in chronic low back pain in postsurgical patients by controlled comparative local anesthetic blocks. *Arch Phys Med Rehabil* **88**, 449-455, doi:10.1016/j.apmr.2007.01.015 (2007).

142 Manchikanti, L., Singh, V., Pampati, V., Beyer, C. D. & Damron, K. S. Evaluation of the prevalence of facet joint pain in chronic thoracic pain. *Pain Physician* **5**, 354-359 (2002).

143 Boswell, M. V., Colson, J. D., Sehgal, N., Dunbar, E. E. & Epter, R. A systematic review of therapeutic facet joint interventions in chronic spinal pain. *Pain Physician* **10**, 229-253 (2007).

144 Sears, W. R., Sergides, I. G., Kazemi, N., Smith, M., White, G. J. & Osburg, B. Incidence and prevalence of surgery at segments adjacent to a previous posterior lumbar arthrodesis. *The Spine Journal* **11**, 11-20, doi:http://dx.doi.org/10.1016/j.spinee.2010.09.026 (2011).

145 Park, P., Garton, H. J., Gala, V. C., Hoff, J. T. & McGillicuddy, J. E. Adjacent Segment Disease after Lumbar or Lumbosacral Fusion: Review of the Literature. *Spine* **29**, 1938-1944 (2004).

146 Serhan, H., Mhatre, D., Defossez, H. & Bono, C. M. Motion-preserving technologies for degenerative lumbar spine: The past, present, and future horizons. *SAS Journal* **5**, 75-89, doi:http://dx.doi.org/10.1016/j.esas.2011.05.001 (2011).

147 Cohen, S. P., Huang, J. H. & Brummett, C. Facet joint pain--advances in patient selection and treatment. *Nat Rev Rheumatol* **9**, 101-116, doi:10.1038/nrrheum.2012.198 (2013).

148 Boswell, M. V., Manchikanti, L., Kaye, A. D., Bakshi, S., Gharibo, C. G., Gupta, S., Jha, S. S., Nampiaparampil, D. E., Simopoulos, T. T. & Hirsch, J. A. A Best-Evidence

Systematic Appraisal of the Diagnostic Accuracy and Utility of Facet (Zygapophysial) Joint Injections in Chronic Spinal Pain. *Pain Physician* **18**, E497-533 (2015).

149 Jaumard, N. V., Welch, W. C. & Winkelstein, B. A. Spinal facet joint biomechanics and mechanotransduction in normal, injury and degenerative conditions. *J Biomech Eng* **133**, 071010, doi:10.1115/1.4004493 (2011).

150 Pal, G. P., Routal, R. V. & Saggu, S. K. The orientation of the articular facets of the zygapophyseal joints at the cervical and upper thoracic region. *J Anat* **198**, 431-441 (2001).

151 Masharawi, Y., Rothschild, B., Dar, G., Peleg, S., Robinson, D., Been, E. & Hershkovitz, I. Facet orientation in the thoracolumbar spine: three-dimensional anatomic and biomechanical analysis. *Spine (Phila Pa 1976)* **29**, 1755-1763 (2004).

152 Tulsi, R. S. & Hermanis, G. M. A study of the angle of inclination and facet curvature of superior lumbar zygapophyseal facets. *Spine* **18**, 1311-1317 (1993).

153 McLain, R. F., Yerby, S. A. & Moseley, T. A. Comparative morphometry of L4 vertebrae: comparison of large animal models for the human lumbar spine. *Spine (Phila Pa 1976)* **27**, E200-206 (2002).

154 Pal, G. P. & Routal, R. V. Mechanism of change in the orientation of the articular process of the zygapophyseal joint at the thoracolumbar junction. *J Anat* **195 (Pt 2)**, 199-209 (1999).

155 Panjabi, M. M., Oxland, T., Takata, K., Goel, V., Duranceau, J. & Krag, M. Articular facets of the human spine. Quantitative three-dimensional anatomy. *Spine* **18**, 1298-1310 (1993).

156 Pal, G. P. & Routal, R. V. The orientation of the articular facets of the zygapophyseal joints at the cervical and upper thoracic region. **198**, 431-441, doi:10.1046/j.1469-7580.2001.19840431.x (2001).

157 White, A. A., 3rd. Analysis of the mechanics of the thoracic spine in man. An experimental study of autopsy specimens. *Acta Orthop Scand Suppl* **127**, 1-105 (1969).

158 White, A. A., 3rd & Panjabi, M. M. The basic kinematics of the human spine. A review of past and current knowledge. *Spine (Phila Pa 1976)* **3**, 12-20 (1978).

159 Colle, K. O., Butler, J. B., Reyes, P. M., Newcomb, A. G. U. S., Theodore, N. & Crawford, N. R. Biomechanical evaluation of a metal-on-metal cervical intervertebral disc prosthesis. *The Spine Journal* **13**, 1640-1649, doi:http://dx.doi.org/10.1016/j.spinee.2013.06.026 (2013).

160 Ivicsics, M. F., Bishop, N. E., Puschel, K., Morlock, M. M. & Huber, G. Increase in facet joint loading after nucleotomy in the human lumbar spine. *J Biomech* **47**, 1712-1717, doi:10.1016/j.jbiomech.2014.02.021 (2014).

161 Niosi, C. A., Wilson Dc Fau - Zhu, Q., Zhu Q Fau - Keynan, O., Keynan O Fau - Wilson, D. R., Wilson Dr Fau - Oxland, T. R. & Oxland, T. R. The effect of dynamic posterior stabilization on facet joint contact forces: an in vitro investigation.

162 Rohlmann, A., Zander, T., Schmidt, H., Wilke, H. J. & Bergmann, G. Analysis of the influence of disc degeneration on the mechanical behaviour of a lumbar motion segment using the finite element method. *J Biomech* **39**, 2484-2490, doi:10.1016/j.jbiomech.2005.07.026 (2006).

163 Rousseau, M. A., Bradford, D. S., Bertagnoli, R., Hu, S. S. & Lotz, J. C. Disc arthroplasty design influences intervertebral kinematics and facet forces. *Spine J* **6**, 258-266, doi:10.1016/j.spinee.2005.07.004 (2006).

164 O'Leary, S. A., Link, J. M., Klineberg, E. O., Hu, J. C. & Athanasiou, K. A. Characterization of facet joint cartilage properties in the human and interspecies comparisons. *Acta Biomater* **54**, 367-376, doi:10.1016/j.actbio.2017.03.017 (2017).

165 Elder, B. D., Vigneswaran, K., Athanasiou, K. A. & Kim, D. H. Biomechanical, biochemical, and histological characterization of canine lumbar facet joint cartilage. *J Neurosurg Spine* **10**, 623-628, doi:10.3171/2009.2.SPINE08818 (2009).

166 Abd Latif, M. J., Jin, Z. & Wilcox, R. K. Biomechanical characterisation of ovine spinal facet joint cartilage. *Journal of biomechanics* **45**, 1346-1352, doi:10.1016/j.jbiomech.2012.03.015 (2012).

167 O'Leary, S. A., White, J. L., Hu, J. C. & Athanasiou, K. A. Biochemical and biomechanical characterisation of equine cervical facet joint cartilage. *Equine Veterinary Journal* **50**, 800-808, doi:10.1111/evj.12845 (2018).

168 Farrell, S. F., Osmotherly, P. G., Cornwall, J. & Rivett, D. A. The anatomy and morphometry of cervical zygapophyseal joint meniscoids. *Surg Radiol Anat* **37**, 799-807, doi:10.1007/s00276-014-1406-3 (2015).

169 Little, J. S. & Khalsa, P. S. Material properties of the human lumbar facet joint capsule. *Journal of biomechanical engineering* **127**, 15-24 (2005).

170 Kallakuri, S., Li, Y., Chen, C. & Cavanaugh, J. M. Innervation of cervical ventral facet joint capsule: Histological evidence. *World journal of orthopedics* **3**, 10-14, doi:10.5312/wjo.v3.i2.10 (2012).

171 Zhou, L., Schneck, C. D. & Shao, Z. The Anatomy of Dorsal Ramus Nerves and Its Implications in Lower Back Pain. *Neuroscience & Medicine* **03**, 192-201, doi:10.4236/nm.2012.32025 (2012).

172 Takigawa, T., Espinoza Orias, A. A., An, H. S., Gohgi, S., Udayakumar, R. K., Sugisaki, K., Natarajan, R. N., Wimmer, M. A. & Inoue, N. Spinal kinematics and facet load transmission after total disc replacement. *Spine (Phila Pa 1976)* **35**, E1160-1166, doi:10.1097/BRS.0b013e3181e5352d (2010).

173 Pal, G. P. & Routal, R. V. A study of weight transmission through the cervical and upper thoracic regions of the vertebral column in man. *J Anat* **148**, 245-261 (1986).

174 Raynor, R. B., Moskovich, R., Zidel, P. & Pugh, J. Alterations in primary and coupled neck motions after facetectomy. *Neurosurgery* **21**, 681-687 (1987).

175 Li, W., Wang, S., Xia, Q., Passias, P., Kozanek, M., Wood, K. & Li, G. Lumbar facet joint motion in patients with degenerative disc disease at affected and adjacent levels: an in vivo biomechanical study. *Spine* **36**, E629-637, doi:10.1097/BRS.0b013e3181faaef7 (2011).

176 Adams, M. A. & Hutton, W. C. The mechanical function of the lumbar apophyseal joints. *Spine (Phila Pa 1976)* **8**, 327-330 (1983).

177 Dreischarf, M., Schmidt, H., Putzier, M. & Zander, T. Biomechanics of the L5-S1 motion segment after total disc replacement - Influence of iatrogenic distraction, implant positioning and preoperative disc height on the range of motion and loading of facet joints. *Journal of biomechanics* **48**, 3283-3291, doi:10.1016/j.jbiomech.2015.06.023 (2015).

178 Bauman, J. A., Jaumard, N. V., Guarino, B. B., Weisshaar, C. L., Lipschutz, D. E., Welch, W. C. & Winkelstein, B. A. Facet joint contact pressure is not significantly affected by ProDisc cervical disc arthroplasty in sagittal bending: a single-level cadaveric study. *Spine J* **12**, 949-959, doi:10.1016/j.spinee.2012.08.013 (2012).

179 Vaccaro, A., Koerner, J., Radcliff, K., Oner, F. C., Reinhold, M., Schnake, K., Kandziora, F., Fehlings, M., Dvorak, M., Aarabi, B., Rajasekaran, S., Schroeder, G., Kepler, C. & Vialle, L. AOSpine subaxial cervical spine injury classification system. *European Spine Journal*, 1-12, doi:10.1007/s00586-015-3831-3 (2015).

180 Kuster, D., Gibson, A., Abboud, R. & Drew, T. Mechanisms of cervical spine injury in rugby union: a systematic review of the literature. *British journal of sports medicine* **46**, 550-554 (2012).

181 Hasler, R. M., Exadaktylos, A. K., Bouamra, O., Benneker, L. M., Clancy, M., Sieber, R., Zimmermann, H. & Lecky, F. Epidemiology and predictors of cervical spine injury in adult

major trauma patients: A multicenter cohort study. *Journal of Trauma and Acute Care Surgery* **72**, 975-981, doi:10.1097/TA.0b013e31823f5e8e (2012).

182 Beyer, C. A. & Cabanela, M. E. Unilateral facet dislocations and fracture-dislocations of the cervical spine: a review. *Orthopedics* **15**, 311-315 (1992).

183 Nadeau, M., McLachlin, S. D., Bailey, S. I., Gurr, K. R., Dunning, C. E. & Bailey, C. S. A Biomechanical Assessment of Soft-Tissue Damage in the Cervical Spine Following a Unilateral Facet Injury. *The Journal of Bone & Joint Surgery* **94**, e156, doi:10.2106/jbjs.k.00694 (2012).

184 Sim, E., Vaccaro, A. R., Berzlanovich, A., Schwarz, N. & Sim, B. In vitro genesis of subaxial cervical unilateral facet dislocations through sequential soft tissue ablation. *Spine* **26**, 1317-1323 (2001).

185 Vaccaro, A. R., Madigan, L., Schweitzer, M. E., Flanders, A. E., Hilibrand, A. S. & Albert, T. J. Magnetic resonance imaging analysis of soft tissue disruption after flexion-distraction injuries of the subaxial cervical spine. *Spine* **26**, 1866-1872 (2001).

186 Lowery, D. W., Wald, M. M., Browne, B. J., Tigges, S., Hoffman, J. R. & Mower, W. R. Epidemiology of cervical spine injury victims. *Annals of Emergency Medicine* **38**, 12-16, doi:http://dx.doi.org/10.1067/mem.2001.116149 (2001).

187 Reinhold, M., Audige, L., Schnake, K. J., Bellabarba, C., Dai, L. Y. & Oner, F. C. AO spine injury classification system: a revision proposal for the thoracic and lumbar spine. *Eur Spine J* **22**, 2184-2201, doi:10.1007/s00586-013-2738-0 (2013).

188 Bogduk, N. Evidence-informed management of chronic low back pain with facet injections and radiofrequency neurotomy. *The Spine Journal* **8**, 56-64, doi:http://dx.doi.org/10.1016/j.spinee.2007.10.010 (2008).

189 Manchikanti, L., Singh, V., Pampati, V., Damron, K. S., Barnhill, R. C., Beyer, C. & Cash, K. A. Evaluation of the relative contributions of various structures in chronic low back pain. *Pain Physician* **4**, 308-316 (2001).

190 Manchikanti, L., Pampati, V., Rivera, J., Fellows, B., Beyer, C. & Damron, K. Role of facet joints in chronic low back pain in the elderly: a controlled comparative prevalence study. *Pain Pract* **1**, 332-337, doi:10.1046/j.1533-2500.2001.01034.x (2001).

191 Gellhorn, A. C., Katz, J. N. & Suri, P. Osteoarthritis of the spine: the facet joints. *Nat Rev Rheumatol* **9**, 216-224, doi:10.1038/nrrheum.2012.199 (2013).

192 Kim, J. S., Ali, M. H., Wydra, F., Li, X., Hamilton, J. L., An, H. S., Cs-Szabo, G., Andrews, S., Moric, M., Xiao, G., Wang, J. H., Chen, D., Cavanaugh, J. M. & Im, H. J. Characterization of degenerative human facet joints and facet joint capsular tissues. *Osteoarthritis Cartilage*, doi:10.1016/j.joca.2015.06.009 (2015).

193 Kalichman, L., Kim, D. H., Li, L., Guermazi, A. & Hunter, D. J. Computed tomography–evaluated features of spinal degeneration: prevalence, intercorrelation, and association with self-reported low back pain. *The Spine Journal* **10**, 200-208, doi:http://dx.doi.org/10.1016/j.spinee.2009.10.018 (2010).

194 Ko, S., Vaccaro, A. R., Lee, S., Lee, J. & Chang, H. The prevalence of lumbar spine facet joint osteoarthritis and its association with low back pain in selected Korean populations. *Clin Orthop Surg* **6**, 385-391, doi:10.4055/cios.2014.6.4.385 (2014).

195 Fujiwara, A., Tamai, K., Yamato, M., An, H. S., Yoshida, H., Saotome, K. & Kurihashi, A. The relationship between facet joint osteoarthritis and disc degeneration of the lumbar spine: an MRI study. *Eur Spine J* **8**, 396-401 (1999).

196 Maataoui, A., Vogl, T. J., Middendorp, M., Kafchitsas, K. & Khan, M. F. Association between facet joint osteoarthritis and the Oswestry Disability Index. *World J Radiol* **6**, 881-885 (2014).

197 Butler, D., Trafimow, J. H., Andersson, G. B., McNeill, T. W. & Huckman, M. S. Discs degenerate before facets. *Spine (Phila Pa 1976)* **15**, 111-113 (1990).

198 Suri, P., Miyakoshi, A., Hunter, D. J., Jarvik, J. G., Rainville, J., Guermazi, A., Li, L. & Katz, J. N. Does lumbar spinal degeneration begin with the anterior structures? A study of the

observed epidemiology in a community-based population. *BMC Musculoskeletal Disorders* **12**, 202-202, doi:10.1186/1471-2474-12-202 (2011).

199 Goode, A. P., Marshall, S. W., Renner, J. B., Carey, T. S., Kraus, V. B., Irwin, D. E., Stürmer, T. & Jordan, J. M. Lumbar spine radiographic features and demographic, clinical, and radiographic knee, hip, and hand osteoarthritis. *Arthritis Care & Research* **64**, 1536-1544, doi:10.1002/acr.21720 (2012).

200 Kalichman, L., Suri, P., Guermazi, A., Li, L. & Hunter, D. J. Facet orientation and tropism: associations with facet joint osteoarthritis and degeneratives. *Spine (Phila Pa 1976)* **34**, E579-585, doi:10.1097/BRS.0b013e3181aa2acb (2009).

201 Linov, L., Klindukhov, A., Li, L. & Kalichman, L. Lumbar facet joint orientation and osteoarthritis: a cross-sectional study. *J Back Musculoskelet Rehabil* **26**, 421-426, doi:10.3233/bmr-130401 (2013).

202 Fujiwara, A., Tamai, K., An, H. S., Lim, T. H., Yoshida, H., Kurihashi, A. & Saotome, K. Orientation and osteoarthritis of the lumbar facet joint. *Clin Orthop Relat Res*, 88-94 (2001).

203 Park, M. S., Lee, Y. B., Moon, S.-H., Lee, H.-M., Kim, T.-H., Oh, J. B. & Riew, K. D. Facet Joint Degeneration of the Cervical Spine: A Computed Tomographic Analysis of 320 Patients. *Spine* **39**, E713-E718 710.1097/BRS.0000000000000326 (2014).

204 Uhrenholt, L., Hauge, E., Charles, A. V. & Gregersen, M. Degenerative and traumatic changes in the lower cervical spine facet joints. *Scandinavian Journal of Rheumatology* **37**, 375-384, doi:doi:10.1080/03009740801998770 (2008).

205 Park, M. S., Moon, S. H., Kim, T. H., Lee, S. Y., Jo, Y. G. & Riew, K. D. Relationship between modic changes and facet joint degeneration in the cervical spine. *Eur Spine J*, doi:10.1007/s00586-015-4257-7 (2015).

206 Lee, M. J. & Riew, K. D. The prevalence cervical facet arthrosis: an osseous study in a cadveric population. *The Spine Journal* **9**, 711-714, doi:http://dx.doi.org/10.1016/j.spinee.2009.04.016 (2009).

207 Kalichman, L., Li, L., Kim, D., Guermazi, A., Berkin, V., O'Donnell, C. J., Hoffmann, U., Cole, R. & Hunter, D. J. Facet joint osteoarthritis and low back pain in the community-based population. *Spine* **33**, 2560 (2008).

208 Kirkaldy-Willis, W. & Farfan, H. Instability of the lumbar spine. *Clinical orthopaedics and related research* **165**, 110-123 (1982).

209 Eubanks, J. D., Lee, M. J., Cassinelli, E. & Ahn, N. U. Does lumbar facet arthrosis precede disc degeneration? A postmortem study. *Clin Orthop Relat Res* **464**, 184-189, doi:10.1097/BLO.0b013e3181583d4e (2007).

210 Bough, B., Thakore, J., Davies, M. & Dowling, F. Degeneration of the lumbar facet joints. Arthrography and pathology. *J Bone Joint Surg Br* **72**, 275-276 (1990).

211 Li, J., Muehleman, C., Abe, Y. & Masuda, K. Prevalence of facet joint degeneration in association with intervertebral joint degeneration in a sample of organ donors. *J Orthop Res* **29**, 1267-1274, doi:10.1002/jor.21387 (2011).

212 Virk, S. S., Niedermeier, S., Yu, E. & Khan, S. N. Adjacent segment disease. *Orthopedics* **37**, 547-555, doi:10.3928/01477447-20140728-08 (2014).

213 HILIBRAND, A. S., CARLSON, G. D., PALUMBO, M. A., JONES, P. K. & BOHLMAN, H. H. Radiculopathy and Myelopathy at Segments Adjacent to the Site of a Previous Anterior Cervical Arthrodesis*. *The Journal of Bone & Joint Surgery* **81**, 519-528 (1999).

214 Hellum, C., Berg, L., Gjertsen, O., Johnsen, L. G., Neckelmann, G., Storheim, K., Keller, A., Grundnes, O. & Espeland, A. Adjacent level degeneration and facet arthropathy after disc prosthesis surgery or rehabilitation in patients with chronic low back pain and degenerative disc: second report of a randomized study. *Spine (Phila Pa 1976)* **37**, 2063-2073, doi:10.1097/BRS.0b013e318263cc46 (2012).

215 Nunley, P. D., Jawahar, A., Kerr, E. J., 3rd, Gordon, C. J., Cavanaugh, D. A., Birdsong, E. M., Stocks, M. & Danielson, G. Factors affecting the incidence of symptomatic adjacent-level disease in cervical spine after total disc arthroplasty: 2- to 4-year follow-up of 3 prospective randomized trials. *Spine (Phila Pa 1976)* **37**, 445-451, doi:10.1097/BRS.0b013e31822174b3 (2012).

216 Ciol, M. A., Deyo, R. A., Howell, E. & Kreif, S. An assessment of surgery for spinal stenosis: time trends, geographic variations, complications, and reoperations. *J Am Geriatr Soc* **44**, 285-290 (1996).

217 Jansson, K. A., Blomqvist, P., Granath, F. & Nemeth, G. Spinal stenosis surgery in Sweden 1987-1999. *Eur Spine J* **12**, 535-541, doi:10.1007/s00586-003-0544-9 (2003).

218 Du Bois, M., Szpalski, M. & Donceel, P. A decade's experience in lumbar spine surgery in Belgium: sickness fund beneficiaries, 2000-2009. *Eur Spine J* **21**, 2693-2703, doi:10.1007/s00586-012-2381-1 (2012).

219 LEE, C. K., Rauschning, W. & GLENN, W. Lateral lumbar spinal canal stenosis: classification, pathologic anatomy and surgical decompression. *Spine* **13**, 313-320 (1988).

220 Lee, S. Y., Kim, T.-H., Oh, J. K., Lee, S. J. & Park, M. S. Lumbar Stenosis: A Recent Update by Review of Literature. *Asian Spine Journal* **9**, 818-828, doi:10.4184/asj.2015.9.5.818 (2015).

221 Kalichman, L., Kim, D. H., Li, L., Guermazi, A., Berkin, V. & Hunter, D. J. Spondylolysis and spondylolisthesis: prevalence and association with low back pain in the adult community-based population. *Spine (Phila Pa 1976)* **34**, 199-205, doi:10.1097/BRS.0b013e31818edcfd (2009).

222 Aebi, M. The adult scoliosis. *Eur Spine J* **14**, 925-948, doi:10.1007/s00586-005-1053-9 (2005).

223 van Dam, B. E. Nonoperative treatment of adult scoliosis. *Orthop Clin North Am* **19**, 347-351 (1988).

224 Pichaisak, W., Chotiyarnwong, C. & Chotiyarnwong, P. Facet joint orientation and tropism in lumbar degenerative disc disease and spondylolisthesis. *J Med Assoc Thai* **98**, 373-379 (2015).

225 Xu, C., Lin, B., Ding, Z. & Xu, Y. Cervical degenerative spondylolisthesis: analysis of facet orientation and the severity of cervical spondylolisthesis. *Spine J*, doi:10.1016/j.spinee.2015.09.035 (2015).

226 Nakayama, T. & Ehara, S. Spondylolytic spondylolisthesis: various imaging features and natural courses. *Jpn J Radiol* **33**, 3-12, doi:10.1007/s11604-014-0371-4 (2015).

227 Bao, H., Zhu, F., Liu, Z., Bentley, M., Mao, S., Zhu, Z., Ding, Y. & Qiu, Y. Vertebral rotatory subluxation in degenerative scoliosis: facet joint tropism is related. *Spine (Phila Pa 1976)* **39**, B45-51, doi:10.1097/brs.0000000000000494 (2014).

228 Manchikanti, L., Singh, V., Falco, F. J., Cash, K. A. & Pampati, V. Evaluation of lumbar facet joint nerve blocks in managing chronic low back pain: a randomized, double-blind, controlled trial with a 2-year follow-up. *Int J Med Sci* **7**, 124-135 (2010).

229 Fotiadou, A., Wojcik, A. & Shaju, A. Management of low back pain with facet joint injections and nerve root blocks under computed tomography guidance. A prospective study. *Skeletal Radiol* **41**, 1081-1085, doi:10.1007/s00256-011-1353-6 (2012).

230 Cohen, S. P., Williams, K. A., Kurihara, C., Nguyen, C., Shields, C., Kim, P., Griffith, S. R., Larkin, T. M., Crooks, M., Williams, N., Morlando, B. & Strassels, S. A. Multicenter, randomized, comparative cost-effectiveness study comparing 0, 1, and 2 diagnostic medial branch (facet joint nerve) block treatment paradigms before lumbar facet radiofrequency denervation. *Anesthesiology* **113**, 395-405, doi:10.1097/ALN.0b013e3181e33ae5 (2010).

231 Schwarzer, A. C., Aprill, C. N., Derby, R., Fortin, J., Kine, G. & Bogduk, N. The false-positive rate of uncontrolled diagnostic blocks of the lumbar zygapophysial joints. *Pain* **58**, 195-200 (1994).

232 Manchikanti, L., Pampati, V., Bakhit, C. E., Rivera, J. J., Beyer, C. D., Damron, K. S. & Barnhill, R. C. Effectiveness of lumbar facet joint nerve blocks in chronic low back pain: a randomized clinical trial. *Pain Physician* **4**, 101-117 (2001).

233 Staal, J. B., de Bie, R. A., de Vet, H. C., Hildebrandt, J. & Nelemans, P. Injection therapy for subacute and chronic low back pain: an updated Cochrane review. *Spine (Phila Pa 1976)* **34**, 49-59, doi:10.1097/BRS.0b013e3181909558 (2009).

234 Carette, S., Marcoux, S., Truchon, R., Grondin, C., Gagnon, J., Allard, Y. & Latulippe, M. A controlled trial of corticosteroid injections into facet joints for chronic low back pain. *N Engl J Med* **325**, 1002-1007, doi:10.1056/nejm199110033251405 (1991).

235 Chou, R., Loeser, J. D., Owens, D. K., Rosenquist, R. W., Atlas, S. J., Baisden, J., Carragee, E. J., Grabois, M., Murphy, D. R., Resnick, D. K., Stanos, S. P., Shaffer, W. O., Wall, E. M. & American Pain Society Low Back Pain Guideline, P. Interventional therapies, surgery, and interdisciplinary rehabilitation for low back pain: an evidence-based clinical practice guideline from the American Pain Society. *Spine (Phila Pa 1976)* **34**, 1066-1077, doi:10.1097/BRS.0b013e3181a1390d (2009).

236 Dagenais, S., Yelland, M. J., Del Mar, C. & Schoene, M. L. Prolotherapy injections for chronic low-back pain. *Cochrane Database Syst Rev*, CD004059, doi:10.1002/14651858.CD004059.pub3 (2007).

237 Vekaria, R., Bhatt, R., Ellard, D. R., Henschke, N., Underwood, M. & Sandhu, H. Intra-articular facet joint injections for low back pain: a systematic review. *European Spine Journal* **25**, 1266-1281, doi:10.1007/s00586-016-4455-y (2016).

238 Wu, T., Zhao, W. H., Dong, Y., Song, H. X. & Li, J. H. Effectiveness of Ultrasound-Guided Versus Fluoroscopy or Computed Tomography Scanning Guidance in Lumbar Facet Joint Injections in Adults With Facet Joint Syndrome: A Meta-Analysis of Controlled Trials. *Arch Phys Med Rehabil* **97**, 1558-1563, doi:10.1016/j.apmr.2015.11.013 (2016).

239 Maas, E. T., Ostelo, R. W., Niemisto, L., Jousimaa, J., Hurri, H., Malmivaara, A. & van Tulder, M. W. Radiofrequency denervation for chronic low back pain. *Cochrane Database Syst Rev* **10**, CD008572, doi:10.1002/14651858.CD008572.pub2 (2015).

240 Nath, S., Nath, C. A. & Pettersson, K. Percutaneous lumbar zygapophysial (Facet) joint neurotomy using radiofrequency current, in the management of chronic low back pain: a randomized double-blind trial. *Spine (Phila Pa 1976)* **33**, 1291-1297; discussion 1298, doi:10.1097/BRS.0b013e31817329f0 (2008).

241 Tekin, I., Mirzai, H., Ok, G., Erbuyun, K. & Vatansever, D. A comparison of conventional and pulsed radiofrequency denervation in the treatment of chronic facet joint pain. *Clin J Pain* **23**, 524-529, doi:10.1097/AJP.0b013e318074c99c (2007).

242 Stovner, L. J., Kolstad, F. & Helde, G. Radiofrequency denervation of facet joints C2-C6 in cervicogenic headache: a randomized, double-blind, sham-controlled study. *Cephalalgia* **24**, 821-830, doi:10.1111/j.1468-2982.2004.00773.x (2004).

243 Leclaire, R., Fortin, L., Lambert, R., Bergeron, Y. M. & Rossignol, M. Radiofrequency facet joint denervation in the treatment of low back pain: a placebo-controlled clinical trial to assess efficacy. *Spine (Phila Pa 1976)* **26**, 1411-1416; discussion 1417 (2001).

244 van Wijk, R. M., Geurts, J. W., Wynne, H. J., Hammink, E., Buskens, E., Lousberg, R., Knape, J. T. & Groen, G. J. Radiofrequency denervation of lumbar facet joints in the treatment of chronic low back pain: a randomized, double-blind, sham lesion-controlled trial. *Clin J Pain* **21**, 335-344 (2005).

245 Poetscher, A. W., Gentil, A. F., Lenza, M. & Ferretti, M. Radiofrequency denervation for facet joint low back pain: a systematic review. *Spine (Phila Pa 1976)* **39**, E842-849, doi:10.1097/BRS.0000000000000337 (2014).

246 Garrido, E. & Connaughton, P. N. Unilateral facetectomy approach for lateral lumbar disc herniation. *J Neurosurg* **74**, 754-756, doi:10.3171/jns.1991.74.5.0754 (1991).

247 Sanderson, P. L. & Getty, C. J. Long-term results of partial undercutting facetectomy for lumbar lateral recess stenosis. *Spine (Phila Pa 1976)* **21**, 1352-1356 (1996).

248 Zander, T., Rohlmann, A., Klockner, C. & Bergmann, G. Influence of graded facetectomy and laminectomy on spinal biomechanics. *Eur Spine J* **12**, 427-434, doi:10.1007/s00586-003-0540-0 (2003).

249 Cusick, J. F., Yoganandan, N., Pintar, F., Myklebust, J. & Hussain, H. Biomechanics of cervical spine facetectomy and fixation techniques. *Spine (Phila Pa 1976)* **13**, 808-812 (1988).

250 Jacobs, R. R., Montesano, P. X. & Jackson, R. P. Enhancement of lumbar spine fusion by use of translaminar facet joint screws. *Spine (Phila Pa 1976)* **14**, 12-15 (1989).

251 Park, Y. K. & Chung, H. S. Instrumented facet fusion for the degenerative lumbar disorders. *Acta Neurochir (Wien)* **141**, 915-920 (1999).

252 Heggeness, M. H. & Esses, S. I. Translaminar facet joint screw fixation for lumbar and lumbosacral fusion. A clinical and biomechanical study. *Spine (Phila Pa 1976)* **16**, S266-269 (1991).

253 Grob, D., Bartanusz, V., Jeszenszky, D., Kleinstuck, F. S., Lattig, F., O'Riordan, D. & Mannion, A. F. A prospective, cohort study comparing translaminar screw fixation with transforaminal lumbar interbody fusion and pedicle screw fixation for fusion of the degenerative lumbar spine. *J Bone Joint Surg Br* **91**, 1347-1353, doi:10.1302/0301-620X.91B10.22195 (2009).

254 Akbay, A., Inceoglu, S., Milks, R., Schlenk, R., Palaoglu, S. & Benzel, E. C. Thoracic transfacet pedicle screw fixation: a new instrumentation technique. *J Neurosurg Spine* **3**, 224-229, doi:10.3171/spi.2005.3.3.0224 (2005).

255 Chin, K. R., Reis, M. T., Reyes, P. M., Newcomb, A. G., Neagoe, A., Gabriel, J. P., Sung, R. D. & Crawford, N. R. Stability of transforaminal lumbar interbody fusion in the setting of

retained facets and posterior fixation using transfacet or standard pedicle screws. *Spine J* **15**, 1077-1082, doi:10.1016/j.spinee.2013.06.103 (2015).

256 Luo, P., Chen, Y. H., Wu, Y. S., Dou, H. C., Chi, Y. L. & Lin, Y. Comparison of transforaminal lumbar interbody fusion performed with unilateral pedicle screw fixation or unilateral pedicle screw-contralateral percutaneous transfacet screw fixation. *Br J Neurosurg*, 1-5, doi:10.3109/02688697.2015.1071324 (2015).

257 Chin, K. R., Seale, J. & Cumming, V. Mini-open or percutaneous bilateral lumbar transfacet pedicle screw fixation: a technical note. *J Spinal Disord Tech* **28**, 61-65, doi:10.1097/BSD.0b013e31827fe17e (2015).

258 Fisher, M. A., O'neil, M. J. & Serhan, H. A. (Google Patents, 2008).

259 Hartensuer, R., Riesenbeck, O., Schulze, M., Gehweiler, D., Raschke, M. J., Pavlov, P. W. & Vordemvenne, T. Biomechanical evaluation of the Facet Wedge: a refined technique for facet fixation. *Eur Spine J* **23**, 2321-2329, doi:10.1007/s00586-014-3533-2 (2014).

260 Goel, A. & Shah, A. Facetal distraction as treatment for single- and multilevel cervical spondylotic radiculopathy and myelopathy: a preliminary report. *J Neurosurg Spine* **14**, 689-696, doi:10.3171/2011.2.SPINE10601 (2011).

261 Goel, V. K., Mehta, A., Jangra, J., Faizan, A., Kiapour, A., Hoy, R. W. & Fauth, A. R. Anatomic Facet Replacement System (AFRS) Restoration of Lumbar Segment Mechanics to Intact: A Finite Element Study and In Vitro Cadaver Investigation. *SAS J* **1**, 46-54, doi:10.1016/SASJ-2006-0010-RR (2007).

262 Sjovold, S. G., Zhu, Q., Bowden, A., Larson, C. R., de Bakker, P. M., Villarraga, M. L., Ochoa, J. A., Rosler, D. M. & Cripton, P. A. Biomechanical evaluation of the Total Facet Arthroplasty System(R) (TFAS(R)): loading as compared to a rigid posterior instrumentation system. *Eur Spine J* **21**, 1660-1673, doi:10.1007/s00586-012-2253-8 (2012).

263 Zhu, Q., Larson, C. R., Sjovold, S. G., Rosler, D. M., Keynan, O., Wilson, D. R., Cripton, P. A. & Oxland, T. R. Biomechanical evaluation of the Total Facet Arthroplasty System: 3-dimensional kinematics. *Spine (Phila Pa 1976)* **32**, 55-62, doi:10.1097/01.brs.0000250983.91339.9f (2007).

264 Phillips, F. M., Tzermiadianos, M. N., Voronov, L. I., Havey, R. M., Carandang, G., Renner, S. M., Rosler, D. M., Ochoa, J. A. & Patwardhan, A. G. Effect of the Total Facet Arthroplasty System after complete laminectomy-facetectomy on the biomechanics of implanted and adjacent segments. *Spine J* **9**, 96-102, doi:10.1016/j.spinee.2008.01.010 (2009).

265 Wilke, H. J., Schmidt, H., Werner, K., Schmolz, W. & Drumm, J. Biomechanical evaluation of a new total posterior-element replacement system. *Spine (Phila Pa 1976)* **31**, 2790-2796; discussion 2797, doi:10.1097/01.brs.0000245872.45554.c0 (2006).

266 McAfee, P., Khoo, L. T., Pimenta, L., Capuccino, A., Sengoz, A., Coric, D., Hes, R., Conix, B., Asgarzadie, F., Hamzaoglu, A., Mirofsky, Y. & Anekstein, Y. Treatment of lumbar spinal stenosis with a total posterior arthroplasty prosthesis: implant description, surgical technique, and a prospective report on 29 patients. *Neurosurg Focus* **22**, E13 (2007).

267 Anekstein, Y., Floman, Y., Smorgick, Y., Rand, N., Millgram, M. & Mirovsky, Y. Seven years follow-up for total lumbar facet joint replacement (TOPS) in the management of lumbar spinal stenosis and degenerative spondylolisthesis. *Eur Spine J* **24**, 2306-2314, doi:10.1007/s00586-015-3850-0 (2015).

268 de Kelft, E. V. Lumbar Facet Resurfacing: First Experience With the FENIX Implant. *Clin Spine Surg* **29**, E475-E481, doi:10.1097/BSD.0b013e31828f92a7 (2016).

269 Elder, B. D., Kim, D. H. & Athanasiou, K. A. Developing an articular cartilage decellularization process toward facet joint cartilage replacement. *Neurosurgery* **66**, 722-727; discussion 727, doi:10.1227/01.neu.0000367616.49291.9f (2010).

270 Ateshian, G. A., Soslowsky, L. J. & Mow, V. C. Quantitation of articular surface topography and cartilage thickness in knee joints using stereophotogrammetry. *J Biomech* **24**, 761-776 (1991).

271 Shepherd, D. E. T. & Seedhom, B. B. Thickness of human articular cartilage in joints of the lower limb. *Annals of the Rheumatic Diseases* **58**, 27-34, doi:10.1136/ard.58.1.27 (1999).

272 Athanasiou, K. A., Darling, E. M., Hu, J. C., DuRaine, G. D. & Reddi, A. H. *Articular Cartilage*. (CRC Press, 2017).

273 Gratz, K. R., Wong, V. W., Chen, A. C., Fortier, L. A., Nixon, A. J. & Sah, R. L. Biomechanical assessment of tissue retrieved after in vivo cartilage defect repair: tensile modulus of repair tissue and integration with host cartilage. *Journal of Biomechanics* **39**, 138-146, doi:http://dx.doi.org/10.1016/j.jbiomech.2004.10.016 (2006).

274 Shelburne, K. B., Torry, M. R. & Pandy, M. G. Muscle, ligament, and joint-contact forces at the knee during walking. *Med Sci Sports Exerc* **37**, 1948-1956 (2005).

275 (ed Centers for Disease Control and Prevention) (2010).

276 Kelly, T. A., Ng, K. W., Wang, C. C., Ateshian, G. A. & Hung, C. T. Spatial and temporal development of chondrocyte-seeded agarose constructs in free-swelling and dynamically loaded cultures. *J Biomech* **39**, 1489-1497, doi:10.1016/j.jbiomech.2005.03.031 (2006).

277 Makris, E. A., MacBarb, R. F., Paschos, N. K., Hu, J. C. & Athanasiou, K. A. Combined use of chondroitinase-ABC, TGF-beta1, and collagen crosslinking agent lysyl oxidase to engineer functional neotissues for fibrocartilage repair. *Biomaterials* **35**, 6787-6796, doi:10.1016/j.biomaterials.2014.04.083 (2014).

278 Natoli, R. M., Skaalure, S., Bijlani, S., Chen, K. X., Hu, J. & Athanasiou, K. A. Intracellular Na+ and Ca2+ modulation increases the tensile properties of developing engineered articular cartilage. *Arthritis & Rheumatism* **62**, 1097-1107 (2010).

279 Giannini, S., Buda, R., Vannini, F., Cavallo, M. & Grigolo, B. One-step Bone Marrow-derived Cell Transplantation in Talar Osteochondral Lesions. *Clinical Orthopaedics and Related Research®* **467**, 3307-3320, doi:10.1007/s11999-009-0885-8 (2009).

280 Kon, E., Filardo, G., Roffi, A., Andriolo, L. & Marcacci, M. New trends for knee cartilage regeneration: from cell-free scaffolds to mesenchymal stem cells. *Curr Rev Musculoskelet Med* **5**, 236-243, doi:10.1007/s12178-012-9135-x (2012).

281 Athanasiou, K., Korvick, D. & Schenck Jr, R. Biodegradable implants for the treatment of osteochondral defects in a goat model. *Tissue Engineering* **3**, 363-373 (1997).

282 Chu, C. R., Dounchis, J. S., Yoshioka, M., Sah, R. L., Coutts, R. D. & Amiel, D. Osteochondral repair using perichondrial cells. A 1-year study in rabbits. *Clin Orthop Relat Res*, 220-229 (1997).

283 Fickert, S., Gerwien, P., Helmert, B., Schattenberg, T., Weckbach, S., Kaszkin-Bettag, M. & Lehmann, L. One-Year Clinical and Radiological Results of a Prospective, Investigator-Initiated Trial Examining a Novel, Purely Autologous 3-Dimensional Autologous Chondrocyte Transplantation Product in the Knee. *Cartilage* **3**, 27-42, doi:10.1177/1947603511417616 (2012).

284 Gunja, N. J., Huey, D. J., James, R. A. & Athanasiou, K. A. Effects of agarose mould compliance and surface roughness on self-assembled meniscus-shaped constructs. *J Tissue Eng Regen Med* **3**, 521-530 (2009).

285 Butscher, A., Bohner, M., Hofmann, S., Gauckler, L. & Müller, R. Structural and material approaches to bone tissue engineering in powder-based three-dimensional printing. *Acta Biomaterialia* **7**, 907-920, doi:http://dx.doi.org/10.1016/j.actbio.2010.09.039 (2011).

286 Bose, S., Vahabzadeh, S. & Bandyopadhyay, A. Bone tissue engineering using 3D printing. *Materials Today* **16**, 496-504, doi:http://dx.doi.org/10.1016/j.mattod.2013.11.017 (2013).

287 Noyori, K., Takagi, T. & Jasin, H. E. Characterization of the macromolecular components of the articular cartilage surface. *Rheumatol Int* **18**, 71-77 (1998).

288 Jay, G. D. & Waller, K. A. The biology of Lubricin: Near frictionless joint motion. *Matrix Biology* **39**, 17-24, doi:https://doi.org/10.1016/j.matbio.2014.08.008 (2014).

289 Morrell, K. C., Hodge, W. A., Krebs, D. E. & Mann, R. W. Corroboration of in vivo cartilage pressures with implications for synovial joint tribology and osteoarthritis causation. *Proc Natl Acad Sci U S A* **102**, 14819-14824, doi:10.1073/pnas.0507117102 (2005).

290 Bergmann, G., Graichen, F. & Rohlmann, A. Hip joint loading during walking and running, measured in two patients. *Journal of Biomechanics* **26**, 969-990, doi:https://doi.org/10.1016/0021-9290(93)90058-M (1993).

291 Maiese, K. Picking a bone with WISP1 (CCN4): new strategies against degenerative joint disease. *Journal of translational science* **1**, 83-85 (2016).

292 Zappone, B., Greene, G. W., Oroudjev, E., Jay, G. D. & Israelachvili, J. N. Molecular Aspects of Boundary Lubrication by Human Lubricin: Effect of Disulfide Bonds and Enzymatic Digestion. *Langmuir* **24**, 1495-1508, doi:10.1021/la702383n (2008).

293 Ghosh, S., Bowen, J., Jiang, K., Espino, D. M. & Shepherd, D. E. Investigation of techniques for the measurement of articular cartilage surface roughness. *Micron* **44**, 179-184, doi:10.1016/j.micron.2012.06.007 (2013).

294 Ghosh, S. & Abanteriba, S. Status of surface modification techniques for artificial hip implants. *Science and technology of advanced materials* **17**, 715-735, doi:10.1080/14686996.2016.1240575 (2016).

295 Moa-Anderson BJ, C. K., Hung CT, Ateshian GA. in *Proceedings of 2003 Summer Bioengineering Conference* (2003).

296 Middendorf, J. M., Griffin, D. J., Shortkroff, S., Dugopolski, C., Kennedy, S., Siemiatkoski, J., Cohen, I. & Bonassar, L. J. Mechanical properties and structure-function relationships

of human chondrocyte-seeded cartilage constructs after in vitro culture. *J Orthop Res* **35**, 2298-2306, doi:10.1002/jor.23535 (2017).

297 McCutchen, C. W. The frictional properties of animal joints. *Wear* **5**, 1-17, doi:https://doi.org/10.1016/0043-1648(62)90176-X (1962).

298 Woydt, M. & Wäsche, R. The history of the Stribeck curve and ball bearing steels: The role of Adolf Martens. *Wear* **268**, 1542-1546, doi:https://doi.org/10.1016/j.wear.2010.02.015 (2010).

299 Tamer, T. M. Hyaluronan and synovial joint: function, distribution and healing. *Interdisciplinary Toxicology* **6**, 111-125, doi:10.2478/intox-2013-0019 (2013).

300 Flowers, S. A., Zieba, A., Örnros, J., Jin, C., Rolfson, O., Björkman, L. I., Eisler, T., Kalamajski, S., Kamali-Moghaddam, M. & Karlsson, N. G. Lubricin binds cartilage proteins, cartilage oligomeric matrix protein, fibronectin and collagen II at the cartilage surface. *Scientific reports* **7**, 13149-13149, doi:10.1038/s41598-017-13558-y (2017).

301 Majd, S. E., Kuijer, R., Kowitsch, A., Groth, T., Schmidt, T. A. & Sharma, P. K. Both hyaluronan and collagen type II keep proteoglycan 4 (lubricin) at the cartilage surface in a condition that provides low friction during boundary lubrication. *Langmuir* **30**, 14566-14572, doi:10.1021/la504345c (2014).

302 Chan, S. M. T., Neu, C. P., DuRaine, G., Komvopoulos, K. & Reddi, A. H. Tribological altruism: A sacrificial layer mechanism of synovial joint lubrication in articular cartilage. *Journal of Biomechanics* **45**, 2426-2431, doi:https://doi.org/10.1016/j.jbiomech.2012.06.036 (2012).

303 Peng, G., McNary, S. M., Athanasiou, K. A. & Reddi, A. H. The distribution of superficial zone protein (SZP)/lubricin/PRG4 and boundary mode frictional properties of the bovine diarthrodial joint. *J Biomech* **48**, 3406-3412, doi:10.1016/j.jbiomech.2015.05.032 (2015).

304 Chang, D. P., Guilak, F., Jay, G. D. & Zauscher, S. Interaction of lubricin with type II collagen surfaces: adsorption, friction, and normal forces. *J Biomech* **47**, 659-666, doi:10.1016/j.jbiomech.2013.11.048 (2014).

305 Warnecke, D., Schild, N. B., Klose, S., Joos, H., Brenner, R. E., Kessler, O., Skaer, N., Walker, R., Freutel, M., Ignatius, A. & Durselen, L. Friction properties of a new silk fibroin scaffold for meniscal replacement. *Tribol Int* **109**, 586-592, doi:10.1016/j.triboint.2017.01.038 (2017).

306 Greene, G. W., Banquy, X., Lee, D. W., Lowrey, D. D., Yu, J. & Israelachvili, J. N. Adaptive mechanically controlled lubrication mechanism found in articular joints. *Proceedings of the National Academy of Sciences* **108**, 5255 (2011).

307 Cowman, M. K., Lee, H.-G., Schwertfeger, K. L., McCarthy, J. B. & Turley, E. A. The Content and Size of Hyaluronan in Biological Fluids and Tissues. *Frontiers in immunology* **6**, 261-261, doi:10.3389/fimmu.2015.00261 (2015).

308 Higaki, H., Murakami, T., Nakanishi, Y., Miura, H., Mawatari, T. & Iwamoto, Y. The lubricating ability of biomembrane models with dipalmitoyl phosphatidylcholine and gamma-globulin. *Proc Inst Mech Eng H* **212**, 337-346, doi:10.1243/0954411981534114 (1998).

309 Comper, W. D. & Laurent, T. C. Physiological function of connective tissue polysaccharides. *Physiol Rev* **58**, 255-315, doi:10.1152/physrev.1978.58.1.255 (1978).

310 Šimkovic, I., Hricovíni, M., Šoltés, L., Mendichi, R. & Cosentino, C. Preparation of water-soluble/insoluble derivatives of hyaluronic acid by cross-linking with epichlorohydrin in aqueous NaOH/NH4OH solution. *Carbohydrate Polymers* **41**, 9-14, doi:https://doi.org/10.1016/S0144-8617(99)00061-2 (2000).

311 Sun, S.-F., Hsu, C.-W., Lin, H.-S., Liou, I.-H., Chen, Y.-H. & Hung, C.-L. Comparison of Single Intra-Articular Injection of Novel Hyaluronan (HYA-JOINT Plus) with Synvisc-One

for Knee Osteoarthritis: A Randomized, Controlled, Double-Blind Trial of Efficacy and Safety. **99**, 462-471, doi:10.2106/jbjs.16.00469 (2017).

312 Bell, C. J., Ingham, E. & Fisher, J. Influence of hyaluronic acid on the time-dependent friction response of articular cartilage under different conditions. *Proc Inst Mech Eng H* **220**, 23-31, doi:10.1243/095441105x69060 (2006).

313 Murakami, T., Higaki, H., Sawae, Y., Ohtsuki, N., Moriyama, S. & Nakanishi, Y. Adaptive multimode lubrication in natural synovial joints and artificial joints. *Proc Inst Mech Eng H* **212**, 23-35, doi:10.1243/0954411981533791 (1998).

314 Ambrosio, L., Borzacchiello, A., Netti, P. A. & Nicolais, L. Rheological study on hyaluronic acid and its derivative solutions. *Journal of Macromolecular Science, Part A* **36**, 991-1000, doi:10.1080/10601329908951195 (1999).

315 Hyun, K., Kim, S. H., Ahn, K. H. & Lee, S. J. Large amplitude oscillatory shear as a way to classify the complex fluids. *Journal of Non-Newtonian Fluid Mechanics* **107**, 51-65, doi:https://doi.org/10.1016/S0377-0257(02)00141-6 (2002).

316 McCutchen, C. W. Mechanism of Animal Joints: Sponge-hydrostatic and Weeping Bearings. *Nature* **184**, 1284, doi:10.1038/1841284a0 (1959).

317 Lewis, P. R. & McCutchen, C. W. Experimental evidence for weeping lubrication in mammalian joints. *Nature* **184**, 1285 (1959).

318 Walker, P. S., Dowson, D., Longfield, M. D. & Wright, V. "Boosted lubrication" in synovial joints by fluid entrapment and enrichment. *Ann Rheum Dis* **27**, 512-520 (1968).

319 Gleghorn, J. P. & Bonassar, L. J. Lubrication mode analysis of articular cartilage using Stribeck surfaces. *J Biomech* **41**, 1910-1918, doi:10.1016/j.jbiomech.2008.03.043 (2008).

320 Chan, S. M. T., Neu, C. P., DuRaine, G., Komvopoulos, K. & Reddi, A. H. Atomic force microscope investigation of the boundary-lubricant layer in articular cartilage. *Osteoarthritis and Cartilage* **18**, 956-963, doi:https://doi.org/10.1016/j.joca.2010.03.012 (2010).

321 Neu, C. P., Komvopoulos, K. & Reddi, A. H. The interface of functional biotribology and regenerative medicine in synovial joints. *Tissue engineering. Part B, Reviews* **14**, 235-247, doi:10.1089/ten.teb.2008.0047 (2008).

322 Jahn, S., Seror, J. & Klein, J. Lubrication of Articular Cartilage. *Annu Rev Biomed Eng* **18**, 235-258, doi:10.1146/annurev-bioeng-081514-123305 (2016).

323 McNary, S. M., Athanasiou, K. A. & Reddi, A. H. Engineering Lubrication in Articular Cartilage. *Tissue Engineering. Part B, Reviews* **18**, 88-100, doi:10.1089/ten.teb.2011.0394 (2012).

324 Marcelino, J., Carpten, J. D., Suwairi, W. M., Gutierrez, O. M., Schwartz, S., Robbins, C., Sood, R., Makalowska, I., Baxevanis, A., Johnstone, B., Laxer, R. M., Zemel, L., Kim, C. A., Herd, J. K., Ihle, J., Williams, C., Johnson, M., Raman, V., Alonso, L. G., Brunoni, D., Gerstein, A., Papadopoulos, N., Bahabri, S. A., Trent, J. M. & Warman, M. L. CACP, encoding a secreted proteoglycan, is mutated in camptodactyly-arthropathy-coxa vara-pericarditis syndrome. *Nat Genet* **23**, 319-322, doi:10.1038/15496 (1999).

325 Waller, K. A., Zhang, L. X., Elsaid, K. A., Fleming, B. C., Warman, M. L. & Jay, G. D. Role of lubricin and boundary lubrication in the prevention of chondrocyte apoptosis. *Proceedings of the National Academy of Sciences* **110**, 5852-5857, doi:10.1073/pnas.1219289110 (2013).

326 Grenier, S., Bhargava, M. M. & Torzilli, P. A. An in vitro model for the pathological degradation of articular cartilage in osteoarthritis. *J Biomech* **47**, 645-652, doi:10.1016/j.jbiomech.2013.11.050 (2014).

327 Jay, G. D., Torres, J. R., Rhee, D. K., Helminen, H. J., Hytinnen, M. M., Cha, C. J., Elsaid, K., Kim, K. S., Cui, Y. & Warman, M. L. Association between friction and wear in diarthrodial joints lacking lubricin. *Arthritis Rheum* **56**, 3662-3669, doi:10.1002/art.22974 (2007).

328 Coles, J. M., Zhang, L., Blum, J. J., Warman, M. L., Jay, G. D., Guilak, F. & Zauscher, S. Loss of cartilage structure, stiffness, and frictional properties in mice lacking PRG4. *Arthritis Rheum* **62**, 1666-1674, doi:10.1002/art.27436 (2010).

329 Park, J. Y., Duong, C. T., Sharma, A. R., Son, K. M., Thompson, M. S., Park, S., Chang, J. D., Nam, J. S., Park, S. & Lee, S. S. Effects of hyaluronic acid and gamma-globulin concentrations on the frictional response of human osteoarthritic articular cartilage. *PLoS One* **9**, e112684, doi:10.1371/journal.pone.0112684 (2014).

330 Antonacci, J. M., Schmidt, T. A., Serventi, L. A., Cai, M. Z., Shu, Y. L., Schumacher, B. L., McIlwraith, C. W. & Sah, R. L. Effects of Equine Joint Injury on Boundary Lubrication of Articular Cartilage by Synovial Fluid: Role of Hyaluronan. *Arthritis and rheumatism* **64**, 2917-2926, doi:10.1002/art.34520 (2012).

331 Gleghorn, J. P., Jones, A. R. C., Flannery, C. R. & Bonassar, L. J. Alteration of articular cartilage frictional properties by transforming growth factor β, interleukin-1β, and oncostatin M. *Arthritis & Rheumatism* **60**, 440-449, doi:10.1002/art.24259 (2009).

332 Jia, H., Ma, X., Tong, W., Doyran, B., Sun, Z., Wang, L., Zhang, X., Zhou, Y., Badar, F., Chandra, A., Lu, X. L., Xia, Y., Han, L., Enomoto-Iwamoto, M. & Qin, L. EGFR signaling is critical for maintaining the superficial layer of articular cartilage and preventing osteoarthritis initiation. *Proc Natl Acad Sci U S A* **113**, 14360-14365, doi:10.1073/pnas.1608938113 (2016).

333 Sanchez-Guerrero, E., Chen, E., Kockx, M., An, S. W., Chong, B. H. & Khachigian, L. M. IL-1beta signals through the EGF receptor and activates Egr-1 through MMP-ADAM. *PLoS One* **7**, e39811, doi:10.1371/journal.pone.0039811 (2012).

334 Schmidt, T. A., Gastelum, N. S., Nguyen, Q. T., Schumacher, B. L. & Sah, R. L. Boundary lubrication of articular cartilage: role of synovial fluid constituents. *Arthritis Rheum* **56**, 882-891, doi:10.1002/art.22446 (2007).

335 Shi, L., Sikavitsas, V. I. & Striolo, A. Experimental friction coefficients for bovine cartilage measured with a pin-on-disk tribometer: testing configuration and lubricant effects. *Ann Biomed Eng* **39**, 132-146, doi:10.1007/s10439-010-0167-3 (2011).

336 Kanca, Y., Milner, P., Dini, D. & Amis, A. A. Tribological evaluation of biomedical polycarbonate urethanes against articular cartilage. *J Mech Behav Biomed Mater* **82**, 394-402, doi:10.1016/j.jmbbm.2018.04.001 (2018).

337 Bonnevie, E. D., Puetzer, J. L. & Bonassar, L. J. Enhanced boundary lubrication properties of engineered menisci by lubricin localization with insulin-like growth factor I treatment. *J Biomech* **47**, 2183-2188, doi:10.1016/j.jbiomech.2013.10.028 (2014).

338 Nečas, D., Vrbka, M., Křupka, I. & Hartl, M. The Effect of Kinematic Conditions and Synovial Fluid Composition on the Frictional Behaviour of Materials for Artificial Joints. *Materials (Basel, Switzerland)* **11**, 767, doi:10.3390/ma11050767 (2018).

339 Grad, S., Loparic, M., Peter, R., Stolz, M., Aebi, U. & Alini, M. Sliding motion modulates stiffness and friction coefficient at the surface of tissue engineered cartilage. *Osteoarthritis Cartilage* **20**, 288-295, doi:10.1016/j.joca.2011.12.010 (2012).

340 Blum, M. M. & Ovaert, T. C. Low friction hydrogel for articular cartilage repair: evaluation of mechanical and tribological properties in comparison with natural cartilage tissue. *Mater Sci Eng C Mater Biol Appl* **33**, 4377-4383, doi:10.1016/j.msec.2013.06.035 (2013).

341 Park, S., Costa, K. D. & Ateshian, G. A. Microscale frictional response of bovine articular cartilage from atomic force microscopy. *Journal of biomechanics* **37**, 1679-1687, doi:10.1016/j.jbiomech.2004.02.017 (2004).

342 Sedin, D. L. & Rowlen, K. L. Influence of tip size on AFM roughness measurements. *Applied Surface Science* **182**, 40-48, doi:https://doi.org/10.1016/S0169-4332(01)00432-9 (2001).

343 Singh, A., Corvelli, M., Unterman, S. A., Wepasnick, K. A., McDonnell, P. & Elisseeff, J. H. Enhanced lubrication on tissue and biomaterial surfaces through peptide-mediated binding of hyaluronic acid. *Nature Materials* **13**, 988, doi:10.1038/nmat4048 (2014).

344 Henrotin, Y., Chevalier, X., Raman, R., Richette, P., Montfort, J., Jerosch, J., Baron, D., Bard, H., Carrillon, Y., Migliore, A. & Conrozier, T. EUROVISCO Guidelines for the Design and Conduct of Clinical Trials Assessing the Disease-Modifying Effect of Knee Viscosupplementation. *Cartilage*, 1947603518783521, doi:10.1177/1947603518783521 (2018).

345 Flannery, C. R., Zollner, R., Corcoran, C., Jones, A. R., Root, A., Rivera-Bermúdez, M. A., Blanchet, T., Gleghorn, J. P., Bonassar, L. J., Bendele, A. M., Morris, E. A. & Glasson, S. S. Prevention of cartilage degeneration in a rat model of osteoarthritis by intraarticular treatment with recombinant lubricin. *Arthritis & Rheumatism* **60**, 840-847, doi:10.1002/art.24304 (2009).

346 Morgese, G., Cavalli, E., Rosenboom, J. G., Zenobi-Wong, M. & Benetti, E. M. Cyclic Polymer Grafts That Lubricate and Protect Damaged Cartilage. *Angew Chem Int Ed Engl* **57**, 1621-1626, doi:10.1002/anie.201712534 (2018).

347 Morgese, G., Cavalli, E., Muller, M., Zenobi-Wong, M. & Benetti, E. M. Nanoassemblies of Tissue-Reactive, Polyoxazoline Graft-Copolymers Restore the Lubrication Properties of Degraded Cartilage. *ACS Nano* **11**, 2794-2804, doi:10.1021/acsnano.6b07847 (2017).

348 Cooper, B. G., Lawson, T. B., Snyder, B. D. & Grinstaff, M. W. Reinforcement of articular cartilage with a tissue-interpenetrating polymer network reduces friction and modulates interstitial fluid load support. *Osteoarthritis Cartilage* **25**, 1143-1149, doi:10.1016/j.joca.2017.03.001 (2017).

349 Kanca, Y., Milner, P., Dini, D. & Amis, A. A. Tribological properties of PVA/PVP blend hydrogels against articular cartilage. *Journal of the Mechanical Behavior of Biomedical Materials* **78**, 36-45, doi:https://doi.org/10.1016/j.jmbbm.2017.10.027 (2018).

350 Liao, I. C., Moutos, F. T., Estes, B. T., Zhao, X. & Guilak, F. Composite three-dimensional woven scaffolds with interpenetrating network hydrogels to create functional synthetic articular cartilage. *Adv Funct Mater* **23**, 5833-5839, doi:10.1002/adfm.201300483 (2013).

351 Rongen, J. J., van Tienen, T. G., van Bochove, B., Grijpma, D. W. & Buma, P. Biomaterials in search of a meniscus substitute. *Biomaterials* **35**, 3527-3540, doi:10.1016/j.biomaterials.2014.01.017 (2014).

352 Galley, N. K., Gleghorn, J. P., Rodeo, S., Warren, R. F., Maher, S. A. & Bonassar, L. J. Frictional properties of the meniscus improve after scaffold-augmented repair of partial meniscectomy: a pilot study. *Clin Orthop Relat Res* **469**, 2817-2823, doi:10.1007/s11999-011-1854-6 (2011).

353 Peng, G., McNary, S. M., Athanasiou, K. A. & Reddi, A. H. Surface zone articular chondrocytes modulate the bulk and surface mechanical properties of the tissue-engineered cartilage. *Tissue Eng Part A* **20**, 3332-3341, doi:10.1089/ten.TEA.2014.0099 (2014).

354 Iwasa, K. & Reddi, A. H. Optimization of Methods for Articular Cartilage Surface Tissue Engineering: Cell Density and Transforming Growth Factor Beta Are Critical for Self-Assembly and Lubricin Secretion. *Tissue Eng Part C Methods* **23**, 389-395, doi:10.1089/ten.TEC.2017.0121 (2017).

355 Iwakura, T., Sakata, R. & Reddi, A. H. Induction of chondrogenesis and expression of superficial zone protein in synovial explants with TGF-beta1 and BMP-7. *Tissue Eng Part A* **19**, 2638-2644, doi:10.1089/ten.TEA.2013.0047 (2013).

356 Peng, G., McNary, S. M., Athanasiou, K. A. & Reddi, A. H. Superficial Zone Extracellular Matrix Extracts Enhance Boundary Lubrication of Self-Assembled Articular Cartilage. *Cartilage* **7**, 256-264, doi:10.1177/1947603515612190 (2016).

357 Bonnevie, E. D., McCorry, M. C. & Bonassar, L. J. Mesenchymal Stem Cells Enhance Lubrication of Engineered Meniscus Through Lubricin Localization in Collagen Gels. *Biotribology* **8**, 26-32, doi:https://doi.org/10.1016/j.biotri.2016.11.001 (2016).

358 Park, I. S., Choi, W. H., Park, D. Y., Park, S. R., Park, S. H. & Min, B. H. Effect of joint mimicking loading system on zonal organization into tissue-engineered cartilage. *PLoS One* **13**, e0202834, doi:10.1371/journal.pone.0202834 (2018).

359 Wu, Y., Stoddart, M. J., Wuertz-Kozak, K., Grad, S., Alini, M. & Ferguson, S. J. Hyaluronan supplementation as a mechanical regulator of cartilage tissue development under joint-kinematic-mimicking loading. *J R Soc Interface* **14**, doi:10.1098/rsif.2017.0255 (2017).

360 Boushell, M. K., Hung, C. T., Hunziker, E. B., Strauss, E. J. & Lu, H. H. Current strategies for integrative cartilage repair. *Connect Tissue Res* **58**, 393-406, doi:10.1080/03008207.2016.1231180 (2017).

361 Groen, W. M., Diloksumpan, P., van Weeren, P. R., Levato, R. & Malda, J. From intricate to integrated: Biofabrication of articulating joints. *J Orthop Res* **35**, 2089-2097, doi:10.1002/jor.23602 (2017).

362 Yodmuang, S., Guo, H., Brial, C., Warren, R. F., Torzilli, P. A., Chen, T. & Maher, S. A. Effect of interface mechanical discontinuities on scaffold-cartilage integration. *Journal of Orthopaedic Research* **37**, 845-854, doi:10.1002/jor.24238 (2019).

363 Arvayo, A. L., Wong, I. J., Dragoo, J. L. & Levenston, M. E. Enhancing Integration of Articular Cartilage Grafts via Photochemical Bonding. *J Orthop Res*, doi:10.1002/jor.23898 (2018).

364 de Girolamo, L., Ragni, E., Cucchiarini, M., van Bergen, C. J. A., Hunziker, E. B. & Chubinskaya, S. Cells, soluble factors and matrix harmonically play the concert of allograft integration. *Knee Surg Sports Traumatol Arthrosc* **27**, 1717-1725, doi:10.1007/s00167-018-5182-1 (2019).

365 Khan, I. M., Gilbert, S. J., Singhrao, S. K., Duance, V. C. & Archer, C. W. Cartilage integration: evaluation of the reasons for failure of integration during cartilage repair. A review. *Eur Cell Mater* **16**, 26-39 (2008).

366 Hunziker, E. B. & Quinn, T. M. Surgical removal of articular cartilage leads to loss of chondrocytes from cartilage bordering the wound edge. *J Bone Joint Surg Am* **85-A Suppl 2**, 85-92, doi:10.2106/00004623-200300002-00011 (2003).

367 Liebesny, P. H., Mroszczyk, K., Zlotnick, H., Hung, H.-H., Frank, E., Kurz, B., Zanotto, G., Frisbie, D. & Grodzinsky, A. J. Enzyme Pretreatment plus Locally Delivered HB-IGF-1 Stimulate Integrative Cartilage Repair In Vitro. *Tissue Engineering Part A* **25**, 1191-1201, doi:10.1089/ten.tea.2019.0013 (2019).

368 Davies, L. C., Blain, E. J., Caterson, B. & Duance, V. C. Chondroitin sulphate impedes the migration of a sub-population of articular cartilage chondrocytes. *Osteoarthritis Cartilage* **16**, 855-864, doi:10.1016/j.joca.2007.12.005 (2008).

369 Lim, J. J. & Temenoff, J. S. The effect of desulfation of chondroitin sulfate on interactions with positively charged growth factors and upregulation of cartilaginous markers in encapsulated MSCs. *Biomaterials* **34**, 5007-5018, doi:10.1016/j.biomaterials.2013.03.037 (2013).

370 DiMicco, M. A., Waters, S. N., Akeson, W. H. & Sah, R. L. Integrative articular cartilage repair: dependence on developmental stage and collagen metabolism. *Osteoarthritis Cartilage* **10**, 218-225, doi:10.1053/joca.2001.0502 (2002).

371 Asanbaeva, A., Masuda, K., Thonar, E. J., Klisch, S. M. & Sah, R. L. Mechanisms of cartilage growth: modulation of balance between proteoglycan and collagen in vitro using chondroitinase ABC. *Arthritis Rheum* **56**, 188-198, doi:10.1002/art.22298 (2007).

372 Asanbaeva, A., Tam, J., Schumacher, B. L., Klisch, S. M., Masuda, K. & Sah, R. L. Articular cartilage tensile integrity: modulation by matrix depletion is maturation-dependent. *Arch Biochem Biophys* **474**, 175-182, doi:10.1016/j.abb.2008.03.012 (2008).

373 Natoli, R. M., Revell, C. M. & Athanasiou, K. A. Chondroitinase ABC treatment results in greater tensile properties of self-assembled tissue-engineered articular cartilage. *Tissue engineering. Part A* **15**, 3119-3128, doi:10.1089/ten.TEA.2008.0478 (2009).

374 Prabhakar, V., Raman, R., Capila, I., Bosques, C. J., Pojasek, K. & Sasisekharan, R. Biochemical characterization of the chondroitinase ABC I active site. *The Biochemical journal* **390**, 395-405, doi:10.1042/BJ20050532 (2005).

375 Lee, M. C., Sung, K. L., Kurtis, M. S., Akeson, W. H. & Sah, R. L. Adhesive force of chondrocytes to cartilage. Effects of chondroitinase ABC. *Clin Orthop Relat Res*, 286-294, doi:10.1097/00003086-200001000-00029 (2000).

376 Seol, D., Yu, Y., Choe, H., Jang, K., Brouillette, M. J., Zheng, H., Lim, T. H., Buckwalter, J. A. & Martin, J. A. Effect of short-term enzymatic treatment on cell migration and cartilage regeneration: in vitro organ culture of bovine articular cartilage. *Tissue Eng Part A* **20**, 1807-1814, doi:10.1089/ten.TEA.2013.0444 (2014).

377 Janssen, L. M., In der Maur, C. D., Bos, P. K., Hardillo, J. A. & van Osch, G. J. Short-duration enzymatic treatment promotes integration of a cartilage graft in a defect. *Ann Otol Rhinol Laryngol* **115**, 461-468, doi:10.1177/000348940611500611 (2006).

378 Bos, P. K., DeGroot, J., Budde, M., Verhaar, J. A. & van Osch, G. J. Specific enzymatic treatment of bovine and human articular cartilage: implications for integrative cartilage repair. *Arthritis Rheum* **46**, 976-985, doi:10.1002/art.10208 (2002).

379 van de Breevaart Bravenboer, J., In der Maur, C. D., Bos, P. K., Feenstra, L., Verhaar, J. A., Weinans, H. & van Osch, G. J. Improved cartilage integration and interfacial strength after enzymatic treatment in a cartilage transplantation model. *Arthritis Res Ther* **6**, R469-476, doi:10.1186/ar1216 (2004).

380 Natoli, R. M., Responte, D. J., Lu, B. Y. & Athanasiou, K. A. Effects of multiple chondroitinase ABC applications on tissue engineered articular cartilage. *J Orthop Res* **27**, 949-956, doi:10.1002/jor.20821 (2009).

381 Cissell, D. D., Link, J. M., Hu, J. C. & Athanasiou, K. A. A Modified Hydroxyproline Assay Based on Hydrochloric Acid in Ehrlich's Solution Accurately Measures Tissue Collagen Content. *Tissue Eng Part C Methods* **23**, 243-250, doi:10.1089/ten.tec.2017.0018 (2017).

382 Naffa, R., Watanabe, S., Zhang, W., Maidment, C., Singh, P., Chamber, P., Matyska, M. T. & Pesek, J. J. Rapid analysis of pyridinoline and deoxypyridinoline in biological samples by liquid chromatography with mass spectrometry and a silica hydride column. *Journal of Separation Science* **42**, 1482-1488, doi:10.1002/jssc.201801292 (2019).

383 Brown, W. E., Huey, D. J., Hu, J. C. & Athanasiou, K. A. Functional self-assembled neocartilage as part of a biphasic osteochondral construct. *PLoS One* **13**, e0195261, doi:10.1371/journal.pone.0195261 (2018).

384 Mow, V. C., Gibbs, M. C., Lai, W. M., Zhu, W. B. & Athanasiou, K. A. Biphasic indentation of articular cartilage--II. A numerical algorithm and an experimental study. *J Biomech* **22**, 853-861, doi:10.1016/0021-9290(89)90069-9 (1989).

385 Athanasiou, K. A., Agarwal, A., Muffoletto, A., Dzida, F. J., Constantinides, G. & Clem, M. Biomechanical properties of hip cartilage in experimental animal models. *Clin Orthop Relat Res*, 254-266 (1995).

386 Fisher, M. B., Henning, E. A., Soegaard, N. B., Dodge, G. R., Steinberg, D. R. & Mauck, R. L. Maximizing cartilage formation and integration via a trajectory-based tissue engineering approach. *Biomaterials* **35**, 2140-2148, doi:10.1016/j.biomaterials.2013.11.031 (2014).

387 Obradovic, B., Martin, I., Padera, R. F., Treppo, S., Freed, L. E. & Vunjak-Novakovic, G. Integration of engineered cartilage. *Journal of Orthopaedic Research* **19**, 1089-1097, doi:https://doi.org/10.1016/S0736-0266(01)00030-4 (2001).

388 Hunter, C. J. & Levenston, M. E. Maturation and Integration of Tissue-Engineered Cartilages within an in Vitro Defect Repair Model. *Tissue Engineering* **10**, 736-746, doi:10.1089/1076327041348310 (2004).

389 Erickson, I. E., Kestle, S. R., Zellars, K. H., Dodge, G. R., Burdick, J. A. & Mauck, R. L. Improved cartilage repair viain vitropre-maturation of MSC-seeded hyaluronic acid hydrogels. *Biomedical Materials* **7**, 024110, doi:10.1088/1748-6041/7/2/024110 (2012).

390 Sennett, M. L., Meloni, G. R., Farran, A. J. E., Guehring, H., Mauck, R. L. & Dodge, G. R. Sprifermin Treatment Enhances Cartilage Integration in an In Vitro Repair Model. *J Orthop Res*, doi:10.1002/jor.24048 (2018).

391 Paschos, N. K., Lim, N., Hu, J. C. & Athanasiou, K. A. Functional properties of native and tissue-engineered cartilage toward understanding the pathogenesis of chondral lesions at the knee: A bovine cadaveric study. *Journal of orthopaedic research : official publication of the Orthopaedic Research Society* **35**, 2452-2464, doi:10.1002/jor.23558 (2017).

392 Chang, C., Lauffenburger, D. A. & Morales, T. I. Motile chondrocytes from newborn calf: migration properties and synthesis of collagen II. *Osteoarthritis Cartilage* **11**, 603-612, doi:10.1016/s1063-4584(03)00087-6 (2003).

393 Hu, J. C. & Athanasiou, K. A. A self-assembling process in articular cartilage tissue engineering. *Tissue Eng* **12**, 969-979, doi:10.1089/ten.2006.12.969 (2006).

394 Theodoropoulos, J. S., DeCroos, A. J., Petrera, M., Park, S. & Kandel, R. A. Mechanical stimulation enhances integration in an in vitro model of cartilage repair. *Knee Surg Sports Traumatol Arthrosc* **24**, 2055-2064, doi:10.1007/s00167-014-3250-8 (2016).

395 Donahue, R. P., Gonzalez-Leon, E. A., Hu, J. C. & Athanasiou, K. Considerations for translation of tissue engineered fibrocartilage from bench to bedside. *J Biomech Eng*, doi:10.1115/1.4042201 (2018).

396 Donahue, R. P., Hu, J. C. & Athanasiou, K. A. Remaining Hurdles for Tissue-Engineering the Temporomandibular Joint Disc. *Trends Mol Med* **25**, 241-256, doi:10.1016/j.molmed.2018.12.007 (2019).

397 Fernandes, T. L., Gomoll, A. H., Lattermann, C., Hernandez, A. J., Bueno, D. F. & Amano, M. T. Macrophage: A Potential Target on Cartilage Regeneration. *Frontiers in immunology* **11**, 111-111, doi:10.3389/fimmu.2020.00111 (2020).

398 Camarero-Espinosa, S., Rothen-Rutishauser, B., Foster, E. J. & Weder, C. Articular cartilage: from formation to tissue engineering. *Biomater Sci* **4**, 734-767, doi:10.1039/c6bm00068a (2016).

399 Centers for Disease Control and Prevention. *Osteoarthritis*, <https://www.cdc.gov/arthritis/basics/osteoarthritis.htm> (2020).

400 Centers for Disease Control and Prevention. *Arthritis-Related Statistics*, <https://www.cdc.gov/arthritis/data_statistics/arthritis-related-stats.htm> (2018).

401 Perrier-Groult, E., Pérès, E., Pasdeloup, M., Gazzolo, L., Duc Dodon, M. & Mallein-Gerin, F. Evaluation of the biocompatibility and stability of allogeneic tissue-engineered cartilage in humanized mice. *PloS one* **14**, e0217183-e0217183, doi:10.1371/journal.pone.0217183 (2019).

402 Koh, T. J. & DiPietro, L. A. Inflammation and wound healing: the role of the macrophage. *Expert Rev Mol Med* **13**, e23, doi:10.1017/S1462399411001943 (2011).

403 Mantovani, A., Sica, A., Sozzani, S., Allavena, P., Vecchi, A. & Locati, M. The chemokine system in diverse forms of macrophage activation and polarization. *Trends Immunol* **25**, 677-686, doi:10.1016/j.it.2004.09.015 (2004).

404 Van Dyken, S. J. & Locksley, R. M. Interleukin-4- and interleukin-13-mediated alternatively activated macrophages: roles in homeostasis and disease. *Annu Rev Immunol* **31**, 317-343, doi:10.1146/annurev-immunol-032712-095906 (2013).

405 Martinez, F. O. & Gordon, S. The M1 and M2 paradigm of macrophage activation: time for reassessment. *F1000Prime Reports* **6**, 13, doi:10.12703/P6-13 (2014).

406 Fang, H., Pengal, R. A., Cao, X., Ganesan, L. P., Wewers, M. D., Marsh, C. B. & Tridandapani, S. Lipopolysaccharide-induced macrophage inflammatory response is regulated by SHIP. *J Immunol* **173**, 360-366, doi:10.4049/jimmunol.173.1.360 (2004).

407 Bogdan, C., Vodovotz, Y. & Nathan, C. Macrophage deactivation by interleukin 10. *J Exp Med* **174**, 1549-1555, doi:10.1084/jem.174.6.1549 (1991).

408 Müller, R. D., John, T., Kohl, B., Oberholzer, A., Gust, T., Hostmann, A., Hellmuth, M., LaFace, D., Hutchins, B., Laube, G., Veh, R. W., Tschoeke, S. K., Ertel, W. & Schulze-Tanzil, G. IL-10 overexpression differentially affects cartilage matrix gene expression in response to TNF-α in human articular chondrocytes in vitro. *Cytokine* **44**, 377-385, doi:https://doi.org/10.1016/j.cyto.2008.10.012 (2008).

409 Behrendt, P., Preusse-Prange, A., Klüter, T., Haake, M., Rolauffs, B., Grodzinsky, A. J., Lippross, S. & Kurz, B. IL-10 reduces apoptosis and extracellular matrix degradation after injurious compression of mature articular cartilage. *Osteoarthritis and Cartilage* **24**, 1981-1988, doi:https://doi.org/10.1016/j.joca.2016.06.016 (2016).

410 Meli, V. S., Veerasubramanian, P. K., Atcha, H., Reitz, Z., Downing, T. L. & Liu, W. F. Biophysical regulation of macrophages in health and disease. *J Leukoc Biol* **106**, 283-299, doi:10.1002/jlb.Mr0318-126r (2019).

411 Patel, N. R., Bole, M., Chen, C., Hardin, C. C., Kho, A. T., Mih, J., Deng, L., Butler, J., Tschumperlin, D., Fredberg, J. J., Krishnan, R. & Koziel, H. Cell Elasticity Determines Macrophage Function. *PLoS ONE* **7**, e41024, doi:10.1371/journal.pone.0041024 (2012).

412 Sridharan, R., Cavanagh, B., Cameron, A. R., Kelly, D. J. & O'Brien, F. J. Material stiffness influences the polarization state, function and migration mode of macrophages. *Acta Biomaterialia* **89**, 47-59, doi:https://doi.org/10.1016/j.actbio.2019.02.048 (2019).

413 Jansen, L. E., Amer, L. D., Chen, E. Y., Nguyen, T. V., Saleh, L. S., Emrick, T., Liu, W. F., Bryant, S. J. & Peyton, S. R. Zwitterionic PEG-PC Hydrogels Modulate the Foreign Body

Response in a Modulus-Dependent Manner. *Biomacromolecules* **19**, 2880-2888, doi:10.1021/acs.biomac.8b00444 (2018).

414 Brown, W. E., Hu, J. C. & Athanasiou, K. A. Ammonium–Chloride–Potassium Lysing Buffer Treatment of Fully Differentiated Cells Increases Cell Purity and Resulting Neotissue Functional Properties. *Tissue Engineering Part C: Methods* **22**, 895-903 (2016).

415 Link, J. M., Hu, J. C. & Athanasiou, K. A. Chondroitinase ABC Enhances Integration of Self-Assembled Articular Cartilage, but Its Dosage Needs to Be Moderated Based on Neocartilage Maturity. *Cartilage*, 1947603520918653, doi:10.1177/1947603520918653 (2020).

416 Dąbrowska, A. M. & Słotwiński, R. The immune response to surgery and infection. *Cent Eur J Immunol* **39**, 532-537, doi:10.5114/ceji.2014.47741 (2014).

417 Smith, T. D., Tse, M. J., Read, E. L. & Liu, W. F. Regulation of macrophage polarization and plasticity by complex activation signals. *Integrative biology : quantitative biosciences from nano to macro* **8**, 946-955, doi:10.1039/c6ib00105j (2016).

418 Nemir, S., Hayenga, H. N. & West, J. L. PEGDA hydrogels with patterned elasticity: Novel tools for the study of cell response to substrate rigidity. *Biotechnol Bioeng* **105**, 636-644, doi:10.1002/bit.22574 (2010).

419 Bianchi, V. J., Lee, A., Anderson, J., Parreno, J., Theodoropoulos, J., Backstein, D. & Kandel, R. Redifferentiated Chondrocytes in Fibrin Gel for the Repair of Articular Cartilage Lesions. *Am J Sports Med* **47**, 2348-2359, doi:10.1177/0363546519857571 (2019).

420 Wrenshall, L. E., Stevens, R. B., Cerra, F. B. & Platt, J. L. Modulation of macrophage and B cell function by glycosaminoglycans. *J Leukoc Biol* **66**, 391-400, doi:10.1002/jlb.66.3.391 (1999).

421 McCormick, F., Harris, J. D., Abrams, G. D., Frank, R., Gupta, A., Hussey, K., Wilson, H., Bach, B., Jr. & Cole, B. Trends in the surgical treatment of articular cartilage lesions in the

United States: an analysis of a large private-payer database over a period of 8 years. *Arthroscopy* **30**, 222-226, doi:10.1016/j.arthro.2013.11.001 (2014).

422 Huang, B. J., Hu, J. C. & Athanasiou, K. A. Cell-based tissue engineering strategies used in the clinical repair of articular cartilage. *Biomaterials* **98**, 1-22, doi:10.1016/j.biomaterials.2016.04.018 (2016).

423 Adkisson, H. D., Milliman, C., Zhang, X., Mauch, K., Maziarz, R. T. & Streeter, P. R. Immune evasion by neocartilage-derived chondrocytes: Implications for biologic repair of joint articular cartilage. *Stem Cell Research* **4**, 57-68, doi:https://doi.org/10.1016/j.scr.2009.09.004 (2010).

424 Huey, D. J., Sanchez-Adams, J., Willard, V. P. & Athanasiou, K. A. Immunogenicity of bovine and leporine articular chondrocytes and meniscus cells. *Tissue Eng Part A* **18**, 568-575, doi:10.1089/ten.TEA.2011.0226 (2012).

425 Elder, B. D. & Athanasiou, K. A. Systematic assessment of growth factor treatment on biochemical and biomechanical properties of engineered articular cartilage constructs. *Osteoarthritis and Cartilage* **17**, 114-123, doi:http://dx.doi.org/10.1016/j.joca.2008.05.006 (2009).

426 Little, C. J., Bawolin, N. K. & Chen, X. Mechanical properties of natural cartilage and tissue-engineered constructs. *Tissue Eng Part B Rev* **17**, 213-227, doi:10.1089/ten.TEB.2010.0572 (2011).

427 Gunja, N. J., Uthamanthil, R. K. & Athanasiou, K. A. Effects of TGF-β1 and hydrostatic pressure on meniscus cell-seeded scaffolds. *Biomaterials* **30**, 565-573 (2009).

428 Huwe, L. W., Sullan, G. K., Hu, J. C. & Athanasiou, K. A. Using Costal Chondrocytes to Engineer Articular Cartilage with Applications of Passive Axial Compression and Bioactive Stimuli. *Tissue Engineering Part A* **24**, 516-526, doi:10.1089/ten.tea.2017.0136 (2017).

429 Panepinto, L. M. & Phillips, R. W. The Yucatan miniature pig: characterization and utilization in biomedical research. *Lab Anim Sci* **36**, 344-347 (1986).

430 Gutierrez, K., Dicks, N., Glanzner, W. G., Agellon, L. B. & Bordignon, V. Efficacy of the porcine species in biomedical research. *Frontiers in genetics* **6**, 293-293, doi:10.3389/fgene.2015.00293 (2015).

431 Pfeifer, C. G., Fisher, M. B., Saxena, V., Kim, M., Henning, E. A., Steinberg, D. A., Dodge, G. R. & Mauck, R. L. Age-Dependent Subchondral Bone Remodeling and Cartilage Repair in a Minipig Defect Model. *Tissue Eng Part C Methods* **23**, 745-753, doi:10.1089/ten.TEC.2017.0109 (2017).

432 Gotterbarm, T., Breusch, S. J., Schneider, U. & Jung, M. The minipig model for experimental chondral and osteochondral defect repair in tissue engineering: retrospective analysis of 180 defects. *Lab Anim* **42**, 71-82, doi:10.1258/la.2007.06029e (2008).

433 Vapniarsky, N., Aryaei, A., Arzi, B., Hatcher, D. C., Hu, J. C. & Athanasiou, K. A. The Yucatan Minipig Temporomandibular Joint Disc Structure-Function Relationships Support Its Suitability for Human Comparative Studies. *Tissue Eng Part C Methods* **23**, 700-709, doi:10.1089/ten.TEC.2017.0149 (2017).

434 Allen, K. D. & Athanasiou, K. A. Tissue engineering of the TMJ disc: a review. *Tissue Eng* **12**, 1183-1196 (2006).

435 Makris, E. A., MacBarb, R. F., Responte, D. J., Hu, J. C. & Athanasiou, K. A. A copper sulfate and hydroxylysine treatment regimen for enhancing collagen cross-linking and biomechanical properties in engineered neocartilage. *FASEB J* **27**, 2421-2430, doi:10.1096/fj.12-224030 (2013).

436 Evelia, S., Ashkan, A., Nikolaos, P., Eric, B., Heenam, K., Jerry, H. & Kyriacos, A. Shear stress induced by fluid flow produces improvements in tissue-engineered cartilage. *Biofabrication* (2020).

437 Mow, V. C., Kuei, S. C., Lai, W. M. & Armstrong, C. G. Biphasic creep and stress relaxation of articular cartilage in compression? Theory and experiments. *J Biomech Eng* **102**, 73-84, doi:10.1115/1.3138202 (1980).

438 Animal physiotherapy; assessment, treatment and rehabilitation of animals. *Scitech Book News* **31** (2007).

439 Miquelestorena-Standley, E., Jourdan, M. L., Collin, C., Bouvier, C., Larousserie, F., Aubert, S., Gomez-Brouchet, A., Guinebretière, J. M., Tallegas, M., Brulin, B., Le Nail, L. R., Tallet, A., Le Loarer, F., Massiere, J., Galant, C. & de Pinieux, G. Effect of decalcification protocols on immunohistochemistry and molecular analyses of bone samples. *Mod Pathol*, doi:10.1038/s41379-020-0503-6 (2020).

440 Sheikh, Z., Brooks, P. J., Barzilay, O., Fine, N. & Glogauer, M. Macrophages, Foreign Body Giant Cells and Their Response to Implantable Biomaterials. *Materials (Basel, Switzerland)* **8**, 5671-5701, doi:10.3390/ma8095269 (2015).

441 Duan, L., Ma, B., Liang, Y., Chen, J., Zhu, W., Li, M. & Wang, D. Cytokine networking of chondrocyte dedifferentiation in vitro and its implications for cell-based cartilage therapy. *American journal of translational research* **7**, 194-208 (2015).

442 Anderson, J. M., Rodriguez, A. & Chang, D. T. Foreign body reaction to biomaterials. *Semin Immunol* **20**, 86-100, doi:10.1016/j.smim.2007.11.004 (2008).

443 Raggatt, L. J. & Partridge, N. C. Cellular and molecular mechanisms of bone remodeling. *Journal of Biological Chemistry* **285**, 25103-25108 (2010).

444 Feng, X. & McDonald, J. M. Disorders of Bone Remodeling. *Annual Review of Pathology: Mechanisms of Disease* **6**, 121-145, doi:10.1146/annurev-pathol-011110-130203 (2011).

445 Jilka, R. L., Noble, B. & Weinstein, R. S. Osteocyte apoptosis. *Bone* **54**, 264-271, doi:10.1016/j.bone.2012.11.038 (2013).

446 Lackeyram, D., Yang, C., Archbold, T., Swanson, K. C. & Fan, M. Z. Early Weaning Reduces Small Intestinal Alkaline Phosphatase Expression in Pigs. *The Journal of Nutrition* **140**, 461-468, doi:10.3945/jn.109.117267 (2010).

447 Waterlow, J. C. Enzyme changes in malnutrition. *Journal of clinical pathology. Supplement (Association of Clinical Pathologists)* **4**, 75-79, doi:10.1136/jcp.s1-4.1.75 (1970).

448 Gibon, E., Córdova, L. A., Lu, L., Lin, T.-H., Yao, Z., Hamadouche, M. & Goodman, S. B. The biological response to orthopedic implants for joint replacement. II: Polyethylene, ceramics, PMMA, and the foreign body reaction. *Journal of biomedical materials research. Part B, Applied biomaterials* **105**, 1685-1691, doi:10.1002/jbm.b.33676 (2017).

APPENDIX 1 Characterization of facet joint cartilage properties in the human and interspecies comparisons

Abstract

The facet joint, a synovial joint located on the posterior-lateral spine, is highly susceptible to degenerative changes and plays a significant role in back-related morbidities. Despite its significance, the facet is rarely studied, and thus current treatment strategies are lacking. This study aimed to characterize, for the first time, the properties of human, pig, monkey, and rabbit lumbar facet cartilage providing much-needed design criteria for tissue engineering approaches. In this study, where possible, the facet's morphological, histological, mechanical, and biochemical properties were evaluated. Comparisons between the properties of the inferior and superior facet surfaces, as well as among spinal levels were performed within each species. In addition, interspecies comparisons of the properties were determined. The human facet joint was found to be degenerated; 100% of joint surfaces showed signs of pathology and approximately 71% of these were considered to be grade 4. Joint morphology varied among species, demonstrating that despite the mini-pig facet being closest to the human in terms of width and length, it was far more curved than the human or any of the other species. No notable differences were found in the mini-pig, monkey, and rabbit mechanical and biochemical properties, suggesting that these species, despite morphological differences, may serve as suitable animal models for studying structure-function relationships of the human facet joint. The characterization data reported in this study may increase our understanding of this ill-described joint as well as provide the foundation for the development of new treatments such as tissue engineering.

Published as: O'Leary SA, Link JM, Klineberg EO, Hu JC, Athanasiou KA. Characterization of facet joint cartilage properties in the human and interspecies comparisons. Acta Biomaterialia, 54:367-376 (2017)

Statement of significance

This work provides the first comprehensive description of the properties of lumbar facet joint cartilage. Importantly, this work establishes that histological, biochemical, and mechanical properties are comparable between bipedal and quadrupedal animals, helping to guide future selection of appropriate animal models. This work also suggests that the human facet joint is highly susceptible to pathology. The mechanical properties of facet cartilage, found to be inferior to those of other synovial joints, provide a greater understanding of the joint's structure-function relationships as well as the potential etiology of facet joint pathology. Lastly, this work will serve as the foundation for the development of much needed facet joint treatments, especially those based on tissue engineering approaches.

Introduction

Zygapophyseal joints, frequently referred to as facet joints, are highly susceptible to the development of osteoarthritis (OA).[1] These diarthrodial joints, located on the posterior-lateral spine, work with the intervertebral disc to transmit loads experienced by the spine while facilitating appropriate motion of the vertebrae (Fig. A1-1A). Depending on the nature of the spinal movement, the facet joints have been reported to carry up to 25% of the total spine compressive loads.[2] To compensate for a loss in structural integrity of a pathological intervertebral disc, the proportion of load borne by the facet joints can more than double.[3] Loading and abnormal loading of these joints can lead to the development of osteoarthritis.

Facet OA is a universal finding in people over the age of 60 years old and affects approximately 60% of adults over the age of 30 years old.[1] Typical radiographic features of OA include joint space narrowing due to cartilage thinning, development of osteophytes and subchondral cysts, hypertrophy of the articular process, and subchondral bone sclerosis.[4] In a CT scan study of an older population (mean age 67 years old), the prevalence of moderate and severe lumbar facet joint OA was found to be approximately 86% and 50%, respectively.[5]

Degeneration is most commonly found at the lower levels of the lumbar spine, i.e., L4-L5 and L5S1; however, all spinal levels are susceptible.[1,6–10]

Degeneration of the facet joint is known to play a significant role in back-related morbidities.[11] Advanced degeneration and concomitant hypertrophy of the facet joint can reduce the spinal canal size and impinge spinal neural elements, causing degenerative spinal stenosis. Spinal stenosis is the most frequently cited reason for lumbar spine surgery in the United States.[12,13] A similar trend is emerging in some European countries.[14,15] Facet joint pathology can also contribute to degenerative spondylolisthesis, where one vertebra translates with respect to the other. This condition occurs in 13.6% of the adult population[16] and contributes to both back pain and leg pain as the spinal cord or nerve roots are squeezed. In short, the facet joint is a significant source of back-related pathology.

In addition to its role in the aforementioned back-related morbidities, the facet joint is also thought to be the locus of low back pain on its own.[17] Similar to other synovial joints, the way by which pain manifests itself within the joint's structure is not well understood. However, the development of OA of this highly innervated joint has long been implicated as a potential cause of pain.[5] Despite the difficulties associated with diagnosis, the facet joints are estimated to be responsible for approximately 38% of chronic pain felt in the lower back.[18] Low back pain is currently the number one contributor to global disability[19] and is estimated to affect approximately 40% of people in their lifetime.[20] Although the prevalence of low back pain is highest between the ages of 40 and 80 years old,[20] young athletes have 3 to 5 times higher prevalence rates when compared to a general age-related population.[21] The debilitating nature of this disease has a huge impact on both the nation's health and health care system, at a total cost of approximately $200 billion per year.[22,23] Unfortunately, according to the latest global burden of disease report, the scale of the problem remains unchanged from 1990 to 2013. Furthermore, due to an aging population, low back pain has been predicted to increase in the coming years.[19]

Due to the almost avascular and acellular nature of facet cartilage, it is unable to repair itself; pain alleviation is heavily dependent on medical treatment. Currently available, non-invasive treatment options only offer short-term relief. Treatments such as radiofrequency denervation, medial branch blocks, and intraarticular injections may reduce the symptoms temporarily but cannot provide a long-term solution to the problem.[24] In cases of degenerative spinal stenosis and spondylolisthesis, surgical removal of the joints is often the only option. Removal of the facet joints can result in spinal instability necessitating fusion of the entire spinal segment. Like a domino effect, spinal fusion, in turn, is related to adjacent segment disease that encompasses a host of symptoms including hypertrophic facet arthritis in the neighboring vertebral segments.[25] Without suitable therapeutics, tissue engineering of the facet cartilage may serve as an attractive solution for long term motion-preserving pain management.

To date, there has only been one attempt to tissue engineer facet cartilage.[26] The paucity of work may primarily be due to the lack of published data detailing the characteristics of this tissue. In order to successfully engineer facet cartilage, it is critical that appropriate design criteria are established, which will ultimately provide the framework for the regeneration of a functional tissue replacement. Currently, there exist no experimental studies that characterize the biomechanical, biochemical, and histological properties of human cartilage, and only a few detailing the characteristics of animal facet cartilage.[27,28] With regard to the latter, the spines of quadrupeds receive different loading patterns when compared to bipeds, furthering the necessity for comparing the facet joints of humans and animals to develop suitable nonprimate animal models.

Toward the long-term objective of tissue engineering facet cartilage replacements, the objectives of this study are 1) to characterize human lumbar facet cartilage and to compare it to mini-pig, monkey, and rabbit lumbar facet cartilage, using morphological, histological, biochemical, and biomechanical methods where appropriate, and 2) to compare properties according to anatomical location (i.e., spinal level and surface type) within and across species.

The lumbar region of the spine was selected to study as it is associated with a high degree of pathology and is a popular target of therapeutics aimed to alleviate low back pain.

Materials and methods

Specimens

Human spines (n = 7, 4 female and 3 male) were obtained from Science Care and MedCure (see Table A1-1 for details). None of the human specimens were noted to have any known musculoskeletal pathology. Animal facet joints were harvested from the spines of Yucatan mini-pigs (n = 6, all aged approximately 18 months old and male), New Zealand White rabbits (n = 5, all aged 6–8 months old and male) and Rhesus Macaque monkeys (n = 3, aged 1 (male), 6 (male), and 12 (female) years old). All animals used for this study were euthanized as part of other research studies unrelated to the musculoskeletal system. Furthermore, all cadaveric and animal facet tissues were harvested for use in this study only and were not subjected to any testing other than what is outlined in this study. Spines were isolated within 24 h of death and were frozen at 20 C. Lumbar facet joints were accessed proximally; all muscle and soft tissue was removed from the spine, and the intervertebral disc and the facet capsule were carefully severed using a scalpel allowing the facet joints to be easily disarticulated. The facet surfaces along with the underlying bone were removed from the lumbar spine using an oscillating saw. Joints were washed with phosphate buffered saline (PBS), photographed, and wrapped in gauze soaked in PBS containing protease inhibitor (10 mM Nethylmaleimide and 1 mM phenylmethylsulfonyl fluoride, Sigma) and frozen at 20 C until further analysis. The length and width of each joint surface for all examined spines were measured photographically as illustrated in Fig. A1-1B and C. The percentage depth[29] was also calculated for the facet joints of one representative spine for each species by making a cross-sectional cut in the joint and taking measurements according to Fig. A1-1C. The human facet surfaces were also graded by a spine surgeon according to the International Cartilage Repair Society (ICRS) scale (Appendix A: Supplementary data 1).[30] The average

severity index was calculated for each human facet joint surface by averaging the value of the assigned grade (0 to 4) among examined spines. Mechanical testing and biochemical analyses were performed on facet joints harvested from the right and left sides of each spine, respectively. The number of facet surfaces and spinal levels examined, as well as the characterization methods they were subjected to, are found in Table A1-2.

Histology

Samples were fixed in 10% neutral-buffered formalin for 4 to 5 days, rinsed thoroughly in water, and decalcified using 10% formic acid. Samples were embedded in paraffin and sectioned at 6 μm. Sections were stained with hematoxylin and eosin (H&E), Safranin-O, and picrosirius red as previously described.[31]

Biochemistry

Facet cartilage sections were removed from the facet joints using a scalpel and weighed (wet weight). Tissues were frozen at 20 C for 24 h, lyophilized for 48 h, and the dry weight was measured. Tissues were digested in 125 mg/ml papain (Sigma Aldrich) in a phosphate buffer (2 mM N-acetyl cysteine (Sigma Aldrich) and 2 mM EDTA) for 18 h at 60 C. Following digestion, DNA and GAG content were measured using PicoGreen Cell Proliferation Assay kit (Life Technologies) and Blyscan Glycosaminoglycan Assay kit (Biocolor), respectively. Total collagen was determined using a chloramine-T hydroxyproline assay and Sircol collagen standard (Biocolor), following hydrolysis with 2 N NaOH for 20 min at 110 C.

Creep indentation testing

Facet joints were tested under compression creep indentation testing as previously described.[32] All cartilage samples were tested on the bone, and the thickness of the cartilage at the site of testing was determined using a thickness probe.[33] The central region of the articular surface was tested, or, for the mini-pig samples where the surface was curved, the flattest region of the tissue was selected for testing. Care was taken to ensure the same regions on opposing surfaces were

tested for all joint surface pairs. Samples were submerged in PBS for at least 15 min prior to testing. A 0.5 mm indenter tip was used with a tare load of 0.075 g and a test load of 0.25 g to achieve strains in the range of 2–12%. Following testing, a semi-analytical, semi-numerical, linear biphasic model was used to approximate the aggregate modulus, shear modulus, and permeability.

Statistical analysis

Student t-tests were performed to compare the biomechanical and biochemical properties between the inferior and superior facet joint surfaces, for all spinal levels of the mini-pig, monkey, and rabbit spines. One-way ANOVA with Tukey's post hoc test were used to assess biomechanical and biochemical differences among spinal levels and in the case of biomechanical properties across species (mini-pig, monkey, and rabbit). Student t-tests were performed to assess differences between the biochemical properties of the mini-pig and rabbit. Regarding the physical dimensions of the facet surfaces, one-way ANOVA followed by Tukey's post hoc test were used to compare the dimensions of the inferior facet joint at each spinal level and also the superior facet joints at each spinal level for each species (human, mini-pig, rabbit, and monkey). Student t-tests were used to compare average dimensions of the inferior facet versus the superior facet for each species and one-way ANOVA followed by Tukey's post hoc test were used to compare dimensions across species. For all statistical tests, a p value of less than 0.05 indicated statistical significance. In figures displaying quantitative results, groups marked by different letters are statistically different. All data are presented as means ± standard deviations.

Results

Gross morphology

Grading of the human facet cartilage morphology revealed that of the 154 joints examined, all (100%) showed evidence of degradation. A representative image of each human facet joint grade

is illustrated in Fig. A1-2A and several more example images can be seen in Appendix A: Supplementary data 2. In the most severe cases, the facet cartilage had completely degraded leaving the entire underlying bone surface exposed. Other observations included the replacement of cartilage with fibrous like tissue. In general, the cartilage surface morphology was a yellow or reddish color, showing varying degrees of fibrillation, fissuring, flaking, and surface erosion that tended to span the entire surface of the joint.

All joints examined demonstrated varying degrees of degeneration and according to the ICRS scale, 72.1%, 22.7%, 3.2%, 1.9%, and 0% were considered to be grade 4, grade 3, grade 2, grade 1, and grade 0, respectively (Fig. A1-2B). With the exception of a single joint surface, five out of the seven examined cadavers (ages 52, 71, 75, 77, 80 years old) had facet joint surfaces graded 3 or above. The youngest cadaver (age 41 years old) had the most amount of facet joint surfaces graded 2 or below (total of 4 surfaces), followed by the 66-year-old cadaver that had a total of 3 joint surfaces graded 2 or below. Comparing the severity of degradation between the inferior and superior joint surfaces (Fig. A1-2C) showed that in general, the superior facet joint surfaces received a higher average score than the inferior facet joint surfaces. In addition, although all levels of the spine were affected by degeneration, the superior joint surfaces located at spinal levels L4 and L5 were found to have the highest frequency of grade 4 joints.

The gross morphology and average physical dimensions of the facet joints harvested from each species are represented in Fig. A1-1B and Fig. A1-3, respectively. In general, the inferior surface was found to have a more convex shape whereas the superior surface was more concave. The average length and width of the human, mini-pig, monkey, and rabbit inferior facet joints were 16.32 ± 1.95 mm and 13.91 ± 1.42 mm, 10.14 ± 2.15 mm and 7.98 ± 0.91 mm, 5.58 ± 0.70 mm and 5.43 ± 0.41 mm, and 4.75 ± 0.48 mm and 4.26 ± 0.45 mm, respectively. In terms of the superior facet dimensions, the average length and width of the human, mini-pig, monkey, and rabbit joints was 13.07 ± 1.78 mm and 16.52 ± 2.74 mm, 9.33 ± 1.34 mm and 9.63 ± 1.21 mm, 5.27 ± 0.71 mm and 5.27 ± 0.50 mm, and 3.37 ± 0.36 mm and 4.87 ± 0.52 mm. The inferior

surfaces of the rabbit and the human were found to be significantly longer than the superior surfaces. Also, the superior facet joint was significantly wider in the minipig and rabbit, when compared to the inferior facet joint. The human facet joint average length and width for both the inferior and superior surface were significantly greater than any other species. Although the average mini-pig's facet dimensions were significantly smaller than the human, they were significantly larger than the monkey and rabbit, whose dimensions were similar.

Examining the differences in the joint's dimensions at each spinal level shows that the human facet tended to increase in both width and length for both the inferior and superior facet surfaces in the lower lumbar levels (Appendix A: Supplementary data 3). Also, the mini-pig had significantly longer inferior surface at spinal level S1 than the other spinal levels and the superior surface at spinal level S1 was also longer than the superior surfaces at spinal levels L2, L4, L5, and L6. In addition, the width of the mini-pig's superior surface at spinal level S1 was significantly wider than the superior surfaces at spinal levels L1 to L4. In general, the length and width of the inferior and superior surfaces from spinal level to spinal level were not found to change significantly for the monkey and rabbit.

The average percentage depth measured for the inferior and superior surfaces of the human, mini-pig, monkey, and rabbit was 15.86 ± 2.54% and 12.89 ± 2.10%, 56.74 ± 9.65% and 72.25 ± 11.50%, 10.00 ± 3.48% and 8.46 ± 1.49%, and 14.02 ± 3.58% and 8.71 ± 3.69%, respectively (Fig. A1-3C). The inferior surface was found to be significantly more curved than the superior surface for the rabbit and the reverse was found to be true for the mini-pig.

Histology

A histological representation of the deleterious effects of OA of human facet cartilage is depicted in Fig. A1-4A. H&E staining of OA changes through grades 1, 2, 3, and 4 highlighted the complete disruption to the cartilage structure. Specifically, in grade 1, despite some minor fibrillation, the surface was largely intact, and the middle and deep zones of the tissue were well preserved. In

grade 2, greater surface discontinuity and disruption of the structure was observed that was propagated to the middle zone of the tissue. In grade 3, the presence of multiple vertical fissures that almost stretched to the deep zone of the tissue as well as severe surface erosion and loss of cartilage was apparent. Finally, in grade 4, complete denudation of unmineralized cartilage was observed leaving only calcified cartilage and/or bone present. In addition, cellular arrangement and density appear relatively normal in grade 1; however, a rapid decline in both of these metrics was observed as the disease progressed. Similarly, the rapid loss in sulfated GAG was demonstrated as the joint becomes more diseased, represented by the decrease in positive Safranin-O staining from grade 1 through to grade 4.

The results of staining of the mini-pig, monkey, and rabbit facet cartilage with H&E, Safranin-O, and picrosirius red are illustrated in Fig. A1-4B. H&E staining across all animals revealed cells that were smaller and flatter in the superficial region when compared to the intermediate and deep zones of the tissue where cells were observed to be more round and organized in a columnar fashion. All animals had positive Safranin-O staining for sulfated GAGs, and it appeared more intense in the middle and deep zones in comparison to the superficial zone and also highlighted a GAG-rich territorial and interterritorial matrix. A similar staining pattern and intensity was observed for the staining of collagen with picrosirius red across all animals.

Biochemistry

The GAG, collagen, and DNA content, all normalized to wet weight, were compared between the ICRS grades for each human facet joint surface (Table A1-3). Considering the uneven group numbers, statistical comparisons were not deemed appropriate. A similar pattern for both GAG and collagen content was observed across grades. Both properties decreased between grade 1 and 2, partially recovered between grade 2 and 3, and were finally observed to decline again between grade 3 and grade 4. The DNA content was observed to decrease between grade 1 and

2, however it steadily increased between grades 2, 3, and 4 and was considered the highest for grade 4.

In general, Student t-tests comparing the GAG, collagen, and DNA content, all normalized to wet weight, between opposing joint surfaces of the mini-pig and rabbit found that they were not significantly different (Appendix A: Supplementary data 4). The GAG/ww, collagen/ww, and DNA/ww content in the mini-pig and rabbit were not statistically different between spinal levels (Fig. A1-5). However, when the GAG content was averaged across all spinal levels, the overall GAG/ww was found to be higher in the mini-pig than in the rabbit (4.2 ± 0.4% versus 2.4 ± 0.4%). The average measured values of collagen/ww across all spinal levels were 15.77 ± 1.0% and 16.62 ± 1.2% for the mini-pig and rabbit, respectively and these values were not found to be statistically different. The averaged DNA content across spinal levels for each species was found to be higher in the rabbit than in the mini-pig (0.034 ± 0.003% versus 0.030 ± 0.003%).

Mechanical testing

In general, Student t-test's comparing the thickness, shear modulus, aggregate modulus, and permeability between opposing inferior and superior joint surfaces of the mini-pig, monkey, and rabbit found that they were not significantly different (Appendix A: Supplementary data 4). Furthermore, the average measured thickness, shear modulus, aggregate modulus, and permeability between spinal levels were not found to significantly different within the same species (Fig. A1-6). When averaged across all spinal levels the average values for the thickness, shear modulus, aggregate modulus and permeability were 0.37 ± 0.02 mm, 71.49 ± 4.92 kPa, 174.49 ± 19.64 kPa, 4.87 ± 0.74 x 10^{-15} m^4/Ns, for the mini-pig, 0.35 ± 0.01 mm, 60.82 ± 14.76 kPa, 161.17 ± 37.41 kPa, 6.27 ± 2.71 x 10^{-15} m^4/Ns, for the monkey and 0.29 ± 0.01 mm, 54.95 ± 6.39 kPa, 158.95 ± 20.22 kPa, 5.95 ± 1.33 x 10^{-15} m^4/Ns, for the rabbit. The averaged thickness and shear modulus across all levels was found to be significantly lower in the rabbit cartilage compared to

the mini-pig cartilage (0.37 ± 0.02 mm versus 0.29 ± 0.01 mm and 71.49 ± 4.92 kPa versus 54.95 ± 6.39 kPa).

Discussion

Due to the dearth of information regarding the facet joint, as its first objective, this study sought to provide much-needed characterization data of human lumbar facet cartilage and compare to various species. Toward the second objective, facet joint properties were compared with respect to spinal level and joint surface (i.e., inferior versus superior) within and across species. Guided by prior literature in other joints, it was hypothesized that the characterization data would reveal differences between a) the opposing inferior and superior facet joint surfaces and b) joints of differing spinal levels. It was also hypothesized that these trends would persist across all examined species, although differing magnitudes were expected, some more similar than others to properties obtained for the human facet cartilage. Contrary to the hypothesis, results showed that biochemical and biomechanical properties were similar among spinal levels and between the inferior and superior facet joint surfaces. This finding was consistent among species; however, an unexpected high percentage of pathology was found in the human facet joints precluding in depth characterization and comparison to other animal models. Of the 154 human facet joints surfaces analyzed, 146 displayed cartilage degeneration corresponding to ICRS grades 3 or 4. This significant finding thus allowed us to provide characterization of human facet cartilage pathology as a function of ICRS grade. This study provides data that may eventually improve our understanding of functional deterioration of the three-joint complex overall. This investigation also serves as the first source of comprehensive design criteria toward the design of a replacement facet joint and also offers insights into the selection of an appropriate animal model.

The prevalence and degree of degeneration in the human lumbar facet joint were staggeringly high. Advanced pathology was found in all but 8 of the examined joint surfaces. The finding of widespread pathology was consistent with previous findings where pathology was also

observed in the majority of facet surfaces.[34,35] Since these other studies employed their own scoring scale, the calculated severity index, denoted by averaging the scores assigned to a particular surface among examined spines (Fig. A1-2C), was different across this and other studies. For reference, the three scoring scales are presented in Appendix A: Supplementary data 1. Of the scores assigned to surfaces from spinal levels L1 to S1 in a previous study,[34] the lowest severity index was found at L1 inferior and L3 superior (both 2.45), and the highest was found at S1 (2.92). In addition, a similar study found that scoring of facet surfaces from spinal levels L1 to L5 revealed that the superior surface of L1 exhibited the lowest score (2.80), and that the superior and inferior surfaces of L5 exhibited the highest score (3.70).[35] In the current study, the lowest score was found for L4 inferior (3.36); and the highest score was found for L4 superior and L5 superior (3.93) (Fig. A1-2C). In summary, our study reported a similar prevalence in pathology, but a higher degree of severity compared to other studies.

Considering the evaluation of human facet joints here and in other studies, it is clear these joints are particularly prone to degeneration. However, establishing a relationship between the cause and effect is difficult without being able to compare pathological to healthy facet cartilage. In this and other studies, healthy facet cartilage was seldom seen. This may in part be due to the fact that the mean age of the patients examined in these studies were 66 (this study), 76,[34] and 88.[35] In this study, even a 41-year-old donor's facet joints were found to be heavily diseased. Furthermore, literature estimates that 60% of people over 30 years old show evidence of degeneration and facet OA has been reported to develop as young as 15 years old.[1,36] Ideally, to compare the facet joint properties of animals and humans, the samples should be age-matched, therefore, necessitating the use of a young, yet skeletally mature population. Future work needs to access a significant number of spines from multiple ages to ascertain the age at which significant degeneration develops in the facet joint.

In the human facet joints that were characterized, the GAG and collagen contents of relatively healthy cartilage (grade 1) are comparable to those of normal human articular cartilage

found elsewhere in the body (3–6% and 12–24% GAG and collagen contents, respectively). These biochemical components are also comparable to the facet cartilage of the rabbit and mini-pig reported here. The overall GAG and collagen content of facet cartilage decreased as a result of degeneration (Table A1-3). In comparison to the amount of GAG loss, the amount of collagen loss was less. Also, the apparent increase in these properties between grades 2 and 3 may be interpreted as the tissue's attempt at repair.[37,38] The cellularity of the cartilage was also observed to increase in the later stages of disease. Loss of GAG and collagen content, and an increase in cellularity are all consistent with the progression of OA in cartilages of other joints.[39] This work shows that human facet cartilage has similar biochemical properties to those of other species and other human synovial joints. It also demonstrates that human facet cartilage follows the well-characterized progression of OA, suggesting that therapies under development for other cartilages may also hold promise for the facet.

In general, the shape of the opposing inferior and superior facet joint surfaces differ with the superior surface tending to be concave and the inferior surface tending to be convex. The extent to which these surfaces are concave and convex differs greatly among species, with the mini-pig facet joint having a remarkably larger percentage depth (similar to a smaller radius of curvature) compared to the other species (Fig. A1-3). The radius of curvature has previously been linked to spinal kinematics and, specifically, to the spine's ability to rotate axially and to translate. It has been found that a smaller radius of curvature is associated with a reduced range of axial rotation.[29] The degree of axial rotation and flexion/extension has previously been measured in the porcine spine and found to be significantly less than in the human spine.[40] Thus, these data suggest that the mini-pig facet joint mostly allows for articulation in a constrained fashion. Data showing that curvatures among rabbit, monkey, and human are similar concur with the descriptions of similar ranges of axial rotation among these species.[41,42] It is known that the gait of the rabbit and the monkey are different to that of the human; the rabbit and monkey swing their hind legs forward under the torso and then propel them backwards into an extended position. This

may account for the small differences in the facet joint curvature observed between species. It should be noted that the degree of flexion and extension is higher for the rabbit than the human suggesting that perhaps facet radii of curvature are better correlated with rotation than flexion/extension. In terms of selecting an animal model, the dramatic differences between the mini-pig and the human facet joint should be considered. The shape of the facet, which is often intimately linked to joint biomechanics, is an important factor, and the data here suggest that the monkey or even the rabbit model may be most similar to human in terms of shape.

Interestingly, the mechanical and biochemical properties between opposing inferior and superior joint surfaces were not found be different for the animals examined. Dramatic differences in opposing articulating surfaces in other joints have been reported previously. In a study characterizing the bovine ankle joint, the tibial plafond exhibited 3-fold higher tensile properties and 2-fold higher compressive and shear moduli compared with its articulating talar dome.[43] This disparity was hypothesized as the reason for increased rates of pathology found in the talar dome compared to the tibial plafond. Within the human facet literature, there is conflict with regard to disposition of pathology, since some report a higher incidence of degeneration in the inferior facet surface[44] while others have concluded that the superior facet joint surface is more susceptible to pathology.[45] The biomechanical properties of human facet cartilage were not collected in this study due to the high incidences of pathology, and it remains unclear if disparities exist across the articulating surfaces of human facet joints. However, the absence of disparities in the animal data suggests that pathology should not be preferentially observed in either inferior or superior surfaces. Indeed, for human facet joints examined here, only a slight preference for the superior facet joint in terms of rate and severity of pathology could be found between joint surfaces. These findings may help explain why similar amounts of evidence currently exist for pathology of the inferior or superior surfaces.

The properties of canine intervertebral disc have been shown to differ according to the lumbar spinal level,[46] a pattern that was expected to be mirrored in the facet joint. However,

biochemical and biomechanical properties of the animal facet joints were not found to differ according to the spinal level. This finding is interesting considering the aforementioned changes in the disc properties as well as reported changes in the range of spinal motion according to spinal level that was observed for both humans and a wide variety of animals.[47] This suggests that different functional properties should be observed in accordance with the way the cartilage is loaded. Despite this, similar to the findings of our study, it was also reported elsewhere that there were no significant differences in biomechanical and biochemical properties between the canine facet joints at spinal levels L4 and L5.[48] Though the properties are similar across all spinal levels, the lower lumbar facet joints are usually the most problematic and the target of both therapeutic and surgical treatments. Taken together with the epidemiological literature, data collected here suggest that facet pathology is not likely due to inherent cartilage properties. Rather, it is likely the differences in loading experienced in these lower joints, or, perhaps, the high susceptibility of disc degradation at these spinal levels, that render the lower lumber facet joints targets of treatment.

The reported compressive stiffness of facet cartilage, though not different for the mini-pig, rabbit, and monkey, is substantially lower than in other joints within the same species. For example, the aggregate modulus values of the rabbit and monkey (cynomolgus) knee cartilage have been reported to be approximately 600 kPa and 700 kPa, respectively,[32] versus an average of approximately 159 and 161 kPa for the facet cartilage reported in this study. The compressive stiffness of the healthy human facet cartilage was not measured due to the presence of disease, however, given this trend in other species, it is likely that it, too, possesses a lower aggregate modulus than cartilage of the human knee joint, which has an aggregate modulus of approximately 607 kPa.[32] Taken together, the findings of this interspecies study suggest that the facet joint may not be subjected to high compressive loads in vivo compared to other joints of the body. This is consistent with literature reporting that the intervertebral disc is primarily responsible for supporting the compressive loads of the spine,[49] and, therefore, the facet joints may be

shielded from high compressive loads. This finding may help to further elucidate the role of the facet joint and its contribution to spinal biomechanics and also supports the idea that quadrupeds may be suitable animal models. The expectation is that the bipedal model would be the gold standard animal model for studying the facet joint; however, in terms of facet mechanical properties, the rabbit and minipig may also be suitable.

The design criteria for tissue engineering a facet joint replacement may be more easily attainable than other joints, such as the knee, considering the results of this study. The facet joint has a small surface area in comparison to other articular surfaces.[32] Therefore, it may be possible to tissue engineer the entire surface of the facet joint, which would avoid any of the well-known integration issues between the native and engineered cartilage. Furthermore, the facet cartilage is thinner than cartilage of other joints, and, therefore, a full thickness replacement would not be as challenging to engineer. Since both the compressive loads borne by facet joints and the compressive stiffness of facet cartilage are lower than other joints, a biomimetic cartilage replacement may be more readily achieved. The fact that the properties of facet cartilage are not different between the opposing joint surfaces or between the spinal levels is also advantageous since this negates the need to design site-specific replacements. For example, using a scaffoldless approach, self-assembled cartilage constructs have been formed with compressive aggregate modulus values ranging from 100–400 kPa,[43,50–52] shear modulus of 45–76 kPa,[43] and thickness between 260 and 950 μm.[52,53]. Furthermore, self-assembled neocartilage has biochemical properties akin to the facet joint, possessing 2–5% GAG/ww[43,52,54] and 15–20% collagen/ww.[52] Given that engineered cartilage already exhibits similar properties as native facet cartilage, engineering the entire facet joint may be a worthy aspiration in providing novel therapeutics to this oft-degenerated joint.

In conclusion, this study will serve as the first database of human and interspecies facet joint properties. The data reported here will help to further elucidate the role of the facet joint in spinal biomechanics as well as increase our general understanding of this ill-described joint. This

study also provides valuable information regarding the selection of an appropriate animal model. The methods reported here could be used to assess the potential of other large animal models such as sheep and goats. The universal finding of degeneration in examined human facet joints further underscores the importance of this joint and its potential contribution to back-related morbidities. Importantly, this work adds to the literature by providing morphological, histological, biomechanical, and biochemical data for bipedal and quadrupedal animals which will aid in future determinations of suitable animal models as well as new treatment modalities.

References

1 J.D. Eubanks, M.J. Lee, E. Cassinelli, N.U. Ahn, Prevalence of lumbar facet arthrosis and its relationship to age, sex, and race: an anatomic study of cadaveric specimens, Spine (Phila Pa 1976) 32 (19) (2007) 2058–2062.

2 K.H. Yang, A.I. King, Mechanism of facet load transmission as a hypothesis for low-back pain, Spine 9 (6) (1984) 557–565.

3 A. Rohlmann, T. Zander, H. Schmidt, H.-J. Wilke, G. Bergmann, Analysis of the influence of disc degeneration on the mechanical behavior of a lumbar motion segment using the finite element method, J. Biomech. 39 (13) (2006) 2484–2490.

4 L. Kalichman, D.H. Kim, L. Li, A. Guermazi, D.J. Hunter, Computed tomography–evaluated features of spinal degeneration: prevalence, intercorrelation, and association with self-reported low back pain, Spine J. 10 (3) (2010) 200–208.

5 P. Suri, D.J. Hunter, J. Rainville, A. Guermazi, J.N. Katz, Presence and extent of severe facet joint osteoarthritis are associated with back pain in older adults, Osteoarthritis Cartilage 21 (9) (2013) 1199–1206.

6 S. Ko, A.R. Vaccaro, S. Lee, J. Lee, H. Chang, The prevalence of lumbar spine facet joint osteoarthritis and its association with low back pain in selected Korean populations, Clin. Orthop. Surg. 6 (4) (2014) 385–391.

7 L. Kalichman, L. Li, D. Kim, A. Guermazi, V. Berkin, C.J. O'Donnell, U. Hoffmann, R. Cole, D.J. Hunter, Facet joint osteoarthritis and low back pain in the community-based population, Spine 33 (23) (2008) 2560.

8 A. Fujiwara, K. Tamai, M. Yamato, H.S. An, H. Yoshida, K. Saotome, A. Kurihashi, The relationship between facet joint osteoarthritis and disc degeneration of the lumbar spine: an MRI study, Eur. Spine J. 8 (5) (1999) 396–401.

9 A. Maataoui, T.J. Vogl, M. Middendorp, K. Kafchitsas, M.F. Khan, Association between facet joint osteoarthritis and the Oswestry Disability Index, World J. Radiol. 6 (11) (2014) 881–885.

10 D. Butler, J.H. Trafimow, G.B. Andersson, T.W. McNeill, M.S. Huckman, Discs degenerate before facets, Spine (Phila Pa 1976) 15 (2) (1990) 111–113.

11 A.C. Gellhorn, J.N. Katz, P. Suri, Osteoarthritis of the spine: the facet joints, Nat. Rev. Rheumatol. 9 (4) (2013) 216–224.

12 M.A. Ciol, R.A. Deyo, E. Howell, S. Kreif, An assessment of surgery for spinal stenosis: time trends, geographic variations, complications, and reoperations, J. Am. Geriatr. Soc. 44 (3) (1996) 285–290.

13 J.N. Weinstein, J.D. Lurie, P. Olson, K.K. Bronner, E.S. Fisher, M.T.S. Morgan, United States trends and regional variations in lumbar spine surgery: 1992– 2003, Spine 31 (23) (2006) 2707.

14 K.A. Jansson, P. Blomqvist, F. Granath, G. Nemeth, Spinal stenosis surgery in Sweden 1987–1999, Eur. Spine J. 12 (5) (2003) 535–541.

15 M. Du Bois, M. Szpalski, P. Donceel, A decade's experience in lumbar spine surgery in Belgium: sickness fund beneficiaries, 2000–2009, Eur. Spine J. 21 (12) (2012) 2693–2703.

16 L. Kalichman, D.H. Kim, L. Li, A. Guermazi, V. Berkin, D.J. Hunter, Spondylolysis and spondylolisthesis: prevalence and association with low back pain in the adult community-based population, Spine (Phila Pa 1976) 34 (2) (2009) 199– 205.

17 S. Klessinger, Facet Joint Pain: Presentation and Treatment, Is It a Myth?, Springer, Advanced Concepts in Lumbar Degenerative Disk Disease, 2016, pp 219–248.

18 M.V. Boswell, L. Manchikanti, A.D. Kaye, S. Bakshi, C.G. Gharibo, S. Gupta, S.S. Jha, D.E. Nampiaparampil, T.T. Simopoulos, J.A. Hirsch, A best-evidence systematic appraisal of the diagnostic accuracy and utility of facet (zygapophysial) joint injections in chronic spinal pain, Pain Physician 18 (4) (2015) E497–533.

19 T. Vos, R.M. Barber, B. Bell, A. Bertozzi-Villa, S. Biryukov, I. Bolliger, F. Charlson, A. Davis, L. Degenhardt, D. Dicker, et al., Global, regional, and national incidence, prevalence, and years lived with disability for 301 acute and chronic diseases and injuries in 188 countries, 1990–2013: a systematic analysis for the Global Burden of Disease Study 2013, The Lancet 386 (9995) (2015) 743– 800.

20 D. Hoy, C. Bain, G. Williams, L. March, P. Brooks, F. Blyth, A. Woolf, T. Vos, R. Buchbinder, A systematic review of the global prevalence of low back pain, Arthritis Rheum. 64 (6) (2012) 2028–2037.

21 J. van Hilst, N.F. Hilgersom, M.C. Kuilman, F.M.K. PP, M.H. Frings-Dresen, Low back pain in young elite field hockey players, football players and speed skaters: prevalence and risk factors, J. Back Musculoskelet Rehabil. 28 (1) (2015) 67–73.

22 V.Y. Ma, L. Chan, K.J. Carruthers, Incidence, prevalence, costs, and impact on disability of common conditions requiring rehabilitation in the united states: stroke, spinal cord

injury, traumatic brain injury, multiple sclerosis, osteoarthritis, rheumatoid arthritis, limb loss, and back pain, Arch. Phys. Med. Rehabil. 95 (5) (2014) 986–995. e1.

23 J.N. Katz, Lumbar Disc Disorders and Low-Back Pain: Socioeconomic Factors and Consequences, 2006.

24 S.P. Cohen, J.H. Huang, C. Brummett, Facet joint pain–advances in patient selection and treatment, Nat. Rev. Rheumatol. 9 (2) (2013) 101–116.

25 J.Y. Yang, J.-K. Lee, H.-S. Song, The impact of adjacent segment degeneration on the clinical outcome after lumbar spinal fusion, Spine 33 (5) (2008) 503–507.

26 B.D. Elder, D.H. Kim, K.A. Athanasiou, Developing an articular cartilage decellularization process toward facet joint cartilage replacement, Neurosurgery 66 (4) (2010) 722–727. discussion 727.

27 B. Elder, Biomechanical, biochemical, and histological characterization of canine lumbar facet joint cartilage, J. Neurosurg. 10 (6) (2009) 623–628.

28 M.J. Abd Latif, Z. Jin, R.K. Wilcox, Biomechanical characterisation of ovine spinal facet joint cartilage, J. Biomech. 45 (8) (2012) 1346–1352.

29 N.A. Duncan, A.M. Ahmed, The role of axial rotation in the etiology of unilateral disc prolapse. An experimental and finite-element analysis, Spine (Phila Pa 1976) 16 (9) (1991) 1089–1098.

30 International Cartilage Repair Society. The ICRS Clinical Cartilage Injury Evaluation System-2000, 2000. http://cartilage.org/society/publications/icrsscore/. (Accessed December 20th, 2016).

31 W.E. Brown, J.C. Hu, K.A. Athanasiou, Ammonium–chloride–potassium lysing buffer treatment of fully differentiated cells increases cell purity and resulting neotissue functional properties, Tissue Eng. Part C 22 (9) (2016) 895–903.

32 K.A. Athanasiou, M. Rosenwasser, J. Buckwalter, T. Malinin, V. Mow, Interspecies comparisons of in situ intrinsic mechanical properties of distal femoral cartilage, J. Orthop. Res. 9 (3) (1991) 330–340.

33 K.A. Athanasiou, A. Agarwal, A. Muffoletto, F.J. Dzida, G. Constantinides, M. Clem, Biomechanical properties of hip cartilage in experimental animal models, Clin. Orthop. Relat. Res. 316 (1995) 254–266.

34 I. Tanno, G. Murakami, H. Oguma, S. Sato, U.Y. Lee, S.H. Han, T. Yamashita, Morphometry of the lumbar zygapophyseal facet capsule and cartilage with special reference to degenerative osteoarthritic changes: an anatomical study using fresh cadavers of elderly Japanese and Korean subjects, J. Orthop. Sci. 9 (5) (2004) 468–477.

35 T. Tischer, T. Aktas, S. Milz, R.V. Putz, Detailed pathological changes of human lumbar facet joints L1–L5 in elderly individuals, Eur. Spine J. 15 (3) (2006) 308–315.

36 J. Li, C. Muehleman, Y. Abe, K. Masuda, Prevalence of facet joint degeneration in association with intervertebral joint degeneration in a sample of organ donors, J. Orthop. Res. 29 (8) (2011) 1267–1274.

37 E. Vignon, M. Arlot, D. Hartmann, B. Moyen, G. Ville, Hypertrophic repair of articular cartilage in experimental osteoarthrosis, Ann. Rheum. Dis. 42 (1) (1983) 82–88.

38 S. Hosseininia, L.R. Lindberg, L.E. Dahlberg, Cartilage collagen damage in hip osteoarthritis similar to that seen in knee osteoarthritis; a case–control study of relationship between collagen, glycosaminoglycan and cartilage swelling, BMC Musculoskelet. Disord. 14 (1) (2013) 1.

39 K.P.H. Pritzker, S. Gay, S.A. Jimenez, K. Ostergaard, J.P. Pelletier, P.A. Revell, D. Salter, W.B. van den Berg, Osteoarthritis cartilage histopathology: grading and staging, Osteoarthritis Cartilage 14 (1) (2006) 13–29.

40 H.-J. Wilke, J. Geppert, A. Kienle, Biomechanical in vitro evaluation of the complete porcine spine in comparison with data of the human spine, Eur. Spine J. 20 (11) (2011) 1859–1868.

41 J.N. Grauer, J.S. Erulkar, T.C. Patel, M.M. Panjabi, Biomechanical evaluation of the New Zealand white rabbit lumbar spine: a physiologic characterization, Eur. Spine J. 9 (3) (2000) 250–255.

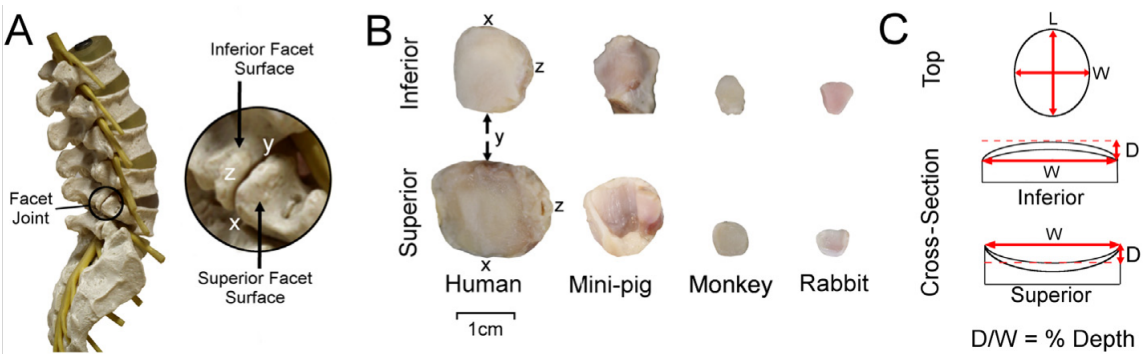

Figure A1-1. Illustration of the facet joint anatomy and the gross morphological measurements of the facet joint surface. A) Location of the facet joint on the lumbar spine. Symbols x, y, and z denote the orientation of the facet joint in situ; this corresponds to the orientation of the joint once it is excised, as illustrated in (B). B) Example scaled images of the opposing inferior and superior facet joint surfaces excised between spinal levels L4 and L5 from the four species examined. C) Top view of the facet joint surface. The left to right and top to bottom arrows denote where the measurements of the width (W) and length (L) were taken for all joint surfaces, respectively. Measurements were taken at the widest and longest regions of the tissue. A cross-sectional view shows the arrows that correspond to the regions from which the W was measured for both the convex inferior and concave superior facet surfaces. A dashed line was constructed such that it ran parallel to the arrow denoting W and also through the lowest or highest point on the facet articular surface. The depth (D) is the perpendicular distance between the dashed line and the arrow. The percentage depth was calculated by normalizing D to WTable A1-1. Patient details of human lumbar spine samples.

Spine	Age	Gender	BMI*
1	52	Female	14.5
2	71	Male	14.4
3	75	Female	48.2
4	77	Female	26.2
5	66	Male	29.3
6	80	Female	26.6
7	41	Male	20.7

* BMI was measured at the time of death and therefore may not be representative of patient's true BMI.

Table A1-2. Interspecies sample numbers and methods used to characterize the facet cartilage.

Species	No.	Spinal levels	Joint surfaces	Morphological measurements	Compression indentation testing	Biochemical analysis	Histological analysis
Human	7	5 (L1-S1)	77	Yes	No**	Yes	Yes
Mini-pig	6	6 (L1-S1)	78	Yes	Yes	Yes	Yes
Monkey	3	5 (L1-L5)*	30	Yes	Yes	No***	Yes
Rabbit	5	8 (L1-S1)	85	Yes	Yes	Yes	Yes

Joints at level L5/S1 were not examined for the monkey due to restricted access to spinal material. **

Human facet cartilage was pathological thus, compression indentation testing could not be performed on this tissue. ***

The Rhesus Macaque is a well-known carrier of herpes B virus. Biochemical analysis was not performed on this cartilage due to the increase in associated handling and subsequent increase in risk to the user.

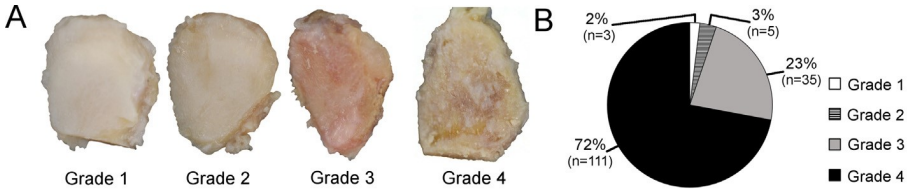

C

Frequency												
Surface	L1-S	L1-I	L2-S	L2-I	L3-S	L3-I	L4-S	L4-I	L5-S	L5-I	S1	Total
Grade 0	0	0	0	0	0	0	0	0	0	0	0	0
Grade 1	1	0	0	0	0	1	0	1	0	0	0	3
Grade 2	0	1	0	2	0	0	0	0	0	2	0	5
Grade 3	4	5	2	4	3	2	1	6	1	3	4	35
Grade 4	9	8	12	8	11	11	13	7	13	9	10	111
Severity Index												
	3.50 ±0.85	3.50 ±0.65	3.86 ±0.36	3.43 ±0.76	3.79 ±0.43	3.64 ±0.84	3.93 ±0.27	3.36 ±0.84	3.93 ±0.27	3.5 ±0.76	3.7 ±0.47	

Figure A1-2. Human facet joint pathology grading. A) Example images of facet cartilage grades 1, 2, 3, and 4. B) Pie chart representing the distribution of grades in the examined population. C) Table describing the frequency of occurrence of grades 1 – 4 for each superior (S) and inferior (I) facet surface at each spinal level. The severity index (please see text for definition) calculated for the facet surfaces at each spinal level demonstrates that human facet cartilage is severely degenerated.

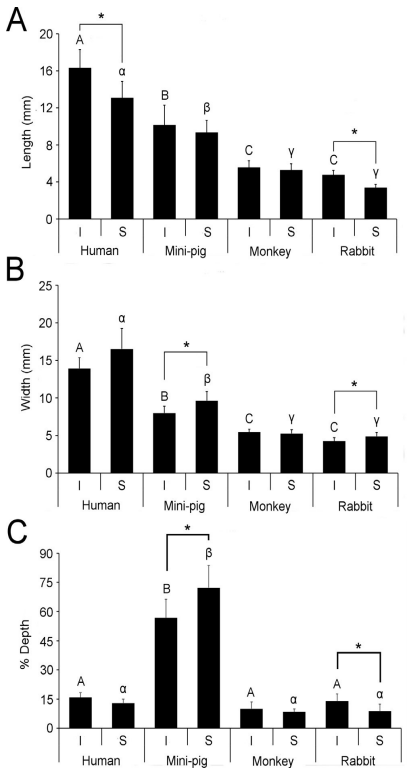

Figure A1-3. Interspecies comparison of the average A) length B) width and C) percentage depth of the inferior (I) and superior (S) facet surfaces. The human facet joint is longer and wider than the other species examined and the mini-pig has a more curved facet surface compared to other species which were relatively flat. Differences between I and S in terms of the average length, width, and percentage depth within species were analyzed using a Student t-test and groups connected by an asterisk are significantly different. An interspecies comparison of the average dimensions of I and S facet surfaces was assessed using a one-way ANOVA, followed by a Tukey's post hoc test, and groups not connected by the same letter or symbol are significantly different. To note, the average values for the percentage depth are based on the joints from one spine however, the average length and width are representative of 7 humans, 6 mini-pig, 3 monkey, and 5 rabbit spines.

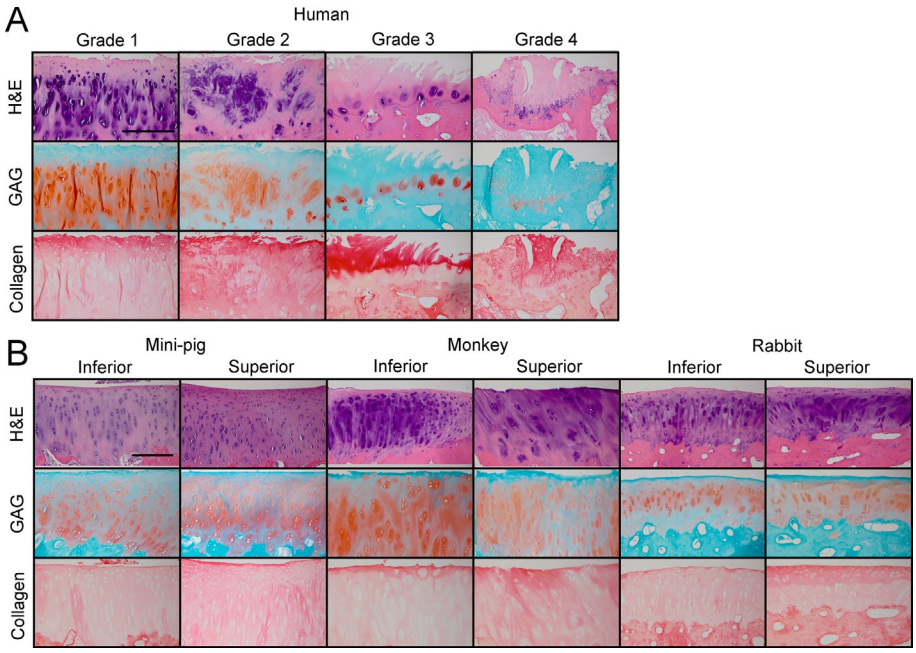

Figure A1-4. Facet joint histology. Hematoxylin and eosin (H&E), Safranin-O, and picrosirius red stain were used to highlight the structure, GAG, and collagen content of the facet cartilage, respectively. A) An interspecies comparison of the inferior and superior facet joint surfaces revealed that the structure is rich in GAG and collagen and has an architecture characteristic of articular cartilage. Scale bar = 500 µm. B) Histological staining of pathological human facet joint illustrated the gradual breakdown in structure and loss of GAG and collagen as the disease progressed. Scale bar = 200 µm. (For interpretation of the references to color in this figure legend, the reader is referred to the web version of this article.)

Table A1-3. Biochemical properties of human facet cartilage as a function of degeneration severity.

Grade	1	2	3	4
Number of samples	n = 3	n = 5	n = 22	n = 75
GAG/ww (%)	2.6 ± 1.4	1.2 ± 0.3	1.4 ± 0.7	1.1 ± 0.7
Collagen/ww (%)	21.6 ± 6.4	14.5 ± 2.4	16.0 ± 2.6	15.6 ± 2.6
DNA/ww (%)	0.07 ± 0.03	0.05 ± 0.02	0.11 ± 0.06	0.12 ± 0.10

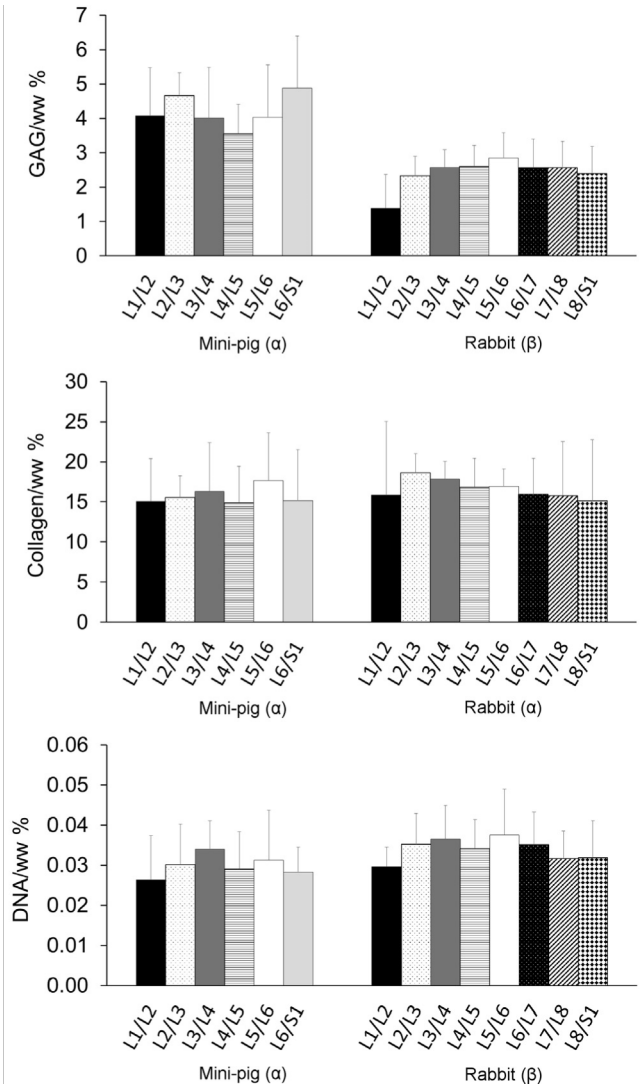

Figure A1-5. Comparison of the biochemical properties of facet cartilage among spinal levels within one species and also among species. A one-way ANOVA determined that there were no differences in biochemical properties of facet cartilage among spinal levels for either the mini-pig or the rabbit. Student t-tests were performed to detect differences in the average biochemical properties between species and species not

connected by the same letter (a, b) are different. Overall, the mini-pig exhibited higher GAG content but lower DNA content than the rabbit.

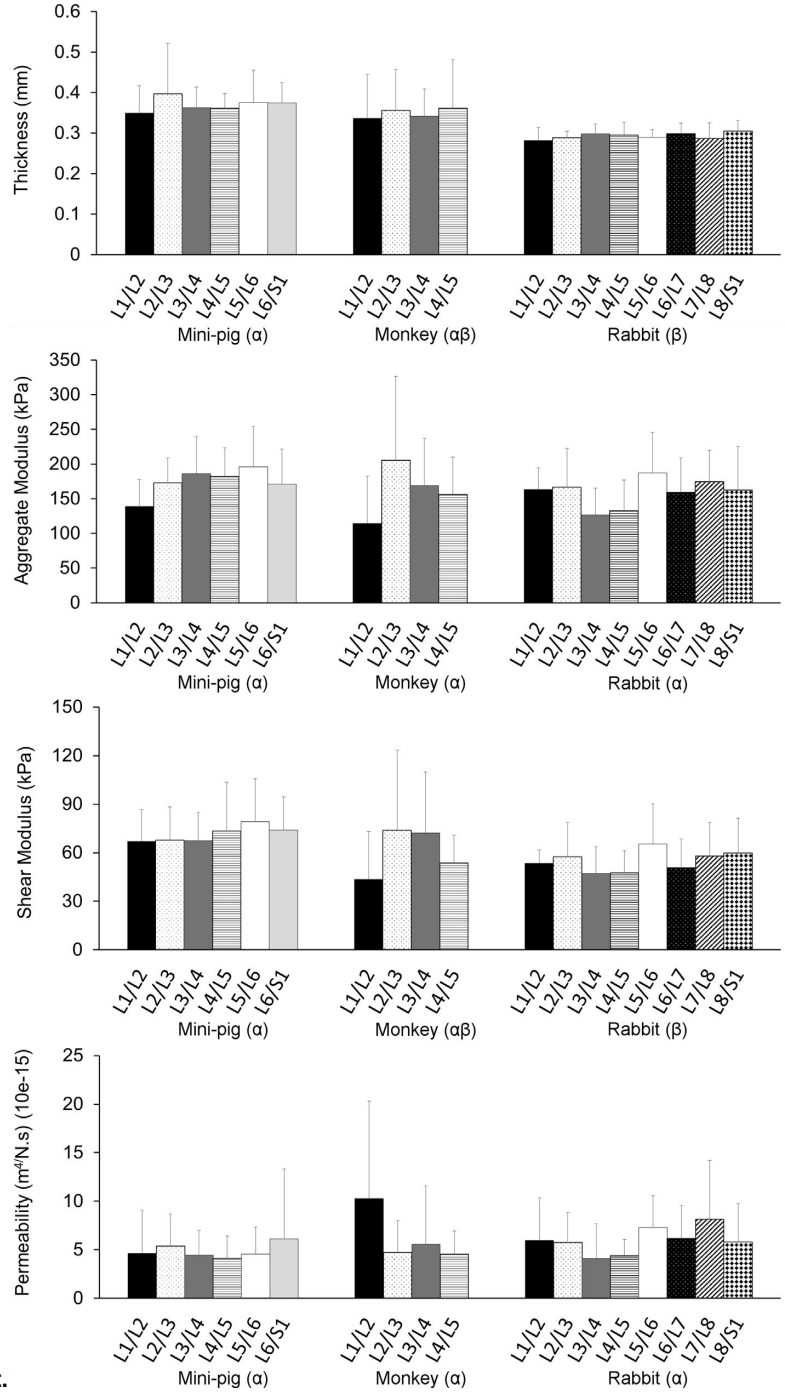

Figure A1-6. Comparison of the mechanical properties of facet cartilage among spinal levels within one species and also among species. One-way ANOVAs determined that there were no differences in mechanical properties of facet cartilage among spinal levels for the mini-pig, monkey, or rabbit. One-way ANOVAs, followed by Tukey's post hoc test, were also performed to detect differences in the average mechanical properties among species and species not connected by the same symbol (a, b) are different. Overall, the mini-pig facet cartilage was found to be thicker and have a higher shear modulus than the rabbit.

APPENDIX 2 Exogenous lysyl oxidase-like 2 and perfusion culture induce collagen crosslink formation in osteogenic grafts

Abstract

Lysyl oxidase (LOX)-mediated collagen crosslinking can regulate osteoblastic phenotype and enhance mechanical properties of tissues, both areas of interest in bone tissue engineering. The objective of this study was to investigate the effect of lysyl oxidase-like 2 (LOXL2) on osteogenic differentiation of mesenchymal stem cells (MSCs) cultured in perfusion bioreactors, enzymatic collagen crosslink formation in the extracellular matrix (ECM), and mechanical properties of engineered bone grafts. We administered exogenous LOXL2 to MSCs seeded in composite scaffolds under perfusion culture for up to 28 days. Constructs treated with LOXL2 appeared brown in color and possessed greater DNA content and osteogenic potential measured by a 2-fold increase in bone sialoprotein gene expression. Collagen expression of LOXL2-treated scaffolds was lower than untreated controls. Functional outputs such as calcium deposition, osteocalcin expression, and compressive modulus were unaffected by LOXL2 supplementation. Excitingly, LOXL2-treated constructs contained 1.8- and 1.4-times more pyridinoline (PYD) crosslinks per mole of collagen and per wet weight, respectively, than untreated constructs. Despite these increases, compressive moduli of LOXL2-treated constructs were similar to untreated constructs over the 28-day culture duration. This is the first report of LOXL2 application to engineered, three-dimensional bony constructs. The results suggest a potentially new strategy for engineering osteogenic grafts with a mature ECM by modulating crosslink formation.

Published as: Mitra D, Yasui OW, Harvestine JN, Link JM, Hu JC, Athanasiou KA, Leach JK. Exogenous lysyl oxidase-like 2 and perfusion culture induce collagen crosslink formation in osteogenic grafts. Biotechnology Journal. 0, 1700763 (2018)

Introduction

The extracellular matrix (ECM) is composed of a tissue-specific repository of proteins, proteoglycans, and sequestered growth factors.[1] Biomaterial-based approaches to bone tissue engineering seek to recapitulate characteristics of the ECM for delivery of bone forming cells such as mesenchymal stem cells (MSCs).[2,3] MSCs are a heterogeneous mixture of progenitor cells with multilineage potential including differentiation to bone forming osteoblasts when given the appropriate signals. Among other components, collagen plays a significant role in the bone ECM, providing a structural framework for mineralization and integrin-binding sites for directing cell function.[3–5] Post-translational modifications of collagen leading to enzymatic crosslink formation are a natural part of ECM maturation that may affect bone healing. Crosslink formation is mediated by lysyl oxidase (LOX) and its isoforms, LOX-like proteins (LOXL1-4).[6,7] LOX deficiency is associated with osteoporosis and weak bones.[8,9] LOX inhibition results in osteolathyrism and impairs bone and cartilage formation and function both in vitro and in vivo.[10] Conversely, increases in crosslink formation correlated with improved mechanical properties of the callus developed in a rat model of fracture repair.[11] Treatment of MC3T3-E1 murine preosteoblasts with beta-aminopropionitrile (β-APN), a well-known specific and irreversible inhibitor of LOX activity[12] that targets the active site of LOX and its isoforms, leads to diminished osteoblastic differentiation and crosslink formation in monolayer culture.[13,14] Collectively, these data suggest that proper enzymatic crosslink formation is essential for osteoblastic differentiation and increases in crosslink formation may provide an avenue to enhance formation of osteogenic grafts. To the best of our knowledge, the relationship between LOX-mediated collagen crosslinks and human MSC osteogenic response has not been reported in 3D culture systems.

LOX is a copper-dependent enzyme produced intracellularly and secreted into the extracellular space where it facilitates pyridinoline (PYD) and deoxypyridinoline (DPD) crosslink formation.[7,15] Copper-activated LOX is necessary for the critical first step in crosslink formation, where telopeptide lysine and hydroxylysine (HL) residues on collagen fibrils are converted to their

aldehyde forms. While lysine is a common component of cell culture media, HL and CuSO4 must be added to culture media to promote LOX function.[15] Endogenous LOX upregulation, stimulated through hypoxia or HL and CuSO4 supplementation, and exogenous LOXL2 supplementation correlate with enhanced compressive and tensile stiffness of native and engineered neocartilage.[15,16]

Overexpression of LOX by genetically modified smooth muscle cells led to increased tensile strength and elastic modulus in engineered vascular constructs.[17] LOXL2 was defined as a critical signaling mediator for chondrogenic differentiation in ATDC5 cells in vitro and was also upregulated in chondrocytes during the chondrogenic phase of fracture healing. However, both LOX and LOXL2 were detected in osteoblasts during early fracture healing, suggesting that each may play a role in osteogenic differentiation.[18] Despite reports of the effect of LOX and its paralogues on enhancing mechanical properties and generating functional cartilage and vascular constructs, literature regarding the effect of LOX in bone is limited to LOX-inhibition studies. As increasing mechanical properties of engineered grafts is a key target for bone tissue engineering and in light of similar successes using exogenous LOXL2, we investigated the effect of LOXL2 supplementation during the formation of three-dimensional engineered bony constructs.

Bioreactor culture of three-dimensional osteogenic constructs can improve nutrient availability, facilitate homogenous cell seeding, and enhance osteogenic differentiation and ECM deposition.[19–21] We recently demonstrated that MSCs on composite scaffolds exhibited superior osteogenic differentiation in vitro when maintained under perfusion culture for at least 14 days, and these constructs resulted in more bone formation in vivo compared to constructs cultured for shorter durations.[21] In this study, we sought to build upon our previous work with perfusion culture by supplementing culture media with LOXL2 to create a mature osteogenic graft. As LOXL2 activity was visible in osteoblasts during fracture healing,[18] we hypothesized that LOXL2 treatment of MSC-seeded constructs cultured under continuous perfusion would provide a novel strategy to further enhance ECM maturity and mechanical properties of these grafts. We seeded MSCs in

hydroxyapatite-poly(lactide-co-glycolide) (HA-PLG) scaffolds and maintained them in direct perfusion bioreactors for up to 28 days in order to answer the following questions: Does LOXL2 treatment 1) induce enzymatic crosslink formation; 2) enhance the osteogenic differentiation potential of MSCs cultured under perfusion; and 3) improve the mechanical properties of engineered constructs?

Materials and methods

Scaffold preparation

Composite scaffolds were fabricated using a gas foaming/particulate leaching method as described previously.[21–23] Briefly, microspheres composed of PLG (85:15, DLG 7E; Lakeshore Biomaterials, Birmingham, AL) were prepared using a double-emulsion process and lyophilized to form a free-flowing powder. 9.2 mg of lyophilized microspheres were combined with 23.1 mg of HA crystals (particle size 100 nm, Berkeley Advanced Biomaterials, Berkeley, CA), and 175.6 mg of NaCl particles (300-500 μm) to yield a 2.5:1:19 mass ratio of ceramic:polymer:salt. The powdered mixture was then compressed for 1 min into solid disks (final dimensions: 8 mm in diameter and 2 mm in height) using a Carver Press (Carver, Inc., Wabash, IN). Compressed disks were exposed to high pressure CO2 (5.5 MPa) for at least 16 hrs followed by rapid pressure release to cause polymer fusion. NaCl particles from the scaffolds were then leached in distilled H2O for 24 hrs. Scaffolds were sterilized by 70% ethanol under gentle vacuum, followed by two rinses in sterile phosphate buffered saline (PBS) and then dried in a sterile biosafety cabinet.

Cell culture

Human bone marrow-derived MSCs (Lonza, Walkersville, MD) were expanded without further characterization in growth medium (GM) consisting of minimum essential alpha medium (α-MEM; Invitrogen, Carlsbad, CA) supplemented with 10% fetal bovine serum (FBS; Atlanta Biologicals,

Flowery Branch, GA) and 1% penicillin/streptomycin (Gemini Bio-Products, Sacramento, CA). Cells were cultured under standard conditions (37°C, 21% O2, 5% CO2) and utilized at passage 5. For all experiments, cells were initially seeded in GM and then exposed to osteogenic medium (OM: GM supplemented with 10 mM βglycerophosphate, 50 μg/mL ascorbate-2-phosphate, and 100 nM dexamethasone, all from Sigma Aldrich, St. Louis, MO).

Hydroxylysine and copper sulfate treatment

Cells were plated in GM at 30,000 cells/cm2 in 12-well plates and allowed to adhere for 1 day. Thereafter, monolayer cultures were exposed to OM supplemented with varying levels of HL and CuSO4 (both from Sigma Aldrich) for up to 21 days to determine potential dose-dependent effects on cell function with these supplements prior to any LOXL2 supplementation studies. HL was added at 0.0146, 0.146, or 1.46 mg/mL, while CuSO4 was added at 0.00016, 0.0016, or 0.016 mg/mL. Following a full-factorial design with two factors of three levels each, we treated MSCs with nine different combinations of supplements. MSCs in OM served as the control group.

Detection of LOX activity

LOX activity in MSCs in monolayer culture was determined using a LOX activity kit (Abcam, Cambridge, MA). Media samples were collected from well plates and analyzed following the manufacturer's instructions. The resulting fluorescence was read on a microplate reader (excitation/emission= 540/590 nm) and recombinant LOXL2 (R&D Systems, Minneapolis, MN) was used as a standard.

Seeding MSCs on HA-PLG constructs in bioreactors and stimulation with LOXL2

Cells were seeded in bioreactors as described.[21,24] Briefly, scaffolds were installed in UCUP flow perfusion bioreactors (Cellec Biotek, Basel, Switzerland) and 10 mL of GM was injected through the bottom port into the bioreactor. Scaffolds were soaked in medium for 30 min before seeding. MSCs (1.2×106 in 2 mL GM) were injected via the top port into the bioreactor. Up to 10 individual

bioreactors were then connected to each syringe pump (Harvard Apparatus, Holliston, MA) to maintain media at a superficial velocity of 3 mL/min for 15-18 hrs. GM was replaced with OM after seeding, and constructs were maintained for up to 28 days in media supplemented with 0.146 mg/mL HL, 0.0016 mg/mL CuSO4, and varying concentrations of LOXL2 (0.0015 ng/mL, 0.015 ng/mL, and 0.15 ng/mL; Signal Chem, Richmond, Canada). Regardless of study duration, media was supplemented with CuSO4/HL/LOXL2 from days 7 to 21 of culture. Constructs received supplements every 3-4 days when media was changed.

Analysis of DNA content, osteogenic differentiation, and construct mechanical properties: Scaffolds were retrieved from bioreactors and washed twice with PBS. A 5 mm biopsy punch (Integra Miltex, York, PA) was used to harvest a disk that was first used for compressive testing and then subsequently for qPCR analysis. The compressive moduli of composite scaffolds were determined using an Instron 5800 Series Testing System (Instron, Norwood, MA). Scaffolds were compressed at a constant deformation rate of 1 mm/min, and compressive modulus was calculated using the linear portion of the stress-strain curve. Samples were processed for qPCR analysis thereafter as described.[25] Samples were collected in TRIzol reagent (Invitrogen) following the manufacturer's protocol. Total RNA was isolated using an RNEasy micro kit (Qiagen, Valencia, CA). RNA was reverse transcribed with the QuantiTect Reverse Transcription kit (Qiagen). qPCR was performed using a QuantiFast Probe PCR kit (Qiagen) on a CFX96 Real-Time System (Bio-Rad, Hercules, CA). Primers and probes for RPL13 (HS00204173_m1), COL1A1 (HS00164004_M1), and IBSP (HS00173720_M1) were purchased from Applied Biosystems (Foster City, CA). Amplification conditions were 95°C for 3 min, followed by 40 cycles at 95°C for 3 sec and 60°C for 30 sec. Quantitative PCR results were normalized to RPL13 transcript levels to yield ΔCt, and fold change in expression relative to the housekeeping gene was calculated using $2^{-\Delta Ct}$. The remainder of the scaffold was collected in 250 μL of passive lysis buffer (Promega, Madison, WI), frozen at −20°C, thawed, sonicated, centrifuged at 5000 rpm for 10 min to pellet the cell debris, and the supernatant was collected for DNA analysis. The

supernatant was analyzed for DNA content using the Quant-iT PicoGreen dDNA Assay Kit (Invitrogen) following manufacturer's instructions. The remaining pellet was resuspended in 0.9 N H2SO4 and incubated overnight at 37°C. Calcium deposition was quantified by reacting with o-cresolphthalein complexone as previously described.[26,27] The calcium content of an unused composite scaffold was subtracted from that of cultured composite scaffolds to determine the amount of calcium deposited by MSCs.

To visualize cell distribution and markers of osteogenic differentiation within constructs, samples were washed twice in PBS and fixed in 10% buffered formalin acetate (Fisher Scientific, Fair Lawn, NJ) for 24 hrs at 4°C. Samples were then washed twice in PBS to remove residual formalin acetate and preserved in 70% ethanol at 4°C until further processing. Prior to cryosectioning, samples were soaked in Tissue-Tek OCT compound (Sakura Finetek, Torrance, CA) overnight to allow OCT to perfuse through the entire scaffold. Constructs were then placed in fresh OCT and frozen on dry ice. 5 μm sections were cut on a Leica CM1850 Cryostat (Leica Microsystems, Bannockburn, IL) and mounted onto microscope slides for analysis. Sections were stained using hematoxylin and eosin (H&E) following standard protocols and immunostained using an anti-osteocalcin (OCN) antibody (1:200, AB13420, Abcam).

Detection and quantification of collagen crosslinks in engineered mineralized tissues: Constructs were washed twice in PBS and tissue wet weight was recorded. Samples were then lyophilized overnight prior to recording dry weight. Samples were decalcified with Calci-Clear Rapid (National Diagnostics, Atlanta, GA) at room temperature for 24 hrs. Decalcified samples were hydrolyzed in 500 μL of 6N HCl at 110°C for 24 hrs. Following hydrolysis, samples were dried using a vacuum concentrator and split into two equal fractions for a collagen content assay and PYD and DPD crosslink analysis. Samples used for HPLC were resuspended in a solution of 10 nmol pyroxidine per mL of water. Samples were then diluted five times with a solution of 10% v/v acetonitrile and 0.5% v/v heptafluorobutyric acid (HFBA) in water to prepare for reverse phase chromatography. For the assay, 50 μL of each sample was injected into the reverse phase column

and eluted over 37 min using the following solvent profile: Solvent A (24% v/v methanol and 0.13% v/v HFBA) from 0-17 min, Solvent B (75% v/v acetonitrile and 0.1% HFBA) from 17-27 min, and Solvent A again from 27-37 min. A PYD/DPD calibrator (Quidel, San Diego, CA) was prepared as a standard and analyzed during each run to permit quantification of pyridinoline content in each sample.

Quantification of collagen content

Collagen content in engineered constructs was determined using a hydroxyproline assay as described previously.[28] Briefly, the remaining portion of hydrolysate from HPLC sample preparation was first reacted with 150 µL Chloramine T (Sigma Aldrich) and incubated at room temperature for 20 min. 150 µL aldehyde-perchloric acid solution (150 µL) was then added to each sample and incubated at 60°C for 15 min. Following incubation, tubes were left to cool for 10 min and sample absorbance was read on a microplate reader. Hydroxyproline was converted to collagen mass assuming that collagen contains 13.7% hydroxyproline.[29]

Statistical analysis

All data are presented as means ± standard deviation of the mean. Statistical analysis was performed using unpaired t-tests, one-way ANOVA, and two-way ANOVA with Tukey's multiple comparison post-hoc test, where appropriate. All statistical analysis was performed in Prism 6 software (GraphPad, San Diego, CA), and p values less than 0.05 were considered statistically significant. Significance is denoted by alphabetical letterings; groups with no significance are linked by the same letters, while groups with significance do not share the same letters.

Results

HL and CuSO4 influence collagen deposition and LOX activity

In the absence of exogenous LOX supplementation, we examined the effect of HL and CuSO4 supplementation on collagen deposition and endogenous LOX activity of MSCs in monolayer

culture at 14 and 21 days to determine necessary concentrations for use in future studies. At 14 days, we observed similar quantities of collagen deposition following MSC stimulation with all levels of HL and CuSO4 (Fig. A2-1A). Importantly, high HL/high CuSO4 yielded lower collagen content than all groups within the medium CuSO4-treated groups. Collagen content in the high HL/low CuSO4 group was also significantly lower than low HL/med CuSO4 group. At 21 days, all groups had similar or higher collagen content than the control group (Fig. A2-1B). Collagen deposition was comparable for low and medium HL groups across all CuSO4 groups. Collagen secreted by MSCs stimulated by medium HL levels was enhanced compared to high HL within the low and high CuSO4 groups.

All treated groups exhibited similar or higher endogenous LOX activity than OM at 14 days. In particular, medium and high HL treatments within the high CuSO4 group exhibited significantly higher activity than all treatments within the low and medium CuSO4 groups (Fig. A2-1C). LOX activity was similar in all low and medium CuSO4 groups. After 21 days in culture, all CuSO4-treated groups except for low HL- and high HL/low CuSO4 had higher LOX activity than the OM control (Fig. A2-1D). LOX activity was reduced in all groups after 21 days compared to 14 days. With a goal of using fewer additives, we supplemented osteogenic media with medium levels of HL and CuSO4 (denoted as OM*) for future studies. This concentration of supplements did not induce detectable differences in proliferation or metabolic activity when measuring DNA content or using an alamarBlue assay, respectively (data not shown).

LOXL2 treatment influences MSC proliferation after 21 days of culture

Constructs were treated low, medium, or high levels of LOXL2 corresponding to 0.0015, 0.015, and 0.15 ng/mL, respectively. Constructs exposed to medium and high levels of LOXL2 had a brownish appearance compared to the pink color of OM- and low LOXL2treated constructs (Fig. A2-2B). We observed homogeneous cell distribution throughout scaffolds of all groups following H&E staining (Fig. A2-2D). DNA content increased with increasing LOXL2 concentration, with

medium and high LOXL2 groups exhibiting significantly higher DNA content than the OM control (Fig. A2-2C). We then evaluated the effect of LOXL2 supplementation on the osteogenic response of MSCs via gene expression, calcium quantification, and immunohistochemistry. Bone sialoprotein (IBSP) gene expression, an intermediate-to-late marker of osteogenic differentiation, was increased in medium and high LOXL2-treated constructs relative to OM control and low LOXL2 groups (Fig. A2-3A). COL1A1 expression exhibited the opposite trend, with decreasing collagen expression as a function of increasing LOXL2 treatment (Fig. A2-3B). Both medium and high LOXL2-treated groups had significantly lower COL1A1 expression than low LOXL2 constructs, but only high LOXL2 was significantly lower than the OM control.

Functional properties of engineered constructs are not affected by LOXL2

Functional properties of engineered constructs were not altered by LOXL2 treatment. Similar levels of total calcium were detected in constructs within all groups of this study (Fig. A2-3C). All LOXL2-treated constructs possessed similar compressive moduli to each other and the control group (Fig. A2-3D). Immunohistochemical evaluation for osteocalcin (OCN) corroborated calcium quantification results. No apparent qualitative differences were observed in OCN expression as a result of LOXL2 supplementation (Fig. A2-3E).

Extended culture duration sustains MSC osteogenic differentiation

In order to allow time for LOXL2-mediated immature crosslinks to form mature enzymatic crosslinks, we cultured constructs for an additional 7 days after the last LOXL2 supplementation and evaluated osteogenic differentiation of MSCs at 28 days (Fig. A2-4A). We treated constructs with medium-level LOXL2 only, since low LOXL2 treatment did not enhance osteogenic differentiation relative to controls and high LOXL2 did not impart significant advantages over medium LOXL2. Similar to the 21-day study, we observed brown discoloration of constructs due to LOXL2 treatment (Fig. A2-4B). We did not observe significant differences in DNA content of

treated constructs compared to OM controls following extended culture (Fig. A2-4C), and H&E stains revealed comparable cell distribution between OM and LOXL2-treated scaffolds (Fig. A2-4D). Similar to the 21-day study, we observed increased osteogenic gene expression of MSCs at 28 days due to LOXL2 supplementation. IBSP expression was significantly greater in LOXL2-treated constructs (Fig. A2-5A). Again, constructs cultured for 28 days exhibited lower COL1A1 expression relative to OM controls (Fig. A2-5B). Even with 28 days of culture, we did not observe increases in calcium content of engineered constructs due to LOXL2 treatment (Fig. A2-5C). Compressive moduli of treated and control samples were not statistically different (Fig. A2-5D), and OCN expression was comparable in both groups (data not shown).

Exogenous LOXL2 supplementation leads to pyridinoline crosslink formation

HPLC analysis of constructs cultured for 28 days under perfusion revealed that LOXL2 supplementation significantly increased PYD crosslinks. Compared to untreated samples, we detected 1.4-fold more total PYD, 1.4-fold more PYD/wet weight, and 1.8-fold more PYD/mol of collagen (Fig. A2-5E-G). We did not detect measurable levels of DPD resulting from LOXL2 treatment (data not shown).

Discussion

We investigated the effect of LOXL2 treatment on the osteogenic potential of MSCs cultured on engineered constructs under perfusion, mechanical properties of engineered bony tissues, and formation of enzymatic crosslinks. LOXL2 supplementation enhanced IBSP gene expression in MSCs, while DNA content was increased with LOXL2 in a dose-dependent manner. Functional properties of LOXL2-treated constructs, such as calcium deposition and compressive moduli, were similar to those of controls. LOXL2 supplementation led to a significant increase in PYD crosslink formation over controls at 28 days. These data demonstrate that exogenous LOXL2

application and perfusion culture may be a novel strategy for inducing enzymatic collagen crosslinks to generate osteogenic constructs with a mature ECM.

Enzymatic collagen crosslink formation in bone is mediated by LOX and its paralogues (LOXL1-LOXL4).[6] While several studies have characterized expression of LOX and its isoforms in MC3T3-E1 cells,[30,31] few studies have reported LOX expression in MSCs. To our knowledge, no reports exist that directly measure LOX and LOXL expression in human MSCs. Fernandes et al. reported that LOX inhibition via β-APN did not affect MSC differentiation; however, this study did not measure LOX or LOXL2 expression.[12] Moreover, β-APN targets the active site of LOX and its isoforms, necessitating further study to determine if a single lysyl oxidase or paralogue is involved in osteogenic differentiation. We measured expression of LOX and its isoforms in human MSCs cultured in monolayer for 14 and 21 days and found that the most prominent LOX and LOXL-genes expressed in human MSCs are LOX, LOXL1, and LOXL2 (data not shown). Both LOX and LOXL2 were detected via immunohistochemistry in osteoblasts during early fracture healing, suggesting that each may play a role in osteogenic differentiation.[18] As LOXL2 was successfully used to enhance the mechanical properties of engineered neocartilage,[15] a shared goal of this study, we supplemented media with LOXL2 given similar levels of gene expression at 21 days. Given the data from these studies and the importance of LOXL2 in chondrogenic differentiation,[18] future work should investigate the effects of LOX and its other isoforms on enzymatic crosslink formation and MSC differentiation.

Copper is an essential co-factor for the activity of the LOX family of enzymes.[32] Since copper is not a common component of cell culture media, endogenous LOX secreted by cells or exogenously supplemented LOX remain in their inactive form during culture.[15] Moreover, the incorporation of both lysine and HL into collagen fibrils is essential for LOX-mediated crosslink formation. While lysine is a common ingredient in media, HL must be exogenously supplemented. Makris et al. demonstrated that supplementing culture medium with 0.146 mg/mL HL and 0.0016 mg/mL CuSO4 synergistically increased PYD formation, tensile properties, and aggregate

modulus of engineered neocartilage.[15] Therefore, we treated MSCs in monolayer with varying levels of both supplements and measured collagen content and LOX activity to ensure that these supplements were not detrimental to either output. From these studies, we determined that medium levels of both supplements (0.146 mg/mL HL, 0.0016 mg/mL CuSO4) were suitable for further studies.

Perfusion culture of MSCs seeded in biomaterial scaffolds provides nutrients for cell survival, enhances extracellular matrix deposition, and increases osteogenic cell differentiation. We recently reported that constructs maintained in perfusion culture for at least 14 days resulted in the greatest expression of osteoblastic markers in vitro and ectopic bone formation when implanted in vivo.[21] The goal of this study was to determine if LOXL2 supplementation and bioreactor culture could synergistically improve ECM maturity and create an enhanced osteogenic graft. The effect of LOX-mediated crosslinking on osteogenic differentiation has been studied with murine osteoblasts in monolayer culture.[14,31] Furthermore, the capacity of LOX and its isoforms to improve mechanical properties of engineered neocartilage or vascular tissues has also been demonstrated in static culture.[16,17,33] However, continuous perfusion culture markedly increases ECM deposition by MSCs during osteogenic differentiation,[21,34,35] providing an abundance of collagen substrate for LOX. Therefore, we applied exogenous LOXL2 to MSCs cultured in HA-PLG scaffolds under perfusion. Constructs treated with medium and high levels of LOXL2 exhibited a brown appearance compared to the pinkish OM controls. Histological evaluation via H&E staining revealed no differences between treated and control scaffolds for either study. LOXL2 treatment increased DNA content of constructs in a dose-dependent manner at 21 days. Though LOX and its isoforms are rarely investigated for their effect on cell proliferation, Pischon et al. demonstrated that knocking out the LOX gene in primary calvarial osteoblasts significantly decreased DNA synthesis.[31] Furthermore, HL supplementation of culture media increased the number of cells per construct in engineered neocartilage.[15] Our data provide further evidence that HL and/or LOXL2 may play a stimulatory role in proliferation of MSCs. However, we did not

observe these differences in the 28-day study in which the LOXL2 supplement cocktail was supplied until day 21 of culture. These results could be attributed to contact inhibition and reduced proliferative capacity of MSCs with increasing osteogenic differentiation, which is present in LOXL2treated constructs relative to MSCs in untreated constructs.[36]

Next, we investigated the effect of LOXL2 supplementation on the osteogenic potential of MSCs. IBSP, an intermediate-to-late marker for osteogenic differentiation, was significantly increased in medium and high level-treated LOXL2 constructs, suggesting that exogenous LOXL2 and mechanical stimulation may synergistically enhance osteogenic gene expression of MSCs. LOX-deficient primary calvarial osteoblasts had reduced IBSP expression and mineralization during osteogenic differentiation in monolayer culture.[31] Others have demonstrated that LOX inhibition by β-APN can downregulate osteocalcin mRNA expression by 75%.[14] In another study, β-APN treatment of MC3T3-E1 cells impaired osteogenic differentiation by downregulating alkaline phosphatase (ALP) activity and calcium deposition, yet human MSCs were unaffected by reduced collagen crosslinking in the same study.[13] Herein, we demonstrate for the first time that mechanically stimulated MSCs cultured in continuous perfusion bioreactors respond to LOXL2 with enhanced IBSP gene expression. Currently, there is no consensus on the effect of LOX on collagen expression during osteogenic differentiation. LOX knockout of murine calvarial primary osteoblasts led to a decrease in COL1A1 expression,[31] while β-APN inhibition of LOX in MC3T3-E1 cultures increased COL1A1 expression by 140%.[14] In this study, we observed increased IBSP expression in human MSCs in 3D perfusion culture, together with decreased COL1A1 expression, due to LOXL2 treatment at both 21 and 28 days. Taken together, our data demonstrate that exogenous LOXL2 administration to MSCs under perfusion initiates a cascade of events in the osteogenic program that require further examination.

Exogenous LOXL2 supplementation is a promising strategy to improve the functional properties of engineered constructs through the formation of enzymatic collagen crosslinks. Despite increases in osteogenic gene expression and DNA content, we did not observe changes

in osteocalcin secretion, a late marker of differentiation, calcium deposition, or compressive modulus. The mechanical properties of bone reflect the inherent material properties of its constituents and the way in which they are arranged and interact. LOX-mediated collagen crosslinks affect the tensile strength and post-yield properties of bone.[7] Although pre-yield properties such as elastic modulus predominantly depend on the mineral phase, collagen crosslinking can influence these as well.[7] Cartilage implants are commonly evaluated using both tensile and compressive testing. Makris et al. demonstrated that increased PYD crosslinks correlated with increased compressive and tensile stiffness in engineered cartilage, which is primarily composed of collagen.[15,16] While the effect of collagen crosslinks may be more easily observed in tension, the physiological role of bone is to withstand compressive stress. Therefore, we chose to measure compressive properties of our constructs. In these studies, MSCs were seeded on clinically relevant, macroporous HAPLG composite scaffolds, which are significantly stiffer than engineered cartilage tissues. Therefore, small changes in compressive modulus due to LOXL2-mediated crosslinking may be masked in stiff biomaterials such as the ones used in this study. Although we did not detect changes in compressive modulus through compressive testing, treated constructs appeared crunchy, indicating that LOXL2 may affect the post-yield properties such as toughness. Further studies are needed to investigate the effect of enzymatic crosslinks on tensile stiffness, strength, and toughness of engineered bony constructs.

LOX and its isoforms mediate the formation of several mature enzymatic collagen crosslinks in bone including PYD and DPD.[7,32] In this study, we detected significant increases in total PYD crosslinks, PYD/wet weight, and PYD/mol of collagen (but not DPD) due to LOXL2 supplementation of culture medium. While total PYD provides a measure for total crosslinks formed in the engineered construct, PYD/wet weight allows us to compare the fraction of crosslinks in our constructs compared to other tissues treated with LOXL2. Moreover, PYD/mol of collagen provides insight into the degree of crosslinking in the collagen present in constructs and enables comparison with native tissues. PYD/wet weight was 1.4-fold that of controls, which

is lower than the improvements in crosslink formation reported for exogenous LOXL2 supplementation of engineered neocartilage.[16] This difference may be attributed to the availability of a continuous matrix of collagen fibrils in neocartilage vs. collagen spatially separated by pores in this study. Moreover, as cartilage is predominantly composed of collagen type II and bone contains primarily collagen type I with the presence of collagen type II, there may be differences in the function of crosslinks formed between collagen subtypes. One might also speculate that this moderate increase in collagen crosslinking could be due to an insufficient amount of collagen substrate. This hypothesis is further corroborated by reduced COL1A1 expression observed due to LOXL2 treatment. Optimizing the timing and duration of LOXL2 administration or increasing the concentration of ascorbate-2-phosphate, a stimulus for matrix deposition, may facilitate enhanced collagen deposition prior to collagen crosslinking. In terms of PYD/mole of collagen, we achieved values higher than the ones reported for native bone,[7] indicating that the major limitation in our study was not the amount of available LOXL2, but rather, the scarcity of substrate in these engineered constructs. Strategies that augment collagen deposition prior to LOXL2 administration could result in a denser ECM, which upon crosslinking, may have more drastic effects on osteogenic differentiation and mechanical properties.

This study provides evidence for LOXL2 treatment as a means to regulate enzymatic collagen crosslink formation within MSC-laden engineered bony constructs. While LOXL2 supplementation led to increases in PYD crosslinks, DNA content, and gene expression of osteogenic markers of differentiation, we did not observe increases in functional outputs of differentiation or compressive modulus of engineered constructs. This work introduces exciting new avenues to the field of bone tissue engineering for improving the functional properties of osteogenic grafts.

References

1 Hynes RO The extracellular matrix: Not just pretty fibrils. Science. 2009, 326, 1216–1219. [PubMed: 19965464]

2 Badylak SF The extracellular matrix as a biologic scaffold material. Biomaterials. 2007, 28, 3587– 3593. [PubMed: 17524477]

3 Cheng CW, Solorio LD and Alsberg E Decellularized tissue and cell-derived extracellular matrices as scaffolds for orthopaedic tissue engineering. Biotechnol Adv. 2014, 32, 462–484. [PubMed: 24417915]

4 Emsley J, Knight CG, Farndale RW, Barnes MJ and Liddington RC Structural basis of collagen recognition by integrin alpha2beta1. Cell. 2000, 101, 47–56. [PubMed: 10778855]

5 Mizuno M, Fujisawa R and Kuboki Y Type I collagen-induced osteoblastic differentiation of bone marrow cells mediated by collagen-alpha2beta1 integrin interaction. J Cell Physiol. 2000, 184, 207–213. [PubMed: 10867645]

6 Trackman PC Enzymatic and non-enzymatic functions of the lysyl oxidase family in bone. Matrix Biol. 2016, 52–54, 7–18.

7 Saito M and Marumo K Collagen cross-links as a determinant of bone quality: A possible explanation for bone fragility in aging, osteoporosis, and diabetes mellitus. Osteoporos Int. 2010, 21, 195–214. [PubMed: 19760059]

8 Oxlund H, Barckman M, Ortoft G and Andreassen TT Reduced concentrations of collagen crosslinks are associated with reduced strength of bone. Bone. 1995, 17, 365S–371S. [PubMed: 8579939]

9 Bailey AJ, Wotton SF, Sims TJ and Thompson PW Biochemical changes in the collagen of human osteoporotic bone matrix. Connect Tissue Res. 1993, 29, 119–132. [PubMed: 8403893]

10 Hong HH, Pischon N, Santana RB, Palamakumbura AH, Chase HB, Gantz D, Guo Y, Uzel MI, Ma D and Trackman PC A role for lysyl oxidase regulation in the control of normal

collagen deposition in differentiating osteoblast cultures. J Cell Physiol. 2004, 200, 53–62. [PubMed: 15137057]

11 Saito M, Shiraishi A, Ito M, Sakai S, Hayakawa N, Mihara M and Marumo K Comparison of effects of alfacalcidol and alendronate on mechanical properties and bone collagen cross-links of callus in the fracture repair rat model. Bone. 2010, 46, 1170–1179. [PubMed: 20026440]

12 Tang SS, Trackman PC and Kagan HM Reaction of aortic lysyl oxidase with beta-aminopropionitrile. J Biol Chem. 1983, 258, 4331–4338. [PubMed: 6131892]

13 Fernandes H, Dechering K, Van Someren E, Steeghs I, Apotheker M, Leusink A, Bank R, Janeczek K, Van Blitterswijk C and de Boer J The role of collagen crosslinking in differentiation of human mesenchymal stem cells and MC3T3-E1 cells. Tissue Eng Part A. 2009, 15, 3857– 3867. [PubMed: 19694522]

14 Turecek C, Fratzl-Zelman N, Rumpler M, Buchinger B, Spitzer S, Zoehrer R, Durchschlag E, Klaushofer K, Paschalis EP and Varga F Collagen cross-linking influences osteoblastic differentiation. Calcif Tissue Int. 2008, 82, 392–400. [PubMed: 18488133]

15 Makris EA, MacBarb RF, Responte DJ, Hu JC and Athanasiou KA A copper sulfate and hydroxylysine treatment regimen for enhancing collagen cross-linking and biomechanical properties in engineered neocartilage. FASEB J. 2013, 27, 2421–2430. [PubMed: 23457219]

16 Makris EA, Responte DJ, Paschos NK, Hu JC and Athanasiou KA Developing functional musculoskeletal tissues through hypoxia and lysyl oxidase-induced collagen cross-linking. Proc Natl Acad Sci U S A. 2014, 111, E4832–4841. [PubMed: 25349395]

17 Elbjeirami WM, Yonter EO, Starcher BC and West JL Enhancing mechanical properties of tissue-engineered constructs via lysyl oxidase crosslinking activity. J Biomed Mater Res A. 2003, 66, 513–521. [PubMed: 12918034]

18 Iftikhar M, Hurtado P, Bais MV, Wigner N, Stephens DN, Gerstenfeld LC and Trackman PC Lysyl oxidase-like-2 (LOXL2) is a major isoform in chondrocytes and is critically required for differentiation. J Biol Chem. 2011, 286, 909–918. [PubMed: 21071451]

19 Yeatts AB and Fisher JP Bone tissue engineering bioreactors: Dynamic culture and the influence of shear stress. Bone. 2011, 48, 171–181. [PubMed: 20932947]

20 Bancroft GN, Sikavitsas VI, van den Dolder J, Sheffield TL, Ambrose CG, Jansen JA and Mikos AG Fluid flow increases mineralized matrix deposition in 3D perfusion culture of marrow stromal osteoblasts in a dose-dependent manner. Proc Natl Acad Sci U S A. 2002, 99, 12600– 12605. [PubMed: 12242339]

21 Mitra D, Whitehead J, Yasui OW and Leach JK Bioreactor culture duration of engineered constructs influences bone formation by mesenchymal stem cells. Biomaterials. 2017, 146, 29–39. [PubMed: 28898756]

22 He J, Genetos DC and Leach JK Osteogenesis and trophic factor secretion are influenced by the composition of hydroxyapatite/poly(lactide-co-glycolide) composite scaffolds. Tissue Eng Part A. 2010, 16, 127–137. [PubMed: 19642853]

23 Vissers CAB, Harvestine JN and Leach JK Pore size regulates mesenchymal stem cell response to bioglass-loaded composite scaffolds. J Mater Chem B. 2015, 3, 8650–8658.

24 Scherberich A, Galli R, Jaquiery C, Farhadi J and Martin I Three-dimensional perfusion culture of human adipose tissue-derived endothelial and osteoblastic progenitors generates osteogenic constructs with intrinsic vascularization capacity. Stem Cells. 2007, 25, 1823–1829. [PubMed: 17446558]

25 Mitra D, Fatakdawala H, Nguyen-Truong M, Creecy A, Nyman J, Marcu L and Leach JK Detection of pentosidine cross-links in cell-secreted decellularized matrices using time resolved fluorescence spectroscopy. ACS Biomater. Sci. Eng. 2017, 3 1944–1954. [PubMed: 28944287]

26 Harvestine JN, Vollmer NL, Ho SS, Zikry CA, Lee MA and Leach JK Extracellular matrix-coated composite scaffolds promote mesenchymal stem cell persistence and osteogenesis. Biomacromolecules. 2016, 17 3524–3531. [PubMed: 27744699]

27 Murphy KC, Stilhano RS, Mitra D, Zhou D, Batarni S, Silva EA and Leach JK Hydrogel biophysical properties instruct coculture-mediated osteogenic potential. FASEB J. 2016, 30 477– 486. [PubMed: 26443826]

28 Hagerty P, Lee A, Calve S, Lee CA, Vidal M and Baar K The effect of growth factors on both collagen synthesis and tensile strength of engineered human ligaments. Biomaterials. 2012, 33, 6355–6361. [PubMed: 22698725]

29 Creemers LB, Jansen DC, van Veen-Reurings A, van den Bos T and Everts V Microassay for the assessment of low levels of hydroxyproline. Biotechniques. 1997, 22, 656–658. [PubMed: 9105617]

30 Atsawasuwan P, Mochida Y, Parisuthiman D and Yamauchi M Expression of lysyl oxidase isoforms in MC3T3-E1 osteoblastic cells. Biochem Biophys Res Commun. 2005, 327, 1042– 1046. [PubMed: 15652501]

31 Pischon N, Maki JM, Weisshaupt P, Heng N, Palamakumbura AH, N'Guessan P, Ding A, Radlanski R, Renz H, Bronckers TA, Myllyharju J, Kielbassa AM, Kleber BM, Bernimoulin JP and Trackman PC Lysyl oxidase (lox) gene deficiency affects osteoblastic phenotype. Calcif Tissue Int. 2009, 85, 119–126. [PubMed: 19458888]

32 Eyre DR, Weis MA and Wu JJ Advances in collagen cross-link analysis. Methods. 2008, 45, 65–74. [PubMed: 18442706]

33 Dahl SL, Rucker RB and Niklason LE Effects of copper and cross-linking on the extracellular matrix of tissue-engineered arteries. Cell Transplant. 2005, 14, 861–868. [PubMed: 16454361]

34 Sikavitsas VI, Bancroft GN, Lemoine JJ, Liebschner MA, Dauner M and Mikos AG Flow perfusion enhances the calcified matrix deposition of marrow stromal cells in

biodegradable nonwoven fiber mesh scaffolds. Ann Biomed Eng. 2005, 33, 63–70. [PubMed: 15709706]

35 Sikavitsas VI, Bancroft GN, Holtorf HL, Jansen JA and Mikos AG Mineralized matrix deposition by marrow stromal osteoblasts in 3D perfusion culture increases with increasing fluid shear forces. Proc Natl Acad Sci U S A. 2003, 100, 14683–14688. [PubMed: 14657343]

36 Banfi A, Muraglia A, Dozin B, Mastrogiacomo M, Cancedda R and Quarto R Proliferation kinetics and differentiation potential of ex vivo expanded human bone marrow stromal cells: Implications for their use in cell therapy. Exp Hematol. 2000, 28, 707–715. [PubMed: 10880757]

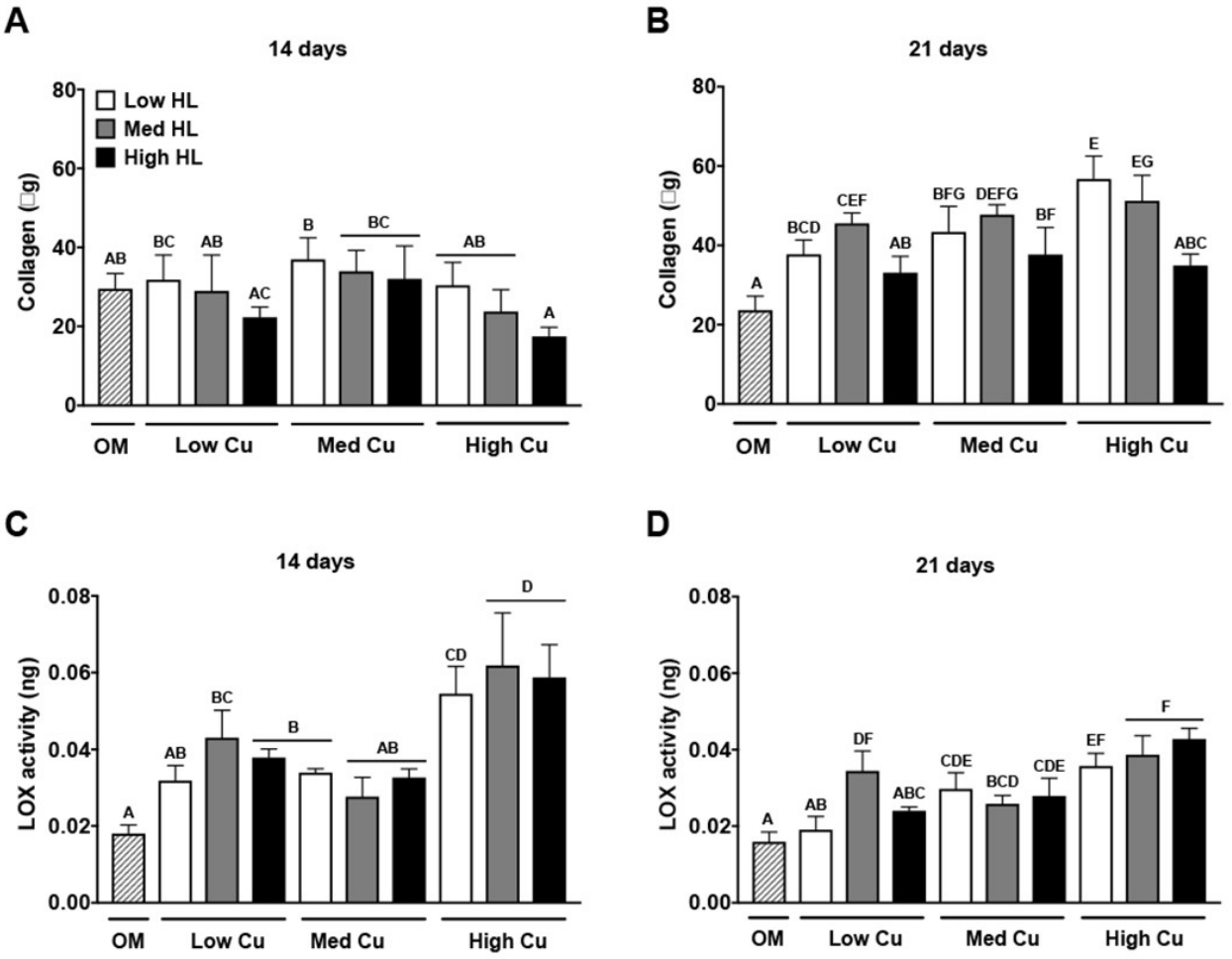

Figure A2-1. Full-factorial study to determine concentrations of HL and CuSO4 required for LOX-mediated crosslinking. Effect of three levels of HL and CuSO4 on collagen deposition in the absence of exogenous LOX at 14 (A) and 21 days (B). LOXL activity at 14 (C) and 21 days (D). For (A)-(D), one-way ANOVA and Tukey's post hoc tests were performed to determine statistical significance, which is denoted by alphabetical letterings; groups with no significance are linked by the same letter, while groups with significance do not share a letter (n=4).

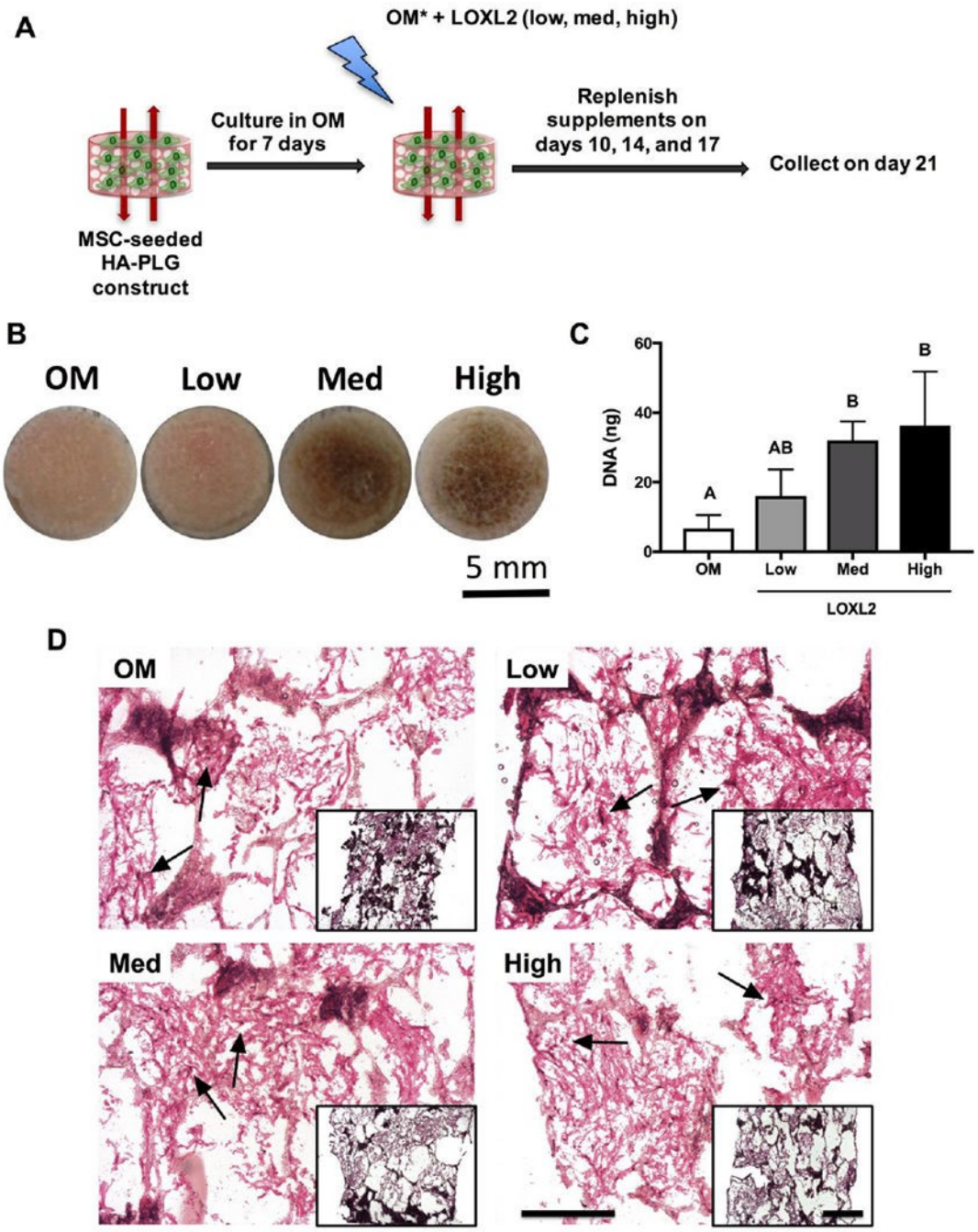

Figure A2-2. Effect of exogenous LOXL2 application on morphology and DNA content of constructs cultured for 21 days. (A) Schematic representing the LOXL2 supplementation regime. (B) Gross morphology of constructs at 21 days. (C) DNA content of constructs at 21 days. (D) Representative H&E images taken at 10× magnification (scale bar represents 200 μm) to visualize cellularity of constructs with insets taken at 4× magnification (scale bar represents 500 μm). Black is indicative of scaffold and some cells are denoted by black arrows. For (C), a one-way ANOVA and Tukey's post hoc test was performed to determine statistical significance, which is denoted by alphabetical letterings; groups with no significance are linked by the same letter, while groups with significance do not share a letter (n=4).

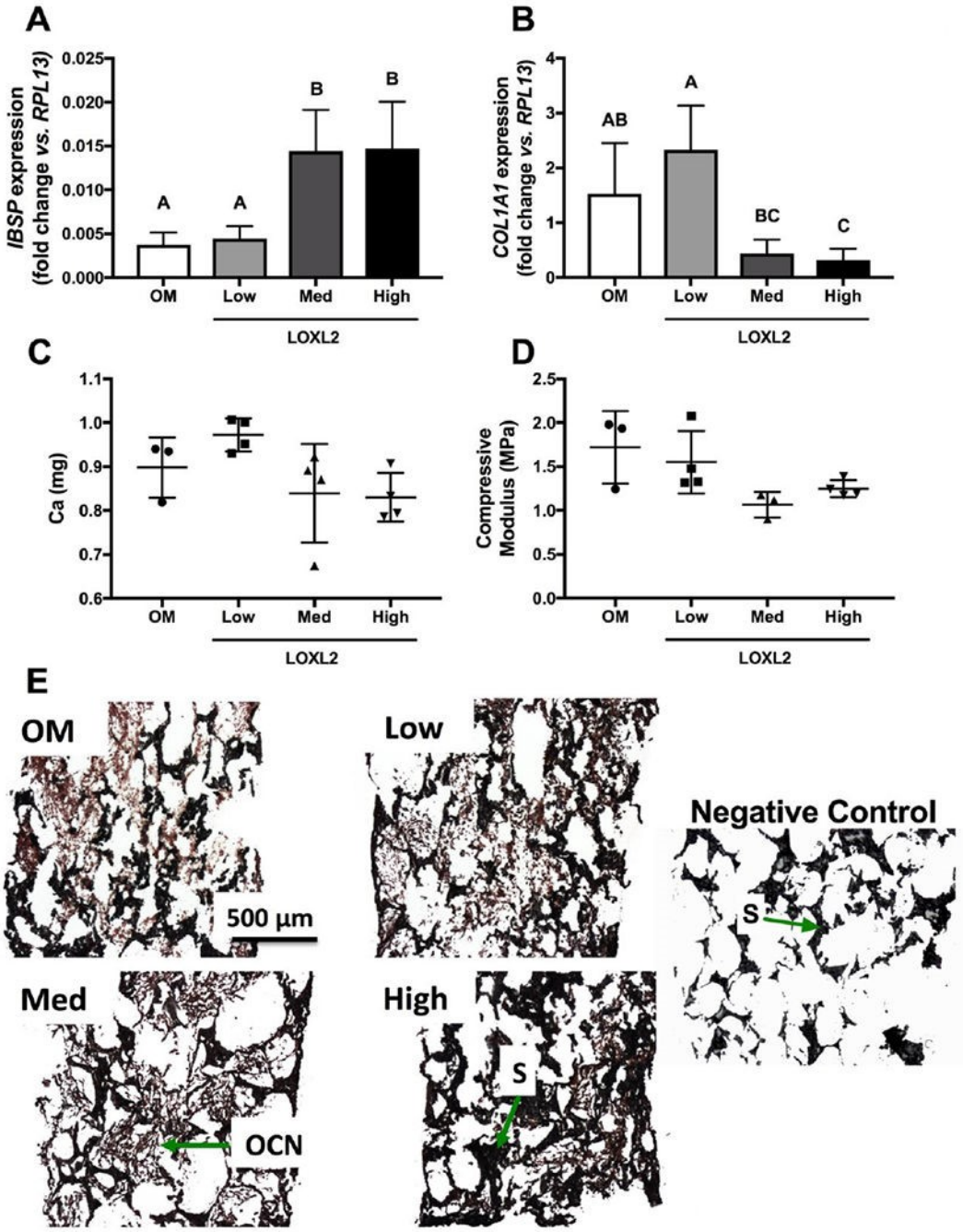

Figure A2-3. Effect of exogenous LOXL2 application on osteogenic differentiation and functional outputs for constructs in perfusion culture for 21 days. (A) IBSP and (B) COL1A1 gene expression. (C) Calcium quantification and (D) compressive moduli of constructs. (E) Representative immunohistochemistry of constructs stained for osteocalcin (OCN). Black is indicative of scaffold (S); brown is indicative of OCN (scale bar represents 500 µm). For (A)-(D), one-way ANOVA and Tukey's post-hoc tests were performed to determine statistical significance, which is denoted by alphabetical letterings; groups with no significance are linked by the same letter, while groups with significance do not share a letter (n=5 for gene expression; n=3-4 for calcium and compressive modulus).

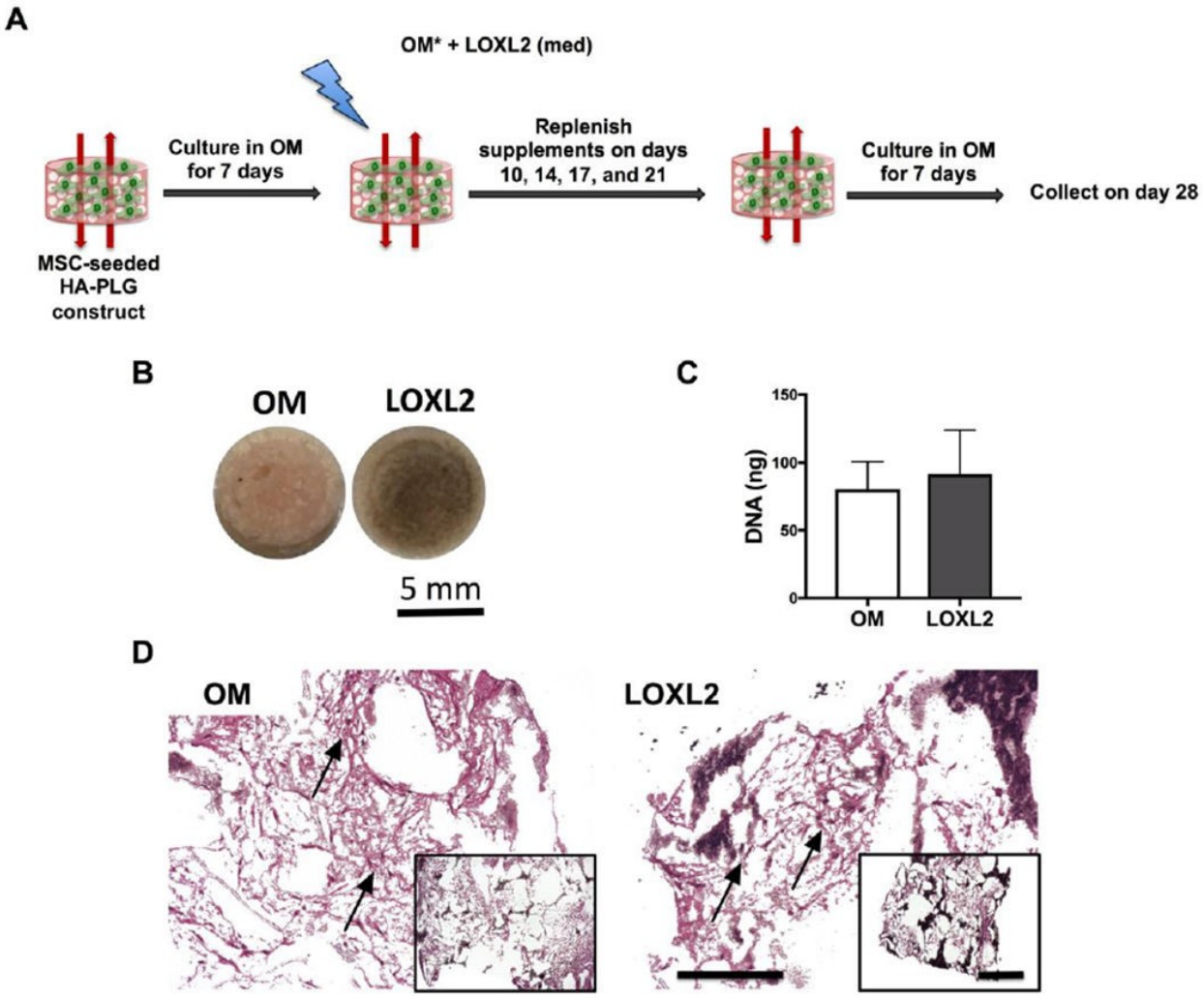

Figure A2-4. Effect of extended culture time on morphology and DNA content. (A) Schematic representing the LOXL2 supplementation regime for the 28-day study. (B) Gross morphology of constructs. (C) DNA content of constructs at 28 days (n=4). (D) Representative H&E images taken at 10× magnification (scale bar represents 200 μm) to visualize cellularity of constructs and insets taken at 4× magnification (scale bar represents 500 μm). Black is indicative of scaffold and some cells are denoted by black arrows. For (C), a lack of statistical significance was determined using an unpaired t-test.

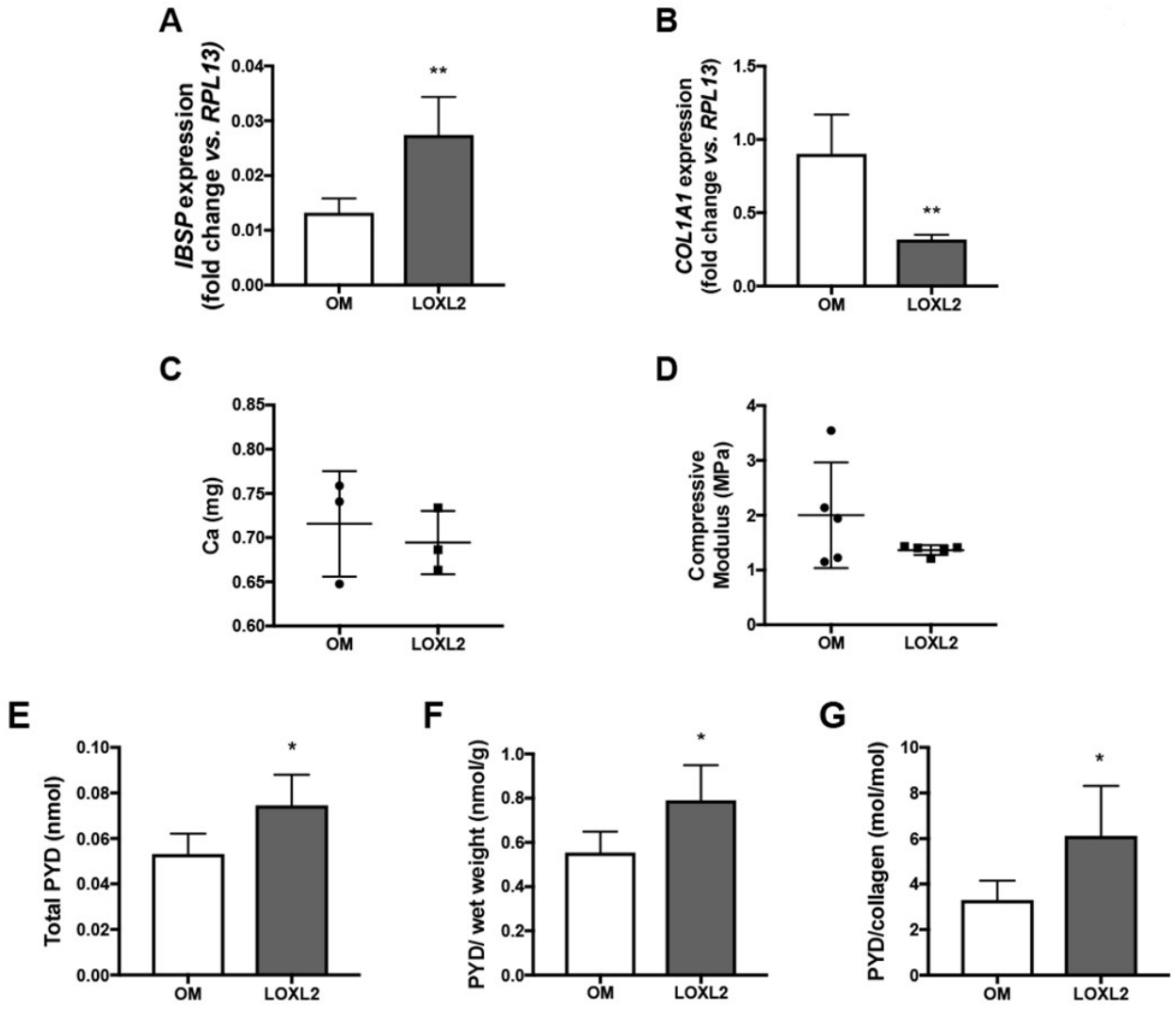

Figure A2-5. Effect of extended culture time on osteogenic differentiation and functional outputs.IBSP and (B) COL1A1 expression at 28 days. (C) Calcium quantification and (D) compressive moduli of constructs at 28 days. (E) Total PYD content at 28 days. (F) PYD content normalized to wet weight at 28 days. (G) PYD content normalized to collagen content at 28 days. For (A)-(G), unpaired t-tests were performed to determine statistical significance, which is denoted by an asterisk; groups with significance are indicated with an asterisk symbol *p<0.05 and **p<0.01 (n=4 for gene expression; n=3 for calcium; n=5 for compressive modulus, n=5 for PYD content).

APPENDIX 3 Characterization of adult and neonatal articular cartilage from the equine stifle

Abstract

Background: A significant portion of equine lameness is localized to the stifle joint. Effective cartilage repair strategies are largely lacking, however, recent advances in surgical techniques, biomaterials, and cellular therapeutics have broadened the clinical strategies of cartilage repair. To date, no studies have been performed directly comparing neonatal and adult articular cartilage from the stifle across multiple sites. An understanding of the differences in properties between the therapeutic target cartilage (i.e., adult cartilage) as well as potential donor cartilage (i.e. neonatal cartilage) could aid in selection of optimal harvest sites within a donor joint as well as evaluation of the success of the grafted cells or tissues within the host. **Objective:** Given the dearth of characterization studies of the equine stifle joint, and in particular neonatal stifle cartilage, the goal of this study was to measure properties of both potential source tissue and host tissue. **Methods:** Articular cartilage of the distal femur and patella was assessed in regard to two specific factors, age of the animal and specific site within the joint. Two age groups were considered: neonatal (<1 week) and adult (4-14 years). Cartilage samples were harvested from 17 sites across the distal femur and patella. It was hypothesized that properties would vary significantly between neonatal and adult horses as well as within age groups on a site-by-site basis. **Results:** Adult thickness varied by site. With the exception of water content, there were no significant biochemical differences among sites within regions of the distal femur (condyles, trochlea) and the patella in either the adult or neonate. Neonatal cartilage had a significantly higher water content than adult. Surprisingly, biochemical measurements of cellularity did not

Submitted to *Journal of Equine Veterinary Science* as: White JL, Salinas EY, Link JM, Hu JC, Athanasiou KA. Characterization of adult and neonatal articular cartilage from the equine stifle. (2020)

differ significantly between neonatal and adult, however adult cartilage had greater variance in cellularity compared to neonatal. Overall, there were no significant differences between neonatal and adult GAG content. Collagen per wet weight was found to be significantly higher in adult cartilage compared to neonatal when averaged across all levels. In terms of biomechanical properties, aggregate modulus varied significantly across the condyles of adult cartilage but not the neonate. Neonatal cartilage was significantly less permeable, and the Young's modulus of neonatal cartilage was significantly higher compared to the adult. The tensile strength did not vary in a statistically significant manner between age groups. **Conclusions:** An understanding of morphological, histological, biochemical, and biomechanical properties enhances the understanding of cartilage tissue physiology and structure-function relationships. This study revealed important differences in biomechanical and biochemical properties among the 17 sites and among the six joint regions, as well as age-related differences between neonatal and adult cartilage. These location and age-related variations are informative toward determining the donor tissue harvest site.

Introduction

The stifle joint is notable as the most complex joint in the body. Damage or developmental abnormalities affecting any component of this complex synovial joint can result in lameness and decreased mobility. Lameness associated with the stifle joint has been reported to comprise approximately 40% of hindlimb lameness cases.[1] The articular cartilage lining the ends of the long bones and articulating surface of the patella, plays a critical role in proper joint function. In addition to developmental disorders, traumatic injury to the articular cartilage of the stifle joint, underlying subchondral bone, or soft tissue structures within and surrounding the joint, such as ligaments, menisci, or joint capsule, can also result in osteoarthritis.[2] Reports of the incidence of osteoarthritis ranges from 3 to 32% of all stifle lameness that may be attributed to the disease process, with the medial femorotibial joint compartment being the most commonly affected in

horses.[3] Effective cartilage repair strategies are largely lacking in both human and veterinary medicine, however, recent advances in surgical techniques, biomaterials, and cellular therapeutics have greatly broadened the clinical strategies of cartilage repair.[4-8]

Advanced strategies for cartilage repair include grafting procedures such as osteochondral allograft transplantation system (OATS) and mosaicplasty, cellular based strategies such as autologous chondrocyte implantation (ACI) and matrix-assisted ACI (MACI), as well as particulated cartilage-based procedures such as cartilage autograft implantation system (CAIS).[8] A handful of these strategies utilize tissue from neonatal and juvenile tissue donor sources, including RevaFlexTM DeNovo® Arthrex Biocartilage®, capitalizing on the higher regenerative capacity of chondrocytes from younger donor sources.[9] While a number of these strategies are utilized routinely in human medicine, they are largely confined to the realm of research in the context of equine medicine. An ideal articular cartilage repair product would result in production of novel hyaline cartilage tissue that recapitulated the zonal architecture and hyaline composition of native articular cartilage and achieve lateral integration into surrounding healthy cartilage and underlying subchondral bone. It is therefore important to understand the properties of native cartilage in order to establish design criteria for potential therapeutics.

Properties of equine articular cartilage in health have been most extensively characterized in the metacarpophalangeal joint,[10-19] however, limited studies have been conducted in other joints such as the carpus,[20-25] cervical facet,[26] and stifle.[27] To date, no studies have been performed directly comparing neonatal and adult articular cartilage from the stifle on a site-by-site basis. An understanding of the differences between neonatal and adult cartilage can inform theories of the post-natal maturation process, especially when interpreted in conjunction with kinematic/loading force studies. Equine neonatal cartilage may also serve as donor tissue, both as a cell source for tissue engineering efforts as well as a matrix source for allograft procedures.[28,29] An understanding of the differences in properties between the therapeutic target cartilage (i.e., adult cartilage) as well as potential donor cartilage (i.e., neonatal cartilage) could aid in selection of

optimal harvest sites within a donor joint as well as evaluation of the success of the grafted cells or tissues within the host.

While a handful of studies have reported properties of stifle cartilage in the adult equine, the majority of these studies have only examined compressive and biochemical properties and have only measured properties from a small number of locations across the joint surface. Given the dearth of characterization studies of the equine stifle joint, and in particular neonatal stifle cartilage, the goal of this study was to measure properties of both potential source tissue and host tissue. Articular cartilage of the distal femur and patella was assessed in regard to two specific factors, age of the animal and location within the joint. It was hypothesized that properties would vary significantly between neonatal and adult horses as well as within age groups by location.

Materials and methods

Native tissue sample preparation

Equine stifle joints were isolated from six skeletally mature horses (4-14 yrs old, mean = 6.7 yrs old) and six neonatal foals (<1 wk old). All animals died or were euthanized for reasons unrelated to stifle joint pathology. Stifle joints were harvested within 48 hours of time of death. Animals were stored at 4˚C during this interim period of up to 48h. Stifle joints were isolated from the animal and stored at -20˚C with joint capsule kept intact until time of tissue harvest and testing. Upon opening the stifle joint, a macroscopic inspection of the cartilage was performed to check for any gross abnormalities suggestive of pathology, including osteoarthritis (OA) and osteochondrosis (OC). Horses whose cartilage showed gross signs of OA were excluded from this study. Articular cartilage samples were isolated from the patella (P) and five different regions of the distal femur – the medial condyle (MC), the lateral condyle (LC) the medial ridge of the trochlea (MR), the lateral ridge of the trochlea (LR), and the trochlear groove (TG). Within each of these regions, multiple sites were tested, three sites on MC, three sites on LC, three sites on MR, three sites on LR, three sites on TG, and two sites on P (Figure A3-1). Sites were isolated using an 8 mm biopsy

punch from the approximate locations detailed in Figure A3-1. For adult samples, the cartilage was trimmed off the underlying subchondral bone with a #10 scalpel blade. Neonatal samples were trimmed to ~2mm thickness (approximate junction between articular cartilage and underlying epiphyseal growth plate cartilage) using a custom jig and microtome blade. Each 8 mm punch was portioned for histological, biochemical, high-performance liquid chromatography, and biomechanical (compressive and tensile) evaluations (Figure A3-1).

Biomechanical evaluation

Creep indentation testing was performed on 3 mm cylindrical punches taken from the central portion of the larger 8 mm specimens collected from each region. This 3 mm punch was then photographed, and digital measuring tools (ImageJ) were used to determine the thickness at the center of the sample where the indenter tip was applied during testing. The sample was subsequently glued to the base of a cylindrical sample holder and submerged in PBS (Sigma). A 0.9 mm diameter, flat, porous indenter tip was applied to the samples under a 2 – 12 g load to achieve ~10% strain. The tissue was allowed to reach creep equilibrium while the deformation was recorded over time. Creep deformation data were then used to determine the aggregate modulus, shear modulus, and permeability of each sample using a linear biphasic model.[30]

For uniaxial tensile testing, specimens were trimmed into a dog-bone shape with a gauge length of 1.3 mm, in adherence with ASTM standards (ASTM D3039). Orientation of collagen fibers was determined by pricking the cartilage sample surface with a needle dipped in India Ink, which allowed for visualization of a split line running parallel to collagen fiber orientation. Specimens were trimmed such that the long-axis of the dog-bone was oriented parallel to collagen fiber alignment based on the India Ink staining. Samples were photographed to obtain the cross-sectional area of each sample using ImageJ. Paper tabs were glued to the samples outside the gauge length. These tabs were loaded into the grips of a TestResources mechanical tester (TestResources Inc.) and pulled at 1% of the gauge length per second until sample failure. Load

measurements were recorded over the duration of the test and used to generate stress-stain curves. Young's modulus was obtained by a least-squares fit of the linear region of the curve and ultimate tensile strength (UTS) was determined from the maximum stress at failure.

Biochemical evaluation

Full-thickness samples were portioned from each 8 mm biopsy punch for biochemical analysis including water, collagen, glycosaminoglycan (GAG), and DNA content. Samples were weighed before and after lyophilization to obtain wet weight (WW) and dry weight (DW) respectively. Water content of the tissues was determined using the difference between wet and dry weight for each sample. Lyophilized samples were digested in 125 μg/mL papain (Sigma) in 50 mM phosphate buffer (pH = 6.5) containing 2 mM N-acetyl cysteine (Sigma) and 2 mM EDTA (Sigma) at 60°C for 18 hours. Sulfated GAG content was measured using the Blyscan dimethyl methylene blue assay kit (Accurate Chemical). Collagen content was quantified by a perchloric acid-free, chloramine-T modified hydroxyproline assay[31] following hydrolysis with 2 N NaOH for 20 mins at 110ºC and using Sircol collagen (Accurate Chemical) as a standard. The Quant-iT PicoGreen dsDNA assay kit (Invitrogen) was used to measure the DNA content.

High-performance liquid chromatography

Full-thickness samples were portioned from each 8 mm biopsy punch for high-performance liquid chromatography (HPLC) in order to quantify pyridinoline crosslink content. For the HPLC assay, lyophilized samples were digested in 6N HCl at 100˚C for 24 h and then dried in a vacuum concentrator. Digested samples were resuspended in 500 μL of a solution containing 1.67 nmol pyroxidine/mL, 8.3% acetonitrile, and 0.41% heptafluorobutyric acid (HFBA) in water and then injected into a 25 mm C18 column (Shimadzu). Two solvents, (1) 24% methanol and 0.13% HFBA in water and (2) 75% acetonitrile and 0.1% HFBA in water, were sequentially flowed through the column for sample elution and column washing, respectively.[32]

Histological and immunohistochemical evaluation

Full-thickness samples partitioned from the 8mm punch for histological processing were fixed in 10% neutral buffered formalin, embedded in paraffin, and sectioned into 4 μm sections to expose the full thickness of the tissue. Sections were stained with Hematoxylin and Eosin, Safranin O/Fast Green for sulfated GAGs, and Picrosirius red for collagen. Immunohistochemistry (IHC) was performed to visualize collagen type I and collagen type 2. Following antigen retrieval with citric acid (pH 6) at 95°C for 20 min and at room temperature for an additional 20 min, anti-collagen I antibody (ab34710, Abcam) was applied at a 1:300 dilution. Antigen retrieval using 4 mg/mL hyaluronidase (Sigma) in PBS for 30 minutes followed by 3 mg/mL pepsin (Sigma) in 0.5% acetic acid for 30 min was used prior to application of anti-collagen II antibody (ab34712, Abcam) at a 1:600 dilution.

Statistical Analysis

An O'Brien test for unequal variances was performed for all quantitative measures. If variances were unequal, a Welch's test was performed. In the case of equal variances, analysis was performed by linear mixed model ANOVA treating animal as a random effect followed by Tukey's post hoc test. The statistical model included site (1, 2, 3), region (lateral condyle, medial condyle, lateral trochlear ridge, medial trochlear ridge, trochlear groove, and patella), age (adult vs. neonatal), and the interaction of joint region and age as fixed effects. Data are presented as mean ± standard deviation, and different letters denote significantly different groups at $p<0.05$.

Results

Gross morphology

All animals used in this study had articular cartilage of the femoropatellar joint that appeared healthy, with a smooth, glossy, white appearance. Thickness was measured for all sites in both neonatal and adult cartilage (Table A3-1). Neonatal cartilage thickness was limited to the depth

of the biopsy punch, and, thus, thickness was only measured for the purpose of compressive testing and was not analyzed for significant differences among sites or regions.

The thicknesses of adult cartilage varied significantly among sites within a region (Figure A3-2A) and among different regions (Figure A3-2B). The thickness of the MC1, MC2, and MC3 sites were 1.51 ± 0.35 mm, 1.80 ± 0.40 mm, and 2.14 ± 0.34 mm, respectively. MC3 was significantly thicker than MC1 and MC2. The thicknesses of the LC1, LC2, and LC3 sites were 1.50 ± 0.51 mm, 0.98 ± 0.21 mm, and 0.75 ± 0.08 mm, respectively. LC1 was significantly thicker than LC3, but not LC2. Interestingly, the thickness increased when moving from cranial to caudal on the medial condyle but decreased when moving from cranial to caudal on the lateral condyle. The thicknesses of the TG1, TG2, and TG3 sites were 1.70 ± 0.23 mm, 1.56 ± 0.30 mm, and 1.60 ± 0.36 mm, respectively. The thicknesses of the MR1, MR2, and MR3 sites were 1.35 ± 0.32 mm, 1.15 ± 0.20 mm, and 1.41 ± 0.38 mm, respectively. The thicknesses of the LR1, LR2, and LR3 sites were 1.95 ± 0.34 mm, 1.78 ± 0.17 mm, and 2.09 ± 0.30 mm, respectively. No significant differences were observed among the three sites for each trochlear region, however, for all trochlear regions the middle site (TG2, MR2, and LR2) was the thinnest site, albeit not significantly thinner that sites 1 and 3. Lastly, the thicknesses of the P1 and P2 sites were 1.95 ± 0.28 mm and 1.66 ± 0.35 mm, respectively, and did not differ significantly. In the adult, the overall thicknesses of each region were also compared, and it was determined that the thickness of MC, TG, LR, and P were significantly higher than those of MR and LC. The average thicknesses of MC, LC, TG, MR, LR and P were 1.82 ± 0.44 mm, 1.08 ± 0.44 mm, 1.62 ± 0.29 mm, 1.30 ± 0.31 mm, 1.94 ± 0.29 mm, and 1.80 ± 0.34 mm.

Histology

Histological staining was used to visualize tissue morphology and distribution of sulfated GAG and collagen (Figure A3-3). H&E staining of adult articular cartilage revealed that the condyles stained basophilic throughout all zones, whereas trochlear cartilage possessed eosinophilic

staining at the surface, and patellar cartilage had an intermediate phenotype that was more basophilic than trochlear cartilage but less basophilic than condylar cartilage. In neonatal articular cartilage, this phenotype was reversed, with the condyles showing less basophilic staining than the trochlea and patella. Overall, neonatal cartilage appeared more homogeneous and more cellular, however cell lacunae were more pronounced in adult cartilage. Safranin-O (with a Fast-green counterstain) was utilized to visualize sulfated GAG distribution. In both neonatal and adult cartilage, stain intensity was generally highest in the deep zone. In many regions of adult cartilage, staining was faint or absent in the most superficial region. This is likely an artifact of tissue processing, however, it suggests that this region may contain less GAG in adult cartilage compared to neonatal cartilage. A picrosirius red stain was used to visualize collagen distribution. Adult cartilage generally had higher staining intensity compared to neonatal cartilage, and in many cases, staining was more intense in the superficial zone. Immunohistochemistry for type I and II collaged showed consistently strong collagen II staining and faint collagen I staining for both adult and neonatal cartilages across all sites (Figure A3-4).

Biochemical properties

The biochemical content of articular cartilage in the different sites for each age group is shown in Tables A3-1 and A3-2. With the exception of water content, there were no significant biochemical differences among sites 1, 2, and 3 for each region (MC, LC, TG, MR, LR, and P) in either the adult or neonate. In the adult, the water content of M1 was significantly greater than that of M2, whereas in the neonate, the water content of M3 was significantly less than M2 and M1, and L1 was significantly less than L3. Averaging across all sites, the water content of neonatal and adult cartilage differed significantly with a mean water content of 80.98 ± 1.33% and 78.36 ± 1.06%, respectively. The variability in water content in neonatal cartilage was also significantly greater than adult cartilage. Comparing different regions within the neonatal cartilage revealed that MR,

LR, and P had significantly higher water content than both condyles, whereas in adult, the lateral and medial condyles had the highest water content (Figure A3-5A).

Collagen crosslinking was measured on a per collagen weight basis. There were no significant differences in collagen crosslinking between age groups or among sites and regions. Crosslinking trended higher in adult cartilage, however, the difference in average crosslink content between adult and neonatal cartilage was not statistically significant. Crosslink content in the adult had greater variance among regions compared to neonatal cartilage (Figure A3-5B).

There were no significant differences between neonatal and adult GAG/WW or GAG/DW, nor were there any significant differences among regions in neonatal cartilage. Adult cartilage, however, did differ significantly among regions with LC having significantly greater GAG/WW and GAG/DW than TG and MC. Interestingly, MC had the lowest GAG content in both adult and neonatal cartilage. GAG/WW averaged 2.86 ± 0.32% and 3.44 ± 0.60% in the neonate and adult, respectively. GAG/DW averaged 15.16 ± 2.20% 16.05 ± 2.70% in neonatal and adult, respectively (Figures A3-5C and A3-5D).

In regard to collagen content, Col/WW varied significantly between neonatal and adult cartilage when averaged across all levels at 10.61 ± 2.23% and 13.80 ± 1.54%, respectively. Col/DW, however, did not, with neonatal cartilage possessing 57.50 ± 14.24% and adult possessing 64.69 ± 9.27%. In the neonate, the regions of the trochlea had the highest collagen content, whereas in the adult, the condyles had the highest collagen content (Figures A3-5E and A3-5F).

Cellularity did not differ significantly between neonatal and adult, however adult cartilage had greater variability in cellularity compared to neonatal. Making the assumption of 7.7 pg of DNA per cell,[33] the cells/WW and cells/DW were calculated and averaged 18,631 ± 1,720 cells/mg and 99,830 ± 12,674 cells/mg, respectively, in the neonate and 24,209 ± 8,466 cells/mg and 112,706 ± 43,074 cells/mg, respectively, in the adult. Also, in the adult, the lateral condyle had significantly greater cellularity than all other regions (Figures A3-5G and A3-5H).

Biomechanical properties

The biomechanical properties at the different sites for each age group are shown in Tables A3-3 and A3-4. In regard to compressive properties, aggregate modulus varied significantly among sites 1, 2, and 3 in MC and LC of adult cartilage but not neonatal. In the adult, LC1 had a significantly higher aggregate modulus than LC3, and both MC1 and MC2 were significantly higher than MC3. Comparing adult and neonatal compressive properties revealed that adult aggregate modulus had a significantly greater amount of variability compared to neonatal, and neonatal cartilage possessed on average a significantly higher aggregate modulus with an average of 354 ± 43 kPa compared to the adult with an average of 282 ± 47 kPa. There were no significant differences among regions in the neonate, but in the adult, P was significantly higher than MC (Figure A3-6A).

Shear moduli also varied significantly among sites 1, 2, and 3 in the adult only, with site 1 significantly higher than site 3 for both MC and LC. There was no significant difference between the overall shear modulus of neonatal and adult cartilage, which were 216 ± 28 kPa and 155 ± 24 kPa, respectively, nor were there significant differences among regions in either age group (Figure A3-6B).

Permeability of adult cartilage was had greater variance than neonatal cartilage and also significantly higher on average. Neonatal cartilage had an average permeability of 3.26 ± 0.41 m4x10-15/N.s, while adult cartilage had an average permeability of 5.09 ± 0.66 m4x10-15/N.s. In the adult, permeability varied significantly among sites on the MC, with MC1 being significantly more permeable than both MC2 and MC3 (Figure A3-6C).

In regard to tensile properties, there were no significant difference among sites 1, 2, and 3 in either the neonatal or adult. The Young's modulus of neonatal cartilage demonstrated greater variance than the adult and was also significantly higher on average. Neonatal cartilage had a Young's modulus of 16.2 ± 3.9 MPa and adult cartilage had a Young's modulus of 9.6 ± 2.1 MPa, on average. In the neonate, the Young's modulus of MR was significantly lower than the condyles

and TG (Figure A3-7A). The UTS did not vary significantly between age groups. In the neonate, however, TG had a significantly higher UTS than MR and LR (Figure A3-7B).

Discussion

Despite its role as the most complex joint in the horse, the stifle joint is largely understudied in terms of its articular cartilage properties. Injury to the stifle joint is common in the equine athlete and repair strategies are lacking. Neonatal cartilage offers a potential source for both allogeneic tissue grafts or chondrocytes that may be used to generate repair tissue in vitro or in vivo. The purpose of this study, therefore, was to characterize the morphological, histological, biochemical, and biomechanical properties of the distal femur and patella in both neonatal and adult horses across the topography of the joint surface. It was hypothesized that these properties would vary between neonatal and adult horses as well as among locations within each age group. The hypothesis was confirmed as significant differences were found between adult and neonatal cartilage and among sites and regions within each age group in regard to morphologic and histologic features, as well as biochemical and biomechanical properties.

In terms of morphology, thickness of adult cartilage was analyzed in this study for variability across sites. Variability in thickness was most pronounced in the condylar regions: MC3 was significantly thicker than MC1 and MC2, whereas LC1 was significantly thicker than LC3, but not LC2. This pattern of increasing thickness of the medial condyle and decreasing thickness of the lateral condyle while moving from cranial to caudal across each condylar surface is consistent with a previous study that topographically examined cartilage thickness of the equine distal femur.[27] The thinner areas of each condyle (the cranial aspect of the medial condyle and caudal aspect of the lateral condyle) correspond to areas that have been demonstrated to experience the greatest amount of contact with underlying meniscal tissue,[34] supporting the theory that cartilage thickness may be influenced by mechanical forces.[17,35]

Similar to thickness, compressive biomechanical properties, aggregate and shear moduli, varied significantly among sites 1, 2, and 3 of the MC and LC of adult cartilage. This variability was not observed in neonatal cartilage. While neonatal cartilage possessed on average a significantly higher aggregate modulus, adult aggregate modulus had a significantly greater amount of variability across locations compared to neonatal cartilage. This finding is consistent with a study comparing biomechanical properties of cartilage in fetal, juvenile and adult equine cartilage at multiple sites, which found that fetal and juvenile cartilage possessed higher compressive properties compared to adult cartilage, but did not vary significantly among sites.[17] The results of this study are also consistent with a previous topographical study of the equine stifle, which found higher compressive properties at the cranial aspect of the condyles in adult horses.[27] Kinematic analysis of the equine study demonstrated that cranial and central area of the condyles corresponded with higher articular contact intensity compared to the more caudal aspect of the condyles.[36] These regions of increased contact intensity correspond with regions of higher compressive properties in the adult but not the neonate, further supporting the concept of a functional adaptation process in response to physiologic loading.

Interestingly, in the adult, the MC region had both the lowest compressive and tensile properties compared to all other regions. In a relatively small study of 47 horses, lesions in the medial femoral condyle and medial meniscus were more prevalent compared to the lateral condyle and meniscus.[37] The cranial pole of the medial meniscus undergoes less cranial-caudal translation and higher axial compressive strain compared to the lateral meniscus during physiologic loading.[38] The forces required to generate this meniscal strain on the cranial pole of the medial meniscus are primarily transmitted through the cranial and central aspect of the medial femoral condyle during locomotion and correspond with areas of higher compressive properties within the medial condyle. Over time, the high strain experience by the medial condyle may result in accelerated wear to the cartilage in this joint compartment and may explain the lower biomechanical properties measured in this region.

Measurements of cellularity did not differ significantly between the neonate and adult, however adult cartilage had greater variance in cellularity compared to neonatal cartilage. Upon histological examination, neonatal cartilage appeared more homogeneous and more cellular compared to adult cartilage. Studies of the equine fetlock joint in the adult have demonstrated variations in DNA content as great as 1.7-fold across this joint surface.[13] In this study, cellular content varied up to 1.9-fold in the adult equine stifle, with areas of higher cell content corresponding to areas with higher GAG content. This correlation between cellularity and GAG content was not found in neonatal cartilage, however. In general, cellularity of cartilage is thought to decrease with age, so the finding in this study of similar cellular content in both age groups was unexpected. Cellularity was determined by measuring DNA content and calculating cell number based on the assumption that most mammalian cells contain approximately 7.7 pg of DNA per cell.[33] This study measuring DNA quantity was performed in adult rat cells, and it is uncertain whether neonatal cells also contain comparable levels of DNA. Histologically, the neonatal chondrocytes appear to be smaller than the adult chondrocytes, and therefore may contain less nuclear DNA. This suggests that assuming neonatal and adult equine chondrocytes have 7.7 pg of DNA per cell may be an oversimplification and could inflate the number of adult chondrocytes compared to neonatal chondrocytes. Another potential explanation for the relatively high cellularity of adult cartilage in this study is that there may have been some early degenerative changes in the samples tested that were not detected upon gross examination, as one of the early changes in osteoarthritis is an increase in cellularity as well as GAG content.[39,40]

Histological staining also revealed that GAG distribution in both neonatal and adult cartilage was generally highest in the deep zone, and the superficial zone contained less GAG in adult cartilage compared to neonatal cartilage. This variation in GAG content corresponding with cartilage depth has also been observed in the equine fetlock.[41] Moreover, similar to fetlock cartilage, the degree of GAG variability across cartilage depth is higher in adult cartilage compared to neonatal cartilage.[41] Biochemical assays revealed that the MC region had the lowest

GAG content in both adult and neonatal cartilage, although, overall, there were no significant differences between neonatal and adult GAG content. This lower GAG content in the MC in the adult may explain lower compressive properties observed in the adult in this region, as GAG content has been shown to correlate positively with compressive properties.[42]

Adult cartilage generally had higher collagen staining compared to neonatal cartilage, and in many cases, staining was more intense in the superficial zone. Supporting this histological observation, Col/WW was found to be significantly higher in adult cartilage compared to neonatal when averaged across all regions. This phenomenon of higher collagen content in the superficial zone of adult equine cartilage compared to neonatal equine cartilage has also been previously observed in the fetlock joint.[41] In the neonatal stifle joint, the regions of the trochlea had the highest collagen content, whereas in the adult, the condyles had the highest collagen content. Collagen crosslinking trended higher in adult cartilage and had greater variance compared to neonatal cartilage. This increase in crosslinking as well as overall collagen content is similar to that observed previously in a study comparing neonatal cartilage and cartilage from yearling horses.[19]

While collagen content and crosslinking generally correlate positively with tensile properties,[42] surprisingly, the stiffness (Young's modulus) of neonatal cartilage was significantly higher on average in the neonate compared to the adult. In the neonate, the Young's modulus of MR was significantly lower than the condyles and TG. Cartilage tensile strength (UTS) did not vary significantly between age groups. In the neonate, however, the TG had significantly higher UTS than the MR and LR. The UTS values measured in the adult stifle in this study are slightly lower (average 5.4 MPa), but comparable to those of a study in which tensile strength was measured at sites on the medial femoral condyle and medial trochlear ridge and found to be 6.7 MPa and 10.7 MPa, respectively.[43] Higher tensile stiffness in neonatal compared to adult cartilage has been observed in a previous study of the equine metacarpophalangeal joint. This study[41] examined tensile properties as well as collagen fiber arrangement in neonatal and adult cartilage and found that tensile stiffness correlated with the amount of collagen fibers that were arranged

perpendicular to the surface (and thus perpendicular to the axis of tension). In adult cartilage, collagen fibers are primarily aligned parallel to the cartilage surface in the superficial zone and perpendicular to the surface in the deep zone. In neonatal cartilage, this collagen fiber alignment has not fully developed and, as a result, a greater proportion of collagen may have been aligned along the axis of tension, perhaps resulting in a higher measured stiffness.[41]

While much of this discussion highlights the differences between neonatal and adult cartilage, there are a number of similarities between cartilages of neonatal and adult horses as well. Neonatal cartilage possesses mechanical and biochemical properties comparable to adult cartilage, suggesting that neonatal cartilage could withstand the loading forces incurred in the adult. This has implications for allograft techniques that may utilize a younger donor source for tissue. Good long-term outcome of a graft is undoubtedly a function of whether the graft tissue adequately recapitulates the properties of surrounding native tissue, such that it is able to withstand physiologic loading.[44,45] Furthermore, mismatch between repair tissue and surrounding native tissue results in stress concentrations at the interface between native and repair tissue, which can result in an acceleration of tissue degradation and failure of repair.[46] Using neonatal donor tissue offers the benefit of increased regenerative capacity of tissue from a younger donor source,[9,28] which may facilitate lateral integration, while still closely matching properties of host cartilage at time of implantation. Similarities between adult and neonatal tissue properties may also be a consideration in regard to use of neonatal chondrocytes harvested from stifle joint tissue for tissue engineering purposes. It has been demonstrated that neocartilage generated from various locations within a joint possess mechanical properties that corresponded to their tissue of origin, i.e. chondrocytes harvested from joint regions with higher mechanical properties produced neocartilage with higher mechanical properties compared to other joint regions.[47] Given that neonatal cartilage possesses properties comparable that of adult cartilage, neonatal chondrocytes may produce tissue engineered neocartilage with comparable properties to adult tissue as well.

Overall, this study characterized multiple locations across the distal femur and patella. As with any topographical study, the resolution of the topographical mapping of the measured properties was limited by the number of sampling sites tested; increasing the number of sample sites would have allowed for a higher level of understanding of the structure-function relationship between tissue properties and tissue location within the joint. Loading forces experienced by the joint vary in a topographical manner as well. Therefore, in order to fully understand the relationship between tissue properties and tissue function, concomitant studies to determine forces experienced by articular cartilage during normal loading cycles will also need to be carried out. Additional age groups would further aid in the understanding of how loading influences maturation of articular cartilage, and how this maturation process manifests in regard to biochemical and biomechanical properties of the tissue. Another limitation of this study was the inability to acquire full-thickness neonatal articular cartilage samples, which prevented comparison to the thickness of the adult cartilage, as well as probing any relationships between cartilage thickness and function in the neonate. However, while trimming may have excluded a small portion of deeper neonatal cartilage, the lack of distinct articular cartilage zonal variation in neonates likely reduced the variability this technique could have caused in the results of other assays. Another major limitation of this study was the heterogeneity of the patient population used in this study, which undoubtedly contributed to the large amount of variability in biochemical and biomechanical results. This study specifically compared neonatal and adult cartilage as neonatal cartilage and chondrocytes may serve as an ideal donor source for allografts or chondrocytes for tissue engineering strategies aimed at repair of damaged articular cartilage in the adult equine athlete. The results of this study, therefore, can be utilized in the establishment of design criteria for future engineered equine articular cartilage products as well as aid in assessment of the performance of engineered tissues in both in vitro and in vivo contexts.

Conclusion

This study provides qualitative and quantitative properties of native articular cartilage from the stifle of both neonatal and skeletally mature adult horses. This study represents the first time neonatal articular cartilage was comprehensively and quantitatively examined from the stifle and compared to adult cartilage in a head-to-head manner. The examination revealed important differences as well as similarities in morphological, histological, biochemical, and biomechanical properties among sites within joint regions as well as age-related differences between neonatal and adult cartilage. An understanding of these location and age-related differences in properties between the therapeutic target cartilage (i.e., adult cartilage) as well as potential donor cartilage (i.e., neonatal cartilage) could aid in selection of optimal harvest sites within a donor joint as well as evaluation of the success of the grafted cells or tissues within the host. Additionally, this work furthers the knowledge of cartilage tissue physiology and structure-function relationships.

References

1 Singer ER, Barnes J, Saxby F, Murray JK. Injuries in the event horse: Training versus competition. The Veterinary Journal 2008;175:76–81. doi:10.1016/j.tvjl.2006.11.009.

2 Jiménez G, Cobo-Molinos J, Antich C, López-Ruiz E. Osteoarthritis: Trauma vs Disease. Osteochondral Tissue Engineering, vol. 1059, Cham: Springer International Publishing; 2018, pp. 63–83. doi:10.1007/978-3-319-76735-2_3.

3 De Lasalle J, Alexander K, Olive J, Laverty S. Comparisons among radiography, ultrasonography and computed tomography for ex vivo characterization of stifle osteoarthritis in the horse. Veterinary Radiology & Ultrasound 2016;57:489–501. doi:10.1111/vru.12370.

4 Huang BJ, Hu JC, Athanasiou KA. Cell-based tissue engineering strategies used in the clinical repair of articular cartilage 2016;98:1–22. doi:10.1016/j.biomaterials.2016.04.018.

5 Makris EA, Gomoll AH, Malizos KN, Hu JC, Athanasiou KA. Repair and tissue engineering techniques for articular cartilage. Nature Publishing Group 2014:1–14. doi:10.1038/nrrheum.2014.157.

6 Cokelaere S, Malda J, van Weeren R. Cartilage defect repair in horses: Current strategies and recent developments in regenerative medicine of the equine joint with emphasis on the surgical approach. The Veterinary Journal 2016;214:61–71. doi:10.1016/j.tvjl.2016.02.005.

7 Ortved KF, Nixon AJ. Cell-based cartilage repair strategies in the horse. The Veterinary Journal 2016;208:1–12. doi:10.1016/j.tvjl.2015.10.027.

8 McIlwraith CW, Fortier LA, Frisbie DD, Nixon AJ. Equine Models of Articular Cartilage Repair. Cartilage 2011;2:317–26. doi:10.1177/1947603511406531.

9 Smeriglio P, Lai JH, Dhulipala L, Behn AW, Goodman SB, Smith RL, et al. Comparative Potential of Juvenile and Adult Human Articular Chondrocytes for Cartilage Tissue Formation in Three-Dimensional Biomimetic Hydrogels. Tissue Engineering Part A 2015;21:147–55. doi:10.1089/ten.tea.2014.0070.

10 Brama PAJ, Holopainen J, van Weeren PR, FIRTH EC, Helminen HJ, Hyttinen MM. Influence of exercise and joint topography on depth-related spatial distribution of proteoglycan and collagen content in immature equine articular cartilage. Equine Veterinary Journal 2009;41:557–63. doi:10.2746/042516409X424162.

11 Brama PAP, Tekoppele JMJ, Bank RAR, van Weeren PRP, Barneveld AA. Influence of different exercise levels and age on the biochemical characteristics of immature equine articular cartilage. Audio, Transactions of the IRE Professional Group on 1999:55–61.

12 Brama PAJ, Holopainen J, van Weeren PR, Firth EC, Helminen HJ, Hyttinen MM. Effect of loading on the organization of the collagen fibril network in juvenile equine articular cartilage. J Orthop Res 2009;27:1226–34. doi:10.1002/jor.20866.

13 Brama PAJ, Tekoppele JM, Bank RA, Karssenberg D, Barneveld A, van Weeren PR.

Topographical mapping of biochemical properties of articular cartilage in the equine fetlock joint 2006:1–8.

14 Hyttinen MM, Holopainen J, René van Weeren P, Firth EC, Helminen HJ, Brama PAJ. Changes in collagen fibril network organization and proteoglycan distribution in equine articular cartilage during maturation and growth. Journal of Anatomy 2009;215:584–91. doi:10.1111/j.1469-7580.2009.01140.x.

15 Holopainen JT, Brama PAJ, Halmesmäki E, Harjula T, Tuukkanen J, van Weeren PR, et al. Changes in subchondral bone mineral density and collagen matrix organization in growing horses. Bone 2008;43:1108–14. doi:10.1016/j.bone.2008.07.254.

16 van der Harst MR, van de Lest CHA, DeGroot J, Kiers GH, Brama PAJ, van Weeren PR. Study of cartilage and bone layers of the bearing surface of the equine metacarpophalangeal joint relative to different timescales of maturation 2005:1–7.

17 Brommer H, Brama PAJ, Laasanen MS, Helminen HJ, van Weeren PR, Jurvelin JS. Functional adaptation of articular cartilage from birth to maturity under the influence of loading: a biomechanical analysis. Equine Veterinary Journal 2005;37:148–54.

18 Weeren PR, Firth EC, Brommer H, Hyttinen MM, Helminen HJ, Rogers CW, et al. Early exercise advances the maturation of glycosaminoglycans and collagen in the extracellular matrix of articular cartilage in the horse. Equine Veterinary Journal 2010;40:128–35. doi:10.2746/042516408X253091.

19 Brama P, Tekoppele JM, Bank RA, Barneveld A, van Weeren PR. Functional adaptation of equine articular cartilage: the formation of regional biochemical characteristics up to age one year. Equine Veterinary Journal 2000;32:217–21.

20 Vachon AM, Keeley FW, McIlwraith CW, Chapman P. Biochemical analysis of normal articular cartilage in horses. Am J Vet Res 1990;51:1905–11.

21 Palmer JL, Bertone AL, Malemud CJ, Carter BG, Papay RS, Mansour J. Site-specific proteoglycan characteristics of third carpal articular cartilage in exercised and

nonexercised horses. Am J Vet Res 1995;56:1570–6.

22 Palmer JL, Bertone AL, Malemud CJ, Mansour J. Biochemical and biomechanical alterations in equine articular cartilage following an experimentally-induced synovitis. Osteoarthritis and Cartilage 1996;4:127–37. doi:10.1016/S1063-4584(05)80321-8.

23 Murray RC, DeBowes RM, Gaughan EM, Zhu CF, Athanasiou KA. The effects of intra-articular methylprednisolone and exercise on the mechanical properties of articular cartilage in the horse. Osteoarthritis and Cartilage 1998;6:106–14. doi:10.1053/joca.1997.0100.

24 Murray RC, DeBowes RM, Gaughan EM, Mosier DE, Athanasiou KA. Variations in the Biomechanical Properties of Articular Cartilage of the Midcarpal Joint of Normal Horses. Veterinary and Comparative Orthopaedics and Traumatology 1995;8:11–8.

25 Murray RC, Zhu CF, Goodship AE, Lakhani KH, Agrawal CM, Athanasiou KA. Exercise affects the mechanical properties and histological appearance of equine articular cartilage. J Orthop Res 1999;17:725–31. doi:10.1002/jor.1100170516.

26 O'Leary SA, White JL, Hu JC, Athanasiou KA. Biochemical and biomechanical characterisation of equine cervical facet joint cartilage. Equine Veterinary Journal 2018;50:800–8. doi:10.1111/evj.12845.

27 Changoor A, Hurtig MB, Runciman RJ, Quesnel AJ, Dickey JP, Lowerison M. Mapping of donor and recipient site properties for osteochondral graft reconstruction of subchondral cystic lesions in the equine stifle joint. Equine Veterinary Journal 2006:1–7.

28 Yanke AB, Tilton AK, Wetters NG, Merkow DB, Cole BJ. DeNovo NT Particulated Juvenile Cartilage Implant. Sports Med Arthrosc Rev 2015;23:125–9. doi:10.1097/JSA.0000000000000077.

29 Taylor SEB, Lee J, Smeriglio P, Razzaque A, Smith RL, Dragoo JL, et al. Identification of Human Juvenile Chondrocyte-Specific Factors that Stimulate Stem Cell Growth. Tissue Engineering Part A 2016;22:645–53. doi:10.1089/ten.tea.2015.0366.

30 Athanasiou KA, Agarwal A, Muffoletto A, Dzida FJ, Constantinides G, Clem M. Biomechanical properties of hip cartilage in experimental animal models. Clinical Orthopaedics and Related Research 1995:254–66.

31 Cissell DD, Link JM, Hu JC, Athanasiou KA. A Modified Hydroxyproline Assay Based on Hydrochloric Acid in Ehrlich's Solution Accurately Measures Tissue Collagen Content. Tissue Engineering Part C: Methods 2017;23:243–50. doi:10.1089/ten.tec.2017.0018.

32 Bank RA, Beekman B, Verzijl N, de Roos JA, Sakkee AN, Tekoppele JM. Sensitive fluorimetric quantitation of pyridinium and pentosidine crosslinks in biological samples in a single high-performance liquid chromatographic run. J Chromatogr B Biomed Sci Appl 1997;703:37–44.

33 Bibbiani C, Tongiani R, Viola-Magni M. I. Quantitative determination of the amount of DNA per nucleus by interference microscopy. J Cell Biol 1969;42:444–51. doi:10.1083/jcb.42.2.444.

34 Ionescu LC, Lee GC, Garcia GH, Zachry TL, Shah RP, Sennett BJ, et al. Maturation state-dependent alterations in meniscus integration: implications for scaffold design and tissue engineering. Tissue Engineering Part A 2011;17:193–204. doi:10.1089/ten.TEA.2010.0272.

35 Wong M, Carter DR. Articular cartilage functional histomorphology and mechanobiology: a research perspective. Bone 2003;33:1–13. doi:10.1016/S8756-3282(03)00083-8.

36 Halley SE, Bey MJ, Haladik JA, Lavagnino M, Arnoczky SP. Three dimensional, radiosteriometric analysis (RSA) of equine stifle kinematics and articular surface contact: A cadaveric study. Equine Veterinary Journal 2013;46:364–9. doi:10.1111/evj.12127.

37 Adrian AM, Barrett MF, Werpy NM, Kawcak CE, Chapman PL, Goodrich LR. A comparison of arthroscopy to ultrasonography for identification of pathology of the equine stifle. Equine Veterinary Journal 2016;49:314–21. doi:10.1111/evj.12541.

38 Fowlie JG, Arnoczky SP, Stick JA, Pease AP. Meniscal translocation and deformation

throughout the range of motion of the equine stifle joint: An in vitro cadaveric study. Equine Veterinary Journal 2010;43:259–64. doi:10.1111/j.2042-3306.2010.00291.x.

39 Poole CA, Matsuoka A, Schofield JR. Chondrons from articular cartilage. III. Morphologic changes in the cellular microenvironment of chondrons isolated from osteoarthritic cartilage. Arthritis Rheum 1991;34:22–35. doi:10.1002/art.1780340105.

40 D'Lima DD, Hashimoto S, Chen PC, Colwell CW, Lotz MK. Impact of mechanical trauma on matrix and cells. Clinical Orthopaedics and Related Research 2001;391:S90–9. doi:10.1097/00003086-200110001-00009.

41 Oinas J, Ronkainen AP, Rieppo L, Finnilä MAJ, Iivarinen JT, van Weeren PR, et al. Composition, structure and tensile biomechanical properties of equine articular cartilage during growth and maturation. Sci Rep 2018;8:1–12. doi:10.1038/s41598-018-29655-5.

42 Athanasiou KA, Darling EM, Hu JC, DuRaine GD, Reddi AH. Articular Cartilage. 2nd Ed. Boca Raton: CRC Press; 2017. doi:10.1201/9781315194158.

43 Lewis CW, Williamson AK, Chen AC, Bae WC, Temple MM, Wong WV, et al. Evaluation of subchondral bone mineral density associated with articular cartilage structure and integrity in healthy equine joints with different functional demands. Am J Vet Res 2005;66:1823–9.

44 Koh Y-G, Lee J-A, Kim YS, Lee HY, Kim HJ, Kang K-T. Optimal mechanical properties of a scaffold for cartilage regeneration using finite element analysis. Journal of Tissue Engineering 2019;10:2041731419832133. doi:10.1177/2041731419832133.

45 Bowland P, Ingham E, Jennings L, Fisher J. Review of the biomechanics and biotribology of osteochondral grafts used for surgical interventions in the knee. Proc Inst Mech Eng H 2015;229:879–88. doi:10.1177/0954411915615470.

46 Kock NB, Smolders JMH, van Susante JLC, Buma P, van Kampen A, Verdonschot N. A cadaveric analysis of contact stress restoration after osteochondral transplantation of a cylindrical cartilage defect. Knee Surg Sports Traumatol Arthrosc 2008;16:461–8.

doi:10.1007/s00167-008-0494-1.

47 Paschos NK, Makris EA, Hu JC, Athanasiou KA. Topographic Variations in Biomechanical and Biochemical Properties in the Ankle Joint: An In Vitro Bovine Study Evaluating Native and Engineered Cartilage. Arthroscopy: the Journal of Arthroscopic and Related Surgery 2014;30:1317–26. doi:10.1016/j.arthro.2014.05.025.

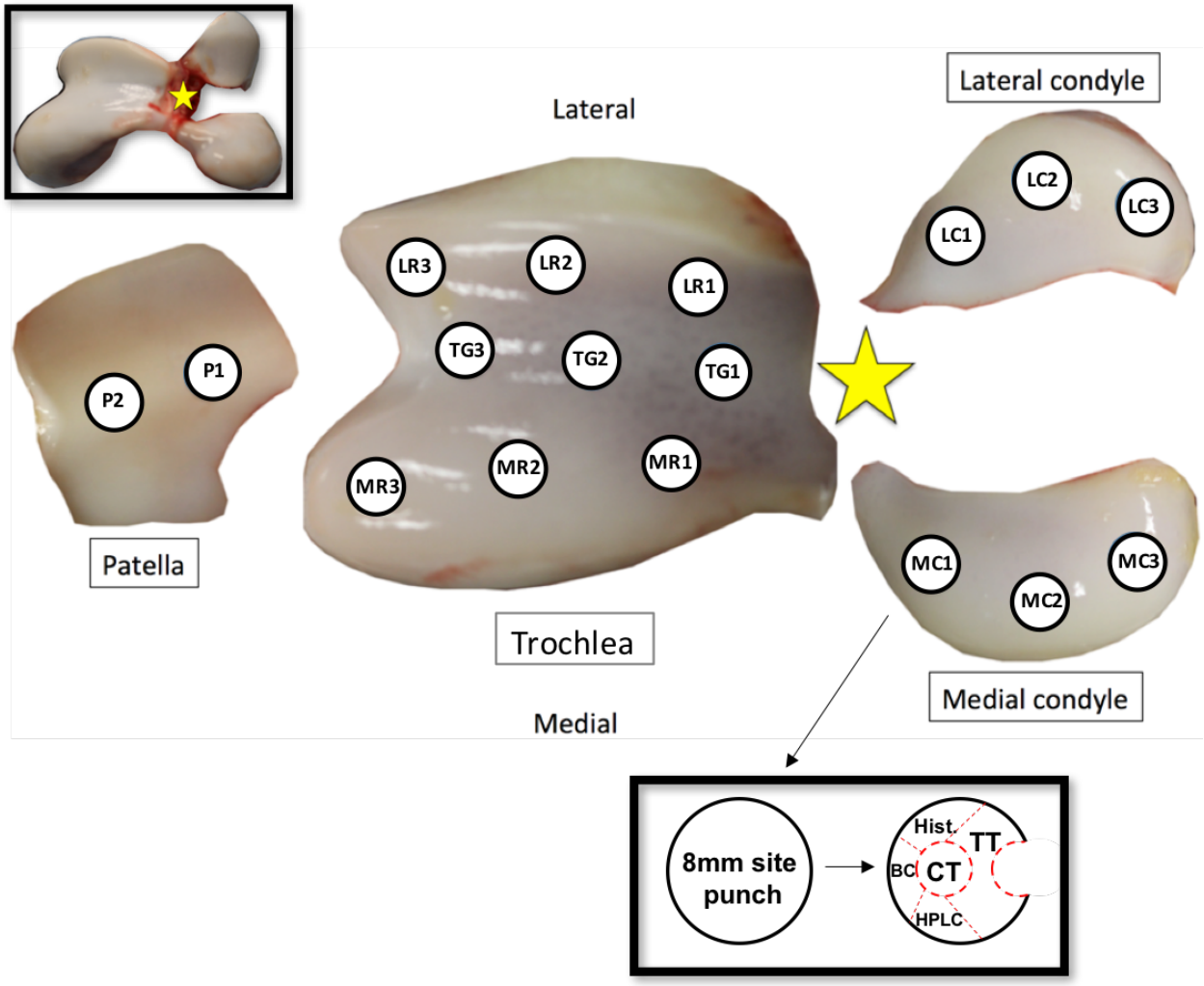

Figure A3-1. Articular cartilage from 17 sites across six regions of the distal femur and patella were characterized morphologically, histologically, biochemically, and biomechanically. The inset image at top left shows the distal femur with the star denoting the most axial portion of the joint surface. MC = medial condyle, LC = lateral condyle, LR = lateral ridge of the trochlea, MR = medial ridge of the trochlea, TG = trochlear groove, P = patella. The inset image at bottom right shows how the 8mm punch from each site was portioned for compression testing (CT), tensile testing (TT), biochemistry (BC), histology (Hist.), and high-performance liquid chromatography (HPLC).

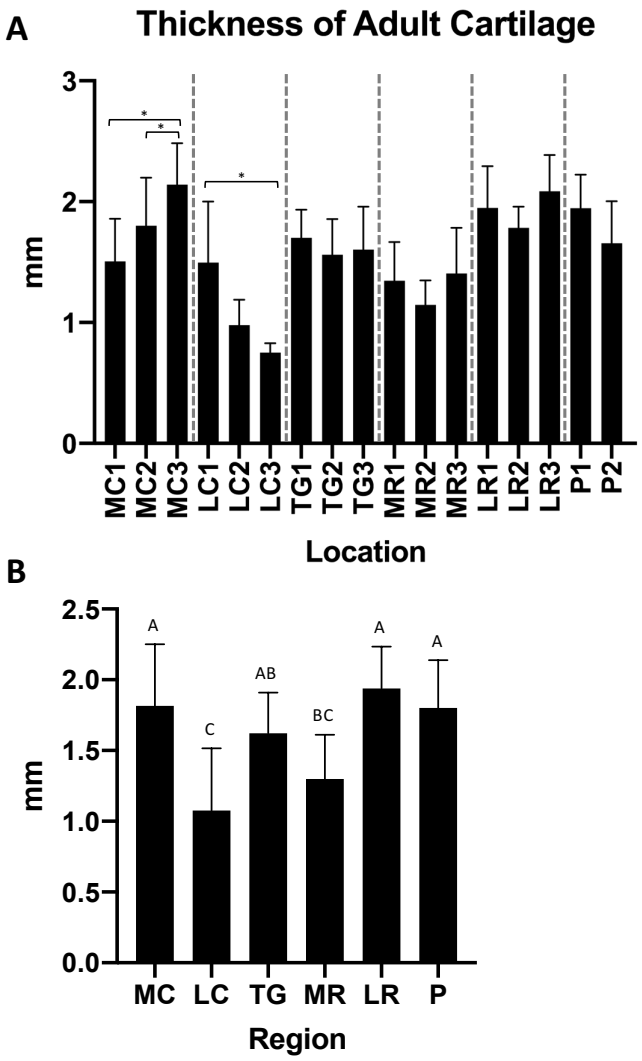

Figure A3-2. Thickness of adult articular cartilage. All values are presented as mean ± s.d. Thickness of neonatal cartilage was not assessed as subchondral bone is not completely mineralized in neonates. A) Average thickness at all sampled sites across the joint. Each region is denoted by dashed gray vertical bars. Sites were compared within each region and starred bars (*) represent significant differences among sites within an individual region. MC3 is thicker than MC1 and MC2, whereas LC1 is significantly thicker than LC3. B) Average thickness across sites within each region. Regions that share the same letter above the error bars do not differ significantly. MC, TG, LR, and P are thicker than LC and MR.

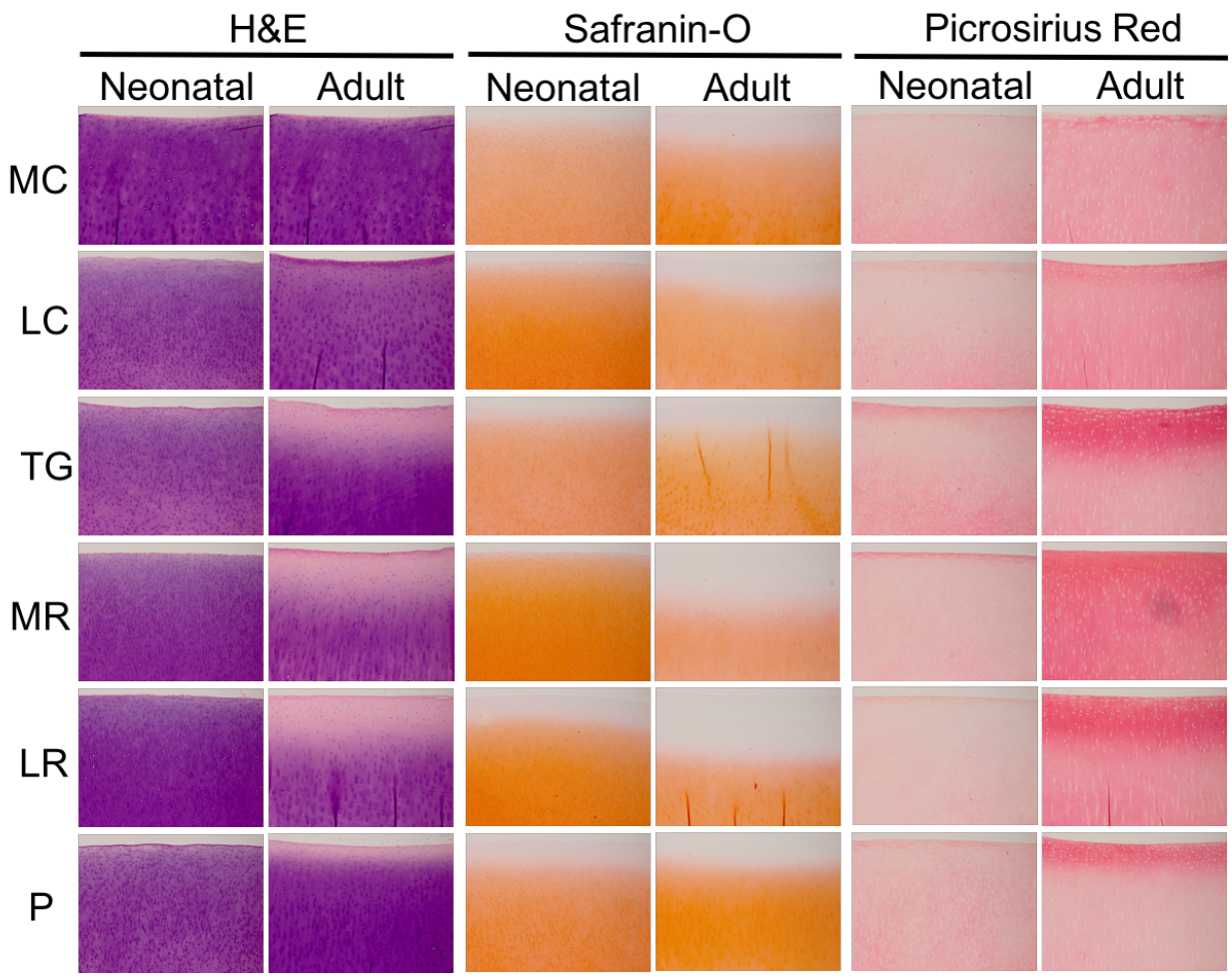

Figure A3-3. Histological evaluation of neonatal and adult articular cartilage cross sections from site 2 of each region. Neonatal cartilage stained more homogeneously basophilic with H&E stain as compared to adult cartilage. Adult cartilage stained eosinophilic in the superficial zone of the trochlear and patellar samples with H&E. Safranin-O stain for GAG was distributed through a greater proportion of neonatal cartilage compared to adult cartilage. Picrosirius red stain for collagen was more intense in adult cartilage compared to neonatal, particularly in the superficial zone.

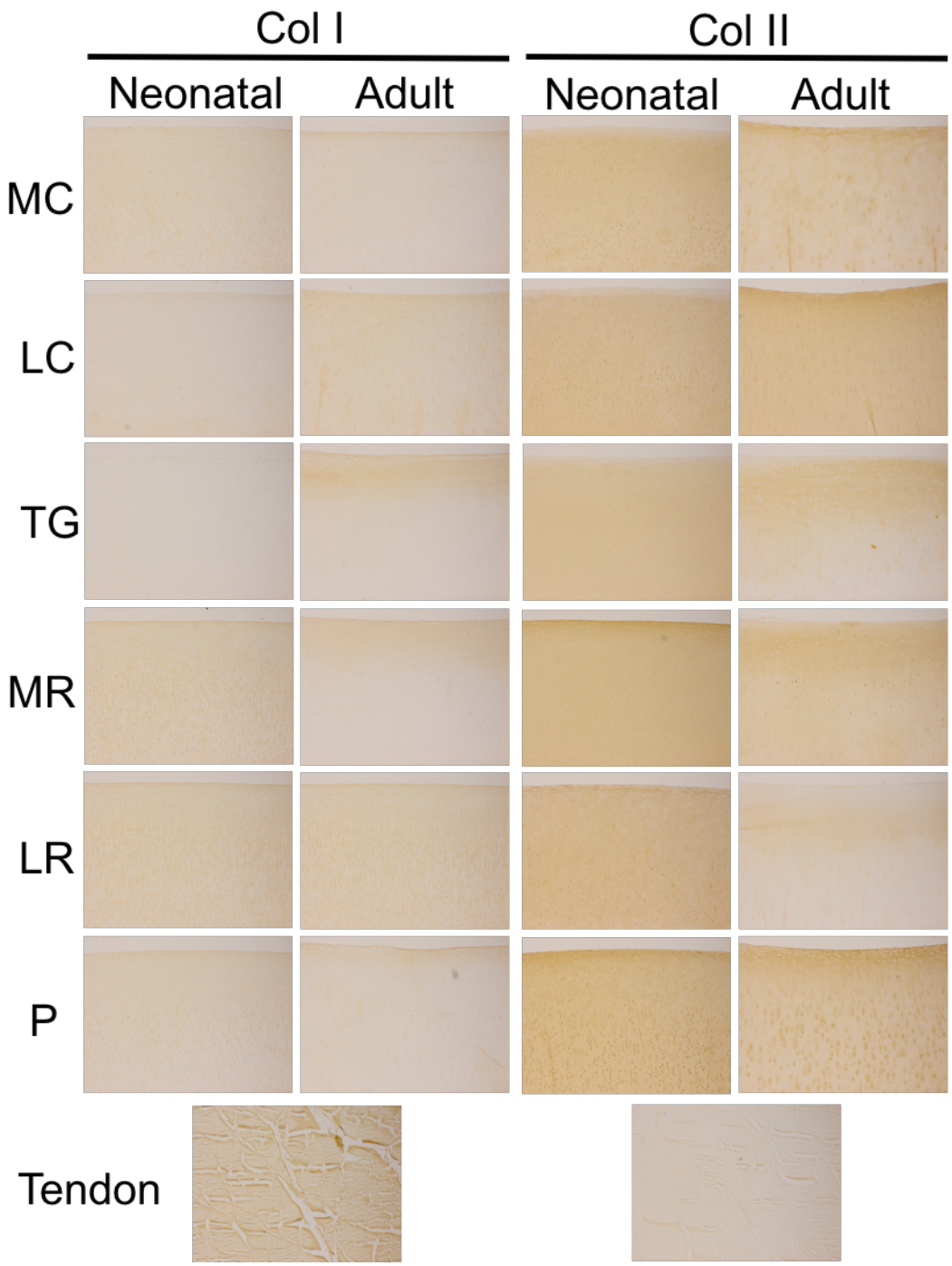

Figure A3-4. Immunohistochemical evaluation of neonatal and adult articular cartilage from site 2 of each region. Tendon, which is primarily comprised of collagen I, served as control. Both adult and neonatal cartilage stained more intensely for collagen II as compared to collagen I, whereas tendon stained more intensely for collagen I compared to collagen II. Overall, there were no dramatic differences between neonatal and adult cartilage in terms of specific collagen content staining using immunohistochemistry.

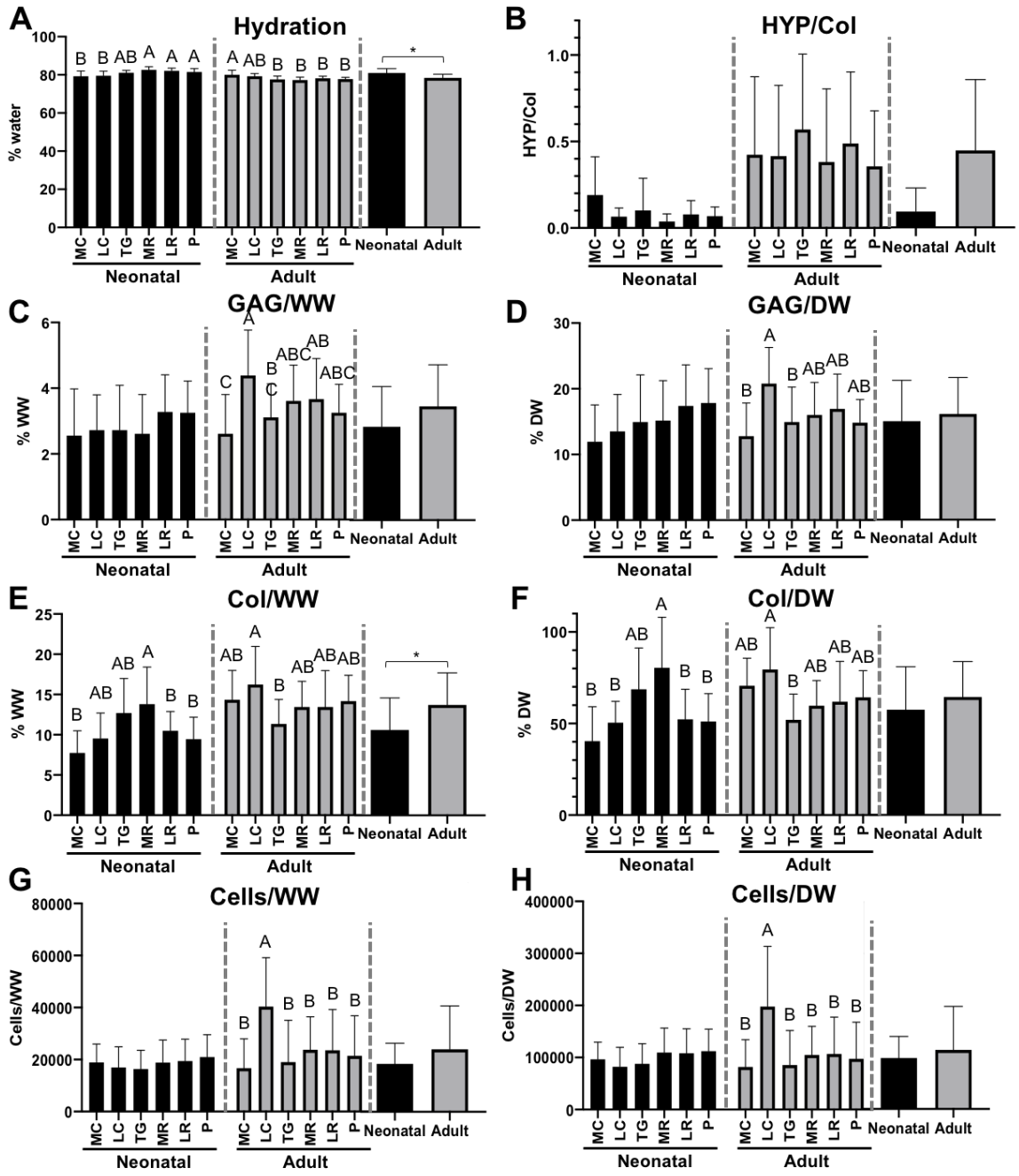

Figure A3-5. Biochemical characterization of regions and overall average for each age group: neonatal and adult. All values are presented as mean ± s.d. Starred bars (*) represent significant differences between age groups while regions that do not share the same letter within each age group differ significantly. (A) Hydration varied among regions in both the neonate and adult, and there was a significant difference of overall hydration between age groups. (B) Collagen cross linking (HYP) on a per collagen weight basis did not vary significantly among regions or between age groups, however, there was a trend for greater crosslinking in the adult. GAG varied among regions in the adult on a per wet weight (WW) (C) and per dry weight (DW) (D) basis. Collagen varied among regions in both the neonate and the adult on a per WW (E) and per DW (F) basis. Additionally, collagen/WW differed overall between the neonate and adult (E). Cellularity varied among regions in the adult on a per WW (G) and per DW (H) basis, but did not vary overall between the neonate and the adult. Topographical biochemical data are available in Tables A3-1 and A3-2.

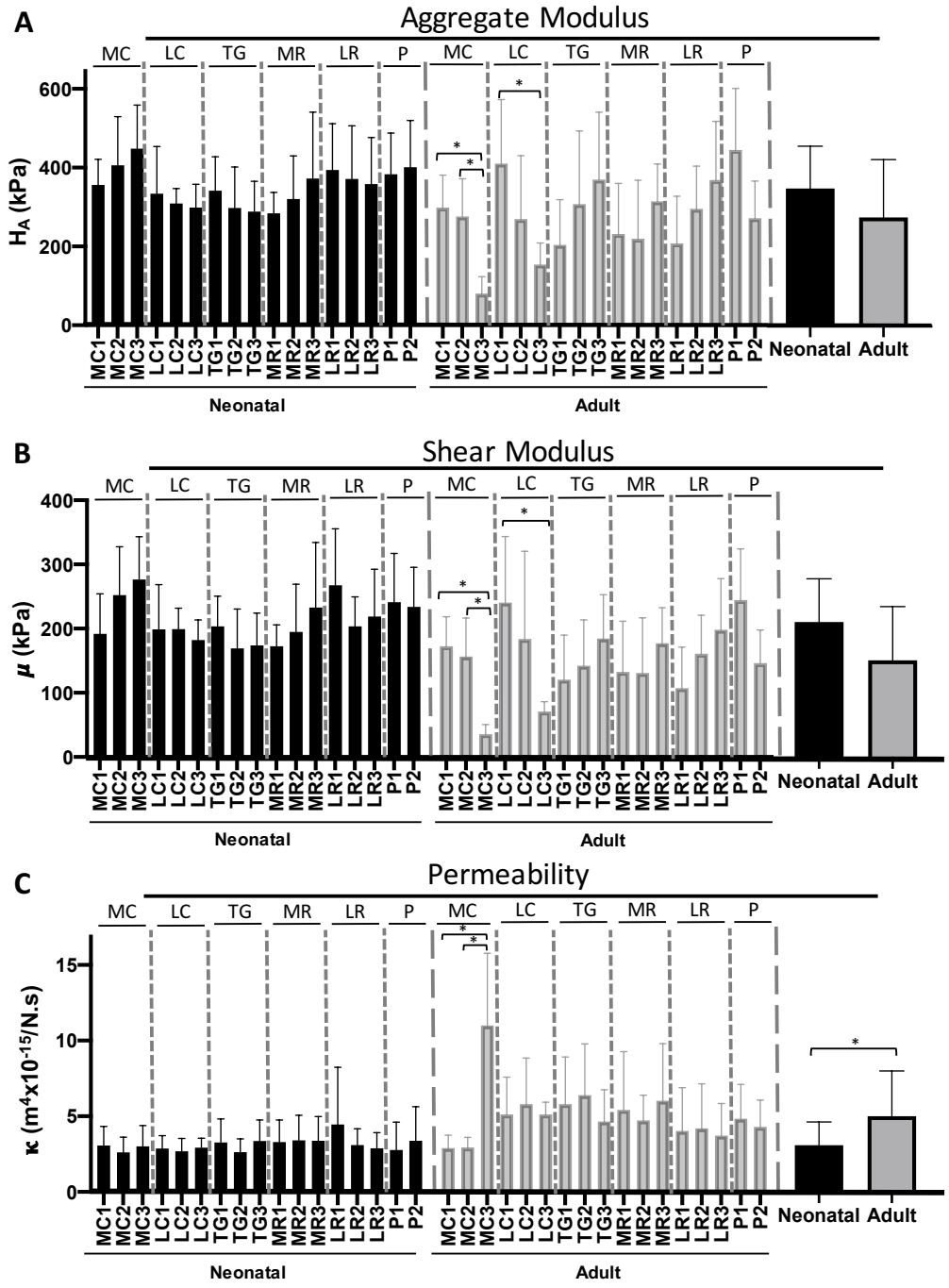

Figure A3-6. Characterization of compressive properties at each site within each region and overall average for each age group: neonatal and adult. All values are presented as mean ± s.d. Starred bars (*) represent significant differences among sites within each region as well as between overall averages of each age group. For both aggregate modulus (A) and shear modulus (B), MC1 and MC2 were significantly greater than MC3 and LC1 was significantly greater than LC3 in the adult. (C) Permeability was significantly greater in MC3 compared to MC1 and MC2 in the adult and varied significantly between the neonate and the adult overall. Topographical compressive property data are available in Table A3-3.

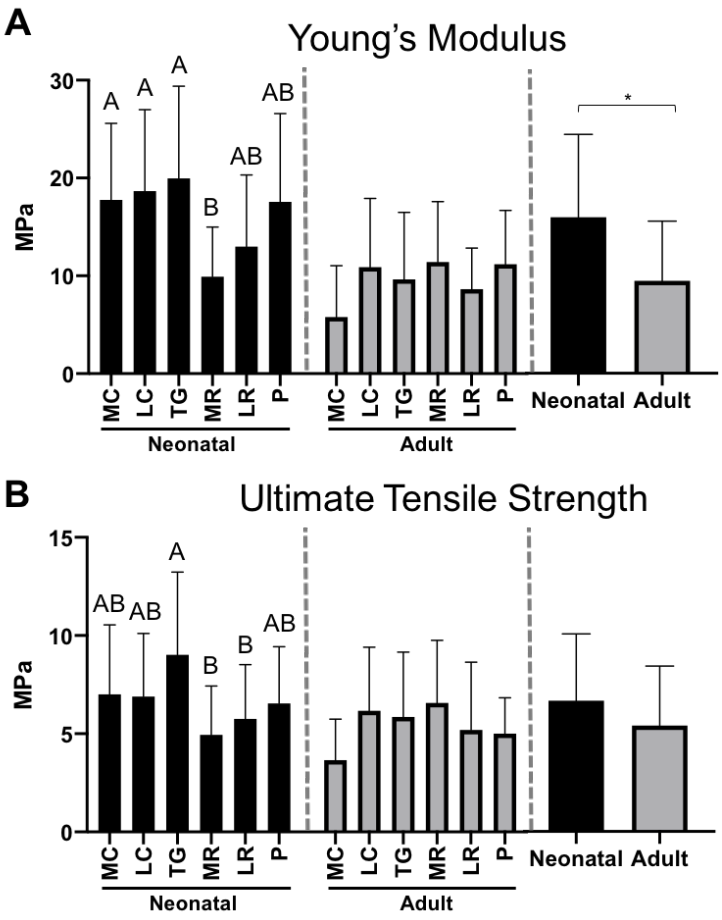

Figure A3-7. Characterization of tensile properties within each region and overall average for each age group: neonatal and adult. All values are presented as mean ± s.d. Starred bars (*) represent significant differences between age groups. Regions that do not share the same letter within each age group differ significantly. For both Young's modulus (A) and ultimate tensile strength (UTS) (B) there were significant differences among regions in the neonate but not adult cartilage. Neonatal cartilage had a significantly higher Young's modulus overall as compared to adult cartilage (A) as well.

Table A3-1. Thickness, hydration, and crosslinks per collagen of neonatal and adult articular cartilage from specific regions and sites within each region. Data are presented as mean ± s.d. Thickness of neonatal cartilage is not presented as neonatal cartilage thickness was limited to the depth of the punch and was only measured for the purposes of mechanical testing.

		Adult	Neonatal	Adult	Neonatal	Adult
Location		Thickness (mm)	Hydration (%)		HPLC/Col (ug/ug)	
Medial Condyle (MC)	1	1.51 ± 0.35	80.33 ± 1.75	78.00 ± 2.10	0.33 ± 0.33	0.19 ± 0.22
	2	1.80 ± 0.40	80.20 ± 3.35	81.33 ± 1.51	0.10 ± 0.10	0.60 ± 0.45
	3	2.14 ± 0.34	77.57 ± 2.07	80.67 ± 2.58	0.14 ± 0.12	0.48 ± 0.59
Lateral Condyle (LC)	1	1.50 ± 0.51	77.33 ± 0.75	78.33 ± 0.82	0.06 ± 0.03	0.40 ± 0.38
	2	0.98 ± 0.21	80.00 ± 1.67	79.17 ± 1.47	0.09 ± 0.08	0.40 ± 0.42
	3	0.75 ± 0.08	81.00 ± 0.75	80.33 ± 1.21	0.05 ± 0.02	0.45 ± 0.51
Trochlear Groove (TG)	1	1.70 ± 0.23	79.83 ± 2.50	78.00 ± 1.22	0.07 ± 0.08	0.65 ± 0.40
	2	1.56 ± 0.30	81.50 ± 1.67	78.00 ± 2.61	0.05 ± 0.02	0.52 ± 0.53
	3	1.60± 0.36	81.83 ± 1.55	76.83 ± 0.98	0.19 ± 0.32	0.54 ± 0.46
Medial Ridge (MR)	1	1.35 ± 0.32	83.33 ± 2.42	76.50 ± 1.05	0.04 ± 0.06	0.55 ± 0.48
	2	1.15 ± 0.20	82.50 ± 3.35	78.17 ± 1.60	0.02 ± 0.01	0.20 ± 0.30
	3	1.41 ± 0.38	81.83 ± 2.07	77.17 ± 1.47	0.06 ± 0.05	0.40 ± 0.48
Lateral Ridge (LR)	1	1.95 ± 0.34	81.67 ± 1.52	77.83 ± 0.75	0.06 ± 0.07	0.56 ± 0.49
	2	1.78 ± 0.17	82.67 ± 1.75	78.33 ± 0.82	0.07 ± 0.07	0.57 ± 0.42
	3	2.09 ± 0.30	81.83 ± 1.63	78.50 ± 1.52	0.11 ± 0.11	0.34 ± 0.38
Patella (P)	1	1.95 ± 0.28	80.50 ± 1.37	77.33 ± 1.21	0.07 ± 0.03	0.32 ± 0.34
	2	1.66 ± 0.35	82.33 ± 1.17	78.17 ± 0.41	0.06 ± 0.07	0.39 ± 0.33

Table A3-2. GAG, collagen, and cell number on a per wet weight (WW) and per dry weight (DW) basis of neonatal and adult articular cartilage from specific regions and sites within each region.

Location		Neonatal		Adult		Neonatal		Adult		Neonatal		Adult	
		GAG/WW (%)	GAG/DW (%)	GAG/WW (%)	GAG/DW (%)	Col/WW (%)	Col/DW (%)	Col/WW (%)	Col/DW (%)	Cell #/WW	Cell #/DW	Cell #/WW	Cell #/DW
Medial Condyle (MC)	1	2.33 ± 0.63	12.12 ± 6,55	3.17 ± 1.17	13.50 ± 3.62	6.67 ± 4.18	34.67 ± 19.03	16.17 ± 4.96	74.00 ± 21.20	19438 ± 7899	99897 ± 31054	22999 ± 13676	104887 ± 62547
	2	2.80 ± 1.47	13.00 ± 8.49	2.50 ± 1.38	13.83 ± 6.11	9.00 ± 1.22	57.00 ± 21.70	13.17 ± 2.79	68.00 12.38	20518 ± 6417	115661 ± 47423	12119 ± 6846	62445 ± 34672
	3	2.57 ± 1.26	11.14 ± 3.18	2.17 ± 0.98	11.00 ± 5.59	7.71 ± 1.80	33.43 ± 7.91	13.67 ± 2.66	69.83 ± 11.97	17330 ± 7519	79692 ± 45869	15005 ± 6967	78300 ± 55154
Lateral Condyle (LC)	1	2.33 ± 1.17	10.83 ± 5.53	4.50 ± 1.05	19.83 ± 4.36	11.67 ± 1.62	54.00 ±10.53	16.33 ± 1.75	75.00 ± 8.85	17186 ± 9244	81223 ± 44140	37912 ± 7211	175210 ± 103385
	2	3.00 ± 1.51	15.83 ± 7.41	4.83 ± 1.94	22.33 ± 7.47	11.20 ± 1.92	55.40 ± 9.10	18.67 ± 6.86	87.83 ± 30.93	17884 ± 7535	87071 ± 30094	51355 ± 20022	201229 ± 124836
	3	2.83 ± 1.51	13.83 ± 2.79	3.83 ±0.98	20.17 ± 4.88	8.67 ± 2.58	42.83 ± 12.06	13.20 ± 2.59	75.83 ± 24.59	15744 ± 8448	78426 ± 43025	32283 ± 8507	217376 ± 133904
Trochlear Groove (TG)	1	3.17 ± 1.37	16.00 ± 5.06	3.33 ± .82	16.50 ± 5.24	15.17 ± 4.67	77.67 ±24.97	11.33 ± 3.83	54.33 ± 20.75	15221 ± 7668	78098 ± 37127	11896 ± 7211	57553 ± 32795
	2	2.67 ± 1.10	15.33 ± 8.55	2.83 ± .75	14.33 ± 4.08	9.83 ± 3.54	55.33 ± 21.15	10.83 ± 3.54	49.67 ± 11.06	15975 ± 7124	86629 ± 37499	13830 ± 8104	64791 ± 3441
	3	2.33 ± 0.75	13.50 ± 8.46	3.17 ± 1.47	14.00 ± 6.90	13.00 ± 3.41	73.00 ± 18.37	11.83 ± 1.94	52.17 ± 9.89	17664 ± 8043	97495 ± 45014	30442 ± 21973	131066 ± 90432
Medial Ridge (MR)	1	3.00 ± 1.75	17.50 ± 5.68	3.50 ± 0.55	15.00 ± 3.52	12.17 ± 3.43	75.33 ± 23.01	13.50 ± 2.43	57.33 ± 10.11	16919 ± 7899	104931 ± 50480	28512 ± 11231	121703 ± 46462
	2	2.83 ±1.92	16.00 ± 5.66	4.00 ± 1.26	17.17 ± 5.71	12.00 ± 4.77	68.67 ± 28.32	12.50 ± 3.83	59.17 ± 16.62	17211 ± 9277	97576 ± 47413	25280 ± 16556	116364 ± 72597
	3	2.00 ± 0.79	12.00 ± 6.45	3.33 ± 1.37	15.83 ± 5.98	17.17 ± 4.12	97.33 ± 26.86	14.33 ± 3.44	62.67 ± 15.63	23163 ± 8873	129168 ± 45869	17374 ± 6967	74565 ± 28750
Lateral Ridge (LR)	1	3.50 ± 0.98	17.50 ± 3.39	3.50 ± 1.22	15.83 ± 4.31	9.67 ± 3.67	50.83 ± 17.17	11.33 ± 3.20	49.67 ± 14.56	15580 ± 7191	83247 ± 35566	20050 ± 17212	88966 ± 76922
	2	3.33 ± 0.82	19.83 ± 6.49	4.00 ± 1.79	19.00 ± 8.02	10.33 ± 3.50	59.33 ± 17.19	13.67 ± 6.50	64.33 ± 31.11	19387 ± 8238	113977 ± 49940	23565 ± 17936	107395 ± 78804
	3	3.00 ± 0.55	14.83 ± 7.99	3.50 ± 0.55	16.00 ± 2.19	8.50 ± 2.51	46.83 ± 14.81	15.33 ± 2.73	71.67 ± 13.03	23282 ± 9342	127229 ± 50080	27729 ± 13210	128023 ± 61199
Patella (P)	1	2.83 ± 1.21	15.17 ± 4.67	3.17 ± 1.17	14.33 ± 4.80	9.50 ± 3.21	48.83 ± 13.41	15.33 ± 3.93	69.50 ± 17.69	19214 ± 8540	97807 ± 39406	17374 ± 12545	77906 ± 55193
	2	3.67 ± 1.55	20.50 ± 4.59	3.33 ± 0.52	15.33 ± 1.97	9.33 ± 2.50	53.33 ± 17.80	13.00 ± 2.00	59.17 ± 9.50	22687 ± 9066	126603 ± 43078	26320 ± 18516	121318 ± 84902

Table A3-3. Compressive properties of neonatal and adult articular cartilage from specific regions and sites within each region.

Location		Neonatal			Adult		
		Aggregate Modulus (kPa)	Shear Modulus (kPa)	Permeability (m^4x10^{-15}/N.s)	Aggregate Modulus (kPa)	Shear Modulus (kPa)	Permeability (m^4x10^{-15}/N.s)
Medial Condyle (MC)	1	356 ± 53	192 ± 62	3.07 ± 1.26	307 ± 82	173 ± 79	2.9 ± 0.84
	2	406 ± 110	252 ± 75	2.61 ± 1.02	370 ± 96	157 ± 86	2.95 ± .65
	3	448 ± 169	277 ± 67	3.01 ± 1.34	81 ± 42	35 ± 56	11.00 ± 4.78
Lateral Condyle (LC)	1	334 ± 120	199 ± 70	2.87 ± 0.84	410 ± 162	241 ± 69	5.12 ± 2.46
	2	309 ± 38	199 ± 33	2.69 ± 0.84	270 ± 161	184 ± 72	5.80 ± 3.05
	3	299 ± 59	182 ± 31	2.92 ± 0.62	204 ± 54	71 ± 68	5.13 ± 0.80
Trochlear Groove (TG)	1	342 ± 86	204 ± 47	3.26 ± 1.57	204 ± 115	120 ± 103	5.80 ± 3.12
	2	297 ± 105	169 ± 61	2.63 ± 0.88	307 ± 186	142 ± 137	6.40 ± 3.39
	3	289 ± 76	174 ± 50	3.36 ± 1.40	370 ± 171	185 ± 15	4.66 ± 2.10
Medial Ridge (MR)	1	284 ± 53	172 ± 33	3.30 ± 1.45	231 ± 128	132 ± 46	5.42 ± 3.86
	2	320 ± 110	195 ± 74	3.40 ± 1.66	220 ± 148	131 ± 60	4.73 ± 1.68
	3	372 ± 169	233 ± 101	3.38 ± 1.60	315 ± 95	177 ± 15	6.03 ± 3.78
Lateral Ridge (LR)	1	394 ± 118	267 ± 88	4.45 ± 3.79	208 ± 120	107 ± 80	4.03 ± 2.87
	2	372 ± 134	204 ± 46	3.09 ± 1.08	295 ± 108	161 ± 52	4.20 ± 2.94
	3	358 ± 118	219 ± 74	2.88 ± 1.04	369 ± 149	198 ± 64	3.72 ± 2.12
Patella (P)	1	394 ± 118	267 ± 88	4.45 ± 3.79	445 ± 156	244 ± 60	4.84 ± 2.27
	2	401 ± 119	234 ± 62	3.38 ± 2.25	272 ± 95	146 ± 80	4.30 ± 1.77

Table A3-4. Tensile properties of neonatal and adult articular cartilage from specific regions and sites within each region.

		Neonatal		Adult	
Location		Young's Modulus (MPa)	UTS (MPa)	Young's Modulus (MPa)	UTS (MPa)
Medial Condyle (MC)	1	14.0 ± 4.1	6.6 ± 3.7	10.9 ± 6.2	4.9 ± 2.3
	2	17 ± 5.9	7.5 ± 3.6	4.1 ± 2.4	2.0 ± 1.7
	3	22.4 ± 10.7	7.0 ± 3.9	2.4 ± 1.1	3.7 ± 4.7
Lateral Condyle (LC)	1	21.2 ± 8.9	6.2 ± 2.5	12.5 ± 11.2	5.8 ± 3.5
	2	16.4 ± 8.9	6.2 ± 3.7	9.1 ± 3.1	5.3 ± 1.8
	3	18.4 ± 10.9	8.2 ± 3.5	11.1 ± 5.1	7.4 ± 4.1
Trochlear Groove (TG)	1	25.3 ± 10.7	12.1 ± 4.9	7.0 ± 7.0	4.1 ± 2.2
	2	22.0 ± 9.6	8.6 ± 2.4	9.4 ± 6.3	6.0 ± 2.8
	3	13.5 ± 4.1	6.4 ± 3.2	12.5 ± 7.1	7.5 ± 4.1
Medial Ridge (MR)	1	10.2 ± 7.3	5.1 ± 2.2	10.3 ± 6.4	7.2 ± 2.8
	2	11.0 ± 4.3	5.4 ± 2.0	9.5 ± 3.5	5.4 ± 1.7
	3	8.6 ± 3.6	4.4 ± 3.4	14.4 ± 7.7	7.1 ± 4.7
Lateral Ridge (LR)	1	15.2 ± 11.0	5.9 ± 2.5	8.8 ± 4.1	6.4 ± 4.3
	2	13.7 ± 6.8	6.4 ± 3.2	9.7 ± 5.3	5.1 ± 3.4
	3	10.1 ± 4.4	4.9 ± 2.9	7.4 ± 3.5	4.0 ± 2.6
Patella (P)	1	20.0 ± 11.3	7.5 ± 2.9	11.4 ± 4.7	5.4 ± 1.7
	2	15.1 ± 4.3	5.6 ± 2.8	11.0 ± 6.6	4.6 ± 2.0

APPENDIX 4 *In Vitro* Effects of Bupivacaine on the Viability and Mechanics of Native and Engineered Cartilage Grafts

Abstract

Background: Although the toxic effects of bupivacaine on chondrocyte monolayer culture have been well-described, its cellular and mechanical effects on native and engineered articular cartilage remain unclear. For the repair of articular cartilage defects, fresh autologous and allogeneic cartilage grafts are commonly used, and engineered cell-based therapies are emerging. The outcome of grafting therapies aimed at repairing damaged cartilage relies largely in maintaining proper viability and mechanical suitability of the donor tissues. **Hypothesis/Purpose:** To investigate the *in vitro* effects of single bupivacaine exposure on the viability and mechanics of two cartilage graft types: native articular cartilage and engineered neocartilage**. Study Design:** Controlled Laboratory Study. **Methods:** Articular cartilage explants were harvested from the bovine stifle femoral condyles, and neocartilage constructs were engineered from bovine stifle chondrocytes using the self-assembling process, a scaffold-free approach to engineer cartilage tissue. Both explants and neocartilage were exposed to chondrogenic medium containing 0.5%, 0.25%, or 0% (control) bupivacaine for 1 hour, followed by fresh medium wash and exchange. Cell viability and matrix content (collagen and glycosaminoglycan [GAG]) were assessed at t=24 hours post-treatment, and compressive mechanical properties were assessed with creep indentation testing at t=5-6 days post-treatment. **Results:** Single bupivacaine exposure was chondrotoxic in both explants and neocartilage, with 0.5% bupivacaine causing a significant decrease in chondrocyte viability compared to controls (55.0±13.4% vs. 71.9±13.5%; p<0.001)). Bupivacaine had no significant effect on matrix content

Submitted to *The American Journal of Sports Medicine* as: Oyadomari S, Brown WE, Kwon H, Otarola G, Link JM, Athanasiou KA, Wang D. *In vitro* Effects of Bupivacaine on the Viability and Mechanics of Native and Engineered Cartilage Grafts. (2020)

for either tissue type. There was significant weakening of the mechanical properties in the neocartilage when treated with 0.5% bupivacaine compared to control with decreased aggregate modulus (415.8±155.1 vs 660.3±145.8 kPa; p=0.003), decreased shear modulus (143.2±14.0 vs 266.5±89.2 kPa; p=0.002), and increased permeability (14.7±8.1 vs 6.6±1.7 $10^{-15}m^4/Ns$; p=0.009). Bupivacaine exposure did not have a significant effect on the mechanical properties of native cartilage explants. **Conclusion:** Single bupivacaine exposure resulted in significant chondrotoxicity in native explants and neocartilage and significant weakening of mechanical properties of neocartilage. The presence of abundant extracellular matrix does not appear to confer any additional resistance to the toxic effects of bupivacaine. **Clinical Relevance:** Clinicians should be judicious regarding use of intra-articular bupivacaine in the setting of articular cartilage repair. **What is known about the subject:** Many studies have shown that bupivacaine is toxic to chondrocytes in a time- and dose-dependent manner. However, the majority of these studies have been performed on monolayer culture. Some studies have suggested that the dense extracellular matrix of articular cartilage may confer a protective effect against the toxicity of these agents. **What this study adds to existing knowledge:** The findings of this study indicate that the dense extracellular matrix of the cartilage tissue does not confer resistance against the chondrotoxic effects of bupivacaine. Additionally, although the cellular toxicity of local anesthetics has been well established, whether the mechanical properties of the articular cartilage are similarly affected is unknown and not well studied to date. To our knowledge, this is the first study to demonstrate weakening of the mechanical properties of cartilaginous tissue induced by bupivacaine exposure, and this phenomenon may be dependent on tissue permeability.

Introduction

Local anesthetics are commonly used as intra-articular injections to reduce pain caused by acute injury, degenerative disease, or surgery.[11,33] Multiple studies have shown the deleterious effects of these anesthetics on chondrocyte viability with chondrotoxic effects occurring in a time- and

dose-dependent manner.[7,8,20,21,29] Historically, continuous infusion intra-articular pain pumps have been associated with frank chondrolysis.[16] Subsequent investigations have reported that significant chondrocyte death can still occur after a short exposure period, raising concern about the potential detrimental effects of single-injection local anesthetics.[8]

Despite concerning evidence demonstrating the chondrotoxicity of local anesthetics, there remains widespread clinical use of these agents for relief of symptoms due to the lack of obvious detrimental effects in the *in vivo* setting.[19,31] In both normal and anterior cruciate ligament (ACL)-transected knees of rats, weekly injections of 0.5% bupivacaine for five consecutive weeks did not induce any changes in chondrocyte viability compared to saline injection.[19] However, unlike humans, rodents can exhibit spontaneous articular cartilage repair due to life-long open growth plates and thinner cartilage.[24,35] Another reason for the skepticism regarding the chondrotoxicity of anesthetics is that the majority of studies examining the toxic effects have been performed on monolayer culture, which does not adequately simulate *in vivo* conditions of chondrocytes embedded within the hyaline extracellular matrix (ECM). Some studies have suggested that an intact ECM may confer a protective effect against the toxicity of these agents.[7,19,32] Even if chondrocyte viability diminishes, changes to the ECM may not occur, and therefore, the mechanical functionality of articular cartilage may remain intact. To date, the effects of local anesthetics on the ECM and mechanical characteristics of articular cartilage have not been well studied.

The purpose of this study is to evaluate the *in vitro* effects of bupivacaine, one of the most commonly used anesthetics, on two types of mature, ECM-dense cartilage grafts: native articular cartilage explants and engineered neocartilage. Native articular cartilage explants are representative of fresh autografts and allografts, which are frequently used clinically to treat articular cartilage damage in patients. Additionally, cell-based engineered cartilaginous tissues are emerging as therapeutic alternatives. The scaffold-free, self-assembling process produces robust neocartilage with abundant extracellular matrix.[18] This biomimetic neocartilage has

histological, biochemical, and mechanical properties similar to native articular cartilage (tensile and compressive stiffness of 6.4 MPa and 326 kPa, respectively, and coefficient of friction of 0.04),[12,13] and is a promising novel strategy being investigated for cartilage repair.[18,26,34] To examine the effects of bupivacaine, native articular cartilage and engineered neocartilage underwent single exposure to bupivacaine followed by quantification of chondrocyte viability, biochemical content, and mechanical properties. It was hypothesized that single bupivacaine exposure would cause chondrotoxicity and decreased mechanical properties in both native explants and neocartilage.

Materials and methods

Explant harvest

Full-thickness cartilage punches, 3 mm in diameter, were harvested from the femoral condyles of juvenile bovine stifle joints (n=3; Research 87, Boston, MA) less than 36 hours after slaughter using aseptic technique. All cadaveric specimens were grossly normal without any abnormalities of the articular cartilage. Punches were rinsed in Dulbecco's modified Eagle's medium (DMEM; Gibco) with high glucose/GlutaMAX™ and with 1% (v/v) penicillin/streptomycin/fungizone (PSF; BD Biosciences). Punches were trimmed to 1 to 2 mm thick, preserving the articular surface, superficial zone, and part of the middle zone. Explants were maintained in chondrogenic (CHG) medium (DMEM with high glucose/GlutaMAX™ containing 1% PSF, 1% (v/v) ITS+ premix, 1% (v/v) non-essential amino acids, 100 nM dexamethasone, 40 µg/mL L-proline, 50 µg/mL ascorbate-2-phosphate, 100 µg/mL sodium pyruvate; all from Sigma) and 3% (v/v) fetal bovine serum (FBS; Atlanta Biologicals) until bupivacaine exposure later that same day..

Neocartilage engineering

Articular cartilage was harvested from the femoral condyles and trochlea of juvenile bovine stifle joints (n=3; Research 87, Boston, MA) within 36 hours of slaughter. The cartilage was minced

into 1-2 mm^3 pieces and digested in 0.2% (w/v) type II collagenase (Worthington, Lakewood, NJ) in DMEM with 1% PSF and 3% FBS for 18 hours on an orbital shaker at 37˚C. Following digestion, chondrocytes were filtered through 70 µm cell strainers, resuspended in DMEM, and frozen in cryovials in liquid nitrogen until use. After thawing, primary (P0) chondrocytes were resuspended in CHG medium, and neocartilage constructs were formed using the self-assembling process as previously described.[18] Briefly, non-adherent self-assembly wells, 3 mm in diameter, were made from 2% (w/v) agarose and saturated with CHG medium for two days prior to construct seeding. Neocartilage constructs were seeded at a density of 1.62 x 10^6 P0 cells per construct in 50 µL of CHG medium into each 3 mm-diameter agarose well. Constructs were maintained at 37˚C and 10% CO_2. On day 7 constructs were unconfined from the self-assembly wells and transferred to a 24-well plate. Medium was changed daily until construct unconfinement, after which medium was exchanged every other day for the remaining duration of the 28-day culture. Constructs were exposed to bupivacaine on day 28 of culture.

Bupivacaine exposure

Both native explants and neocartilage constructs (n=6 per group) were exposed to CHG medium supplemented with 0.5% (w/v) bupivacaine, 0.25% (w/v) bupivacaine, or 0% bupivacaine (control) for 1 hour at 37˚ C at 50 RPM on an orbital shaker. Bupivacaine doses were calculated based on a standard clinical 10 mL bolus injection of medication into an adult human knee and accounting for a dilution from 6.7 mL of synovial joint fluid.[17] For example, a 10 mL bolus of 0.5% bupivacaine injected into a knee joint with 6.7 mL of synovial fluid yields a bupivacaine concentration of 3 mg/mL within the joint. Using this adjusted concentration, each group of native explants or constructs was placed in a well of a 12-well plate and incubated with 1.2 mL of appropriate bupivacaine-CHG medium dilution to allow for complete submersion of the tissues. Following bupivacaine exposure, explants and constructs were washed three times with CHG medium.

Explants and constructs were then maintained in individual wells in a 24-well plate in CHG medium at 37°C and 10% CO_2 until testing.

Viability assessment

Twenty-four hours after bupivacaine exposure, 1 mm thick, vertical cross sections were taken and incubated in 80 µL of CHG medium plus 80 µL of LIVE/DEAD reagent (calcein AM, ethidium homodimer-1; ThermoFisher) for 30 minutes. Sections were viewed with fluorescence microscopy using the Texas Red and GFP filters at 4x and 10x magnification. Images were analyzed with Image J. Three regions of interest (ROI) measuring 150 µm by 150 µm were taken from random, non-overlapping areas at least 100 µm below the surface. A macro was created using the auto local threshold, watershed, and analyze particles functions to count live and dead cells in order to calculate viability. An average was taken from these three ROIs to yield one measurement of viability per explant or construct.

Histological evaluation

Twenty-four hours after exposure, samples from explants and constructs were fixed in 10% neutral buffered formalin and embedded in paraffin. Cross sections, 4 µm thick, were stained with Hematoxylin and Eosin to assess cellular morphology, Picrosirius Red to assess total collagen distribution, and Safranin O to assess glycosaminoglycan (GAG) distribution.

Quantitative biochemistry

Twenty-four hours after exposure, samples from explants and constructs were weighed to measure their wet weights (ww). Samples were then lyophilized and weighed again to measure their dry weights (dw). Water content of the tissues was determined from sample weights before and after lyophilization. Lyophilized tissue samples were digested in 125 µg/mL papain in phosphate buffer at 60°C for 18 hours. Sulfated GAG content was measured using the Blyscan dimethyl methylene blue assay kit (Biocolor Ltd). Collagen content was quantified by a modified colorimetric chloramine-T hydroxyproline assay using a Sircol collagen assay standard (Biocolor

Ltd).[9] DNA content was measured with a PicoGreen cell proliferation assay (Quant-iT PicoGreen dsDNA assay kit). Collagen and GAG content were normalized to wet weight, dry weight, and DNA.

Creep indentation testing

A compression indentation apparatus[1] was used to assess creep of explants and neocartilage on day 5 or 6 post-exposure. Sample thickness was determined prior to testing using ImageJ software. As previously described,[18] a 0.55 mm-diameter, flat-ended, porous indenter tip was applied to the samples under a 2.5–3.5 g or 0.5–4.5 g load, and specimens were allowed to creep until reaching equilibrium, resulting in 5–18% or 8–15% strain for explants and constructs, respectively. A semi-analytical, semi-numerical, linear biphasic model and finite element analysis were used to obtain the aggregate modulus (H_A), shear modulus, and permeability (k) from the experimental data.[2]

Statistical analysis

Statistical analyses were performed using GraphPad Prism 8. Sample size (n=6 per group) was determined based on prior study data using viability as the primary outcome with alpha set at 0.05 and minimum power of 80%. For the mechanical data, all samples that experienced strains below 8% were excluded (n=3) to ensure conformity with the assumptions of the analytical model used. Statistical outliers were identified and removed before additional statistical analyses were performed. A two-way analysis of variance (ANOVA) with Tukey's post-hoc tests were used to determine differences caused by bupivacaine dose within tissue type for all quantitative data. In figures and tables showing quantitative data, statistical significance ($p<0.05$) is indicated by groups marked with different letters. All data are presented as means ± standard deviations.

Results

Chondrocyte viability

Overall, neocartilage had decreased chondrocyte viability compared to native explants (Figure A4-1). Histologically, chondrocyte death was localized at the tissue periphery in both groups (Figure A4-1A). Specimens exposed to bupivacaine exhibited reduced viability compared to control, irrespective of tissue type. Among all specimens (both explants and neocartilage), lower chondrocyte viability was observed in the 0.5% bupivacaine-treated specimens (55.0±13.4%; $p<0.001$) and 0.25% bupivacaine-treated specimens (62.0±13.0%; $p=0.054$) compared to controls (71.9±13.5%). Differences in mean chondrocyte viability between 0.5% and 0.25% bupivacaine-treated specimens were not significant. Both bupivacaine dose ($p=0.001$) and tissue type ($p<0.001$) were significant factors affecting chondrocyte viability with no significant interaction between factors (Figure A4-1B). Among the native explant groups, chondrocyte viability was significantly decreased in 0.5% bupivacaine-treated specimens (65.2±9.9%; $p=0.018$) and 0.25% bupivacaine-treated specimens (67.8±12.8%; $p=0.049$) compared to the control (82.0±9.8%). Among the neocartilage groups, chondrocyte viability was significantly decreased in 0.5% bupivacaine-treated specimens compared to control (44.8±7.0% vs 61.7±7.7%; $p=0.016$).

Histology

Cell morphology in both the native explants and neocartilage constructs did not appear to be affected by bupivacaine treatment (Figure A4-2). This was evident by the presence of many cells within lacunae, with elongated cells in the superficial zone and a columnar arrangement of cells in the deep zone. Collagen distribution within the native explants and neocartilage constructs also appeared unaffected by bupivacaine exposure (Figure A4-2). Among the native explants, collagen staining was more intense in the superficial and deep zones of all treatment groups. Among neocartilage constructs, collagen was homogeneously distributed throughout the tissue except

for intense staining localized at the periphery in all treatment groups. In contrast, GAG distribution did appear to be affected by bupivacaine exposure (Figure A4-2). Among the native explants, GAG staining was less intense in the superficial and mid zones in the groups that received 0.25% and 0.5% bupivacaine treatment. Among the neocartilage constructs, GAG staining was less intense throughout the tissue treated with 0.25% and 0.5% bupivacaine.

Quantitative biochemistry

Tissue type, but not bupivacaine dose, was a significant factor affecting tissue biochemical properties. Collagen/ww, collagen/dw, collagen/DNA, and GAG/DNA were greater in the explant groups compared to the neocartilage groups ($p<0.001$), while hydration, GAG/ww, and GAG/dw were greater in the neocartilage groups compared to the explant groups ($p<0.001$) (Table A4-1). Bupivacaine treatment did not have a significant effect on the biochemical content of both explants and neocartilage (Figure A4-3).

Compressive mechanical properties

Both bupivacaine dose ($p=0.021$) and tissue type ($p<0.001$) were significant factors affecting aggregate modulus, with no significant interaction between factors (Figure A4-4A). Among the self-assembled constructs, mean aggregate modulus for 0.5% bupivacaine-treated specimens (415.8±155.1 kPa) was significantly decreased compared to 0.25% bupivacaine-treated specimens (618.5±103.1 kPa; $p=0.012$) and controls (660.3±145.8 kPa; $p=0.003$). Bupivacaine dose did not have a significant effect on aggregate modulus among native explants.

Both bupivacaine dose ($p=0.015$) and tissue type ($p=0.011$) were significant factors affecting shear modulus, with no significant interaction between factors (Figure A4-4B). Among the self-assembled constructs, mean shear modulus for 0.5% bupivacaine-treated specimens (143.2±14.0 kPa) was significantly decreased compared to 0.25% bupivacaine-treated specimens (237.7±48.6 kPa; $p=0.018$) and controls (266.5±89.2 kPa; $p=0.002$). Bupivacaine dose did not have a significant effect on shear modulus among native explants.

Finally, both bupivacaine dose (p=0.021) and tissue type (p=0.011) were significant factors affecting permeability, with a significant interaction between factors (p=0.021) (Figure A4-4C). Among the self-assembled constructs, mean permeability for 0.5% bupivacaine-treated specimens (14.7±8.1 $10^{-15}m^4/Ns$) was significantly increased compared to 0.25% bupivacaine-treated specimens (4.4±1.8 $10^{-15}m^4/Ns$; p=0.001) and controls (6.6±1.7 $10^{-15}m^4/Ns$; p=0.009). Bupivacaine dose did not have a significant effect on permeability among native explants.

Discussion

In this study, single exposure of native articular cartilage explants and neocartilage constructs to clinically relevant doses of bupivacaine resulted in significant chondrotoxicity and changes in tissue mechanics. The findings of this study suggest that the existence of abundant extracellular matrix within native cartilage and neocartilage tissue does not confer any additional resistance to the chondrotoxic effects of bupivacaine. However, the effect of bupivacaine on tissue mechanics may be less deleterious for native cartilage tissue compared to tissue-engineered neocartilage.

The chondrotoxic effect of bupivacaine is well known and has been the subject of study by a number of groups.[7,8,20,21,29,30] This effect is dose-dependent, with higher concentrations of bupivacaine exhibiting more chondrotoxicity.[4,5,7,10,15,30] Similar dose-dependent effects were observed in both cartilage tissue types in this study. Although the majority of prior studies have been performed using monolayer cell culture, recent studies examining the effects of bupivacaine on intact tissue explants have found similar chondrotoxicity.[10,14,28,30] Sherman et al. found that 1hour exposures of canine cartilage explants to 0.25% and 0.125% bupivacaine both had chondrotoxic effects with corresponding decreases in metabolic activity.[30] In an *in vivo* rat study, Chu et al. demonstrated that a single intra-articular injection of 0.5% bupivacaine resulted in a reduction in chondrocyte density after six months.[6] The outcomes of the present study support the growing body of literature which demonstrates that bupivacaine is chondrotoxic to cartilage, despite the presence of intact extracellular matrix.

The primary function of articular cartilage is to provide low-friction articulation and absorption of joint loads. Thus, it is critical that cartilage mechanics not be affected by the administration of anesthetics. Although the cellular toxicity of local anesthetics has been well established, whether the mechanical properties of the articular cartilage are similarly affected is unknown and not well studied to date. This study found that the aggregate modulus and shear modulus of neocartilage constructs was significantly diminished 5 to 6 days after single bupivacaine exposure, indicating a loss of load-bearing and energy dissipation capabilities of the tissue. It was also shown that 0.5% bupivacaine exposure resulted in an increase of neocartilage permeability compared to 0.25% bupivacaine or control. Furthermore, this study found that neocartilage was more susceptible to an increase in permeability from high-dose bupivacaine exposure compared to native explants. This increased permeability may contribute to the decrease in compressive mechanical properties observed among the neocartilage constructs, but not among native explants, as a result of fluid exudation. Importantly, human cartilage is more permeable than bovine cartilage and, therefore, may be further susceptible to bupivacaine-induced changes than those demonstrated by this study.[3] Although this study did not find any significant changes in the compressive mechanical properties of native explants following bupivacaine exposure, a single measurement at 5 to 6 days after exposure may not have allowed sufficient time for alterations in the matrix and tissue mechanics to develop. It is postulated that substantial chondrocyte death would initiate a cascade of decreased matrix production and consequently, loss of mechanical functionality over time. Therefore, longitudinal assessment of cartilage mechanics over a longer period of time after single bupivacaine exposure is warranted.

The findings of this study caution against the use of intra-articular bupivacaine, which is commonly administered during surgery to reduce postoperative pain, in the setting of articular cartilage repair. Cell-based approaches to cartilage repair, such as Matrix-induced Autologous Chondrocyte Implantation (MACI) are becoming commonly used, with many additional products in clinical development.[22] The neocartilage constructs used in this study are fabricated using the

cell-based, scaffold-free, self-assembling process that generates scaffold-free neocartilage with abundant extracellular matrix and compressive, tensile, and low-friction properties similar to those of native articular cartilage.[12,13,18,23,25,34] This neocartilage has been investigated for cartilage repair in the knee and temporomandibular joint and demonstrated outstanding healing and prevention of osteoarthritis compared to empty defect controls in preclinical animal models.[34] This study showed that neocartilage was more susceptible to bupivacaine-induced reduction in mechanical properties. Compared to self-assembled neocartilage, MACI and other cell-based implants contain less mature matrix and are likely more permeable than the neocartilage tested in this study. Therefore, these implants may be even more susceptible to the chondrotoxic effects of bupivacaine and the corresponding deterioration of mechanical integrity. Additionally, most cartilage repair implants also lack a robust lamina splendens, which serves as a protective barrier to intra-articular elements.[7] Cartilage changes associated with OA, such as fibrillation and increased hydration, may similarly make the tissue more susceptible to bupivacaine toxicity. Greater anesthetic-induced chondrotoxicity has been noted in osteoarthritic cartilage compared to intact cartilage,[5,21] and further weakening in the biomechanical properties of osteoarthritic cartilage may occur from bupivacaine exposure.

While this study presents compelling data demonstrating the negative effects of bupivacaine on chondrocyte viability and cartilage mechanics, there are several notable limitations. Biochemical measurement was performed once at 24 hours after bupivacaine exposure (concurrently with viability measurement) and was not performed at the same time as creep indentation testing, precluding correlation of biochemical and mechanical results. Second, this *in vitro* study may not have accurately represented *in vivo* conditions regarding bupivacaine exposure time, dosage, and clearance from the joint. Third, chondrocytes used to generate neocartilage were isolated from the femoral condyles and the trochlea, whereas the explants were only harvested from the femoral condyles. It has been shown that neocartilage generated from cells derived from different topographical areas within the bovine patellofemoral joint have

different functional properties.[27] Finally, native explants in this study only consisted of the superficial and middle zones and did not contain the deep zone, and bupivacaine sensitivity may differ among each zone of cartilage.[32] Despite these limitations, this study reports the effects of bupivacaine on both native and engineered cartilage tissues and encourages further, in-depth analyses of alterations in cartilage matrix composition and mechanical properties resulting from local anesthetic exposure.

Single bupivacaine exposure resulted in dose-dependent chondrotoxicity to native explants and neocartilage, both extracellular matrix-dense tissues. Additionally, single bupivacaine exposure significantly increased the permeability and weakened the compressive mechanical properties of neocartilage. The existence of abundant extracellular matrix does not appear to confer any additional resistance to the chondrotoxic effects of bupivacaine. Furthermore, tissue permeability appeared to influence the susceptibility of the tissue to dose-dependent decreases in mechanical properties. Clinicians should be judicious regarding use of intra-articular bupivacaine in the setting of articular cartilage repair.

References

1 Athanasiou KA, Agarwal A, Dzida FJ. Comparative study of the intrinsic mechanical properties of the human acetabular and femoral head cartilage. J Orthop Res. 1994;12(3):340-349.

2 Athanasiou KA, Agarwal A, Muffoletto A, Dzida FJ, Constantinides G, Clem M. Biomechanical properties of hip cartilage in experimental animal models. Clin Orthop Relat Res. 1995(316):254-266.

3 Athanasiou KA, Rosenwasser MP, Buckwalter JA, Malinin TI, Mow VC. Interspecies comparisons of in situ intrinsic mechanical properties of distal femoral cartilage. J Orthop Res. 1991;9(3):330-340.

4 Baker JF, Walsh PM, Byrne DP, Mulhall KJ. In vitro assessment of human chondrocyte viability after treatment with local anaesthetic, magnesium sulphate or normal saline. Knee Surg Sports Traumatol Arthrosc. 2011;19(6):1043-1046.

5 Breu A, Rosenmeier K, Kujat R, Angele P, Zink W. The cytotoxicity of bupivacaine, ropivacaine, and mepivacaine on human chondrocytes and cartilage. Anesth Analg. 2013;117(2):514-522.

6 Chu CR, Coyle CH, Chu CT, Szczodry M, Seshadri V, Karpie JC, Cieslak KM, Pringle EK. In vivo effects of single intra-articular injection of 0.5% bupivacaine on articular cartilage. J Bone Joint Surg Am. 2010;92(3):599-608.

7 Chu CR, Izzo NJ, Coyle CH, Papas NE, Logar A. The in vitro effects of bupivacaine on articular chondrocytes. J Bone Joint Surg Br. 2008;90(6):814-820.

8 Chu CR, Izzo NJ, Papas NE, Fu FH. In vitro exposure to 0.5% bupivacaine is cytotoxic to bovine articular chondrocytes. Arthroscopy. 2006;22(7):693-699.

9 Cissell DD, Link JM, Hu JC, Athanasiou KA. A Modified Hydroxyproline Assay Based on Hydrochloric Acid in Ehrlich's Solution Accurately Measures Tissue Collagen Content. Tissue Eng Part C Methods. 2017;23(4):243-250.

10 Dragoo JL, Braun HJ, Kim HJ, Phan HD, Golish SR. The in vitro chondrotoxicity of single-dose local anesthetics. Am J Sports Med. 2012;40(4):794-799.

11 Eker HE, Cok OY, Aribogan A, Arslan G. The efficacy of intra-articular lidocaine administration in chronic knee pain due to osteoarthritis: A randomized, double-blind, controlled study. Anaesth Crit Care Pain Med. 2017;36(2):109-114.

12 Elder BD, Athanasiou KA. Synergistic and additive effects of hydrostatic pressure and growth factors on tissue formation. PLoS One. 2008;3(6):e2341.

13 Elder BD, Athanasiou KA. Systematic assessment of growth factor treatment on biochemical and biomechanical properties of engineered articular cartilage constructs. Osteoarthritis Cartilage. 2009;17(1):114-123.

14 Farkas B, Kvell K, Czompoly T, Illes T, Bardos T. Increased chondrocyte death after steroid and local anesthetic combination. Clin Orthop Relat Res. 2010;468(11):3112-3120.

15 Grishko V, Xu M, Wilson G, Pearsall AWt. Apoptosis and mitochondrial dysfunction in human chondrocytes following exposure to lidocaine, bupivacaine, and ropivacaine. J Bone Joint Surg Am. 2010;92(3):609-618.

16 Hansen BP, Beck CL, Beck EP, Townsley RW. Postarthroscopic glenohumeral chondrolysis. Am J Sports Med. 2007;35(10):1628-1634.

17 Heilmann HH, Lindenhayn K, Walther HU. [Synovial volume of healthy and arthrotic human knee joints]. Z Orthop Ihre Grenzgeb. 1996;134(2):144-148.

18 Hu JC, Athanasiou KA. A self-assembling process in articular cartilage tissue engineering. Tissue Eng. 2006;12(4):969-979.

19 Iwasaki K, Sudo H, Kasahara Y, Yamada K, Ohnishi T, Tsujimoto T, Iwasaki N. Effects of Multiple Intra-articular Injections of 0.5% Bupivacaine on Normal and Osteoarthritic Joints in Rats. Arthroscopy. 2016;32(10):2026-2036.

20 Karpie JC, Chu CR. Lidocaine exhibits dose- and time-dependent cytotoxic effects on bovine articular chondrocytes in vitro. Am J Sports Med. 2007;35(10):1621-1627.

21 Kreuz PC, Steinwachs M, Angele P. Single-dose local anesthetics exhibit a type-, dose-, and time-dependent chondrotoxic effect on chondrocytes and cartilage: a systematic review of the current literature. Knee Surg Sports Traumatol Arthrosc. 2018;26(3):819-830.

22 Kwon H, Brown WE, Lee CA, Wang D, Paschos N, Hu JC, Athanasiou KA. Surgical and tissue engineering strategies for articular cartilage and meniscus repair. Nat Rev Rheumatol. 2019;15(9):550-570.

23 Lee JK, Link JM, Hu JCY, Athanasiou KA. The Self-Assembling Process and Applications in Tissue Engineering. Cold Spring Harb Perspect Med. 2017;7(11).

24 Libbin RM, Rivera ME. Regeneration of growth plate cartilage induced in the neonatal rat hindlimb by reamputation. J Orthop Res. 1989;7(5):674-682.

25 MacBarb RF, Makris EA, Hu JC, Athanasiou KA. A chondroitinase-ABC and TGF-beta1 treatment regimen for enhancing the mechanical properties of tissue-engineered fibrocartilage. Acta Biomater. 2013;9(1):4626-4634.

26 McNary SM, Athanasiou KA, Reddi AH. Transforming growth factor beta-induced superficial zone protein accumulation in the surface zone of articular cartilage is dependent on the cytoskeleton. Tissue Eng Part A. 2014;20(5-6):921-929.

27 Paschos NK, Lim N, Hu JC, Athanasiou KA. Functional properties of native and tissue-engineered cartilage toward understanding the pathogenesis of chondral lesions at the knee: A bovine cadaveric study. J Orthop Res. 2017;35(11):2452-2464.

28 Piper SL, Kim HT. Comparison of ropivacaine and bupivacaine toxicity in human articular chondrocytes. J Bone Joint Surg Am. 2008;90(5):986-991.

29 Seshadri V, Coyle CH, Chu CR. Lidocaine potentiates the chondrotoxicity of methylprednisolone. Arthroscopy. 2009;25(4):337-347.

30 Sherman SL, Khazai RS, James CH, Stoker AM, Flood DL, Cook JL. In Vitro Toxicity of Local Anesthetics and Corticosteroids on Chondrocyte and Synoviocyte Viability and Metabolism. Cartilage. 2015;6(4):233-240.

31 Sola M, Dahners L, Weinhold P, Svetkey van der Horst A, Kallianos S, Flood D. The viability of chondrocytes after an in vivo injection of local anaesthetic and/or corticosteroid: a laboratory study using a rat model. Bone Joint J. 2015;97-B(7):933-938.

32 Syed HM, Green L, Bianski B, Jobe CM, Wongworawat MD. Bupivacaine and triamcinolone may be toxic to human chondrocytes: a pilot study. Clin Orthop Relat Res. 2011;469(10):2941-2947.

33 Turnbull ZA, Sastow D, Giambrone GP, Tedore T. Anesthesia for the patient undergoing total knee replacement: current status and future prospects. Local Reg Anesth. 2017;10:1-7.

34 Vapniarsky N, Huwe LW, Arzi B, Houghton MK, Wong ME, Wilson JW, Hatcher DC, Hu JC, Athanasiou KA. Tissue engineering toward temporomandibular joint disc regeneration. Sci Transl Med. 2018;10(446).

35 Watrin-Pinzano A, Ruaud JP, Cheli Y, Gonord P, Grossin L, Gillet P, Blum A, Payan E, Olivier P, Guillot G, Netter P, Loeuille D. T2 mapping: an efficient MR quantitative technique to evaluate spontaneous cartilage repair in rat patella. Osteoarthritis Cartilage. 2004;12(3):191-200.

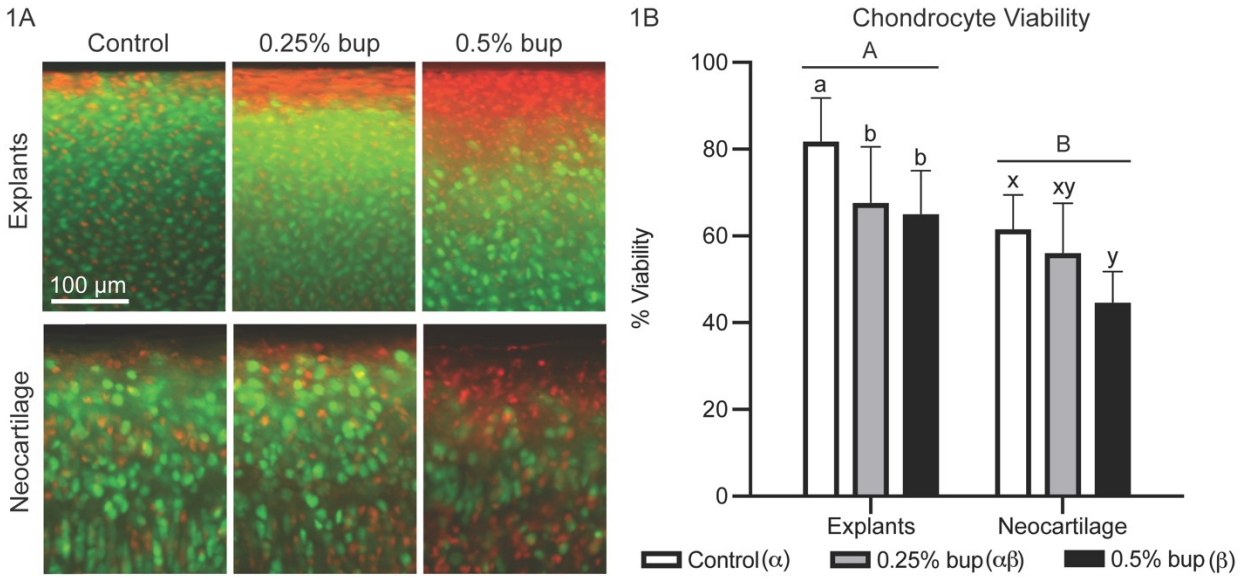

Figure A4-1. Chondrocyte viability in native explants and neocartilage constructs after bupivacaine exposure. (A) Top surface of cartilage tissue (10x). (B) Tissue type and bupivacaine exposure are significant sources of variation in chondrocyte viability. Statistical significance ($p<0.05$) is indicated by groups marked with different letters.

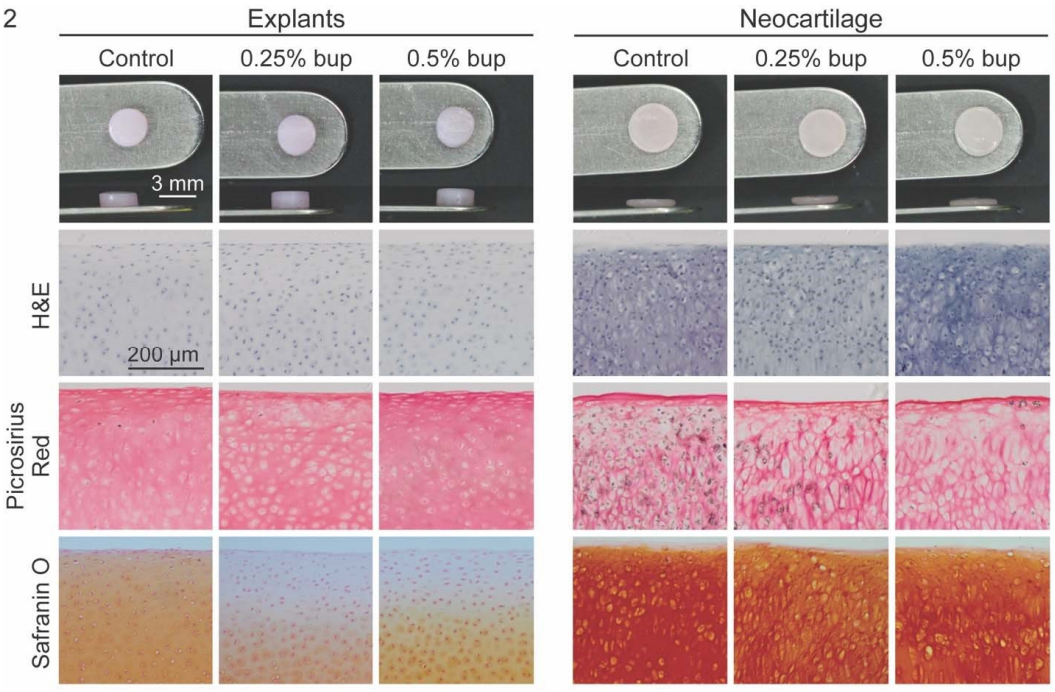

Figure A4-2. Gross and microscopic histology of native explants and neocartilage constructs after exposure to bupivacaine. H&E – hematoxylin and eosin.

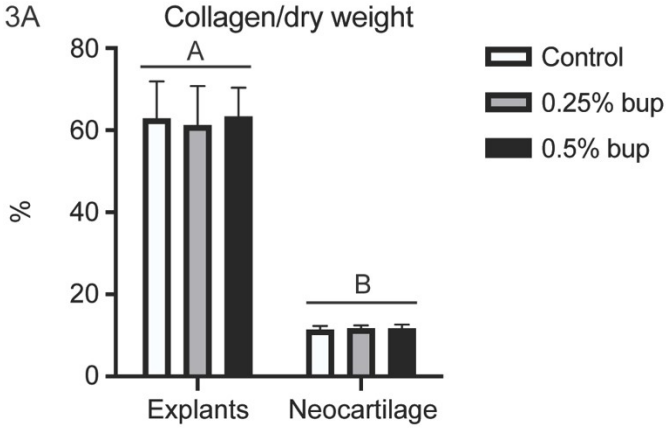

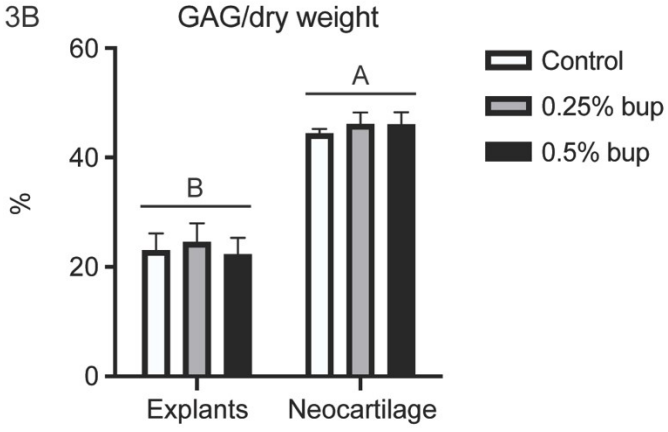

Figure A4-3. Biochemical composition of the extracellular matrix. Tissue type was a significant source of variation in (A) collagen per dry weight and (B) GAG per dry weight.

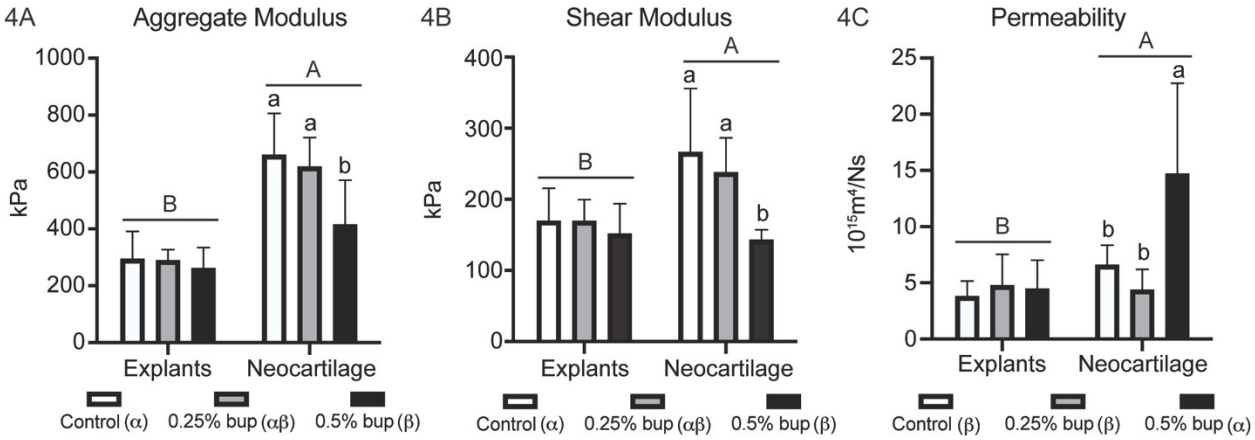

Figure A4-4. Compressive mechanical properties of native explants and neocartilage. Tissue type and bupivacaine exposure were significant sources of variation in (A) aggregate modulus and (B) shear modulus. (C) For permeability, there was a significant interaction between tissue type and bupivacaine exposure. Both factors were also significant sources of variation. Statistical significance ($p<0.05$) is indicated by groups marked with different letters

Table A4-1. Biochemical composition of extracellular matrix

Bupivacaine Treatment		Hydration (%)	Col/ww (%)	Col/dw (%)	Col/DNA (μg/μg)	GAG/ww (%)	GAG/dw (%)	GAG/DNA (μg/μg)
Explants	Control	78.3±2.7	13.8±3.5	62.8±9.1	343.9±102.6	5.0±0.6	23.0±3.1	125.0±33.7
	0.25%	80.2±1.3	12.2±2.5	61.2±9.5	294.4±81.0	4.9±0.7	24.5±3.5	117.2±25.6
	0.5%	80.6±2.5	12.3±2.4	63.3±7.1	359.6±110.9	4.3±0.9	22.3±3.1	128.6±45.9
Neocartilage	Control	82.2±0.7	2.0±0.2	11.4±0.9	22.7±1.2	7.5±1.0	42.3±5.2	84.5±11.9
	0.25%	81.9±0.4	2.1±0.2	11.7±0.8	18.3±2.0	8.3±0.5	46.1±2.2	72.4±7.3
	0.5%	82.6±1.2	1.9±0.4	10.7±2.4	16.6±4.8	8.0±0.5	46.0±2.3	71.1±13.1